Application of mechanistic and mixed effect modelling in the elucidation of developmental factors influencing oral absorption and bioavailability in children

---

A PhD Thesis Presented to
Great Ormond Street Institute of Child Health
University College London

Zoe Anna Kane

December 2023

Declaration

I, Zoe Kane, confirm that the work presented in this thesis is my own. Where information was derived from other sources, I confirm that this was indicated in the thesis.

Acknowledgements

I want to thank UCL and the Great Ormond Street Institute of Child Health for the opportunity to be part of a research community decidated to improving the health and well being of children. While everybody I have met (albeit often virtually) has inspired me to continue to grow and seek new understanding I want to say a special thank you to Professor Standing and Dr Gastine, I have learnt so much from you both, you have pushed me all the way to do my best work, thank you. To Professor Cortina-Borja and Professor Klein you were both instrumental in setting me off on the right path in the early stages of this journey and I am extremely grateful for all of your time and advice. To all the famillies and children whose poor health led to the data that I have worked with thank you, I hope that in some small way my work will contribute to better outcomes for children in the future. To all the amazing researchers across the world who's work I have learnt from, results I have incorporated and methods I have used, thank you. Last but by no means least, Ben, thank you for all your support, this would never have been possible without it.

Abstract

Infectious diseases are the major cause of drug use in children, however even today a significant proportion of paediatric medicines lack rational age appropriate dosing strategies. Most paediatric medicines are administered orally which introduces further complexity to paediatric dose setting beyond scaling of drug clearance. There still remain significant gaps in our understanding of the developmental changes that influence oral drug absorption and bioavailability in children especially during the early years of life, a time when the most significant maturational changes occur in the structure and function of the biological systems affecting drug exposure.

This PhD comprises three distinct chapters. Each chapter focuses on a different antimicrobial with different absorption, distribution, metabolism and elimination (ADME) properties. Either population (nonlinear mixed effects) and/or physiologically based pharmacokinetic (PK) modelling has been utilised to study the age-dependent physiological changes that influence oral drug absorption and bioavailability in children.

In Chapter 1 a fosfomycin population pharmacokinetic model was developed using intravenous and oral PK data collected during the NeoFoso clinical trial. In total, 238 plasma and 15 cerebrospinal fluid concentrations were collected from 60 neonates hospitalised with suspected sepsis. The final model was used alongside currently available pharmacodynamic targets to evaluate neonatal fosfomycin doses based on an infant's post menstrual age, postnatal age and weight. A two-compartment disposition model, with an additional CSF compartment and first-order absorption, best described the data. Neonatal bioavailability was estimated as 0.48 (95% CI = 0.347–0.775) and the cerebrospinal fluid:plasma ratio as 0.32 (95% CI = 0.272–0.409). Allometric weight and post menstrual age scaling was applied *a priori*, additional covariates found by this analysis included postnatal age on clearance and cerebrospinal fluid protein level on cerebrospinal fluid:plasma ratio.

In Chapter 2 population PK modelling was used to quantify age related changes in systemic benznidazole exposure following oral dosing in paediatric and adult Chagas Disease patients. To enable development of a mechanistic explanation for the observed effect of age on oral bioavailability, a PBPK model describing benznidazole pharmacokinetics was also developed. Human pharmacokinetic data included adult PK data (n=16, 168 plasma concentrations) from healthy volunteers (rich single dose PK at 1.6 and 25 mg/kg) and Chagas Disease patients (sparse repeat dosing at 3.4 mg/kg, q12hr, 4 weeks). The paediatric PK data set comprised 109 plasma concen-trations from 35 children aged 2-12 years (5-9 mg/kg/day, q12hr, 60 days). External validation of the PBPK model was performed using a subset of pharmacokinetic data from the BENDITA clinical trial (n=25 adult Chagas Disease patients, 83 plasma concentrations). This study is the first time a physiologically based pharmacokinetic (PBPK) model has been developed for benznidazole and it indicates incomplete oral absorption, low first-pass extraction, and significant renal re-absorption. The PBPK model has been used to test the hypothesis that the age-dependent changes in ben-znidazole oral exposure are due to reduced renal reabsorption in children aged 2-6 years as compared to in adult patients. Further *in-vitro* renal transporter work is required to confirm the feasibility of this hypothesis.

In Chapter 3 real-world intravenous and oral (suspension and tablet) posaconazole therapeutic drug monitoring data was modelled using the population approach. In total, 298 plasma concentrations (10 to 11,400 ng/L) from 104 children were included in this analysis. Median age was 6.2 years (IQR 2.6 to 10.6 years) and median weight 19.5 kg (range 4.3 to 86 kg). The relative proportion of IV:tablet:suspension data was 16:14:70. Sixty nine percent of the plasma concentrations were collected during periods of concomitant proton-pump inhibitor (PPI) administration, 49% during a period of diarrhoea, and 6% were reported as below the limit of quantification. The final model was a one-compartment model with first-order absorption and nonlinear elimination. Tablet bioavailability was estimated to be 66%. Suspension bioavailability was estimated to decrease with increasing doses, ranging from 3.8% to 32.2% in this study population, and reducing by 41% with concomitant use of proton pump-inhibitors. This is the first population pharmacokinetic study to model posaconazole data from hospitalized children following intravenous, tablet, and suspension dosing simultaneously. The incorporation of saturable posaconazole clearance into the model was found to be critical to the credible joint estimation of tablet and suspension bioavailability.

While incomplete absorption was found for the three exemplar drugs evaluated during this research, the ability to estimate between-subject variability in the extent and the rate of oral absorption (Ka) has been a major challenge. This was especially true when modelling the real world posaconazole data where between subject variability in oral bioavailability could not be estimated, and even the population estimates of absorption rate constants (Ka_{tab} and Ka_{sus}) had to be fixed to adult priors. While the challenges of sparse PK data in children makes it difficult to draw conclusions concerning the effect of age on the rate and extent of oral absorption, the work presented in this thesis contributes significant new evidence regarding the pharmacokinetics, and subsequently the optimal dose, of three important antimicrobials in paediatric populations.

UCL Research Paper Declaration Form (Chapter 1):

In accordance with the UCL policy the following publication is declared.

a) What is the title of the manuscript?

- *IV and oral fosfomycin pharmacokinetics in neonates with suspected clinical sepsis*

b) Please include a link to or doi for the work:

- *DOI: 10.1093/jac/dkab083*

c) Where was the work published?

- *Journal of Antimicrobial Chemotherapy*

d) Who published the work?

- *OUP*

e) When was the work published?

- *April 2021*

f) List the manuscript's authors in the order they appear on the publication?

- *Kane, Zoe. Gastine, Silke. Obiero, Christina. Williams, Phoebe. Murunga, Sheila. Thitiri, Johnstone. Ellis, Sally. Correia, Erika. Nyaoke, Borna. Kipper, Karin. Van Den Anker, John. Sharland, Mike. Berkley, James A. Standing, Joseph F.*

g) Was the work peer reviewed?

- *Yes*

h) Have you retained the copyright?

- *Yes; Licence OA-CC-BY*

I) Was an earlier form of the manuscript uploaded to a preprint server (e.g. medRxiv)? If 'Yes', please give a link or doi. If 'No', please seek permission from the relevant publisher and check the box next to the below statement:

- *No*

☒ I acknowledge permission of the publisher named under 1d to include in this thesis portions of the publication named as included in 1c.

UCL Research Paper Declaration Form (Chapter 3):

In accordance with the UCL policy the following publication is declared.

a) What is the title of the manuscript?

- *Model based estimation of posaconazole tablet and suspension bioavailability in hospitalised children using real–world therapeutic drug monitoring data in patients receiving intravenous and oral dosing*

b) Please include a link to or doi for the work:

- *DOI: 10.1128/aac.00077-23*

c) Where was the work published?

- *Antimicrobial Agents and Chemotherapy*

d) Who published the work?

- *American Society for Microbiology (ASM Journals)*

e) When was the work published?

- *June 2023*

f) List the manuscript's authors in the order they appear on the publication?

- *Zoe Kane, Iek Cheng, Orlagh McGarrity, Robert Chiesa, Nigel Klein, Mario Cortina–Borja, Joseph F Standing and Silke Gastine.*

g) Was the work peer reviewed?

- *Yes*

h) Have you retained the copyright?

- *Yes; Licence OA-CC-BY*

I) Was an earlier form of the manuscript uploaded to a preprint server (e.g. medRxiv)? If 'Yes', please give a link or doi. If 'No', please seek permission from the relevant publisher and check the box next to the below statement:

- *No*

☒ I acknowledge permission of the publisher named under 1d to include in this thesis portions of the publication named as included in 1c.

Other Scientific Contributions

In addition to the work presented in this thesis and the research papers declared above, I have been involved in the following publications whilst studying for the degree of Doctor of Philosophy.

- **Kane, Z.**; Picetti, R.; Wilby, A.; Standing, J. F.; Grassin-Delyle, S.; Roberts, I.; Shakur-Still, H. Physiologically Based Modelling of Tranexamic Acid Pharmacokinetics Following Intravenous, Intramuscular, Sub-Cutaneous and Oral Administration in Healthy Volunteers. Eur. J. Pharm. Sci. 2021, 164, 105893. https://doi.org/10.1016/j.ejps.2021.105893.
- Obiero, C. W.; Williams, P.; Murunga, S.; Thitiri, J.; Omollo, R.; Walker, A. S.; Egondi, T.; Nyaoke, B.; Correia, E.; **Kane, Z.**; Gastine, S.; Kipper, K.; Standing, J. F.; Ellis, S.; Sharland, M.; Berkley, J. A. Randomised Controlled Trial of Fosfomycin in Neonatal Sepsis: Pharmacokinetics and Safety in Relation to Sodium Overload. Arch. Dis. Child. 2022, archdischild-2021-322483. https://doi.org/10.1136/archdischild-2021-322483.

Impact Statement

The work presented in Chapter 1 of this thesis on the pharmacokinetics of fosfomycin in neonates is potentially highly impactful for children globally. The population PK model that was developed, along with the resulting neonatal dosing simulations, have already been published in the Journal of Antimicrobial Chemotherapy and fill a key knowledge gap concerning fosfomycin pharmacokinetics in newborns. Thereby enabling researchers to move closer to more efficacious empiric regimens for the treatments of Gram -ve sepsis. Recruitment is currently on-going for the NeoSep1 clinical trial (ISRCTN48721236: `https://doi.org/10.1186/ISRCTN48721236`), a Phase II/III study that aims to recruit 3060 neonates and determine the effectiveness of existing and new antibiotic combinations to treat newborn babies hospitalised with severe sepsis. Fosfomycin will be evaluated in the NeoSep1 study at a total daily dose of 200-300 mg/kg using a q12hr interval for both sepsis and meningitis, and the Global Antibiotic Research & Development Partnership who are funding the NeoSep1 trial, are targeting study completion by Oct 2026. In Chapter 2 the unexpected affect of age on benznidazole pharmacokinetics was investigated. Benznidazole is one of only two treatment options available to patients suffering from Chagas Disease, a condition designated by the WHO as a neglected tropical disease. Benznidazole's PKPD relationship is poorly understood, but the frequency of adverse reactions that are often an issue in adult populations appear reduced in children. This thesis presents the first ever published benznidazole physiologically based PK model, and alongside it, a mechanistic hypothesis for the disconnect in exposure between adult populations and children <6yrs old. With further work to test this hypothesis and validate the models ability to predict benznidazole tissues concentrations it could present a valuable tool to researchers working to discover new chemical entities for the treatment of Chagas Disease (`https://dndi.org/research-development/portfolio/uw-series/`), potentially providing a quantitative link to diminished benznidazole efficacy during chronic disease. In the final chapter of this thesis the impact of formulation, dose and other covariates on the oral bioavailability of posaconazole was estimated using population PK modelling and real-world therapeutic drug monitoring data collected

in paediatric patients. The results of this study analysis have recently been accepted by the journal Antimicrobial Agents and Chemotherapy and will be published soon. The head to head comparison of intravenous, tablet and suspension posaconazole products administered widely to European children has implications for all front line prescribers. Lastly, whilst physiologically based PK (PBPK) modelling has only been performed for benznidazole as part of this thesis, all three of the paediatric oral PK datasets that have been curated will be of value to members of the PBPK research community interested in validating the age dependent system (gastrointestinal) parameters that underpin 'bottom-up' oral absorption predictions for children as more validatory evidence is still needed here.

Dedication

To Peggy and Leni you were only seven and five when I started on this journey. Thank you for being so patient and for all your encouragement, you are my inspiration.

Table of Contents

List of Tables

List of Figures

Abbreviations

Short Form	Definition
-2LL	-2 log likelihood function
ϵ, Σ, RUV	residual unexplained variability
η, Ω, IIV	inter-individual variability
λ_z, K_{el}	terminal elimination rate constant
τ	dosing interval
φ, θ	population parameters
C_{24}	concentration at 24 hours
CL	clearance
CLh	hepatic clearance
CLr	renal clearance
F_a	fraction absorbed
F_g	fraction surviving gut metabolism
F_h	fraction surviving first pass metabolism
F	bioavailability
K_a	absorption rate constant
K	rate constant
PR_i	CSF protein concentration for the ith subject
Q	inter-compartmental clearance
R^2	coefficient of determination
$T_{\frac{1}{2}z}$	terminal half-life
V_c	volume of the central compartment
V_{ss}	volume of distribution at steady state
V_z	terminal phase volume of distribution
V	volume of distribution
AAG	alpha 1 acid-glycoprotein
ABC	ATP-binding cassette
ABCB1/MDR1	P-glycoprotein transporter

ABCC2/MRP2	multi drug resistance-associated protein-2
ABCG2/BCRP	breast cancer resistance protein
ACAT	advanced compartmental absorption and transit
ADEs	age-dependant exponents
ADME	absorption, distribution, metabolism and elimination
ADR	adverse drug reaction
AFE	average fold error
AP	ADMET Predictor
ASF	absorption scale factor
AUC	area under the curve
BCS	biopharmaceutics classification system
BDDCS	biopharmaceutics drug disposition classification system
BID	"bis in die" meaning twice a day
BNZ	benznidazole
BSV	between subject variability
BW	body weight
CI	confidence interval
Cmax	maximum concentration
CNS	central nervous system
CSF	cerebrospinal fluid
CV	coefficient of variation
CWRES	conditional weighted residual
CYP	cytochrome P450
DDI	drug-drug interaction
DF	intestinal regional distribution factor
DNDI	Drugs for Neglected Diseases initiative
DV	dependant variable
Eg	gut wall extraction
Eh	hepatic extraction
EMEA	European Medicines Agency
EU	European Union
FDA	food and drug administration
FE	food effect
FO	first order
FOCE	first order conditional estimation
FOCEI	first-order conditional estimation method with interaction
FOS	fosravuconazole

Fup	fraction unbound in plasma
GE	gastric emptying
GFR	glomerular filtration rate
GOF	goodness of fit
GUI	graphical user interface
GVHD	graft versus host disease
HSA	human serum albumin
HSCT	hematopoietic stem cell transplantation
ICH	International Council for Harmonisation
IFI	invasive fungal infection
IPRED	individual prediction
iPSP	initial paediatric study plan
IQR	inter-quartile range
IV	intravenous
IVIVE	In-vitro in-vivo extrapolation
IWRES	individual weighted residual
Kp	tissue/plasma partition coefficient
LMICs	low and middle income countries
LOESS	locally estimated scatterplot smoothing
MBDD	model based drug development
MDR	multi-drug resistant
MIC	minimum inhibitory concentration
MISO	misonidazole
MLE	maximum likelihood estimation
MNZ	metronidazole
MSD	Merck Sharp and Dohme
NCA	non-compartmental analysis
NDA	new drug application
NFX	nifurtimox
NLME	non-linear mixed effects
ODE	ordinary differential equation
OFV	objective function value
OLS	ordinal least squares
PAMPS	pathogen-associated molecular patterns
PBPK	physiologically based pharmacokinetics
PD	pharmacodynamics
Peff	effective intestinal permeability

PI	simulated prediction interval
PIP	paediatric investigation plan
PK	pharmacokinetics
PMA	postmenstrual age
PNA	postnatal age
PO	“per-os” meaning oral dosing
PopPK	population pharmacokinetics
POSA	posaconazole
PPB	plasma protein binding
PRED	population prediction
PsN	Perl-speaks-NONMEM
PSP	paediatric study plan
PSTc	permeability surface area product
QD	“quaque die” meaning once a day
QSAR	quantitative structure-activity relationship
Rbp	blood to plasma ratio
RMSE	root mean square error
RSE	relative standard error
RW	real world
SCR	serum creatinine
SD	single dose
SEF	surface area enhancement factor
SLC15A1/PEPT1	peptide transporter-1
SLC22A1/OCT1	organic cation transporter-1
SLCO2B1/OATP2B1	organic anion transporting polypeptide 2B1
SOC	standard of care
SS	steady state
TA	target attainment
TAFD	time after first dose
TALD	time after last (most recent) dose
TDM	therapeutic drug monitoring
TID	“ter in die” meaning three times a day
TJ	tight junction
TLRs	toll-like receptors
Tmax	time to maximum concentration
UGT2B7	uridine diphosphate glucuronosyltransferase-2B7
UGTs	uridine diphosphate glucuronosyltransferases

UNGAP	European network on understanding gastrointestinal absorption-related process
UPTK	fractional uptake into the cerebrospinal fluid
VPC	visual predictive check
WHO	World Health Organisation

Introduction

Paediatric pharmacotherapy

The European Paediatric Regulation (Regulation (EC) No 1901/2006) was introduced in 2006 and adopted in 2009, the primary goal being to improve paediatric development of medicinal products[1]. Whilst this and comparable legislation in other territories have been introduced to force investment in paediatric research (Figure 1 summarises key paediatric landmark legislation[2]) key challenges associated with paediatric pharmacotherapy endure. Clinicians are still frequently required to prescribe "off-label" (unlicensed or use outside the terms of the licence) to paediatric patients[3,4], thereby taking a greater burden of personal responsibility for the safety and efficacy of a medicine than when prescribing within the terms of a drugs licence[5].

Year	Regulation	Impact
1997	US FDA Modernization Act (FDAMA)	This act presented the financial incentive of an additional 6 months of market exclusivity to companies undertaking required paediatric studies
1998	US FDA Pediatric Rule	This rule permitted companies to label medicines for use in children based on extrapolation of efficacy from adult trial data, together with paediatric PKPD and safety data
2002	US Best Pharmaceutical for Children Act (BPCA)	Framework for paediatric research in both on and off patent drugs
2003	US Pediatric Research Equity Act (PREA)	Sponsors required to undertake clinical studies in children for new medicines and biological products
2007	EU Paediatric Regulation	Introduction of new legislation in the European Union mandating paediatric medicines research for new medicinal products
2012	US FDA Safety and Innovation Act (FDASIA)	BPCA and PREA became permanent in US Law.

Figure 1: Landmark Paediatric Legislation, recreated from Germovsek et al 2019

Fourteen years since adoption of the EU paediatric regulation there is now increased information on the safety and efficacy of new drugs in children[6], however further measures to promote timely completion of paediatric studies may be required. Hwang et al. found that even after a median time of 4.8 years post approval, 57% of the medicines in question still did not include any paediatric information[7]. The pic-

ture is somewhat better in oncology where a systematic analysis by Neel et al. found that from 1997 to 2017, the median time from first-in-human studies of new cancer drugs (ultimately approved by the US Food and Drug Administration) to "first-in-child studies" was 6.5 years[8]. Hirota et al. looked across regulatory territories and analyzed novel therapeutics approved in Japan, the United States, and the European Union during 2005–2014. At the time of initial approval, 50 out of 319 novel therapeutics (16%) in Japan, 46 out of 263 (17%) in the United States, and 33 out of 242 (14%) in the European Union had approval for some paediatric dosing information. Paediatric labeling was less available in younger age groups such as infants (27/319 (8%) in Japan, 18/263 (7%) in the United States, 15/242 (6%) in the European Union and neonates (16/319 (5%) in Japan, 10/263 (4%) in the United States, 10/242 (4%) in the European Union. As of April 30, 2018, the median duration of supplemental indication approval in paediatric population was 7.3 years (interquartile range (IQR), 5.1 to 10.3) in Japan, 7.3 years (IQR, 5.1 to 10.0) in the United States, and 6.9 years (IQR, 4.7 to 10.0) in the European Union[9]. However of the paediatric studies that are being completed there are still questions over study design. Hampson et al. con-cluded that 41% of the Paediatric Investigation Plans (PIP) studies performed in Europe between 2010–2012 were only dose-evaluating (single dose) in nature rather than dose-finding (multiple dose levels), with pharmacokinetics (PK) as an objective in very few studies[10].

PK is the study of what the body does to the drug, how it is absorbed, where it distributes to in the body, how it is metabolised and finally how it is eliminated from the body. Understanding a drugs pharmacokinetics is fundamental to understanding the dose-concentration-effect relationship, how it evolves with time and therefore what is the right dose in population X to treat disease Y. Drug effect or pharmacodynamics (PD) is usually driven by systemic or tissue drug exposure (AUC), which is indirectly proportional to CL following intravenous administration, and bioavailability following oral administration. As humans grow and age, dosing regimens need to be appropriately scaled to correct for these two correlated processes.

It is widely accepted that paediatric PK data can be used for dose setting without the need for complex/lengthy efficacy studies when the 'disease' can be extrapolated from adult data[11–15]. In some instances it may also be appropriate to extrapolate safety from adult data as was recently proposed for new antibiotics by Pansa et al[16]. For determining when extrapolation is or is not appropriate, a useful point of reference is the US Food and Drug Administration (FDA) Paediatric Study Decision Tree. Figure 2 shows an adapted version as presented by Germovsek et al[2]. However

even 'simple' PK studies in children are not without additional complexities compared to adult PK studies.

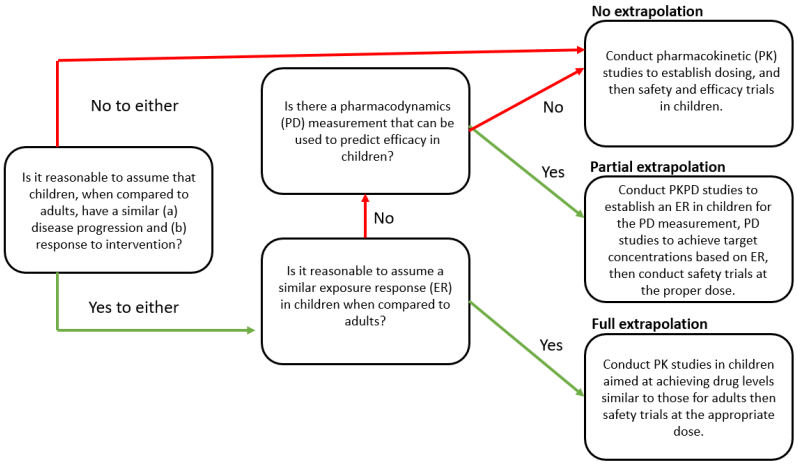

Figure 2: An adapted version of the US FDA Paediatric Study Decision Tree, recreated from Germovsek et al 2019

Neonates are generally considered to be the most vulnerable paediatric group. Pansieri et al. found that among all the trials registered within Clinicaltrials.gov between 1999 and 2012, 22% were paediatric trials, but only 0.2% (n = 288) involved neonates, most neonatal drug trials were classified as pre-marketing trials (84%), and predominantly funded by non-profit organisations (58%)[17]. While drug research in neonates represents only a very small fraction of clinical trials, scientific research in this population is thankfully growing. In 2015 Allegaert et al. reported a 2-4 fold increase since 1975 in publications returned by searching for the words "newborn" and "pharmacotherapy, pharmacokinetics, or drug"[18]. However the relative paucity of neonatal PK data is clear; inclusion of the word "pharmacokinetics" resulted in by far the lowest number of hits (a few hundred) and stands to illustrate that there remain significant challenges and barriers to performing informative PK studies in the neonatal population. In an attempt to drive the global research agenda and address paediatric off-label prescribing, deWildt et al. have identified the drugs and therapy areas for which clinical evidence is lacking regarding dosing in paediatric populations. In the case of neonates; pre-term and term, only 49.1% (n=110) and 48.7% (n=481) of prescribing was found to be supported by high quality evidence; regulatory authorisation, meta-analysis or randomised control trial[19].

It is important to remember that the regulatory requirement for pharmaceutical companies to provide paediatric dosing information, currently in the form of a "Paediatric Investigation Plan" (PIP) in the EU or an "Initial Paediatric Study Plan" (iPSP)

in the US, only applies to recently (since 2009 in the EU) developed medicines, many older drugs still have poorly defined age appropriate dosing[20], that is often complicated by polypharmacy. In a study of 1 million Canadian children 25% of children were responsible for 70% of drug use[21]. These children typically having complex or chronic disorders requiring multiple drugs be taken in parallel[22]. In attempts to address the historic lack of paediatric clinical trials researchers, especially those working in the field of antimicrobial chemotherapy and anaesthetics, have utilised retrospective analysis of data collected during routine clinical care (therapeutic drug monitoring (TDM) or real-world (RW) data to optimise therapeutic outcomes for children[23,24].

In summary paediatric drug research is essential and dosing strategies should be be grounded in a thorough understanding of developmental pharmacology combined with statistical or model-based analysis of data collected in well designed paediatric clinical trials[25,26].

Paediatric infectious diseases

While childhood survival rates have been improving in recent years the UN interagency group for child mortality reported that in 2020 alone 5.0 (4.8-5.5, 90% uncertainty interval) million children died before their fifth birthday, with half of those deaths occurring in newborns[27]. Infectious diseases disproportionately affect children in low- and middle-income countries (LMICs), especially in sub-Saharan Africa.

However even in more affluent countries antimicrobials play a major role in paediatric medicine. Rashed et al. analysed prescribing information from 1278 paediatric patients collected in the paediatric general medical ward of hospitals in five affluent countries: Australia, Germany, Hong Kong, Malaysia and the UK during 2008-2009. The authors found that the majority of patients (67.2%) received 1–4 drugs, most of whom were aged <=2 years and in the total cohort systemic antibacterials accounted for 25.2% of prescriptions with analgesic drugs following in second place at 16.8%.[28]

Sepsis

Sepsis disproportionately affects neonates. In the first month of life 17.0% of neonatal deaths globally are due to neonatal sepsis or other infectious disorders, but in infants 1-12 months old this reduces to 1.5%[29].

In 2012 2.9 million neonatal deaths were reported and an estimated 0.68 million were linked to severe bacterial infection[30]. Nearly 60% of neonatal infections are the

result of Gram-negative bacteria and it has been estimated that approximately 0.2 million neonatal sepsis deaths in the five highest burden countries were caused by bacteria resistant to first line antibiotics[31].

A more recent meta-analysis identified Klebsiella, Escherichia coli spp. and *Staphylococcus aureus* as the main causes of sepsis in neonates in sub-Saharan Africa[32].

Chagas disease

Chagas disease, or American trypanosomiasis, is an infection caused by the single-cell protozoan parasite *Trypanosoma cruzi (T. cruzi)*. More than 100 years since its discovery the condition remains a major problem in Latin America and is classified as a neglected tropical disease by the World Health Organisation (WHO).

Prevalence of the disease has decreased significantly since the early 90s due to vector control programmes and compulsory blood bank testing[33] however the WHO still estimate that 6 to 7 million people are infected worldwide (mostly in Latin America) and that 10,000 people die annually as a result of Chagas disease[34]. Due to large numbers of people emigrating from endemic countries to industrialized regions, particularly in the United States and the European Union transmission in non-endemic regions is growing[35–37].

Chagas disease has an acute and a chronic phase. Acute infections are predominantly asymptomatic and are characterized by high parasitaemia. Death occurs in approximately 5–10% of symptomatic patients during the acute stage of the disease, typically due to meningoencephalitis or myocarditis[33]. Individuals surviving the acute phase progress to chronic Chagas disease. Between 10% and 30% of people chronically infected with *T. cruzi* ultimately develop cardiac or gastrointestinal symptoms caused by pathological processes related to the persistent presence of the parasite. Chronic cardiac Chagas Disease typically involves rhythm disturbances and cardiomyopathy, while gastrointestinal problems can include megaesophagus and megacolon.

Two drugs, benznidazole (BNZ) and nifurtimox (NFX), are licensed for the treatment of Chagas disease although they have both safety and efficacy challenges. Benznidazole treatment in adults has >30% incidence of adverse effects, including neuropathy and severe dermatological and gastrointestinal symptoms, with adverse drug reactions (ADRs) causing over 20% of benznidazole therapy to be suspended[38]. However, in children an inverse correlation between age and ADR incidence has been reported. In one study out of 107 infants and children (median age: 6.9 years, range:

10 days to 19 years, 36% < 2 years old) treated with BNZ, 77.3% of ADRs were in children over 7 years of age[39].

Invasive fungal infections

Hematopoietic stem cell transplantation (HSCT) is a well established procedure used in the treatment of many disorders of the hematopoietic system.[40]. Infection accounts for most of the morbidity and mortality after HSCT. Autologous transplant recipients rarely experience opportunistic infections however allogeneic HSCT recipients who take chronic immunosuppressive drugs for several months are at a much greater risk of infection. The severity of infectious complications varies according to the phase post-transplant, type of transplantation, graft versus host disease (GVHD), and the degree of immunosuppression or reconstitution.

The post-HSCT period can be divided into the pre-engraftment period, immediate post-engraftment period and late post-engraftment period. Generally, neutrophils recover two to three weeks post transplant, however functional recovery of other immune cell types is also important and can take much longer; 3-6 months for NK cells, 6-12 months for B-cells and CD8 T-cells, and 1-2 years for CD4 T-cells[41].

HSCT patients are vulnerable to fungal infections, with *Aspergillus* species and *Candida spp* causing most cases of invasive fungal infections (IFIs) in HSTC patients. Azoles are considered the first choice for primary antifungal prophylaxis[42] however therapeutic drug monitoring (TDM) is recommended and drug-drug interactions (DDIs) with immunosuppressants typically employed in paediatric HSCT patients are well established[43]. Even with TDM of antifungal plasma concentrations breakthrough IFIs can still occur. Unfortunately, not all licensed antifungals are approved for paediatric use and for those that are optimal dosing regimens may not have been identified for all age groups or indications[44,45].

Developmental pharmacology

Age is a well recognised patient related factor that can alter a drug's pharmacokinetics or pharmacodynamics resulting in either deficient or excessive therapeutic effects, or unwanted side effects[46–48].

The International Council for Harmonisation (ICH) E11 guidance "Clinical investigation of medicinal products in the paediatric population"[12] suggests key age categories that should be considered when defining paediatric doses, however these

are presented as potentially relevant age categories whilst the guidance acknowledges that ultimately these should be selected based on the development of relevant physiological/mechanistic processes for specific drugs/diseases.

Neonates are a group of particular interest and represent children from birth up to 28 days, or the equivalent postmenstrual age (44 weeks), and covers both preterm (<37 weeks gestational age at birth) and full term (>37 weeks gestational age at birth) neonates.

Developing ADME systems

Following oral drug delivery there are four processes that a drug will go through: Absorption, Distribution, Metabolism (pre-systemic and systemic) and Elimination (ADME). Each of these plays a role in determining the levels of drug present in the blood and body tissues at any given time. Understanding absorption and pre-systemic metabolism in isolation does not allow oral pharmacokinetics to be predicted but as they are the main focus of this study they are discussed in more detail in the subsequent sections.

Bioavailability (F) is a important concept in oral drug delivery and can be calculated by comparing drug exposure (AUC) following oral and IV dosing.

$$Bioavailability\,(F) = \frac{AUC_{\,oral}}{AUC_{\,iv}} \times \frac{DOSE_{\,iv}}{DOSE_{\,oral}}$$

Depending on the properties of a drug F may be dependent on the oral dose, the formulation, concomitant co-medication or the fed state of a subject. Ideally F is calculated using PK data obtained in a crossover study and the IV dose as much as possible exposes the key metabolising organs to comparable drug concentrations as the oral dose, thereby avoiding issues with non-linear metabolism or transporter mediated distribution. Bioavailability is often also expressed as a product of the fraction absorbed (Fa), the fraction surviving gut metabolism (Fg) and the fraction surviving first pass liver metabolism (Fh), see Figure 3. Alternatively, F may be expressed in terms of gut wall extraction (E_g, where $F_g = 1 - E_g$) and hepatic extraction (E_h, where $F_h = 1 - E_h$). However, determining these fractions *in-vivo* is challenging, often requiring model based PK analysis or assumptions such as $F_g = 1$ and clearance is only either hepatic or renal.

The question of the impact of population demographics; ethnicity, weight, age, disease state on bioavailability is an interesting one, and the ability to predict such effects relies on an understanding of the drug properties and the factors that influence

either absorption, distribution, metabolism or elimination.[48,49].

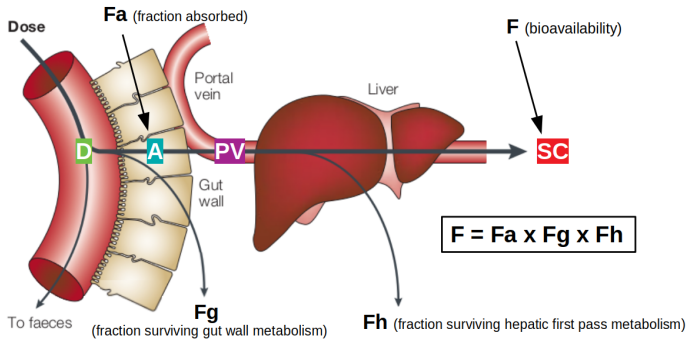

Figure 3: Schematic overview of the factors that contribute to bioavailability, modified from van de Waterbeemd 2003. D; amount of drug dosed. A; amount absorbed into the enterocyte. PV; amount of drug entering the portal vein. SC; amount of drug reaching the systemic circulation.

Absorption

In order to be absorbed drug must be in solution and pass from the intestinal lumen into the enterocyte. Therefore, the primary drug properties that determine how well a drug is absorbed are solubility and permeability. These properties like many others must always be considered in the context of the oral dose given. These primary determinants of Fa are reflected in the BCS criteria, a classification system first introduced in the mid 90s as a regulatory framework to enable the use of biowaivers; in vitro based bioequivalence studies[50]. However the nuanced challenges of defining 'high solubility' and 'high permeability'; this depends on dose, which can vary with the patient population and the specific indication, has meant that the the EMEA only adopted the ICHM9 guidance this year[51].

While solubility and permeability are considered the primary drug properties that together determine Fa, many other drug characteristics influence these properties; ionisation state, lipophilicity, crystal structure and molecular weight. Dissolution rate and precipitation kinetics are important secondary factors and since most licensed drugs have been formulated into 'optimised' drug products, excipient effects are also important to understand, with some having potential to influence both solubility, permeability and also metabolism.[52,53].

Solubility is a thermodynamic property determined by physico-chemical properties. Intestinal permeability is a biological process and is therefore more difficult to study. Drugs can move from the intestinal lumen into the systemic circulation via ei-

ther transcellular or paracellular transport, the first of which may be either a passive (down a concentration gradient) or active (transporter mediated) process, with the main barrier to paracellular diffusion across the epithelial cell layer being the tight junction (TJ) complex, see Figure 4. Studies in T84 monolayers reported that restrictive paracellular pores typically had a radius of ~4.5 Å[54]. The importance of the intestinal tight junction in immunity is also established, with TJ dysfunction highly associated with metabolic and inflammatory diseases[55].

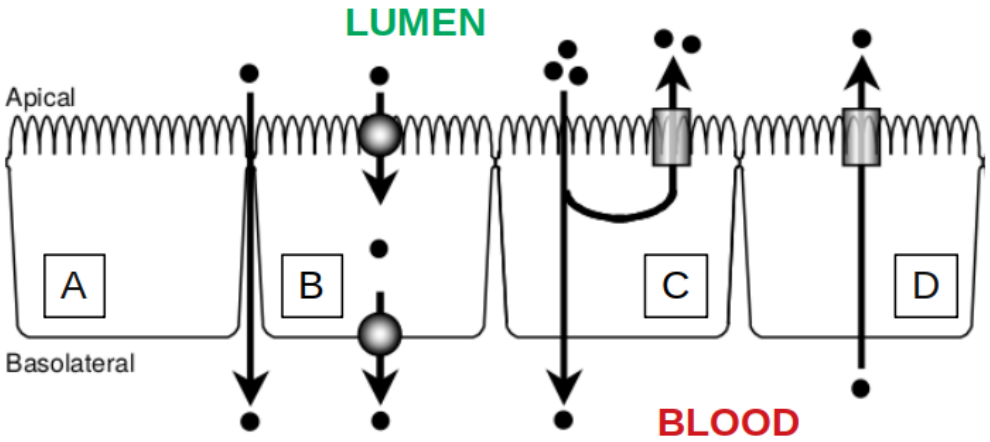

Figure 4: Schematic overview of intestinal permeability. (A) paracellular absorption restricted by tight junctions. (B) Transcellular carrier mediated absorption. (C) Efflux transporter reducing drug absorption. (D) Efflux transporter facilitating intestinal secretion from the blood. Modified from Chan 2004

It is the physiological environment of the GIT that determines how a given drug will behave, and it is these conditions that potentially differ in special populations such as paediatrics. Conditions such as the pH, composition and volume of the gastrointestinal fluid, intestinal surface area, gastrointestinal transit times, thickness and viscosity of the mucus layer, integrity of the epithelial barrier, and the expression and function of uptake/efflux transporters are all important to understand if attempting to predict F% in children[56,57].

On top of age dependent changes in GI physiology, disease also plays an important role. Pathophysiological changes in patients with GI disease include transit time/motility, pH, composition of luminal contents, permeation and transport systems, metabolism and were reviewed by Effinger et al. The authors conclude by advocating for further elucidation of drug absorption profiles (derived from pharmacokinetics) in patients with GI diseases as more quantitative data is needed[58]. The health and diversity of the microbiome is another GI related variable that has

been linked to clinical outcomes in children undergoing Haematopoietic Stem Cell Transplantation[59] and for drugs processed by bacterial enzymatic action, an influence on drug absorption may also be expected.

The European network on understanding gastrointestinal absorption-related processes (UNGAP) have published comprehensive review articles dealing with the key themes concerning the oral absorption landscape, one of which relates to the insufficient mechanistic understanding of the processes critical to oral drug absorption in specific patient populations. The objective of the review by Vinarov et al. was to identify gaps/controversies in current understanding, and create a roadmap for future oral drug absorption research[60]. The 'way-forward' for age-segregated oral absorption proposed by UNGAP is to focuses on four research themes; 1) determination of age segregated GI fluid volumes and compositions, 2) further characterise intestinal drug-metabolising enzymes and drug transporters, 3) generation of quality clinical PK in paediatric populations and 4) further develop and *verify* in-vitro and in-silico models[60]. These research themes are all in consistent with knowledge gaps highlighted in an earlier UNGAP review by Stillhart et al. where the authors conclude that current knowledge about GI conditions in special populations and their impact on drug absorption is still limited, and call for further research to improve confidence in pharmacokinetic predictions and dosing recommendations in the 'special patient populations' (paediatrics, geriatrics, obese, pregnant, and GI disease pateints) thereby ensuring safe and effective drug therapies[61].

Intestinal permeability is known to decrease to adult levels during the immediate postnatal period, with the process of 'gut closure' taking between 7-30 days and occurring faster in babies fed with breast milk rather than formula[62]. A more recent study evaluated intestinal permeability markers on day 1, 8 and 15 post birth with the aim of exploring whether feeding and antibiotic exposures affected intestinal barrier maturation in pre term infants. This work also found a maturational affect of breast milk feeding and that intestinal barrier maturation in pre term infants is both GA and postnatal age dependent[63]. However, while intestinal permeability may be elevated in the first month of life, the intestinal surface-to-volume ratio is believed to be reduced in children when compared with adults[64].

Gastric pH is frequently quoted as being neutral initially post birth and declining to adult like acidic conditions over either hours or days, however arguments to the contrary are increasingly being made and clear consensus is still missing on this subject[56]. Gastric emptying (GE) is often reported to be slower and more irregular in newborns and young infants, and in the case of paracetamol was used to explain a

higher absorption half-life in neonates compared to older children/adults, see Figure 5[65,66].

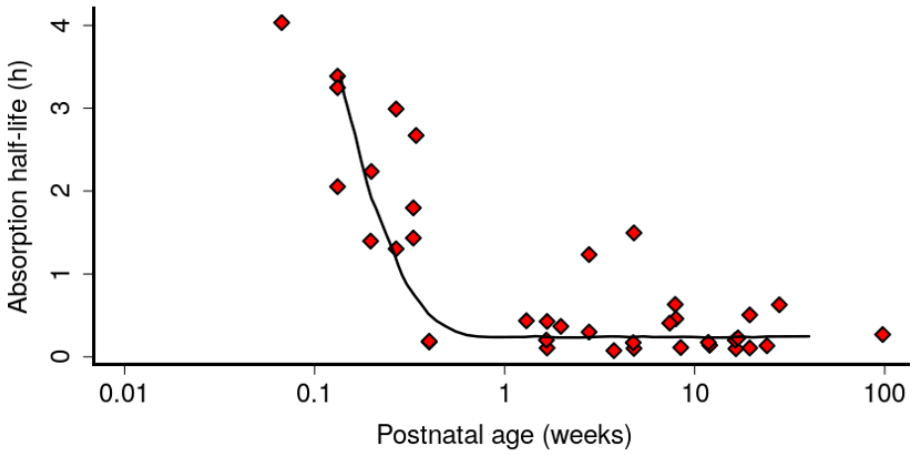

Figure 5: Age dependent GE affects on paracetamol absorption, recreated from Anderson et al 2002

However a meta analysis performed in 2015 evaluated data from 49 clinical studies (n=1457 subjects, pre-term neonates to adults) and concluded that age is not a significant covariate for GE, but instead reinforced the significance of food type (liquid vs solid, high vs low fat) in modulating GE[67]. Gastric volume is considered to be fairly comparable between adults and children when normalized per kg body weight, with a fasted gastric content volume of 0.25-0.56 mL/kg in children and 0.36-0.50 mL/kg in adults[56]. However, combined with developmental changes in GI fluid composition[68] and differing age dependent oral doses (mg/kg) solubility limitations may be different in different age groups[69].

In 2018 Johnson et al[70] published algorithms to describe paediatric age-specific salivary flow, gastric pH, gastric emptying (and associated food effects), duodenal bile salt concentrations, intestinal CYP3A4, P-glycoprotein (ABCB1/MDR1) and multi drug resistance-associated protein 2 (ABCC2/MRP2) expression. The model was tested using PK data for paracetamol, ketaconazole and theophylline collected in different age groups. Oral neonatal pharmacokinetics of paracetamol and theophylline (BCS I) and indomethacin and ibuprofen (BCS II) were also modelled by Somani *et. al.* who concluded that increasing absorption rates within the first few days after birth are a system-specific property, recommending their approach be used to guide oral dosing of BCS class I and BCS class II compounds in neonates[71].

Presystemic metabolism and drug transport

Drug absorption can be sensitive to the expression and activity of intestinal transporters. P-glycoprotein (ABCB1/MDR1/P-gp), multidrug resistance-associated protein 2 (ABCC2/MRP2) and breast cancer resistance protein (ABCG2/BCRP) are three of the most well characterised members of ATP-binding cassette (ABC) transporters family that are also functionally expressed in the human intestine. With intestinal expression often varying throughout the length of intestine as well as along the crypt-villous axis, see Figure 6[72,73].

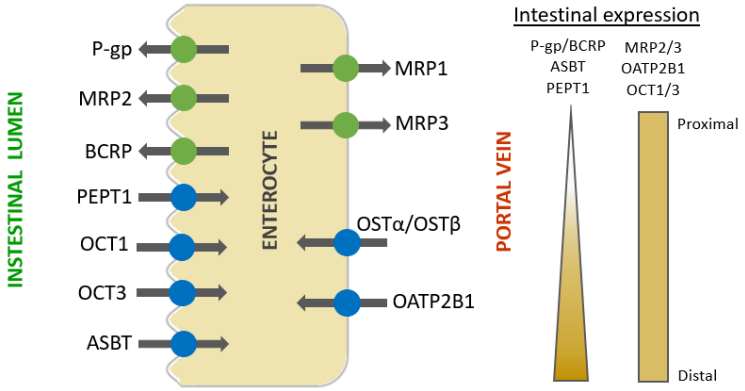

Figure 6: Schematic overview of intestinal drug transporters, recreated from Muller et al 2017

P-gp, MRP2, and BCRP are major efflux transporters found on the apical enterocyte membrane and are responsible for limiting drug absorption. Organic anion transporting polypeptide 2B1 (SLCO2B1/OATP2B1) and organic cation transporter 1 (SLC22A1/OCT1) have been suggested to participate in intestinal absorption (uptake), although there is still some uncertainty as to the apical or basolateral localisation of OATP2B1[74,75]. Peptide transporter 1 (SLC15A1/PEPT1) is another major uptake intestinal transporter that facilitates absorption of peptide-like drugs such as β-lactam antibiotics[76].

The majority of research into human transporter ontogeny has focused on understanding age related effects in renal and hepatic transporter expression and activity[77]. The limited studies into intestinal transporter ontogeny have mostly involved either analysis of mRNA expression levels or localization studies using immunohistochemistry[78–80] however age specific protein expression information in the intestine is still lacking. Of the intestinal transporter ontogeny literature reviewed OATP2B1 appears most noteworthy with evidence of significantly more expression in neonates compared to adults[81].

As well as transporters metabolising enzymes are expressed within enterocytes potentially reducing bioavailability due to pre-systemic metabolism[82,83]. Cytochrome P450 expression decreases down the intestine with the upper small intestine (duodenum and jejunum) serving as the major site for intestinal first pass extraction by CYP3A4[84]. CYP3A4/5 and CYP2C9 account for the majority of CYP expression in mature human small intestine, other less abundant isoforms include 1A1/2, 2C19, 2J2, and 2D6[85]. A study that quantified CYP3A4 expression in duodenal biopsies from 104 paediatric patients (age range 2 weeks to 17 years) concluded that duodenal CYP3A4 is present at significantly lower levels in neonates potentially having clinical significance with respect to the oral bioavailability of CYP3A4 substrates[86]. A study recently reported by Brussee *et. al.* supports this conclusion, having used a hybrid semi-physiological population PK model and oral plus IV pharmacokinetics from 37 pre term neonates to estimate separately Fg and Fh for midazolam. The extraction was found to be very low for both organs, with a median of 0.04 in the gut wall (range 0.026–0.046) and a similar median of 0.04 (range 0.01–0.31) in the liver. This combined with complete absorption resulted in 92% of midazolam (0.1 mg/kg via nasogastric tube) reaching the systemic circulation, a bioavailability significantly higher than seen in adults where median extraction ratios of 0.59 and 0.34 have been reported for the gut and liver respectively, resulting in a lower total bioavailability of around 30%[87].

Another important group of metabolising enzymes found in the intestine are the uridine diphospho-glucuronosyltransferase enzymes (UGTs) which mediate conjugation of glucuronic acid with exogenous and endogenous substances, such as bilirubin, to increase water solubility for elimination. Glucuronidation by UGTs form a major phase II biotransformation pathway and inter individual variability in UGT activity can be significant[88]. The most abundantly expressed UGTs in the mature small intestine are 2B7 (20%), 2B17 (19%), 1A10 (17%), 1A1 (13%), 1A6 (9%)[88]. UGT1A1 is a polymorphic enzyme for which functional variants have been linked to both hereditary disease (e.g. Crigler–Najjar and Gilbert Syndrome) and altered substrate pharmacology[89]. While there has been a significant amount of work published regarding the impact of UGT polymorphism[89–91], human intestinal ontogeny data is lacking.

Distribution

Growth during the first year of life[92] has a significant impact on a number of factors that determine a drug's volume of distribution, including tissue/organ size[93], tissue

composition (protein, lipid, water) and the abundance of plasma proteins (e.g. serum albumin (HSA) and alpha 1 acid-glycoprotein (AAG)). Infants have relatively more extracellular water than older children[94] and conversely lower percentage body fat[95], which can result in increased weight corrected volume of distribution for hydrophilic drugs compared to adults. Plasma protein levels are lower in neonates than in the adults, gradually increasing with age. The ratio of the protein concentrations also changes with age[96] as can the percent of drug binding[97]. These physiological or system parameters that contribute to understanding how tissue distribution and hence volume of distribution is likely to change with age have recently been extended to pre-term neonates and to describe the foetal period[98–100]. As with increased intestinal permeability in neonates, there are also reports of increased CNS penetration for small hydrophilic molecules such as meropenem[101], which may be indicative more broadly of greater tissue penetration due to increased paracellular permeation in neonatal epithelium.

Systemic metabolism and elimination

The liver is the major drug metabolism organ in the human body containing both Phase I and Phase II metabolising enzymes. Metabolism is possible in other major organs and even in the blood but typically these tissues play a less significant role in drug metabolism than the liver. The primary purpose of metabolism in the context of pharmacokinetics is the chemical conversion or breakdown of drugs such that they are more easily eliminated by the body through either biliary, intestinal secretion or renal elimination.

Only unbound/free drug is available to be metabolised, so as as described in section 1.3.1.3, for drugs that are highly plasma protein bound age dependent changes in the concentration and ratio of HSA and AAG also has a potential impact in the extent of metabolism seen in children. For example, the mean percentage of free (unbound) ciclosporin in plasma drops from 20% at birth to below 5% in adults due to increasing albumin concentration with age[102]. While both allometric and physiologically based methods aim to deal with the scaling of body and organ size it is also important to understand the metabolic pathways for an individual drug in order to make use of enzyme ontogeny and polymorphism data, which for the cytochrome P450 family is well characterised[103–107].

While ontogeny of intestinal glucuronidation is lacking, some age-related information on Phase II enzymes does exist for the liver[108]. One study compared foetal and adult UGT mRNA expression in liver and olfactory epithelium, finding that

UGT2B4 was by far the most abundant isoform in the foetal liver (90% of total) and that in olfactory epithelium high UGT2A1 and UGT2A2 expression in the foetus was replaced by high UGT1A6 expression in the adult[109]. Miyagi *et. al.* studied the development of UGT1A1 and 1A6 in 50 paediatric liver samples and found that UGT activity developed with age, while protein expression was not age-dependent and that maximal activity was achieved at 3.8 and 14 months for UGT1A1 and UGT1A6 respectively[110]. Interestingly, unlike UDP-glucuronosyltransferases and cytochrome P450 enzymes, cytosolic sulfotransferases SULT1A1 and SULT2A1 showed the highest abundance in human liver during early childhood (1 to <6 years), which gradually decreased by approx. 40% in adolescents and adults[111].

Teasing apart the factors contributing to a drugs F when the drug in question has never been dosed intravenously has an additional level of complexity since the true clearance of the drug is unknown. In such situations predicting a suitable paediatric dose becomes even more complicated and necessitates the use of cross species allometric scaling[112] and *in-vitro/in-vivo* extrapolation (IVIVE)[113,114] to make reasonable assumptions about human adult clearance prior to any paediatric scaling.

Renal Elimination

Renal clearance is achieved in the nephron, which comprises the glomerulus, proximal tubule, loop of Henle, distal tubule and collecting tubule. As blood carries drug molecules into the glomerulus, about 10% is filtered as plasma water into the renal tubule. The glomerulus contains relatively large, leaky pores that exclude cells, proteins and bound drugs, but allows unbound drug molecules to be filtered with water. In humans, the glomerular filtration rate (GFR) is about 120 mL/min.[115]

In the proximal tubule, drug molecules can also be actively secreted into the renal tubule by transporters such as the OATs (organic anion transporters), OCT2 (organic cation transporter 2), and P-gp. Alternatively some drug will be actively reabsorbed by uptake transporters; PEPT1/2, OCTN1/2 (organic cation/L-carnitine transporter 1 or 2), URAT1 (urate anion transporter 1).[116]

Drugs with good passive permeability will be passively reabsorbed along the renal tubules, as well as 99% of the water. Drug molecules and water that are not absorbed will enter into the collecting tubule, ureter and bladder for excretion. Renal clearance can be described according to Eq. (1)[117], where CLr is renal clearance, Fup is fraction unbound in plasma, CLr_{sec} is renal clearance due to active secretion, CLr_{reabs} is renal

reabsorption due to active and passive mechanisms.

$$\mathrm{CLr} = \mathrm{GFR} \times \mathrm{Fup} + \mathrm{CLr}_{\mathrm{sec}} - \mathrm{CLr}_{\mathrm{reabs}} \tag{1}$$

For compounds with good passive permeability, renal clearance is typically less than GFR×Fup, due to passive reabsorption[117], if however the compound has inherently poor passive permeability, then a CLr less than GFR×Fup is likely indicative of active (transporter mediated) renal reabsorption[116]. Conversely, a CLr > than GFR×Fup is indicative of active renal secretion.

The usefulness of plasma or serum creatinine measurements for the identification of renal insufficiency is often employed but made challenging by its covariates; sex, age, race, diet, and muscle mass. Moreover, the analytical quality of the quantitative test is often sub optimal, as with the non-specific Jaffe method used in most routine laboratories[118]. However in 2008 Ceriotti et al sought to define scientifically sound creatinine reference intervals via systematic review, and based on published literature defined a function to estimate a typical serum creatinine concentration (TSCR) based on age for white individuals[119].

$$\mathrm{TSCR}(\mu\mathrm{mol}) = 2.37330 - 12.91367 \times \ln_{(\mathrm{PNA}_{\mathrm{years}})} + 23.93581 \times (\mathrm{PNA}_{\mathrm{years}})^{0.5} \tag{2}$$

In 2009 Rhodin et.al[120] attempted to do something similar pooling published data to describe the increase in glomerular filtration rate (GFR) from very premature neonates to young adults. A nonlinear mixed effects approach was used to examine the influences of size and maturation on renal function. Size was the primary covariate, on GFR postmenstrual age (PMA) was found to be a better descriptor of maturational changes than postnatal age (PNA). A sigmoid hyperbolic model (Hill function) was used to describe the nonlinear relationship between GFR maturation and PMA, and depending on the how GFR was scaled for body size, the time to 50% maturation ranged from 48 to 55 weeks, and the Hill coefficient ranged from 3.3 to 3.4[120].

Renal function in the neonate undergoes significant changes over the course of days to weeks[121]. It is therefore important to evaluate CLr in neonates dynamically. The diuretic phase takes place within 2–3 days after birth, during which urine production is relatively high. This phase also coincides with the reduction in total body water and weight. By the 5th–7th postnatal day, renal function starts to stabilize and slowly progresses to ultimately reach the adult state[121].

While renal membrane transporters play key roles in the disposition of many drugs and endogenous substrates, their ontogeny is largely unknown. In 2019 Cheung *et.*

al.[77] analysed both mRNA and protein abundance of several renal transporters in postmortem frozen renal cortical tissues (preterm newborns to adults) and found that expression of P-gp, URAT1, OAT1, OAT3 and, OCT2 increased with age. The authors highlight the different rates and patterns of maturation exhibited by different renal transporters, and show that several are associated with slow maturation (incomplete maturation by the age of 2 years). Using OAT1 as an example, children older than 2 years of age (PNA $>$ 102 weeks) had highly variable expression levels, while the typical 2 year old (Hill function: TM_{50} = 19.71 [7.81, 36.95] weeks, Hill exponent = 0.43 [0.27, 0.61]) is predicted to only have 67% of adult protein abundance[77].

Allometric scaling:

In the allometric size adjustment approach, PK parameters, typically volume and clearance are related to the body weight (BW) of an individual via a power model, see below equation. Where P_i is the individual PK parameter of interest, and A is the y-axis intercept when BW and P_i are plotted on a log-log scale, and b the allometric exponent. Conceptually A represents P_i for an individual with the (theoretical) weight of 1 kg. It is common to express BW relative to a standard weight BW_s, typically either a 70-kg reference individual, or the mean or median weight of the study population. When bodyweight is standardised and its effects disentangled from age in this way, developmental/maturational changes can be understood more clearly; age-related versus size-related.

$$\mathrm{P_i} = \mathrm{A} \times (\mathrm{BW}/\mathrm{BW_s})^{\mathrm{b}} \tag{3}$$

Allometry is now such a well established approach for scaling PK parameters that often the exponent b is fixed, thereby allowing secondary covariate effects to be explored[122–126]. Although much debated it is generally believed that allometry means a fixed exponent of 0.75 for clearance and 1.0 for volume of distribution. This standardisation of the allometric exponent has significant advantages as it facilitates cross study comparisons and when Germovsek *et. al.* evaluated 18 allometrically based models for scaling paediatric clearance estimates, no significant evidence was found for the rejection of this standard exponent when used in conjunction with a sigmoidal maturation function[127].

Recently however the question of the exponent returned when Mahmood reported a comparative study designed to evaluate the accuracy of paediatric clearance predictions achieved through PBPK versus allometric methods[128]. Mahmood found that for

children <2 years old (n = 130), typically the most difficult to predict, PBPK and allometric models had 89% and 87% of observations within the 0.5- to 2-fold prediction error, respectively and concluded that the predictive power of PBPK and allometric models was essentially similar for the prediction of clearance or AUC in paediatric subjects ranging from neonates to adolescents. However, in the allometric scaling in this study Mahmood employed age-dependent exponents (ADEs), citing evidence for the under/over estimation of clearance in children <2 years old by use of a 0.75 allometric exponent when used in isolation[129]. The ADEs employed by Mahmood were not used in conjunction with a sigmoidal maturation function as proposed by Germovsek et al[127] and where b = 1.2, 1.1, 1.0, 0.9 and 0.75 in paediatric age groups; preterm, term neonates, age 0-3 months, >3 months to 2 years, >2-5 years and >5 years respectively[128].

The developing immune system

The human immune system is a highly complex multifaceted system of defences and can be broadly classified as comprising the innate, the adaptive and the complement systems. The complement cascade bridges the innate and adaptive immune systems working to enhance (complement) the ability of antibodies and phagocytic cells to clear microbes and damaged cells from the host, promote inflammation, and attack a pathogen's cell membrane by formation of the membrane attach complex.

Innate immunity is available right from the beginning of life and is particularly important in newborns and during invasive infections like sepsis and meningitis. Innate immunity describe the defences that target invading pathogens in a non-specific manner and can be categorised as either physical/mechanical, chemical, or cellular in nature. All of the formed components of blood are derived from pluripotent hematopoietic stem cells (HTCs) that are produced in the bone marrow. HTCs differentiate into different types of blood cell that, once mature circulate in peripheral blood and lymph. The main leukocytes of the innate immune system include neutrophils, basophils, eosinophils, mast cells and natural killer cells along with antigen presenting dendritic cells and macrophages. Phagocytes like monocytes and macrophages contain various catabolic and digestive enzymes and use toll-like receptors (TLRs) to recognise pathogen-associated molecular patterns (PAMPs) that are common to many groups of pathogenic microbes[130].

In contrast to innate defences the individually developed adaptive immune system is one that evolves over time in response to a variety of factors, it is pathogen specific

and has memory. T lymphocytes (T cells) and B lymphocytes (B cells) are the main cellular components of the adaptive immune system but their sites of maturation and roles in adaptive immunity are very different. T cells mature in the thymus and differentiate into various sub-types including T helper (Th or CD4+) cells and cytotoxic T lymphocytes (CTLs or CD8+) that are responsible for the destruction of cells infected with intracellular pathogens, a process referred to as cellular immunity. While naive B cells mature in the bone marrow and differentiate into antibody (immunoglobulins) producing plasma cells and memory B cells that importantly can respond rapidly to subsequent exposure to a given pathogen[130].

While genetic factors undoubtedly play a part, non-genetic factors are thought to play a dominant role in defining the composition of the immune system, with an individual's age, their environment, and previous chronic viral infections all key factors in human immune variation over time[131–133].

Van den Heuvel *et. al.* used flow cytometry (6-color) and linear mixed effect modelling to characterise the dynamics of 62 leukocyte subsets from birth to 6 years of age (n=1182 children). Hierarchical clustering of functionally similar leukocyte populations resulted in 4 distinct clusters of leukocyte dynamics. The non-genetic determinants affecting the innate leukocytes and naive memory lymphocyte dynamics were categorised into one of 4 groups: birth characteristics, prenatal maternal life style, maternal immune-mediated diseases and bacterial/viral exposure-related characteristics[132].

Pharmacokinetic modelling and simulation

Pharmacokinetic data and analysis methods

To ensure patients receive medication according to a dosing regimen that is both safe and effective, a quantitative understanding of the dose-response, or PK/PD relationship is required. This relationship is established using model-informed drug development to consolidate the PK and PD data collected during phase I-III clinical trials[134,135]. At a very high level MIDD refers to the application of quantitative clinical pharmacology models to inform decision making concerning clinical trial design and critically optimal dose selection in patient populations[136]. Understanding and describing a drugs pharmacokinetics is the first step in establishing a PKPD relationship.

Pharmacokinetics is often described as what the body does to a drug, it seeks to quantitatively describe the time course of the movement of drug into, around, and out of the body. Pharmacokinetic data routinely consists of drug concentration data, typically measured in plasma, and critically this concentration data must be supported by accurate information regarding the dose and PK sampling schedule; time between measuring a concentration in plasma and administration of the last dose. There are a number of different ways that PK data can be analysed and often the method employed will depend on the nature of the PK data available.

In Phase I clinical studies (healthy volunteer trials) PK data are often described as 'rich', meaning the time course is well characterised by a frequent PK sampling schedule, and 'balanced', meaning each subject provides the same number of samples at the same time. Paediatric PK data is almost always the exact opposite; 'sparse' and 'unbalanced'. There are a number of reasons for this, foremost is the fact that the Helsinki declaration precludes the use of healthy paediatric volunteers in paediatric clinical trials[137], and while PK sampling schedules are often designed to ensure precise PK parameter estimation is possible, for ethical reason the frequency of PK sampling is always minimised as far as possible. Figure 7 illustrates graphically the difference between rich/balanced and sparse/unbalance PK data.

When analysing rich/balanced PK data, non-compartmental analysis (NCA) is the preferred method of analysis. See Figure 7A for an illustration of rich/balanced PK data. NCA relies upon algebraic equations, including extrapolations, and linear or exponential relationships are assumed between adjacent time points. The results of an NCA are summary statistics that can be used to describe the drug's concentration-time profile, the most important of which include; area under the curve (AUC), max-

imum concentration (Cmax), time to maximum concentration (Tmax), the terminal rate constant (λ_z) and terminal half-life ($T_{1/2z}$).

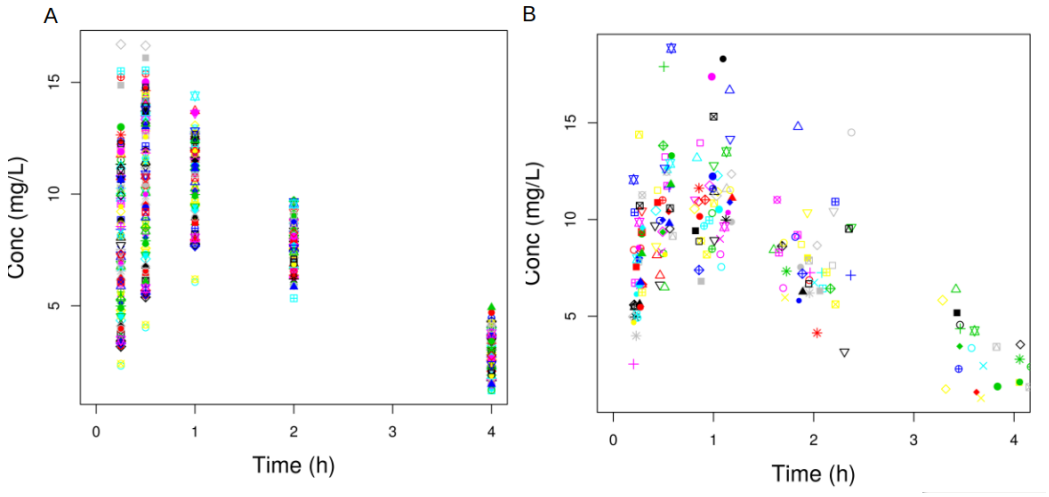

Figure 7: Hypothetical PK data A) Rich/Balanced (Phase I); all subjects contribute the same number of observations at the same timepoint and the PK profile is well characterised in all subjects. B) Sparse/Unbalanced (Phase II-IV and real-world data); the number of observations may differ across subjects as may the timing of the observations. In these hypothetical PK datasets colour and shape are used to represent observations from different subjects.

NCA calculates AUC using the trapezoidal method which involves calculating the individual areas between each adjacent observed concentration as if they formed a trapezoid. AUC_{last} is the total AUC from time zero (drug administration) to the last evaluated time point, calculated by summing the areas of all the trapezoids. AUC can be approximately extrapolated from time zero to infinity (AUC_{∞}), however, this is only reliable under certain conditions, including if AUC_{last} would compromise at least 80% of the calculated AUC_{∞}. The linear-log trapezoidal method often called "linear-up log-down" utilises the linear trapezoidal rule (Equation (4)) when concentrations are increasing (as in the absorption phase), and when concentrations are decreasing (as in the elimination phase), the logarithmic trapezoidal method (Equation (5)) is used. This method is thought to be the most "accurate" because the linear method is the best approximation of drug absorption, while drug elimination is best modeled using the logarithmic method[138].

$$\text{Linear AUC interval} = \frac{(\text{t2} - \text{t1}) \times (\text{c1} + \text{c2})}{2} \tag{4}$$

$$\text{Logarithmic AUC interval} = \frac{(\text{t2} - \text{t1}) \times (\text{c2} - \text{c1})}{\ln(\text{c2}/\text{c1})} \tag{5}$$

At some time point post administration, and at all time points thereafter, the concentration of a drug in the plasma will decline in a mono-exponential fashion. The portion of the plasma profile that shows this behavior is referred to as the terminal phase. The PK parameters that define this phase are the terminal rate constant (λ_z), and the terminal half-life ($T_{1/2z}$). The terminal rate constant can be calculated from the slope of a linear regression fit to the log-transformed late concentration-time data and this can subsequently be used to calculate the terminal half-life according to Equation (6).

$$\text{T}_{1/2\text{z}} = \frac{\ln(2)}{\lambda_\text{z}} = \frac{0.693}{\lambda_\text{z}} \tag{6}$$

It is not uncommon for λ_z to be referred to as the terminal elimination rate constant; K_{el}, and $T_{1/2z}$ as the terminal elimination phase half-life, this is however misleading as the kinetics of the terminal phase usually depends on concurrent drug elimination and drug distribution/redistribution. Indeed, a slow rate of drug redistribution can sometimes be the major determinant of terminal phase kinetics. Additionally, for some drugs, the terminal phase kinetics reflect not the elimination, or redistribution rate, but rather a slow rate of uptake from an extravascular site of drug administration, for example the rate of absorption through the gastrointestinal tract following oral administration, a phenomenon typically referred to as 'flip-flop' or 'absorption rate limited elimination'[139,140]. When a drug exhibits only mono-exponential decline or first order elimination, the rate of elimination following intravenous dosing, where A is the amount of drug in the body, is given by[115];

$$\text{Rate of Elimination} = -\frac{\text{dA}}{\text{dt}} = \text{K}_\text{el} \cdot \text{A} \tag{7}$$

Which on integration allows the amount of drug in the body (A) at any given time can be calculated according to[115]:

$$\text{A} = \text{A}(0) \cdot \text{e}^{-\text{K}_\text{el} \cdot \text{t}} \tag{8}$$

With an estimate of λ_z determined from intravenous PK data, further important PK parameters can be calculated, the two most noteworthy are the systemic or total clearance (CL) and the (apparent) volume of distribution (V). Clearance is the volume of plasma effectively cleared of drug per unit time and along with the drug concentration (C) determines the rate of elimination from the body. The volume of

distribution is the volume of plasma at the drug concentration (C) that is required to account for the entire amount of drug in the body (A). If the PK data under analysis is collected following extra-vascular dosing then the equations presented below (Equations (9)) derive CL/F and V/F where F represents oral bioavailability[115].

$$\mathrm{CL} = \frac{\mathrm{dose}}{\mathrm{AUC}_\infty} \quad \text{and} \quad \mathrm{V} = \frac{\mathrm{A}}{\mathrm{C}} = \frac{\mathrm{dose}}{\lambda_\mathrm{z} \times \mathrm{AUC}_\infty} = \frac{\mathrm{CL}}{\lambda_\mathrm{z}} \tag{9}$$

After repeat dosing concentrations in the body will accumulate until steady state has been reached. Steady state is achieved when the rate of drug input to the body is equal to the rate of drug elimination. The time to reach steady state is dependent on the elimination half-life of the drug, five half-lives is generally considered a reasonable estimation of the time to reach steady state. The extent to which concentrations will accumulate on repeat dosing is dependent on two things, the dosing interval (τ) and the elimination rate constant (K_{el} or λ_z) Assuming the absence of both concentration and time dependent non-linearity once steady state has been reached the AUC for a given dosing interval (AUC_τ) will equal the $AUC_{0-\infty}$ after a single dose[138].

Sometimes however NCA is either not feasible or there is a need to take a model based approach to the PK data analysis. Fitting a compartmental model or non-linear regression model to PK data can be advantageous for a number of reasons. Importantly it enables a continuous description of the PK profile, in certain cases this can give a more accurate estimation of important features such as Cmax, Tmax and AUC, and by accounting for the whole concentration-time course, a compartmental PK model, such as the simple first order absorption and elimination model presented in Figure 8, can allow a more dynamic relationship to be constructed between changing drug concentration in the body and a subsequent pharmacodynamic effect, be that toxic or beneficial.

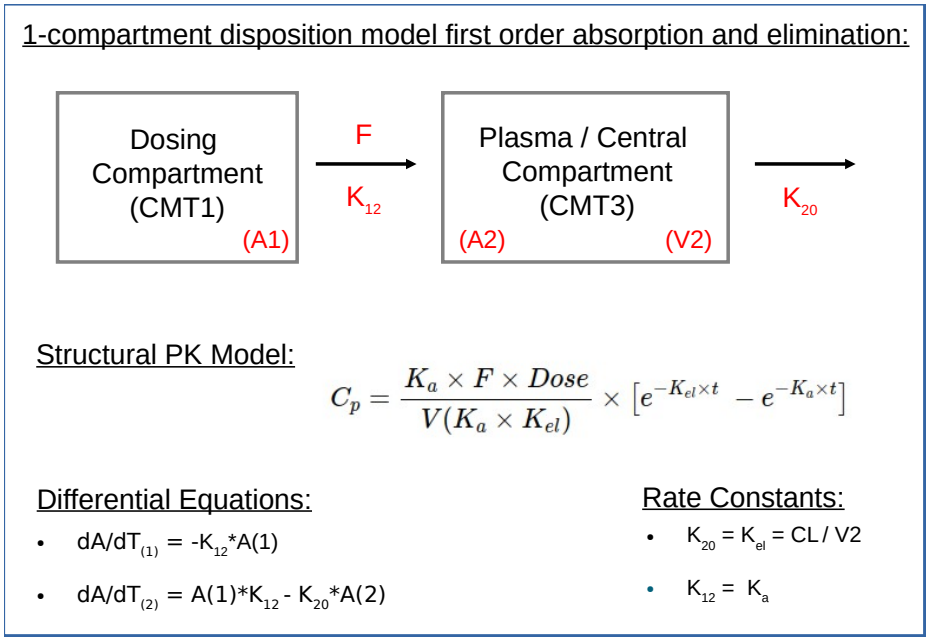

Figure 8: Example of a simple PK model; 1-compartment disposition model with first order absorption and elimination. Ka; absorption rate constant. Kel; elimination rate constant. Cp; concentration in plasma. F; bioavailability. CL; clearance. V; volume. A; amount of drug.

Figure 9 illustrates the difference between estimating AUC_∞ after a single dose by NCA versus using regression analysis and fitting a compartmental PK model such as that described in Figure 8[141,142]. Compartmental PK models typically utilise, 1, 2 or 3 compartments to describe absorption from an extra-vascular space, distribution within and elimination from the body, and can be written as a series of ordinary differential equations (ODE's).

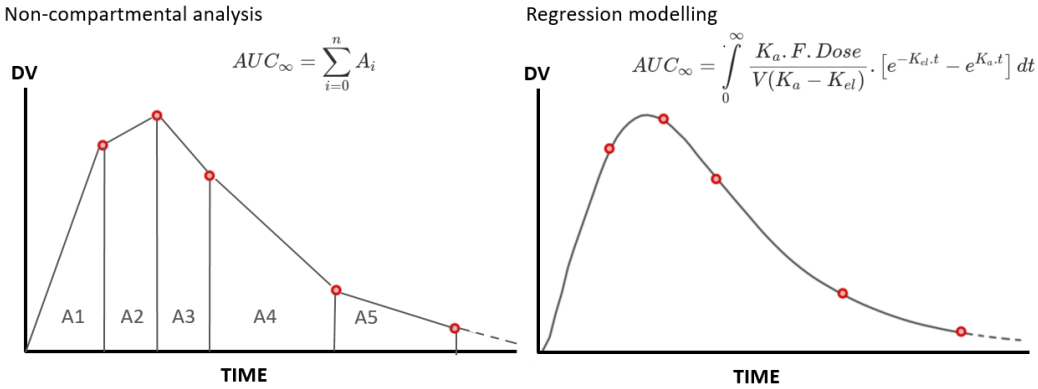

Figure 9: Non-compartmental versus regression analysis, recreated from Gabrielsson et al 1997

The number of distributional compartments, or structural model complexity is

driven by the available data. Regression analysis is used to estimate model parameters using statistical methods such as ordinary least squares (OLS) regression or maximum likelihood estimation (MLE). The OLS method minimizes the square of the residuals between the observed and model predicted plasma concentration-time (Cp-time) data, while the MLE method maximizes the probability of observing the dataset given a model and its parameters. The structure of a PK model is very importantly informed by biological "prior" information on the system that generated the data and therefore typically follows a specific structural form based on the multi-compartment mammillary system characterised by means of a number of peripheral compartments which are connected to a single central compartment. Input and irreversible loss of drug is generally assumed to occur only from the central compartment[142,143].

When compartmental PK modelling, or non-linear regression modelling, is performed at an individual subject level and population estimates are subsequently obtained by calculating the geometric mean and geometric variance of a given PK parameters, it is called the two-stage (TS) approach. An important assumption here is that the responses are independent, even within the same subject. Population parameters calculated in this way can be biased, especially when the number of subjects is large[144,145].

Other approaches to summarising the average trend of a PK profile in a given population or for a given formulation include the naive pooled (NP) and naive average (NA) approach. However these are more problematic. In the NP method, all PK data is analysed as if it has come from a single subject. This method ignores that data came from individuals with inter-individual variability and can result in biased estimates[145].

In the NA method the average drug concentration at any given timepoint is calculated and the average value at is used to construct a 'average' concentration time profile and PK parameters estimated using the 'average' concentration time profile. This is a popular but crude approach because it too does not consider between subject variability and is only ever suitable for a balanced study design[2,145].

Consider however the scenario that arises in paediatrics; sparse unbalanced PK data (differing number of observations, j (j = 1, ...) across individuals, i (i = 1,....) most likely taken at different time points, in a relatively limited number of subjects. In such scenarios 'mixed effect' (ME) modelling is preferable. With ME modelling data is fitted simultaneously, but model parameters are allowed to differ between subjects. Population pharmacokinetic (PopPK) modelling, as it has become known, has become standard practice during drug development and provides unbiased pharmacokinetic estimates through simultaneous determination of between subject variability at the

parameter level, and observation level residual variability.

Mixed effect / population PK modelling

Non-linear mixed effect (NLME) modelling became a main stay of quantitative clinical pharmacology, or pharmacometrics thanks to Lewis Sheiner and Stuart Beal who started publishing on the benefits of their software NONMEM for population PK parameter estimation over 50 years ago[146].

Mixed effects models are often used in the analysis of longitudinal data comprised of multiple measurements from within the same subject over time. Data (the dependent variables) may be unevenly spaced, with a different number of observations in each subject, it is also possible to deal with time varying covariates like age, weight and serum creatinine. The incorporation of subject specific characteristics in this way make mixed effect models far more versatile than fixed effect models[144].

Because a mixed effect, also referred to as a pharmacometric or population PK model comprises both a mathematical and statistical model, it enables the determinants of PK variability to be quantified. A population PK model is able to relate subject-specific covariates (for example; age, weight, sex) to individual pharmacokinetic parameters, such as bioavailability or clearance and thereby reduce unexplained (residual) variability. To do this pharmacometric or population PK models estimate two types of parameters: fixed-effects and random-effects, hence 'mixed-effects'. Fixed-effects, are structural PK model parameters, e.g clearance, volume, bioavailability and they take a single value that represents the population typical value. Random-effects also take a single value for the whole population, but represent the variance of a distribution of some element of the model.

For example Figure 10 presents some hypothetical IV concentration–time profiles collected in a population that includes young and elderly patients, however the dose administered is the same irrespective of age and the resulting plasma concentrations show two separate groups, see Figure 10A and Figure 10B. By incorporating age into a population PK model the between subject variability in clearance (and thus AUC) is reduced, see Figure 10c. In this hypothetical scenario, adjusting dose based on whether the patient is 'young' or 'elderly' would result in more consistent exposure within each group[147].

In NONMEM, linearisation of the model in the random effects is typically effected using the first-order (FO) Taylor series expansion with respect to the random effect variables η_i (inter-subject variability) and ε_{ij} (residual variability). The jth obser-

vation in the ith individual of the population (y_{ij}) can be described by the random effects (η_i and ε_{ij}), a vector of fixed effects or model parameters (φ) and individual covariates (x_{ij}) for example, time, dose or subject weight. In the context of a population *PK* model, 'model parameters' (φ) refers to the structural PK model parameters, for example; clearance, volume, and bioavailability[145,148].

$$\mathrm{y_{ij}} = \mathrm{f}(\varphi, \mathrm{x_{ij}}, \eta_\mathrm{i}) + \varepsilon_\mathrm{ij} \tag{10}$$

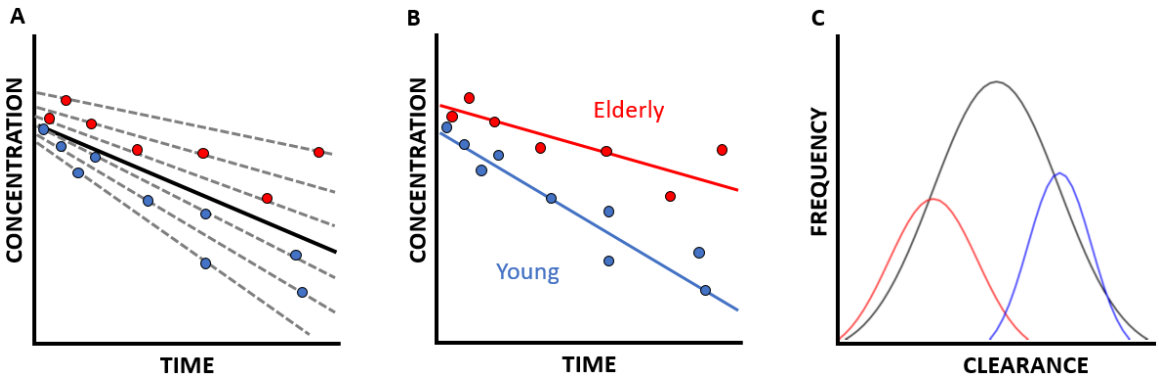

Figure 10: The impact of PK variability in special populations, recreated from Mould et al 2012. This figure illustrates that model estimated variability in clearance within this hypothetical population can be reduced by accounting for age as a catagorical covariate; elderly (red observations) v's young (blue observations), in a mixed effect or population PK model.

Figure 11 illustrates the mathematical (structural compartmental PK model) and statistical components of a one compartment intravenous mixed effect/population PK model, for simplicity only observed data from two subjects are shown.

In Figure 11 y_{ij} are individual plasma concentrations (observations, dependent variable) from the ith subject at the jth time and x_{ij} is a vector of known quantities (eg, dose, time, subject covariates). φ_{ip} is the vector of model parameters (fixed effects) for the ith individual. Post model expansion pharmacokinetic model parameters; φ are typically denoted as θ. It follows that individual parameter estimates φ_{ip} are related to the population parameter estimate μ_p by the random effects; η_{ip}, the departure of subject i from the population average and the residual (unexplained) error; ε_{ij}. The random effect parameters η_{ip} and ε_{ij} are assumed to be independent (multivariate) and normally distributed with zero means and variances of ω^2 and σ^2 respectively.

Structural PK Model

$$C_{pred,i} = C_0 e^{K_{el} t_i}$$
$$ln\, C_{pred,i} = ln\, C_0 - K_{el} t_i$$

Statistical Model

$$y_{ij} = f(\varphi, x_{ij}, \eta_i) + \varepsilon_{ij}$$
$$\varphi_{ip} = \mu_p + \eta_{ip}$$
$$\eta_{ip} \sim D(0, \omega_p^2)$$
$$\epsilon_{ij} \sim N(0, \sigma^2)$$

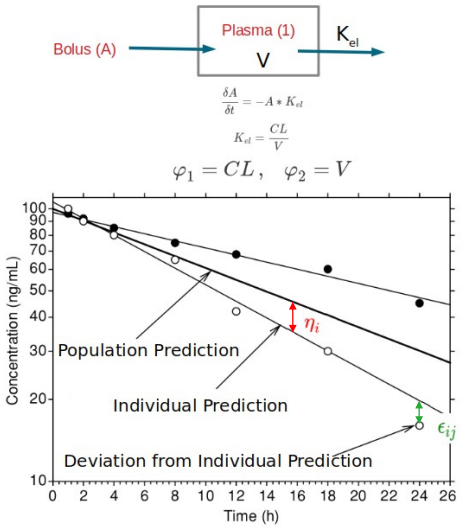

Figure 11: Schematic of a one compartment IV mixed effect/population PK model. Observed concentration-time data are shown as circles, model predicted concentration-time profiles are shown as solid black lines. Fixed effects, such as clearance (CL) and volume (V) are defined by the mathematical/structural PK model, are estimated using regression analysis and produce a population/typical concentration-time profile. Inter-subject variability is a random effect that is estimated using the statistical model and accounts for variability in the population estimated fixed effects, thereby enabling description of individual subject concentration-time profiles. The remaining residual/unexplained variability accounts for the deviation of an individual observation from an individual predicted concentration-time profile.

In summary a population PK model estimates structural model parameters (fixed effects) at the population level, variance of the population parameters between individuals, often referred to as the inter-individual variability (IIV) or between subject variability (BSV), and a variance describing the residual unexplained variability (RUV).

Because pharmacokinetic data are often modeled assuming log-normal distributions (parameters must be positive and are often right-skewed), the clearance (CL) of the ith subject (CL_i) and volume (V) of the ith subject (V_i) would be written as:

$$\mathrm{CL_i} = \theta_1 \ + \ \mathrm{e}^{\,\eta_{1i}} \tag{11}$$

$$\mathrm{V_i} = \theta_2 \ + \ \mathrm{e}^{\,\eta_{2i}} \tag{12}$$

Where θ_1 and θ_2 are the population CL and V estimate, and η_{1i} and η_{2i} are the

deviation from the population values (θ_1 and θ_2) for the ith subject. The log-normal function is a transformation of the distribution of η values, such that the distribution of CL_i values may be log-normally distributed but the distribution of η_{1i} values is normal. When parameters are treated as arising from a log-normal distribution, the variance estimate (ω^2) is the variance in the log-domain, which does not have the same magnitude as the θ values. For small values of (ω^2) (e.g., <30%) the coefficient of variation (CV) can be approximated as the square root of (ω^2)[140].

Three common RUV models include additive error (Eq. (13)), proportional error (Eq. (14)), and the combined additive and proportional error model (Eq. (15)), where the observed concentration (y_{ij}) for the ith subject at the jth time point can be written. Here $\hat{y}_{ij}$ is the subject and time specific predicted concentration and ε_{ij} is the error, which like BSV is estimated as a variance.[140,149].

$$\mathrm{y_{ij}} = \hat{\mathrm{y}}_{\mathrm{ij}} + \varepsilon_{\mathrm{ij}} \tag{13}$$

$$\mathrm{y_{ij}} = \hat{\mathrm{y}}_{\mathrm{ij}} \times (1 + \varepsilon_{\mathrm{ij}}) \tag{14}$$

$$\mathrm{y_{ij}} = \hat{\mathrm{y}}_{\mathrm{ij}} \times (1 + \varepsilon_{1\mathrm{ij}}) + \varepsilon_{2\mathrm{ij}} \tag{15}$$

Evaluating how well a model describes an observed dataset is crucial during model development. Typically employed diagnostics include:

1. Visual goodness of fit plots such as; DV (dependant variable) versus PRED (population prediction), DV versus iPRED (individual prediction), CWRES (conditional weighted residual) versus time and IWRES (individual weighted residual) versus IPRED[150].

2. Diagnostics such as the 'Visual Predictive Check (VPC)' involve simulating from the model parameters and plotting the 95% prediction interval (calculated from the simulations) around the 2.5th, 50th and 97.5th percentiles of the observe data[151].

3. Bootstrapping. In performing a bootstrap analysis, the study population is randomly sampled with replacement to create multiple new populations and then model parameters are re-estimated for each 'new' population. The bootstrap results allow confidence intervals for each parameter to be calculated and thereby tests the robustness of population parameter estimates to the dataset/influential individuals.

4. Minimisation of the -2 log likelihood function (-2LL), which in NONMEM is re-

ferred to as the objective function value (OFV) and is equivalent to maximising the likelihood (L).

If Y is the measured observation, $\hat{Y}$ the prediction of that observation by the model, and σ^2 is the variance of the model, then the likelihood (probability) of the observation given the model is:

$$L = \frac{1}{\sqrt{2\pi\sigma^2}} exp\left(\frac{(Y_i - \hat{Y}_i)^2}{2\sigma^2}\right)$$

If there are n observations, the probability is the product of all the individual probabilities:

$$L = \prod_{i=1}^{n} \frac{1}{\sqrt{2\pi\sigma_i^2}} exp\left(\frac{(Y_i - \hat{Y}_i)^2}{2\sigma_i^2}\right)$$

Then taking logs and dividing through by -2 the equation for the likelihood is transformed into the -2 log likelihood (-2LL). The second part of the equation below is sometimes referred to as the "extended least squares" objective function.

$$-2\ log(L) = n\ log(2\pi) + \sum_{i=1}^{n}\left(log(\sigma_i^2) + \frac{(Y_i - \hat{Y}_i)^2}{\sigma_i^2}\right)$$

If comparing two nested models, the significance of parameters which differ between the two models can be tested by using the likelihood ratio (L_1/L_2). The distribution of -2 log of the likelihood ratio, or the difference between the -2LL values follows a χ^2 distribution, where the degrees of freedom are the difference in the number of parameters. Thus, if the difference in the -2LL values (or ΔOFV) between 2 nested models that differ by only 1 parameter exceeds 3.84, then the additional parameter is significant at $p < 0.05$, if ΔOFV is > 6.64 then the additional parameter is significant at $p < 0.01$.

Physiologically based (PB) PK modelling

Physiologically based PK (PBPK) models attempt to marry the complex interplay of physiological parameters; demographics, organ size/composition, enzyme/transporter expression, and blood flows with drug-related properties that importantly, can be measured in vitro; pKa, pH dependent aqueous (aq) solubility, lipid solubility, enzyme and transporter kinetics, permeability, plasma protein binding etc. and thus represent a mechanistic approach to predicting the PK of specific drugs in different populations[152,153].

Built up through a series of ODEs that bring together the different ADME processes PBPK is typically used to predict an 'average/typical' PK profile, and any subsequent population simulations are achieved through Monte-Carlo sampling of user defined parameter distributions, which may (or may not) be related by a covariance matrix[154–156].

Importantly PBPK methods offer the opportunity to perform 'bottom-up' PK predictions based on pre-clinical and *in-vitro* data prior to there being clinical PK data available in humans or a given special population; elderly, paediatric, renal impairment etc. This is an important differentiator to PopPK/NLME models, where models while still informed by prior information are fitted to observed clinical PK data[157,158].

While PopPK has been an integral part of drug development and pharmacometrics for probably the last 40 years, PBPK has been adopted by pharmaceutical companies and drug regulatory agencies more recently[159], and since 2018 both the US FDA and European Medicines Agency (EMEA) have finalised industry guidance on PBPK[160,161].

Key milestones in the evolution of PBPK as a branch of pharmaceutical MBDD (model-based drug development) include the publication of the compartmental absorption and transit (CAT) model in the late 90's[162,163] quickly followed by the advanced CAT (ACAT) model[164] for predicting the impact of physiological and biochemical processes on oral drug bioavailability.

Experimentally effective jejunal permeability (Peff) in humans is calculated by measuring the rate of disappearance of a drug from a section of the GI tract at steady state[165,166]. The calculations involved in the estimation of Peff and the absorption rate coefficient (ka) are shown below, where Q is the volumetric flow rate, Cin and Cout are the concentrations at the input and output ports, and R and L are the radius and length of the perfused section (always taken as 1.75 cm radius and 10 cm length in these experiments)[167], and α is the surface area to volume ratio.

$$Peff = \frac{Q(C_{in} - C_{out})}{2\pi \cdot R \cdot L \cdot C_{out}}$$

Since;

$$Concentration\ (C) = \frac{Mass\ (M)}{Volume\ (V)}$$

and;

$$\alpha = \frac{cylinder\ surface\ area}{cylinder\ volume} = \frac{2\pi \cdot R \cdot L}{\pi \cdot R^2 \cdot L} = \frac{2}{R}$$

then;

$$\frac{dM}{dt} = Peff \cdot alpha \cdot M \qquad and \qquad Absorption\ Rate\ (ka) = Peff \cdot \alpha$$

At the same time as the ACAT model was being developed other research groups were exploring how to predict tissue-plasma partition coefficients from physico-chemical properties[168–171]. Then in 1998 the first graphical user interface (GUI) based PBPK platform GastroPlus was released by Simulations Plus and early publications on its utility began emerging[172].

Within GastroPlus to try and account for some of the factors that contribute to regional differences in passive transcellular permeability along the GIT, compartment-dependent absorption rate coefficients ($ka_i{}'$) are implemented within the ACAT model[164]. Consideration of the regional differences in surface area (A) due to the density of villi and microvilli are incorporated through surface area enhancement factors (SEFs). Where;

$$A = \frac{2}{R \cdot SEF}$$

Changes in passive transcellular permeability due to changes in a drugs ionisation state (resulting from pH differences along the GIT) are incorporated through four fitted constants: C1- C4, where ASF_{SI} and ASF_{LI} are absorption scale factors (ASFs) related to the regions of the small and large intestine respectively;

$$ASF_{SI} = A \cdot C2 \cdot 10^{\left(C1\left(\frac{\Delta logD_{ph}-C}{\Delta logD_{6.5}-C}\right)\right)} \quad , \quad ASF_{LI} = A \cdot C3 \cdot 10^{C4 \cdot logD}$$

Finally in the absence of intestinal transporters and paracellular absorption, passive absorption into the enterocyte sub-compartments from each luminal compart-ment is then predicted employing the compartment dependant absorption rate coeffi-cient $k_a(i)$

$$\frac{dM(i)_{absorbed}}{dt} = ka_i'(i) \cdot V(i)\left(C_{lumen}(i) - C_{ent,u}(i)\right) \quad , where \quad ka_i' = Peff\ .\ ASF(i)$$

In parallel to the emergence of GastroPlus as a commercially available PBPK platform, pharmaceutical companies were developing their own in-house PBPK software, examples include Gi-Sim by AstraZeneca and PK-Sim by Bayer. The Bayer platform has since gone on to be released as an OpenSource platform[173]. In 2000, the University of Sheffield and several pharmaceutical companies formed a global consortium with the specific aim of producing an automated platform for IVIVE (*in-vitro/in-vivo* extrapolation) in virtual populations to aid the prediction of metabolic drug-drug interactions[174], the resulting platform SimCYP was later acquired by Certara in 2012.

Regarding the differences in functionality, between the main commercially available PBPK platforms; SimCYP and GastroPlus, these are diminishing with each new version of the software as each developer (Certara and Simulations Plus respectively) seeks to incorporate functionality historically considered to be the specialist area of the other[175,176]. When the Innovative Medicines Initiative (IMI) Oral Biopharmaceutics Tools (OrBiTo) project evaluated the predictive performance of three PBPK software packages (GI-Sim (ver.4.1), Simcyp® Simulator (ver.15.0.86.0), and GastroPlus™ (ver.9.0.00xx)) they used data for 58 active pharmaceutical ingredients (APIs) and predicted clinical PK for over 200 studies, and found the average predictive performance did not clearly differ between software packages[177].

Paediatric PBPK models can account for the rapid development of organs and the ontogeny of specific enzymes and transporters, key determinants of age-related PK. In 2006 Johnson et al reported on PBPK based prediction of clearance in neonates, infants, and children for 11 compounds eliminated primarily through Phase I metabolism (CYP mediated) and/or passive renal filtration[114]. In 2016 Upreti performed a meta analysis of hepatic cytochrome P450 ontogeny and described the development of ontogeny functions for all the major hepatic CYPs based on in vitro or in vivo data[178]. Subsequently studies have incorporated ontogeny information on liver uptake transporters (OCT1) and Phase II metabolism (UGT2B7) to enable prediction of age dependent increases in morphine clearance[179]. And more recently the physiological descriptors required for PBPK modelling have now even been extended to cover pre-term neonates[98] and these descriptors evaluated against pre term PK data for alfentanil, midazolam, caffeine, ibuprofen, gentamicin and vancomycin[180]. Brussee also evaluated pre-term neonatal midazolam PK, finding that the highly variable and high total oral bioavailability of 92.1% (range, 67–95%) in pre term neonates, (30% in adults) is explained by, likely age-related, low CYP3A activity in the liver and even lower CYP3A activity in the gut wall[87].

In a review of the utility of PBPK in paediatric dose selection Templeton *et al* concluded that PBPK modelling will become a highly valuable tool for the prediction of paediatric dosing regimens[181], with the evidence now considered by some to be so strong that PBPK modelling in the *clinical* setting has been suggested by van der Heijden *et. al.* as a pragmatic solution to the challenge of low-evidence-based off-label paediatric dosing[182].

However parameter non-identifiability can be a challenge when it comes to establishing confidence in PBPK models. When scientifically well-founded, the mechanistic basis of physiologically based pharmacokinetic (PBPK) models can help reduce the uncertainty and increase confidence in extrapolations outside the studied scenarios or studied populations. However, it is not always possible to establish mechanistically credible PBPK models, and when this cannot be established, Peters *et. al.* advocate for the use of simpler models or evidence-based approaches[183].

PhD project aims

Chapter 1

Fosfomycin PK data in neonates is extremely limited. No previous study has analysed oral fosfomycin PK data from neonates and flip-flop kinetics have previously been described following oral fosfomycin dosing in adults. Chapter 1 analysed the intravenous and oral fosfomycin plasma and CSF PK data collected as part of the the NeoFosfo clinical trial[184].

The aim of this chapter was to use the crossover IV and oral PK data collected as part of the NeoFosfo trial and apply model-based estimation methods to determine the oral bioavailability of fosfomycin in neonates, consequently allowing a comparison of fosfomycin bioavailability in neonates and adults. The resulting population PK model was also used to simulate oral and IV neonatal dosing regimens in the context of neonatal sepsis.

Chapter 2

The aim of this study was to use population and physiologically based PK modelling methods to develop and test a mechanistic hypothesis for previously reported age-dependent changes in benznidazole oral bioavailability[185]. This chapter comprised four main aims. Firstly the affect of age on oral bioavailability was quantified using conventional allometric approaches, thereby enabling delineation of age effects. Secondly, based on a platform of evidence, initial benznidazole PBPK parameter estimates and modelling strategy were defined. Thirdly an adult PBPK model was be developed and verified. Finally the adult PBPK model was extrapolated to enable simulation of oral paediatric PK.

Chapter 3

In the final chapter the aim was to perform a population PK analysis of real-world posaconazole TDM data from hospitalized children receiving both intravenous and oral (suspension and tablet) posaconazole. While previous studies have reported pediatric posaconazole PK data, or modelled oral paediatric PK data in isolation, simultaneous model-based analysis of intravenous, suspension, and tablet data to enable estimation of formulation-dependent bioavailability in children has never been previously reported.

Chapter 1

Fosfomycin - oral bioavailability in neonates

1.1 Introduction

Antimicrobial resistance is a global health priority[186]. Due to their immature immune systems, young children are a population particularly vulnerable to bacterial infectious diseases. Sepsis disproportionately affects neonates and mortality rates are highest in low-middle income countries (LMICs). In 2013 infection accounted for 1/4 of all neonatal deaths globally[187] and in Asia and Africa 50-88% of clinical isolates were reported as resistant to WHO first line antibiotics ampicillin and gentamicin[188,189]. The situation continues to deteriorate and in 2021 the BARNARDS group reported that out of 390 Gram -ve isolates, 97% were resistant to ampicillin and 70% to gentamicin. Such wide spread resistance to first-line antibiotics means there is an urgent need for alternative treatment regimens for Gram –ve sepsis[190].

Fosfomycin an affordable and effective antibiotic has emerged as one potential solution[191,192]. It has recently been shown that community acquired Gram-negative bacteraemia isolates are significantly more likely (96% vs 59%, p <0.0001) to be susceptible to fosfomycin than empirical ampicillin/gentamicin therapy[193]. Therefore, used in combination with another appropriate antibiotic, fosfomycin may present an alternative treatment strategy for empirical management of hospital- or community-acquired multi-drug resistant (MDR) Gram-negative sepsis in neonates. However, optimal fosfomycin dosing in neonates is currently uncertain, including whether oral (PO) therapy is feasible[192]. The limited neonatal PK studies that have been published are mostly 30 to 40 years old,[194–197] small studies (n~10 babies) that only evaluated intravenous (IV) fosfomycin PK. Oral fosfomycin PK and consequently bioavailability (F) has never previously been reported for a neonatal population. Predicting neona-tal oral PK is challenging since in adults F depends on the fosfomycin salt form and physiological gastrointestinal conditions[198,199]. Finally, neonates suffering from sep-sis, may also have bacterial meningitis, so evaluating the extent of fosfomycin CNS penetration is highly desirable.

In adults 85-95% of a fosfomycin dose is excreted unchanged in the urine[200] with clearance similar to glomerular filtration rate, the volume of distribution is 0.42 L/Kg, half-life 2.4-2.8 hours and bioavailability is 0.53 for a 3 g dose of the tromethamine salt, a regimen that sees plasma levels sustained >1 μg/mL for 48 hours due to absorption rate limited elimination[201]. In fact the average plasma concentration at 24 hours (C_{24}) after the 3 gram oral dose was almost 2-fold higher than after a 8 gram intravenous dose (1-hour infusion). Others have also confirmed flip-flop kinetics are a feature of fosfomycin's pharmacokinetics[202]. Because of fosfomycin's low molecular mass and

despite its hydrophilicity, it enters the central nervous system (CNS) regardless of meningeal inflammation[203],[204].

In this chapter plasma and cerebrospinal fluid (CSF) pharmacokinetic data from neonates with suspected clinical sepsis was analysed using the population approach.

1.2 Aims and objectives

Fosfomycin PK data in neonates is extremely limited. No previous study has analysed oral fosfomycin PK data from neonates and flip-flop kinetics have previously been described following oral fosfomycin dosing in adults. This chapter analyses the intravenous and oral fosfomycin plasma and CSF PK data collected as part of the the NeoFosfo clinical trial[184].

The overall aim of this study was to use the crossover IV and oral PK data collected as part of the NeoFosfo clinical trial and apply model-based estimation methods to determine the oral bioavailability of fosfomycin in neonates, thereby allowing a comparison of fosfomycin bioavailability in neonates and adults. The resulting population PK model was then used to simulate oral and IV neonatal dosing regimens in the context of neonatal sepsis. Specific study objectives included:

1. Study design: Generate summary statistics describing the Neofosfo neonatal PK population and compare to the much larger neonatal sepsis population studied as in the NeoAMR[205] study.
2. Pharmacokinetic data: Visualise the fosfomycin plasma and CSF concentration data collected during the Neofosfo trial.
3. PopPK Model Development: Clean the source (bioanalytical, biochemical, dose and demographic) data and prepare a NONMEM ready datafile. Select the structural and statistical model. Incorporate significant covariate effects and extend the model to describe CSF concentrations in addition to plasma concentrations.
4. The final PopPK model: Review the model parameter estimates, covariate effects and visual diagnostics, including goodness of fit (GOF)[150] plots and visual predictive checks (VPCs)[151].
5. Neonatal PK simulations: Create a hypothetical neonatal population for use in PK simulation and apply the final model to simulate oral and IV neonatal dosing regimens in the context of neonatal sepsis considering relevant PD targets.

1.3 Methods

1.3.1 Study design and neonatal population

The NeoFosfo study (www.ClinicalTrials.gov: NCT03453177[206]) ran between March 2018 and March 2019 at Kilifi County Hospital in Kenya. Neonates aged 0 to 28 days old, weighing > 1500g, born at >34 weeks' gestation (using Ballard Maturational Assessment), with at least one sign of clinical sepsis and eligible to receive IV antibiotics (according to national guidelines) were included. The protocol was approved by the KEMRI Scientific and Ethical Review Unit (KEMRI/SERU/CGMRC/097/3513), Kenya Pharmacy and Poisons Board (PPB/ECCT/17/10/01/2017(200)) and Oxford Tropical Research Ethics Committee (26- 17). Written informed consent was sought by trained field assistants in the carer's preferred language. Participants gave informed consent to participate in the study before taking part. Provenance[184]. Neonates were randomised to standard of care (SOC) consisting of ampicillin and gentamicin or SOC plus 100 mg/kg fosfomycin twice daily (BID). Patients in the fosfomycin arm received a minimum of four IV fosfomycin doses (Fomicyt 40 mg/mL solution, Infectopharm, Germany) over 48 hours at 12-hour intervals. Once tolerating oral fluids IV fosfomycin was changed to oral (PO) fosfomycin (Fosfocina 250 mg/5mL suspension, ERN Laboratories, Spain) therapy at 100 mg/kg BID. The IV dose was given as a slow push while oral fosfomycin was given via oral syringe, spoon, or nasogastric tube. Once reconstituted fosfomycin was stored below 25°C.

In a neonatal observational study (the NeoAMR Observational Study in Neonatal Sepsis; NCT03721302[207]) hospitalized infants <60 days with clinical sepsis were enrolled during 2018 to 2020 by 19 sites in 11 countries (mainly Asia and Africa). Information regarding ethics approval can be found elsewhere[205]. Prospective daily observational data was collected on clinical signs, supportive care, antibiotic treatment, microbiology, and 28-day mortality[205]. To allow comparisons to be made between the small NeoFosfo neonatal sepsis population and the much larger neonatal sepsis population investigated by the NeoAMR study a demographics comparison was made between the two studies.

1.3.2 Pharmacokinetic data

Simulation based sample size calculations were performed by Professor J. Standing using previously described methods[208,209] to inform study design and the PK sampling schedule. A cross-over design with each subject providing two IV and two PO plasma

samples was predicted to estimate clearance, central volume, and bioavailability with a power of >85% to have 95% confidence intervals (CIs) within a 20% precision level, if 45 patients were included. Due to uncertainty regarding the shape of the PK profile, patients were randomised to a single early (0.08, 0.5 or 1 hour post dose) and single late (2, 4 or 8 hours post dose) PK sample following the first IV and oral doses. Patients who remained hospitalised underwent a final safety blood sample following the last PO dose at day 7, and if there was sufficient blood volume drawn this was also assayed for PK. In addition, if a lumbar puncture was undertaken for clinical investigation during treatment, fosfomycin concentration was also measured in the cerebrospinal fluid (CSF)[@ 184].

Plasma and CSF samples were centrifuged at 3,000 RPM for 5 minutes then separated and frozen (at -80°C) within 30 minutes of collection. Frozen samples were shipped to Analytical Services International Ltd., St. Georges University of London, UK. Analysis of fosfomycin concentration in plasma and CSF samples was assessed via Liquid Chromatography Tandem Mass Spectrometry assay. The lower limit of quantification for plasma was 5 µg/ml and for CSF was 1 µg/ml. The method was fully validated according to European Medicines Agency guidelines[210]. Assay methodology and fosfomycin stability data are described elsewhere[211].

1.3.3 Population PK model development

Model based estimation of PK parameters was undertaken using the first-order conditional estimation method with interaction (FOCEI) in NONMEM (Version 7.4; ICON Development Solutions, Ellicott City, MD)[212].

One and two-compartment structural models were compared. Between subject or inter-individual variability (IIV) was assumed to follow a log-normal distribution for clearance, volume and absorption rate constants, and a logit distribution for bioavailability. IIV and was tested on all parameters. An additive, a proportional and combined error model were tested. In line with the Chi-squared distribution, a drop in the log likelihood ratio of >6.64 per degree of freedom was needed to be significant at a level of $p<0.01$ and >3.84 at a level of $p<0.05$.

Covariate effects:

Allometric (weight) scaling was included using a fixed exponent of 0.75 on clearance terms and linear scaling on volume terms. A standard weight of 70 kg was used to allow comparison of parameter estimates with previous studies. A previously pub-

lished neonatal renal maturation function[120] was also added to clearance. Due to the narrow postmenstrual age range of babies included in this study the Hill coefficient and time to 50% maturation (PMA_{50}) were fixed as with previous similar neonatal studies[213,214].

$$CL_i = CL_{std} \times \left(\frac{WT_i}{70}\right)^{0.75}$$

$$V_i = V_{std} \times \left(\frac{WT_i}{70}\right)$$

$$maturation = \frac{{PMA_i}^{3.4}}{47.7^{3.4} + {PMA_i}^{3.4}}$$

While the Rhodin maturation function[120] accounts for development of renal maturation in early life, there may also be a further effect on clearance maturation after birth regardless of gestational age that occurs over the first few days/weeks of life[215]. This covariate may be best related to postnatal age (PNA) as has been observed by others[213]. Therefore, $PNA_{function}$ was also evaluated as shown in the equation below, θ_M; fraction of clearance on the first day of life, set to day = 0 and θ_N; postnatal maturation rate constant.

$$PNA_{function} = \theta_M + (1 - \theta_M) \times (1 - e^{-PNA_i \times \theta_N})$$

The influence of serum creatinine on clearance was also tested according to the following equations, where the measured serum creatinine concentration (SCR) was standardized using typical serum concentration (TSCR) for age calculated using the Ceriotti equation:[119].

$$TSCR(\mu mol) = -2.37330 - 12.91367 \times ln_{(PNA_{years})} + 23.93581 \times (PNA_{years})^{0.5}$$

The ability of measured serum creatinine concentration (SCR) to explain and reduce IIV on clearance was then tested according to the equation below, where the measured SCR was standardized using the age typical serum concentration (TSCR)[119]. The SCR levels utilised by Ceriotti *et. al.* in defining the TSCR function were quantified using the more specific enzymatic method, while the less accurate Jaffe method was used in this study[118].

$$SCR_{function} = \frac{{SCR_i}^{\theta_{SCr}}}{TSCR}$$

CSF modelling:

Having defined the plasma PopPK model including covariate effects, an additional peripheral compartment was added to model the available CSF data. This introduced three additional parameters: inter-compartmental clearance between the central and CSF compartments (Q2), volume of the CSF compartment (V4) and the CSF/plasma ratio or fractional uptake into CSF (UPTK).

The initial modelling strategy aimed to estimate the inter-compartmental clearance between the central and CSF compartments and the uptake into CSF while the volume of the CSF compartment was fixed to 0.15 L/70Kg with linear weight scaling[216]. However due to model instability, OFV profiling and modelling of adult fosfomycin plasma and CSF concentration-time data published by Kuhnen *et. al.*[203] was used to define and subsequently fix Q2 in the Neofosfo model. OFV profiling involved manually fixing the value of Q2 prior to executing the model with the Neo-Fosfo dataset, and then exploring the impact on model stability, parameter estimates and parameter precision.

Finally CSF protein concentration was tested as a covariate on the uptake into CSF according to equations shown below, where PR_i is the individual's measured CSF protein level, and 0.94 is the population's median CSF protein level.

Like bioavailability the fractional uptake into CSF is a model parameter that can range from values of 0 to 1, and as such the logit transformation was implemented prior to testing the effect of CSF protein concentration on CSK uptake.

$$UPTK1 \;=\; ln\left(\frac{\theta_{UPTK}}{1-\theta_{UPTK}}\right)$$

$$UPTK2 \;=\; UPTK1 \;\times((1+\theta_{PR}) \;\times(PR_i - 0.94))$$

$$UPTK_i \;=\; \frac{1}{1+e^{-UPTK2}} \;=\; Fractional\ uptake\ into\ CSF\ for\ the\ ith\ individual$$

1.3.4 The final PopPK model

The final PopPK model was selected based on the likelihood ratio test, goodness of fit (GOF) p lots[217] and visual predictive checks (VPC). A non-parametric bootstrap (n=1000) was performed on the final model to test parameter robustness and derive parameter uncertainty. Perl-speaks-NONMEM (PsN)[218] was used for the bootstrap analysis and to produce the VPC, which was visualized using Xpose4[219]. Covariate effects were visualised to aid interpretation of the final model.

1.3.5 Neonatal PK simulations

Using the final model parameter estimates, half-life for each phase of the PK profile was calculated using methods reported by Upton et al[220]. The Upton method solves the differential equations of a three-compartment model by transformation into the Laplace domain then matrix manipulation, enabling calculation of hybrid (macro) rate constants (λ_1, λ_2, λ_3), from the micro rate constants (K_{12}, K_{21}, K_{13}, K_{31}, K_{10}). Thereby allowing calculation of the half life of each phase of decline, see Figure 1.1.

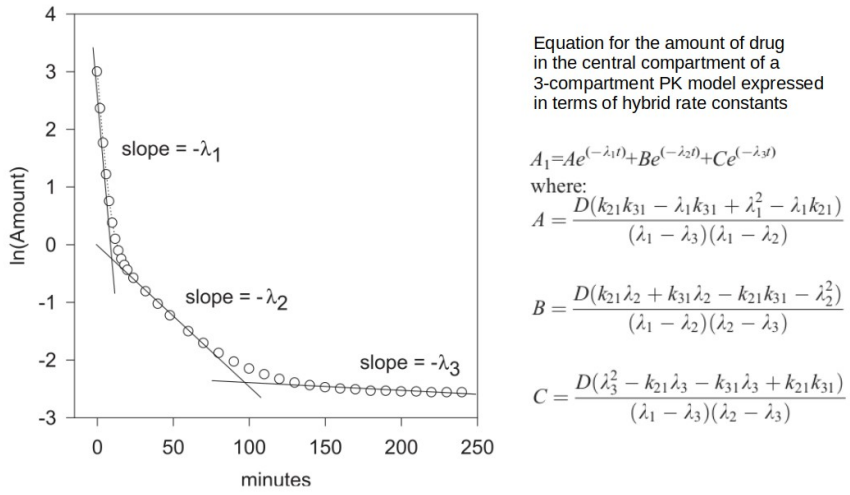

Figure 1.1: Illustrative 3 compartmental PK Model - Taken from R.Upton 2004

A hypothetical neonatal population of 10,000 subjects was created using observed demographics from the present study (Neofosfo, NCT03453177[184,206]) combined with data from an international multi-centre neonatal observational study; the NeoAMR Observational Study in Neonatal Sepsis (NCT03721302, n=3,204 infants)[207,205]. The hypothetical population along with the final model were used to simulate fosfomycin plasma concentrations at steady state for different dosing regimens. The simulations were all executed in R using the linpk package[221].

Neonatal sub-populations were defined based on weight and postnatal age to further explore optimal dosing in specific neonatal populations. The following sub-populations were evaluated:

- Group 1: WT $>$ 1.5kg and PNA $\leq$ 7days
- Group 2: WT $>$ 1.5kg and PNA $>$ 7days
- Group 3: WT $\leq$ 1.5kg and PNA $\leq$ 7days
- Group 4: WT $\leq$ 1.5kg and PNA $>$ 7days

Simulated concentration versus time profiles and summary statistics (T>MIC) considered the then current EUCAST breakpoint for Enterobacteriaceae of ≤ 32 mg/L[193].

Target attainment (TA) plots were generated considering two potentially relevant pharmacodynamic targets; AUC/MIC ratio[222] and T>MIC[223]. For T>MIC target values were defined as 60%, 80% and 100% of time over an minimum inhibitory concentration (MIC) of 32 mg/L[193]. For AUC/MIC previously published target ratios for Escherichia coli (*E.coli*) were considered; stasis (19.3), 1-log kill (87.5)[224] and resistance suppression (3136)[225]. The fosfomycin MIC for the five *E.coli* strains evaluated by Lepak *et. al.*[224] ranged from 1 to 16 mg/mL, the single strain against which Decobo-Perez *et. al.*[225] demonstrated suppression of resistance had a fosfomycin MIC of 1 mg/L. Due to uncertainty regarding the specific target value required for predicting the efficacy of fosfomycin in bacteraemia a previously suggested approach[226] was employed, and TA rather than 'probability of target attainment' was presented for ascending MIC values.

1.4 Results

1.4.1 Study design and neonatal population

61 babies were recruited into the SOC plus fosfomycin arm of the study, with fosfomycin PK sampling performed in 60 babies. Key baseline demographic information is summarized in Table 1.1 for the Neofosfo babies that received fosfomycin plus SOC and for babies included in the larger (n=3204) observational neonatal sepsis study (NeoAMR)[205].

Table 1.1: Key baseline covariates of all fosfomycin receiving patients in the NeoFosfo Study compared to the NeoAMR study population.

	NeoFosfo Study (NCT03453177)		**NeoAMR Study (NCT03721302)**	
Covariates[a]	**Median (IQR)**	**Mean (SD)**	**Median (IQR)**	**Mean (SD)**
GA (weeks)	40	39.8	37	35.4
	(38.4 – 40.8)	(2.1)	(31.0 – 39.0)	(4.9)
PNA (days)	1	2.7	5	10.4
	(0.0 - 3.0)	(4.9)	(2.0 – 15.0)	(12)
WT (grams)	2805	2871.5	2500	2353
	(2500.0 – 3233.8)	(674.6)	(1400.0 – 3197.0)	(992.2)
PMA (weeks)	40.1	40.3	38.1	36.8
	(38.7 – 41.3)	(2.4)	(32.4 – 40.3)	(5.2)
CSF Protein (g/L)	0.94	1.074	0.923	1.241
	(0.777 – 1.160)	(0.673)	(0.639 – 1.391)	(1.185)

[a] GA; gestational age. PNA; postnatal age. WT; weight. PMA; postmenstrual age. CSF; cerebrospinal fluid.

1.4.2 Pharmacokinetic data

In total 238 fosfomycin plasma samples were collected. Two babies died during the intravenous fosfomycin phase of the study resulting in complete intravenous and oral PK data being collected in 58 babies. Plasma protein binding of fosfomycin is negligible[227,228] therefore calculation of free concentrations were not performed.

Fifteen CSF samples from 15 subjects were collected. Five of the CSF samples were collected during intravenous treatment and 10 during oral. Individual CSF protein concentrations (PR_i) were available for 12 subjects. No samples (plasma or CSF) were below the limit of quantification.

Pooled plasma and CSF concentration-time data is presented in Figure 1.2. Individual concentration-time data are shown in Appendix Figures A.1 and A.2.

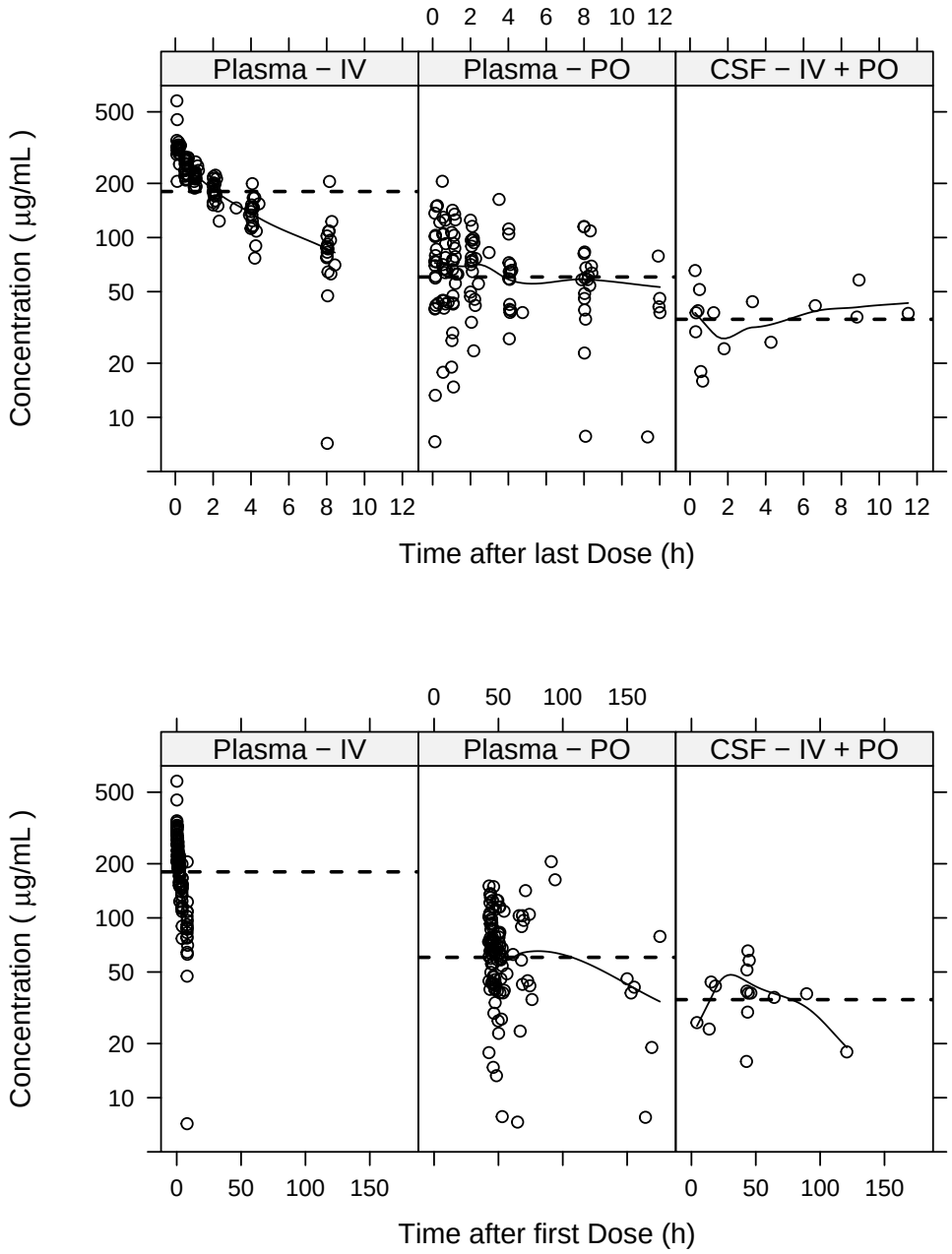

Figure 1.2: Pooled CSF and plasma concentrations versus time after LAST dose (top) and time after FIRST (bottom) for all patients. The dashed lines represent mean concentrations which are 37.6 μg/mL in CSF and 70.1 and 201.7 μg/mL in plasma following oral and IV dosing respectively, the solid lines represent the loess smooth curves.

1.4.3 Population PK model development

A two-compartment IV structural model was superior to a one-compartment model (-ΔOFV 31, $p < 0.01$). When modelling the IV data in isolation it was only possible to estimate IIV on CL, however increasing the dataset to include the oral plasma data enabled estimation of IIV on CL, Vc and F (-ΔOFV 22, $p < 0.01$).

The correlations between key demographic and biochemical covariates were analysed and correlation coefficients calculated, see Figure 1.3. The strongest correlation was observed between SCR and PNA (r^2 =0.52), SCR showed a slight initial increase with PNA followed by a rapid then slower decline. Weight correlated to a lesser extent with the different measures of age (PNA; $r^2 = 0.32$, PMA; $r^2 = 0.33$) whilst PMA and SCR appear essentially independent ($r^2 = 0.1$).

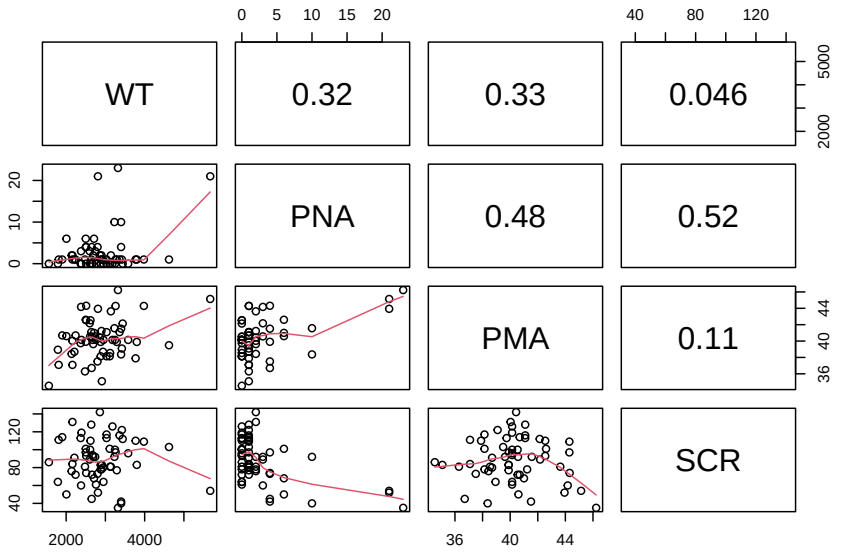

Figure 1.3: Baseline covariate correlations, plots in lower triangle, correlation coefficients in upper triangle. WT; weight (grams). PNA; postnatal age (days). PMA; postmenstrual age (weeks). SCR; serum creatinine (μmol/L)

Inclusion of allometric scaling and the Rhodin maturation function resulted in a drop in OFV of 84 and inclusion of the PNA function previously described gave a further OFV decrease of 43 ($p< 0.01$). However, inclusion of SCR instead of PNA, or in conjunction with PNA, did not improve the model compared to just using allometric scaling and the Rhodin function (-ΔOFV by < 1).

The CSF data available from this study was not sufficiently rich to support esti-

mation of Q2. The decision therefore was made to manually explore OFV sensitivity and precision of the UPTK estimate to Q2. The effects of fixing Q2 to a range of values are presented in Figure 1.4 and Table 1.2. Based on this OFV and UPTK precision profiling the optimal value of Q2 was expected to fall between 0.01 and 0.05 L/hr/70kg.

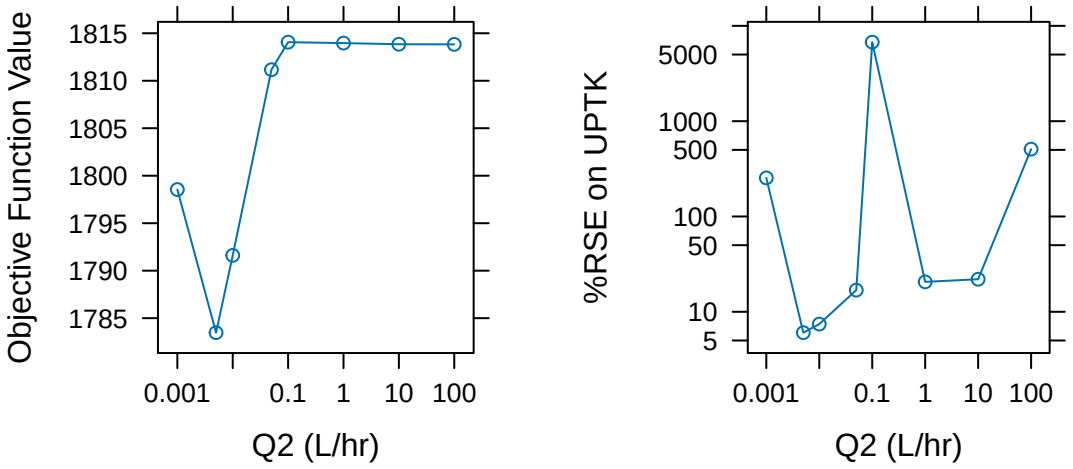

Figure 1.4: Impact of fixing Q2 when modelling the Neofosfo study data. Left; impact on the OFV. Right; impact on UPTK %RSE.

Table 1.2: Q2 Parameter Profiling using the Neofosfo study data.

Q2 (L/hr)	OFV	CL(L/hr)	%RSE on CL	UPTK	%RSE on UPTK
0.001	1798.54	8.87	5413.74	0.69	254.04
0.005	1783.47	8.78	83.60	0.39	6.04
0.01	1791.61	8.84	33.30	0.36	7.43
0.05	1811.16	8.92	8.38	0.31	16.88
0.1	1814.06	8.93	3579.74	0.30	6741.83
1	1813.96	8.93	14.99	0.33	20.61
10	1813.84	8.93	35.37	0.33	21.97
100	1813.83	8.93	786.33	0.33	508.81

Next the possibility of using adult prior information to inform Q2 was explored. Kuhnen *et. al.*[203] report full plasma and CSF concentration-time profiles after 5 and 10 grams of intravenous fosfomycin. The mean age of subjects was 47 years (range 18 to 69), and each patient obtained an intra-operative or therapeutic CSF drain that was required for a neurosurgical indication. Both 5 and 10 g datasets were extracted

from the publication and individually modelled, no covariates or BSV were included in the model as only a single average plasma/CSF profile was available at each dose. The fixed effects and residual errors associated with modelling the 5 gram data, along with GOF plots are provided in Figure 1.5.

The value of Q2 that was manually estimated based on OFV profiling fell between 0.01 and 0.05 L/hr/70kg. This was in good agreement with the average Q2 estimated from modelling the adult fosfomycin plasma and CSF PK data published by Kuhnen *et. al.*; 0.017 L/hr/70kg 2.d.p[203]. Therefore in the final neofosfo model Q2 was fixed to 0.017 L/hr/70kg.

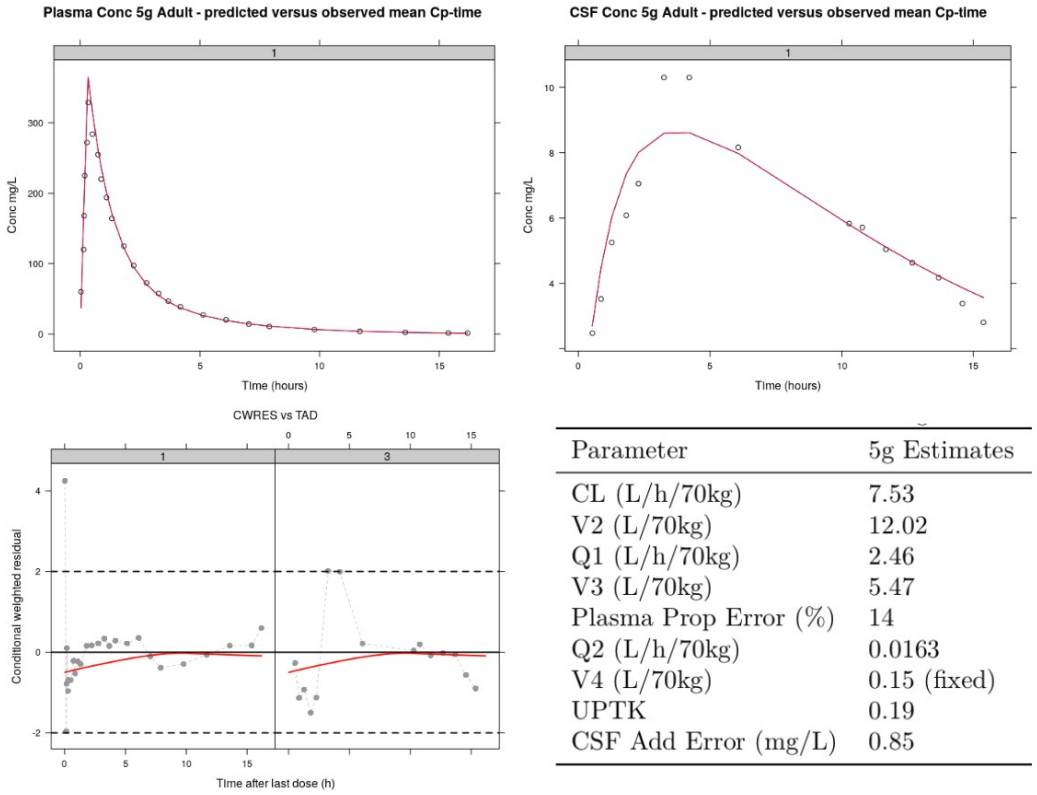

Parameter	5g Estimates
CL (L/h/70kg)	7.53
V2 (L/70kg)	12.02
Q1 (L/h/70kg)	2.46
V3 (L/70kg)	5.47
Plasma Prop Error (%)	14
Q2 (L/h/70kg)	0.0163
V4 (L/70kg)	0.15 (fixed)
UPTK	0.19
CSF Add Error (mg/L)	0.85

Figure 1.5: Adult plasma and CSF PK modelling. Shown are the results from modelling of the 5 gram IV infusion PK data (n=35 adult patients) published by Kuhnen et al (Penetration of fosfomycin into cerebrospinal fluid across non-inflamed and inflamed meninges, Infection 15, 422–424, 1987). Top left; observed (open circles) and predicted (solid red line) fosfomycin plasma concentration. Top right; observed (open circles) and predicted (solid red line) fosfomycin CSF concentration. Bottom left; CWRES versus time since last dose GOF plots (left facet; plasma, right facet; CSF). Bottom right; Adult modelling parameter estimates.

1.4.4 The final PopPK model

An illustration of the final model is presented in Figure 1.6 and model parameters along with their associated relative standard errors and 95% CIs (%RSE) are presented in Table 1.3.

Visual predictive checks are shown in Figure 1.7 and goodness of fit plots in Figure 1.8 and 1.9 for plasma and CSF concentrations respectively. The estimated postnatal age function is visualised in Figure 1.10 and compared with clearance estimates for each subject at each time point. Figure 1.10 illustrates the fractional change in clearance for each subject at each time point as a function of just the change in postnatal age, i.e. the effect of weight and postmenstrual age (the other covariates included in the model on clearance) have already been accounted for. The final model employed three residual (unexplained) error terms; separate proportional error models were used to describe the intravenous and oral plasma levels and an additive error model was used for CSF concentrations. The NONMEM code is included in Appendix A.1.

Final Model

- K_0 = Infusion rate
- K_{el} = CL/V2
- C_p = A(2)/V2
- C_{csf} = A(4)/V4
- $dA/dT_{(1)} = -K_a * A(1)$
- $dA/dT_{(2)} = A(1) * K_A + A(3) * K_{32} + A(4) * K_{42} - A(2) * (K_{el} + K_{23} + K_{24})$
- $dA/dT_{(3)} = A(2) * K_{23} - A(3) * K_{32}$
- $dA/dT_{(4)} = A(2) * K_{24} - A(4) * K_{42}$

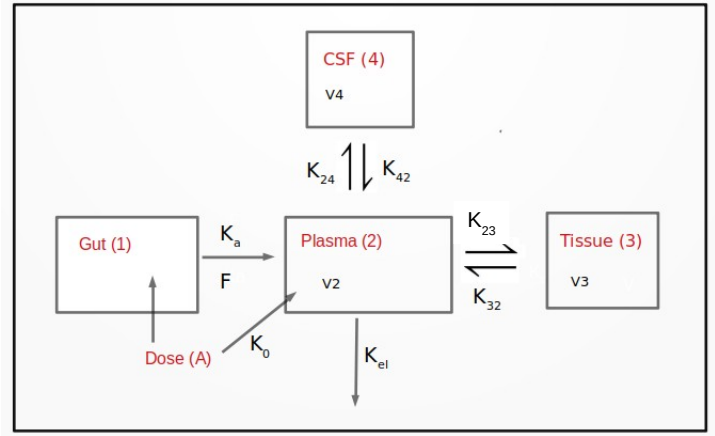

Rate Constants

- K_{23} = Q1 / V2
- K_{32} = Q1 / V3
- K_{24} = Q2 * UPTK / V2
- K_{42} = Q2 / V4

Covariates

- PMA, PNA and WT on CL terms
- WT on V terms
- CSF protein on CSF uptake

Figure 1.6: Structural PK Model including CSF Compartment. Inter-compartmental clearances and volumes are derived from the following rate constants as follows; Kel, K23, K32, K24, K42. Ka is the first order absorption rate constant. The intravenous infusion rate is nominally 6000mg/kg/h. WT; weight (grams). PNA; postnatal age (days). PMA; postmenstural age (weeks). CL; clearance. V2; central volume. V3; peripheral volume. V4; volume of the CSF compartment. CSF; cerebrospinal fluid. UPTK; is the fractional uptake into the CSF and is an estimated model parameter.

Table 1.3: Population pharmacokinetic model parameter estimates. All disposition terms are centred on a fully mature 70 kg individual using allometric scaling with exponents of 1 for volume terms and 0.75 for clearance terms.

Parameter	**Estimate (%RSE)**	**IIV %CV (%RSE)**	**Bootstrap 95%CI**	**Median**
CL (L/h/70kg)	8.94 (14.5)	24.5% (30.5)	7.10 - 13.2	9.13
V2 (L/70kg)	19.1 (8.8)	14.2% (41.8)	11.2 – 21.3	19
Q1 (L/hr/70kg)	8.01 (49.6)	-	4.54 – 39.30	8.24
V3 (L/70kg)	7.53 (14.0)	-	5.69 14.30	7.61
Q2 (L/hr/70kg)	0.017(fixed)	-	-	-
V4 (L/70kg)	0.15 (fixed)	-	-	-
θ_{UPTK}	0.321 (12.0)	-	0.272 – 0.409	0.32
Ka (/hr)	0.0987 (21.7)	-	0.057 – 0.148	0.0994
F	0.478 (15.0)	0.269 (60.2)	0.347 – 0.775	0.483
θ_M	0.449 (22.9)	-	0.277 – 0.567	0.42
θ_N (/day)	0.117 (29.4)	-	0.053 – 0.259	0.121
θ_{PR}	-0.952 (22.4)	-	2.88 - -0.62	-1.081
IV Plasma Prop Error (%)	7.69 (46.4)	-	3.78 – 12.08	8.22
PO Plasma Prop Error (%)	18.6 (37.5)	-	7.36- 24.31	16.6
CSF Add Error (mg/L)	10.9 (35.3)	-	5.47 – 14.63	10.2

Note: CL, total plasma clearance; Vc, central volume; Q1, intercompartmental clearance between central and main peripheral compartment; V3, volume of main peripheral compartment; Q2, intercompartmental clearance between central and CSF compartment; V4, volume of CSF compartment; θ_{UPTK}, CSF/plasma ratio; Ka, absorption rate constant; F, oral bioavailability; θ_M, population estimate of te fraction of clearance on the first day of life, set to day = 0; θ_N, represents the postnatal maturation rate constant; θ_{PR}, CSF protein coefficient; %RSE, asymptotic standard error; %CV, coefficient of variation; IIV, interindividual variability. IIV on F reported directly as OMEGA value due to logit transformation.

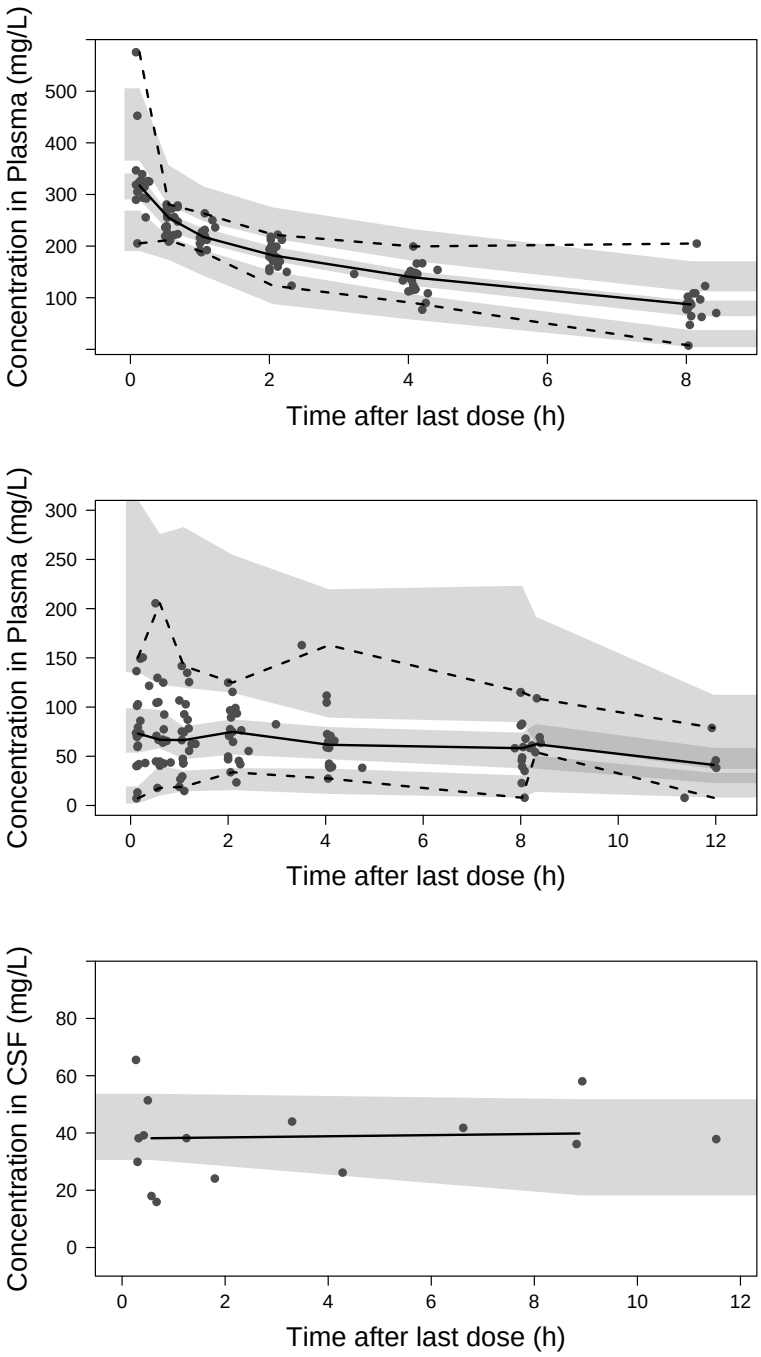

Figure 1.7: Visual predictive check showing the 2.5th, 50th and 97.5th percentiles of the observed data (lines and closed circles) compared with 95 percent CIs of the corresponding simulations from the final model (shaded areas) versus time after last dose. The top panel shows the fosfomycin plasma concentrations following IV dosing, the middle shows fosfomycin plasma concentrations following oral dosing and the bottom panel shows fosfomycin CSF concentrations. The 2.5th or 97.5th percentiles and corresponding prediction intervals have not been presented in the bottom panel due to the size of the CSF dataset evaluated.

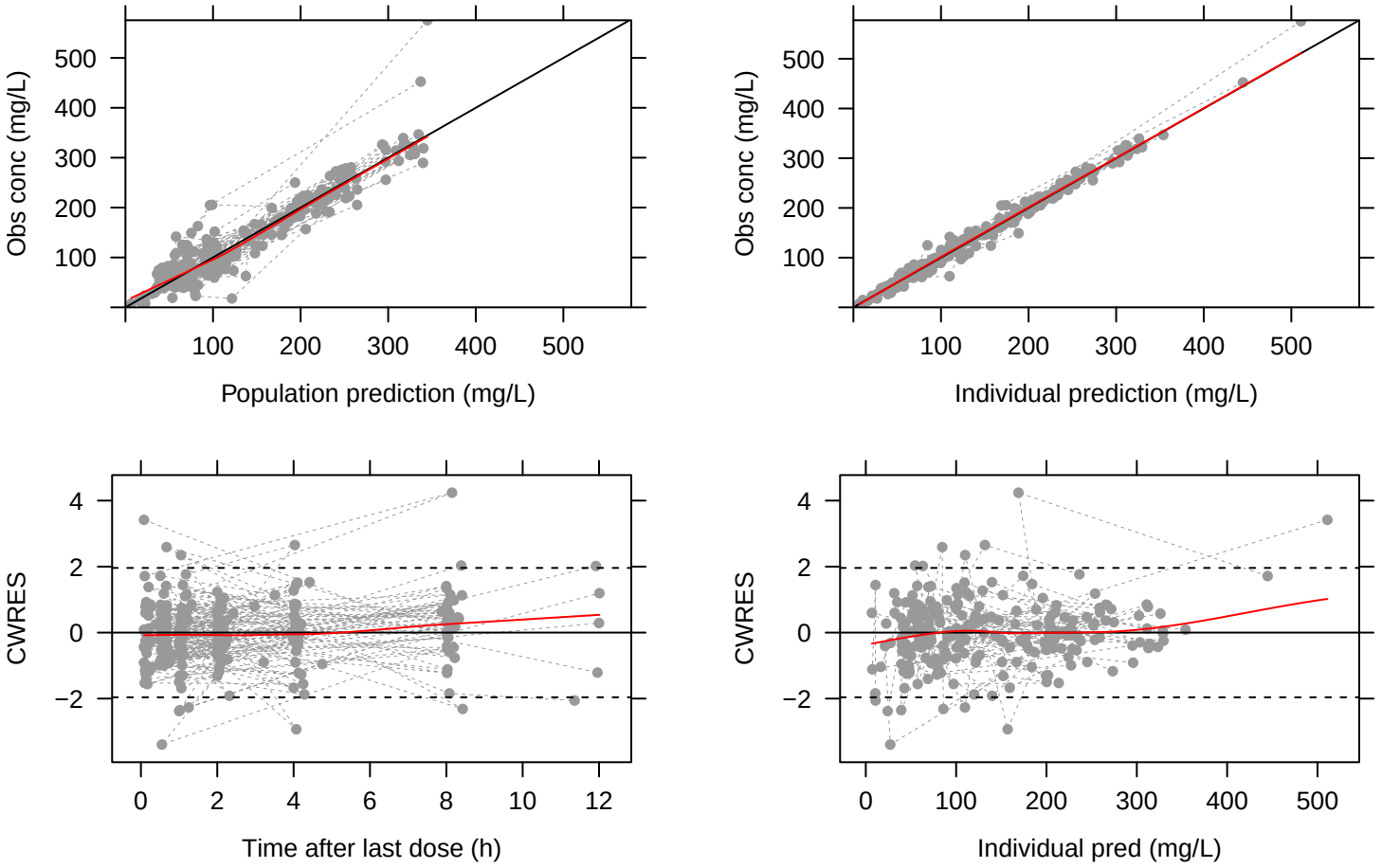

Figure 1.8: Plasma goodness of fit plots. Top; observed fosfomycin plasma concentrations versus the population (PRED) predicted plasma concentration (left) and the individual predicted (iPRED) plasma concentration (right). Bottom; conditional weighted residual (CWRES) versus time since last dose (left) and conditional weighted residual versus individual predicted plasma concentration (right).

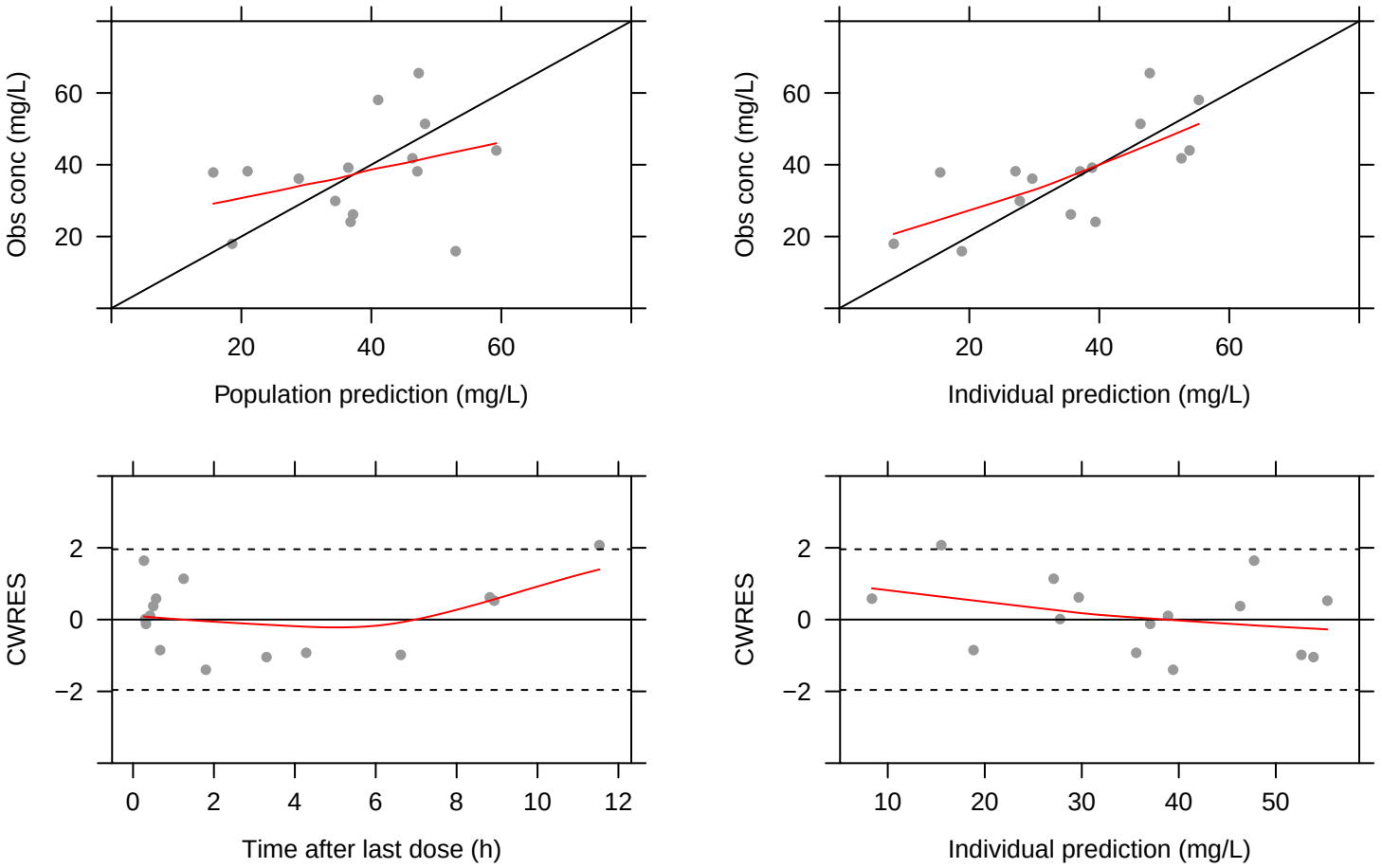

Figure 1.9: CSF goodness of fit plots. Top; observed fosfomycin CSF concentrations versus the population (PRED) predicted CSF concentration (left) and the individual (iPRED) CSF plasma concentration (right). Bottom; conditional weighted residual versus time since last dose (left) and conditional weighted residual versus individual predicted CSF concentration (right).

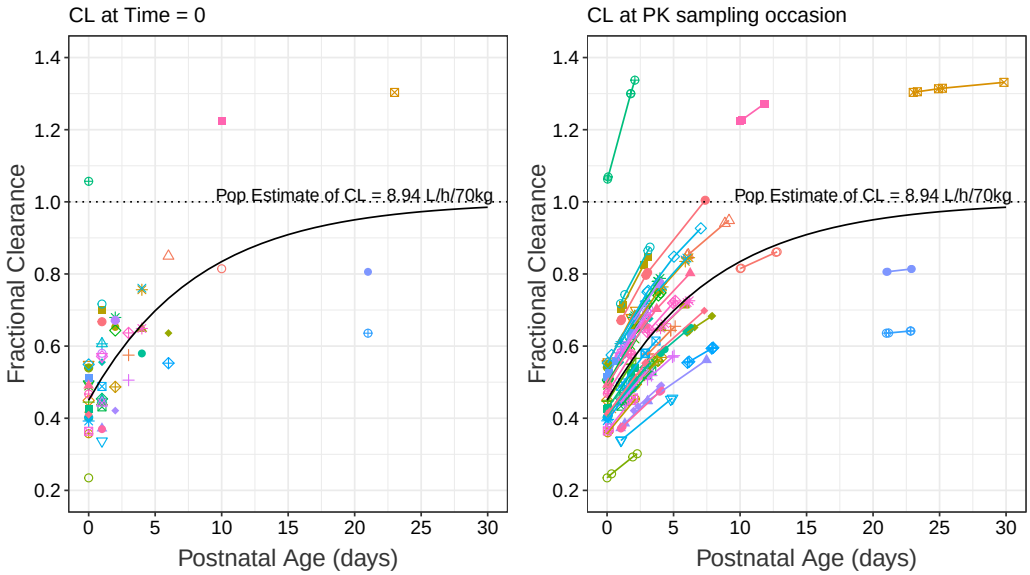

Figure 1.10: Visualisation of the PNA effect on clearance, the effect of postmenstrual age and weight on clearance has been accounted for, hence the change in clearance is expressed as the fractional change that results solely from increasing postnatal age. Data points are grouped by subject ID (n=60), the left panel shows an individual's fractional clearance at Time = 0 (the first PK time point for each individual patient), and the right panel shows individual fractional clearance at all PK sampling timepoints. The solid black line in each panel represents the model estimated postnatal age maturation function.

1.4.5 Neonatal PK simulations

The demographics of the full hypothetical neonatal simulation population is presented in Figure 1.11.

Simulation Population Covariates

	GA	PNA	WT	PMA	Protein
Min	23	0	400	23.1	0.03
1st Qu	31	2	1400	32.4	0.48
Med	37	5	2500	38.1	0.90
Mean	35	10	2355	36.9	1.36
3rd Qu	39	15	3166	40.3	1.69
Max	44	59	5670	51.7	12.00

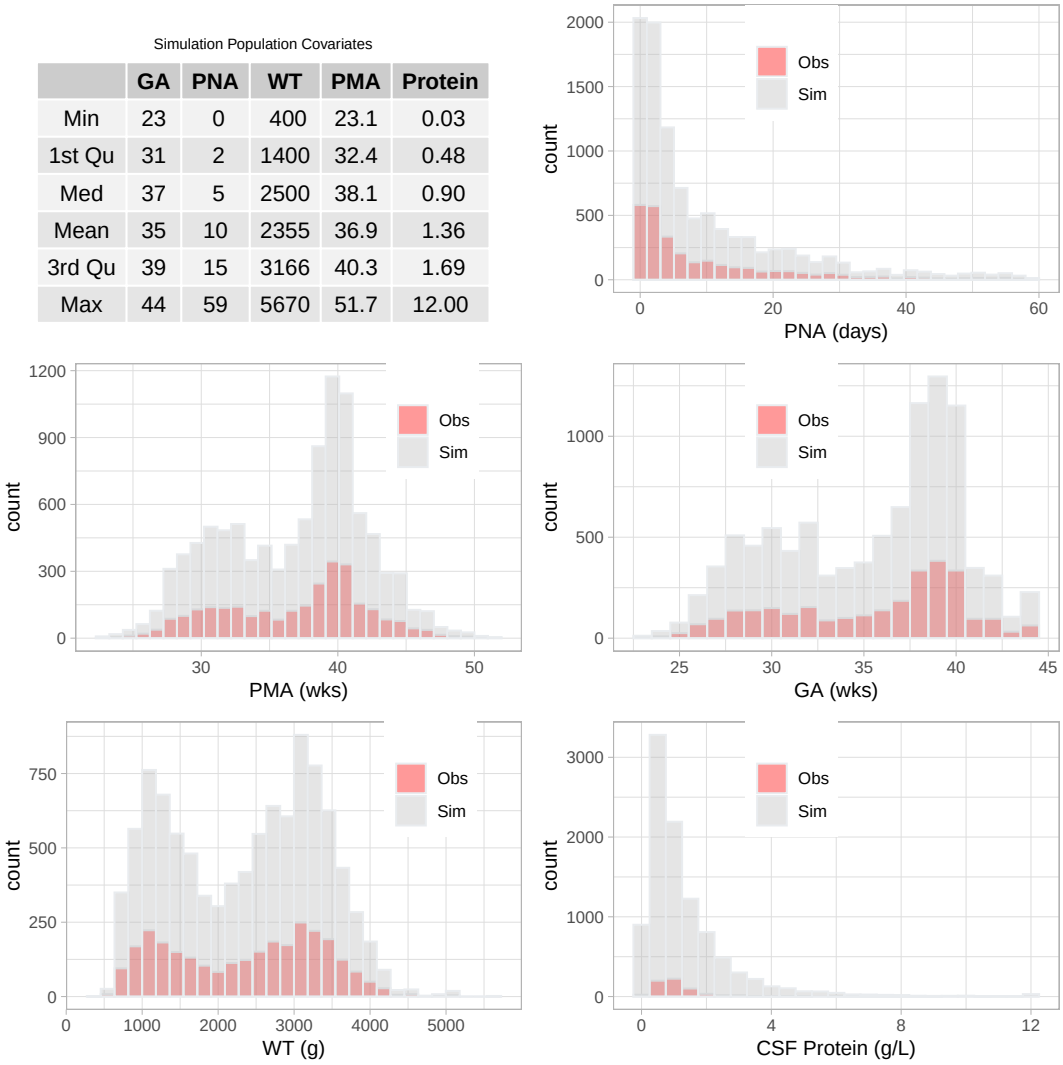

Figure 1.11: Hypothetical Population Demographics (n=10,000). GA; gestational age (wks). PNA; postnatal age (days). WT; weight (grams). PMA; postmenstrual age (wks). Protein; CSF protein concentration (g/L)

Illustrative simulated Cp-time profiles using the full hypothetical population are presented in Figure 1.12 assuming 100mg/kg BID intravenous and oral dosing out to steady state. Predicted steady state PK parameters (AUC, C_{max} and C_{min}) using the final model and the full hypothetical population are summarised in Table 1.4. Half-lives for the typical (median) trial neonate (WT = 2805 g, PNA = 1 day, PMA

40 weeks) for each elimination phase were longer than those predicted in a 70 kg adult: Neonate: 0.2, 5.2 and 8.7 hours. Adult: 0.4, 2.3 and 6.1 hours.

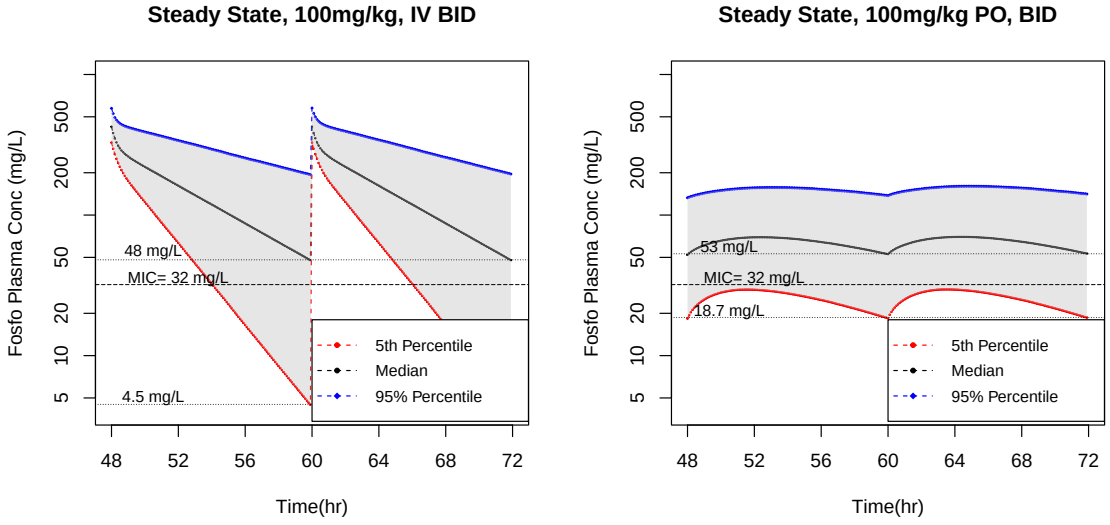

Figure 1.12: Plasma concentration-time curves for IV (left) and oral (right) fosfomycin administered at 100mg/kg/dose twice daily. Simulations use the full hypothetical population. BID; twice a day.

Table 1.4: Simulated IV Steady State PK Summary - Full Population. P5; 5th percentile. P50; 50th percentile. P95; 95th percentile.

	AUC48-72 (hr*mg/L)			Cmin (mg/L)			Cmax (mg/L)			T>MIC (hr)		
Regimen	P5	P50	P95	P5	P50	P95	P5	P50	P95	P5	P50	P95
100 BID_IV	1539.1	3387.2	7406.7	4.5	47.8	195.8	327.8	425.5	577.1	12.2	24	24
150 BID_IV	2308.6	5080.9	11110.1	6.7	71.6	293.7	491.8	638.2	865.6	14.6	24	24
200 BID_IV	3078.1	6774.5	14813.4	9.0	95.5	391.6	655.7	850.9	1154.2	16.2	24	24
100 BID_PO	607.8	1528.8	3629.5	18.7	53.3	141.2	29.6	70.0	160.3	0.0	24	24
200 BID_PO	1215.6	3057.7	7258.9	37.3	106.5	282.3	59.3	139.9	320.6	24.0	24	24
300 BID_PO	1823.4	4586.5	10888.4	56.0	159.8	423.5	88.9	209.9	480.9	24.0	24	24

[1] T>MIC assumes MIC = 32 mg/L

AUC/MIC and T>MIC target attainment plots are presented in Figure 1.13 and Figure 1.14 respectively. For pathogens with an MIC of 32 and 4 mg/L, a BID 100 mg/kg IV regimen was predicted to achieve a plasma AUC/MIC ratio of 48 and 385 respectively in 95% of neonates. Following oral dosing of 100 mg/kg BID and evaluating the same MICs, the predicted plasma AUC/MIC ratios are 19 and 152 in 95% of neonates. Considering T>MIC, and a BID 100 mg/kg IV regimen, 95% of neonates are predicted to exceed 32 mg/L 51% of the time. The flatter profile shape that results from slow absorption following oral administration (Tmax ~ 3-4 hours)

and oral bioavailability means that at 100 mg/kg BID, 5% of neonates were predicted to never exceed 32 mg/L.

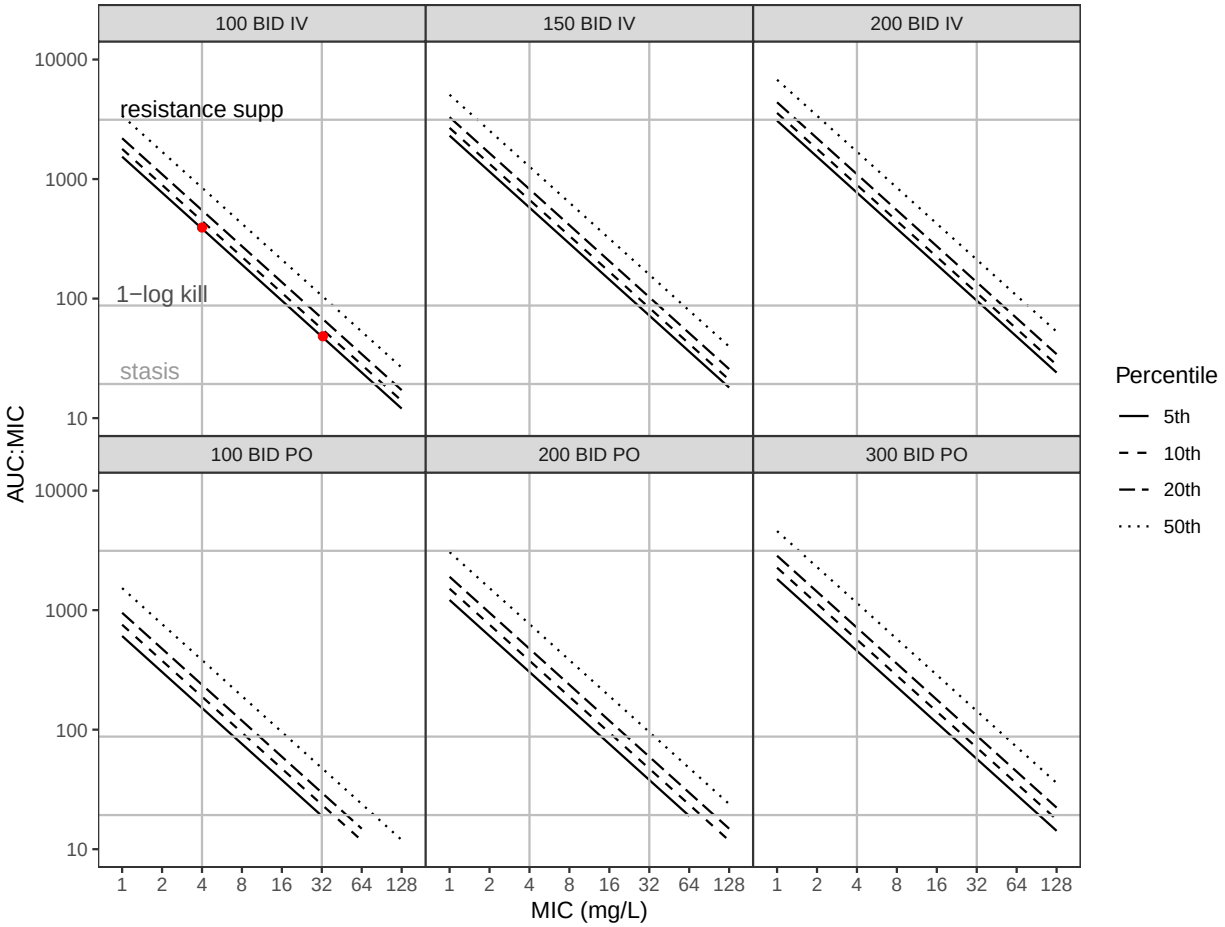

Figure 1.13: Target attainment plots for various dose schemes using the full simulation population. The top row presents predicted AUC/MIC ratio in plasma following IV dosing while the bottom row shows results following oral dosing. A comparison of 100, 150 and 200 mg/kg BID is given for IV and 100, 200 and 300 mg/kg BID for oral. The continuous black line is the predicted AUC/MIC ratio achieved by 95% of the population (5th percentile) while the typical patient (50th percentile) is shown by the dotted line. AUC/MIC target ratios for stasis (19.3), 1-log reduction (87.5) and resistance suppression (3136) are shown by the grey horizontal reference lines. The grey vertical reference lines highlight MIC values of 4 and 32 mg/L. Red circles highlight that 95% of the population are predicted to achieve an AUC/MIC ratio $\geq$ 48 and 385 for a pathogen with a fosfomycin MIC of 32 and 4 mg/L respectively.

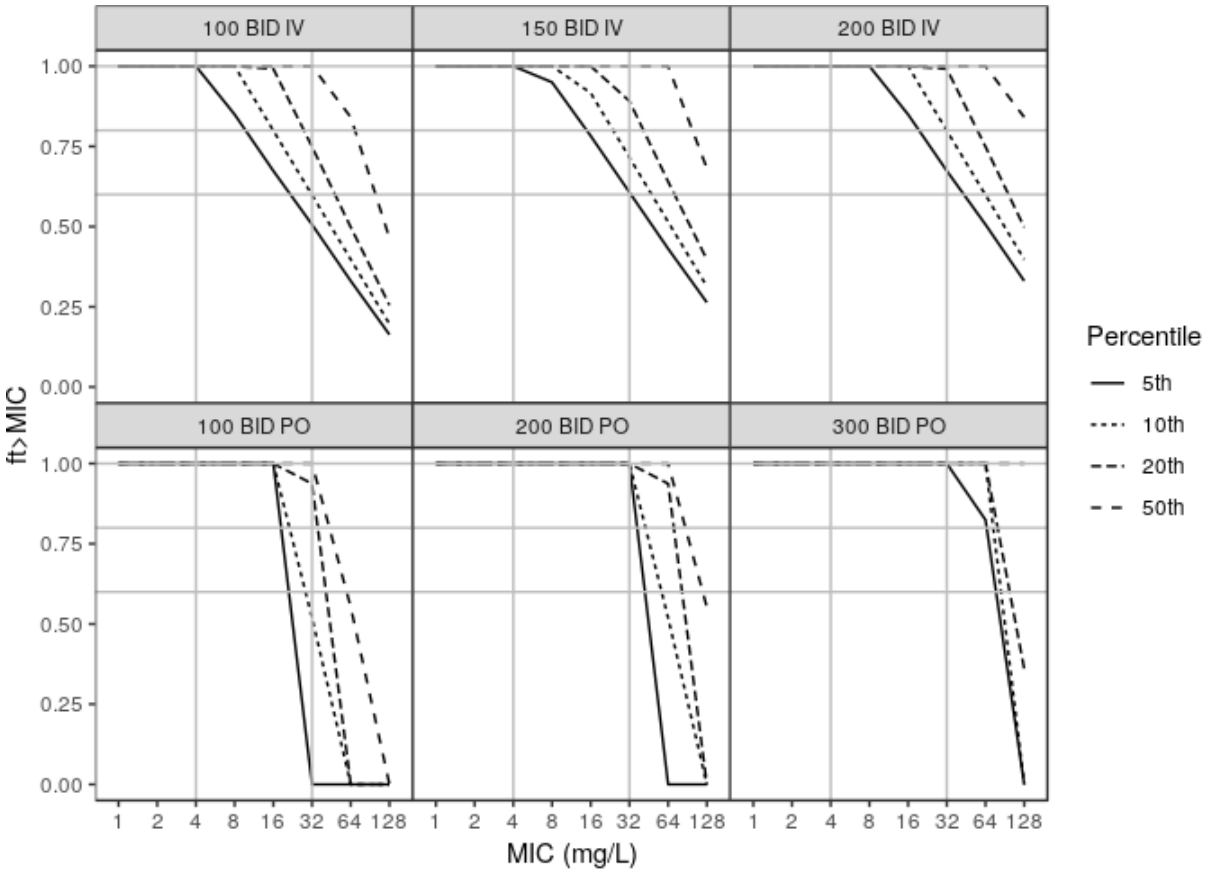

Figure 1.14: Target Attainment, plasma fT>MIC, IV and PO Simulations, Full Population. The top row presents predicted ft>MIC in plasma following IV dosing while the bottom row shows results following oral dosing. A comparison of 100, 150 and 200 mg/kg BID is given for IV and 100, 200 and 300 mg/kg BID for oral. The continuous black line is the predicted ft>MIC achieved by 95% of the population (5th percentile) while the typical patient (50th percentile) is shown by the dotted line. ft>MIC target ratios for stasis (19.3), 1-log reduction (87.5) and resistance suppression (3136) are shown by the grey horizontal reference lines. The grey vertical reference lines highlight MIC values of 4 and 32 mg/L

To illustrate further the implications of PNA on predicted target attainment, simulations were catagorised according to WT and PNA age; Groups 1-4. Predicted steady state PK parameters (AUC, C_{max} and C_{min}) using the final model are summarised for each neonatal subpopulations in Table 1.5. Target attainment plots analogous to Figure 1.13 were also constructed for these neonatal sub-populations and are presented in Figure 1.15 for IV dosing and Figure 1.16 for PO dosing.

Table 1.5: Simulated Neonatal Steady State PK - Summary Statistics

		AUC48-72 (hr*mg/L)			Cmin (mg/L)			Cmax (mg/L)			T>MIC (hr)		
Regimen	Group	P5	P50	P95	P5	P50	P95	P5	P50	P95	P5	P50	P95
100_IV	1	2962.5	5554.6	10019.0	34.2	126.6	304.9	379.3	497.8	687.7	24.0	24.0	24
150_IV	1	4443.8	8331.9	15028.4	51.2	189.9	457.3	568.9	746.6	1031.6	24.0	24.0	24
200_IV	1	5925.0	11109.3	20037.9	68.3	253.2	609.7	758.6	995.5	1375.4	24.0	24.0	24
100_PO	1	1115.2	2542.9	4968.8	38.8	95.8	200.5	51.0	113.3	218.6	24.0	24.0	24
200_PO	1	2230.3	5085.8	9937.6	77.7	191.5	401.1	102.0	226.6	437.2	24.0	24.0	24
300_PO	1	3345.5	7628.7	14906.4	116.5	287.3	601.6	153.0	340.0	655.7	24.0	24.0	24
100_IV	2	1256.5	2086.9	3606.5	1.8	13.8	56.9	308.6	385.2	478.8	9.8	17.0	24
150_IV	2	1884.7	3130.3	5409.7	2.7	20.7	85.4	462.9	577.8	718.2	11.8	20.4	24
200_IV	2	2512.9	4173.8	7212.9	3.5	27.5	113.9	617.2	770.4	957.5	13.2	22.6	24
100_PO	2	464.5	959.9	1890.0	13.4	30.4	66.3	23.0	46.1	86.0	0.0	22.1	24
200_PO	2	929.1	1919.9	3779.9	26.8	60.8	132.5	45.9	92.2	172.0	19.0	24.0	24
300_PO	2	1393.6	2879.8	5669.9	40.1	91.2	198.8	68.9	138.3	258.0	24.0	24.0	24
100_IV	3	1659.3	3056.4	5508.1	6.4	38.3	120.6	325.2	413.4	517.4	13.4	24.0	24
150_IV	3	2488.9	4584.6	8262.2	9.5	57.4	180.8	487.8	620.1	776.1	16.2	24.0	24
200_IV	3	3318.5	6112.8	11016.2	12.7	76.5	241.1	650.4	826.8	1034.8	18.0	24.0	24
100_PO	3	646.3	1392.7	2817.2	20.2	47.7	104.9	30.8	64.4	125.7	0.0	24.0	24
200_PO	3	1292.6	2785.5	5634.4	40.4	95.5	209.7	61.6	128.7	251.4	24.0	24.0	24
300_PO	3	1938.9	4178.2	8451.6	60.6	143.2	314.6	92.4	193.1	377.0	24.0	24.0	24
100_IV	4	2271.0	3883.8	6805.8	17.5	63.6	173.0	345.9	438.5	567.4	18.6	24.0	24
150_IV	4	3406.5	5825.7	10208.7	26.2	95.4	259.6	518.8	657.7	851.1	22.2	24.0	24
200_IV	4	4541.9	7767.6	13611.6	34.9	127.3	346.1	691.7	877.0	1134.9	24.0	24.0	24
100_PO	4	860.8	1792.9	3500.4	28.5	63.9	132.7	40.2	80.9	154.8	19.0	24.0	24
200_PO	4	1721.7	3585.8	7000.8	57.0	127.8	265.5	80.5	161.8	309.6	24.0	24.0	24
300_PO	4	2582.5	5378.7	10501.2	85.5	191.7	398.2	120.7	242.6	464.4	24.0	24.0	24

Note:

Group1: WT<=1.5kg+PNA<=7days

Group2: WT>1.5kg+PNA>7days

Group3: WT<=1.5kg+PNA>7days

Group4: WT>1.5kg+PNA<=7days

Abbreviations: AUC, area under concentration-time curve; C, plasma concentration; min, minimum; max, maximum; T>MIC, fraction of time plasma concentrations exceeds the MIC (minimum inhibitory concentration); mg, milligram; L, litre; hr, hour; P5, 5th percentile; P50, median; P95, 95th percentile; IV, intravenous; PO, oral; WT, weight; PNA, postnatal age. T>MIC assumes MIC=32mg/L

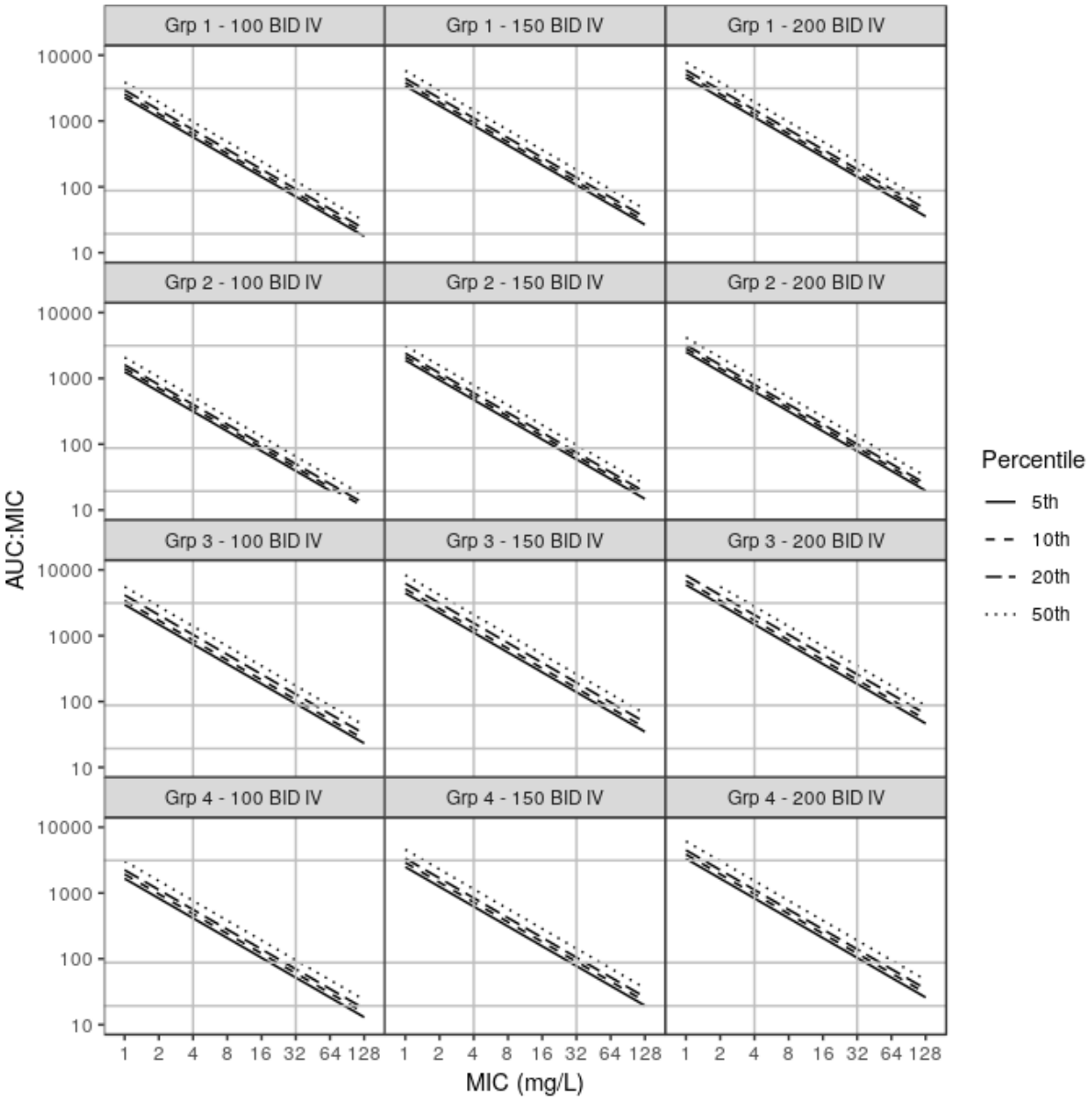

Figure 1.15: Target attainment, plasma AUC:MIC, IV dosing, neonatal subpopulations. Group 1: WT > 1.5kg and PNA ≤ 7days (n=4391). Group 2: WT > 1.5kg and PNA > 7days (n=2798). Group 3: WT ≤ 1.5kg and PNA ≤ 7days (n=1534). Group 4: WT ≤ 1.5kg and PNA > 7days (n=1277). Groups 1 and 2 represent patients similar to those fitting the Neofosfo study inclusion criteria. Groups 3 and 4 represent an extrapolation to preterm neonates that were not studied in the Neofosfo clinical trial.

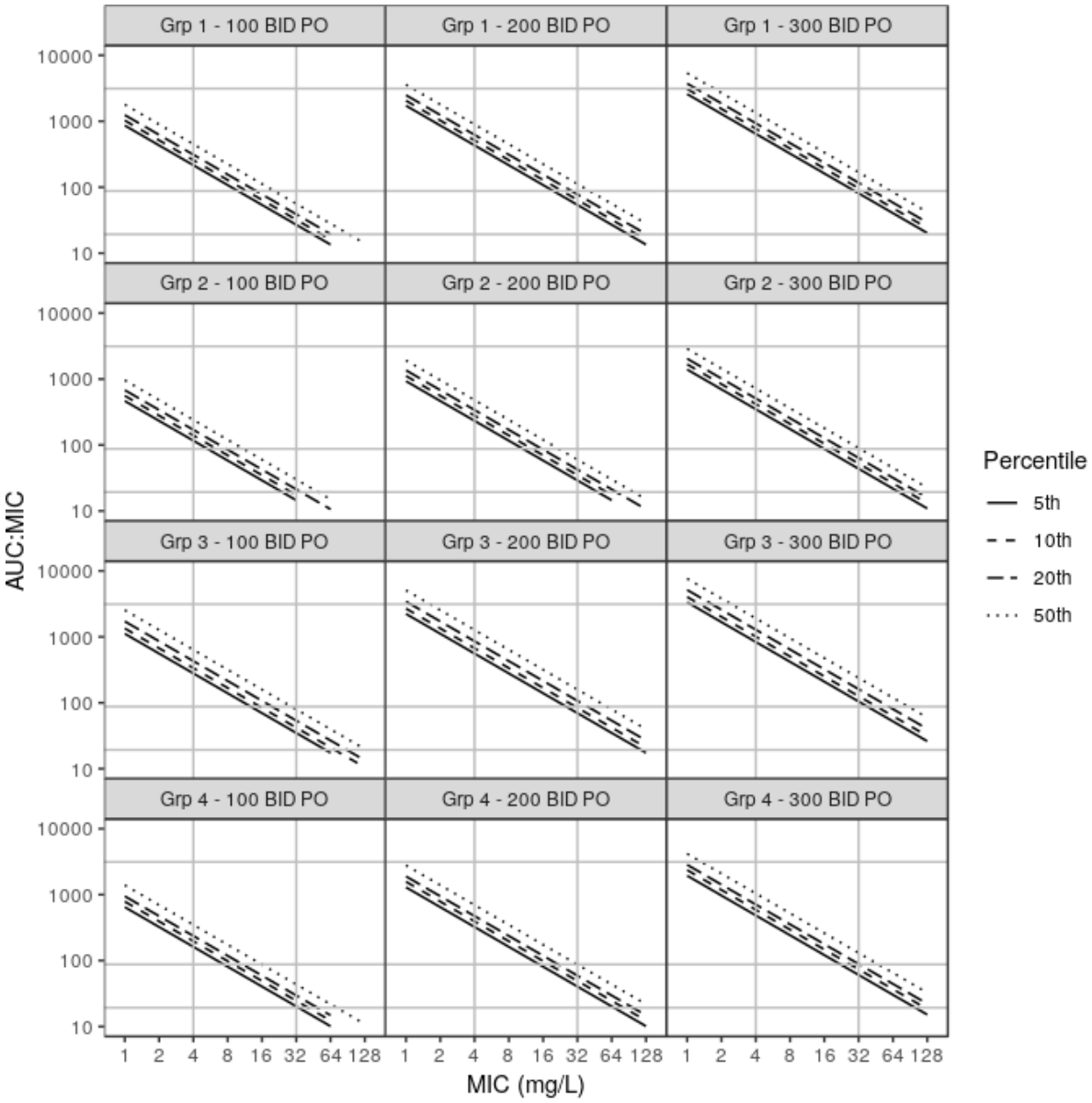

Figure 1.16: Target attainment, plasma AUC:MIC, PO dosing, neonatal subpopulations. Group 1: WT $>$ 1.5kg and PNA $\leq$ 7days (n=4391). Group 2: WT $>$ 1.5kg and PNA $>$ 7days (n=2798). Group 3: WT $\leq$ 1.5kg and PNA $\leq$ 7days (n=1534). Group 4: WT $\leq$ 1.5kg and PNA $>$ 7days (n=1277). Groups 1 and 2 represent patients similar to those fitting the Neofosfo study inclusion criteria. Groups 3 and 4 represent an extrapolation to preterm neonates that were not studied in the Neofosfo clinical trial.

1.5 Discussion

This study is the first neonatal cross-over bioavailability study of fosfomycin, and with a minimally invasive design precise population PK estimates have been derived. This model and subsequent PK simulations should prove useful in determining optimal fosfomycin dosing in neonates.

The population estimates for CL (8.94 L/h/70kg) and Vc (19.11 L/70kg) agree with PK observed in healthy adults as does the calculated β phase half-life of 2.3 hours (after 1 g IV fosfomycin to healthy adults, V = 29.7 ± 5.7 L, CL = 8.7 ± 1.7 L/hr, BW = 70.5 ± 11.1 kg, $T_{\frac{1}{2}} = 2.4 \pm 0.4$)[201]. The calculated adult equivalent γ phase half-life of 6.1 hours, resulting from the additional CSF compartment, is unlikely to be measured clinically. As such the β phase is considered the clinically relevant plasma half-life. Half-lives for the typical (median) trial neonate (WT = 2805 g, PNA = 1 day, PMA 40 weeks) for each elimination phase were longer than those predicted in a 70 kg adult: Neonate: 0.2, 5.2 and 8.7 hours. Adult: 0.4, 2.3 and 6.1 hours.

The Rhodin maturation function[120] describes the development of renal function in early life and was added to the model as fixed biological prior knowledge, as reported in previous similar neonatal PK studies[213,214]. Having adjusted clearance for WT and PMA a strong relationship between CL and PNA remained (see Figure 1.10). The $PNA_{function}$ successfully captured the increases in clearance over the first few days/weeks of life. Nephrogenesis is complete by the 34th–36th week of gestation however the functional maturation of the kidney continues through the postnatal period.[229]. The first days/weeks following birth see a rapid increase in renal blood flow as a function of cardiac output, glomerular filtration rate (GFR) and urine output, all of which are likely to contribute to the significance of PNA as a covariate on fosfomycin clearance.

SCR was not found to be a significant covariate on fosfomycin clearance. As with previous neonatal antimicrobial PK reports[213], the function published by Ceriotti *et. al.*[119] was used to account for expected postnatal changes in SCR. This function accounts for the postnatal decline in SCR due to washout of maternal creatinine and then the subsequent rise with age. Whilst SCR is often used to predict GFR in adults, the relationship between SCR and GFR in the newborn infant is complicated[121] and measured SCR in neonates $<$ 2-3 weeks old is known to be highly variable[119]. In this study 75% of babies were $<$ 3 days old on admission, and a three-fold range in baseline measured SCR was observed, both these factors are thought to have contributed to the lack of correlation between fosfomycin clearance and SCR in this study.

Oral bioavailability was estimated to be 48% (dose was nominally 100 mg/kg), and with limited first pass extraction this is likely indicative of fraction absorbed. Fosfomycin is a low molecular weight (138 g/mol), highly polar (ACD/logP -2.98) phosphonic acid derivative thereby demonstrating pH dependant solubility and ionisation in the GIT. Fosfomycin absorption is likely to be permeability limited which is consistent with the class III Biopharmaceutics Drug Disposition Classification (BDDCS) assigned by Benet et al[230]. *In vitro* intestinal permeability studies suggest fosfomycin is absorbed via both the paracellular and transcellular routes with uptake mediated, in part by the Na+ dependant phosphate transport system[231,232]. However, the fact that fosfomycin F is increased 3 fold by switching from the calcium to tromethamine salt form does indicate solubility and/or stability limitations cannot be disregarded[199,202,233]. The calcium salt form was administered in this study (Fosfocina 259mg/5 mL suspension, ERN Laboratories, Spain) which at the much lower dose of 7.5 mg/kg is reported to be only 37% bioavailable in adults[234]. Interestingly the rate of absorption also seems to be faster than reported in adults. Wenzler *et. al.*[201] report a Ka of 0.0175 /hour following administration of 3g (~43 mg/kg) tromethamine salt in adults, while this study finds a population estimate of 0.0987 /hour, >five-fold faster, which combined with a lower relative clearance due to renal immaturity means flip flop kinetics are not as prominent a feature of fosfomycin PK in the NeoFosfo population as in adults. The elevated rate and extent of absorption seen in this study compared to that reported in adults is attributed to increased permeability of the immature intestinal barrier in neonates < 7days old[62,63] and higher luminal concentrations of fosfomycin.

The final population estimate of CSF UPTK in the NeoFosfo trial population was 0.32 (%RSE = 12.0, 95% CI = 0.27-0.41), Nau et al previously reported that in adults with uninflamed or mildly inflamed meninges fosfomycin AUC_{CSF}/AUC_S was 0.18 (0.09 - 0.27). Since progression from sepsis to meningitis in neonates can be rapid, and less overt than in older children, fosfomycin's good CSF penetration in this population is supportive of its potential role in empiric regimens for neonatal sepsis.

When considering the TA results, it is important to highlight the difference between the median PNA of the hypothetical population and the NeoFosfo trial population, 5 (mean = 10) versus 1 (mean = 3) days respectively, as within a given individual, clearance is predicted to increase by 36% over this time frame (based on just this increase in PNA). A caveat specific to the oral TA predictions concerns the use of a constant Ka in all subjects. Following oral dosing the Ka in an individual will

have a significant impact on the shape of the oral PK profile and therefore this does introduce an element of additional uncertainty compared to the IV TA predictions.

Further *in vitro* work to define target AUC:MIC ratios required to achieve a 2 log kill against pathogens typically responsible for neonatal sepsis is needed as is definition of MIC breakpoints that are relevant for bacteraemia and meningitis.

In conclusion the Neofoso study is the first neonatal cross-over bioavailability study of fosfomycin, and the model and subsequent PK simulations that have been derived from the study should prove useful in determining optimal fosfomycin dosing in neonates. Whilst the NeoAMR demographic data was used to simulate pre-term neonates and those weighing <1500g, a neonatal sub-population not represented in the model building dataset, the mechanistic covariates used with biological priors on allometric weight and PMA scaling give some confidence in this extrapolation. The TA simulations that have been produced assume that the observed PNA maturation effect will follow a similar trajectory in smaller neonates (<1500g), and whilst this assumption may be reasonable, it could only be fully confirmed by collecting data in this population. However, regardless of GA and/or weight, this analysis has found that reducing the dose of fosfomycin in the first week of life due to short-term PNA maturation is required, and this finding may also be applicable to other drugs for which elimination is predominantly mediated through passive renal filtration. The model and target attainment simulations presented here can be used to aid selection of a neonatal IV fosfomycin dose based on an infant's PMA, PNA and WT and an oral step down dose personalised using likely pathogen MIC at 48 hours.

Chapter 2

Benznidazole - oral pharmacokinetics in children

2.1 Introduction

Benznidazole (BNZ) is the first-line treatment for American trypanosomiasis (Chagas Disease), a condition caused by the parasitic protozoan Trypanosoma cruzi[235]. An estimated 6 to 7 million people worldwide are infected with T. cruzi. Chagas disease is found mainly in endemic areas of 21 continental Latin American countries, where it is mostly transmitted when humans come into contact with faeces and/or urine of infected blood-sucking triatomine bugs (vector-borne transmission).

Chagas disease is named after Carlos Ribeiro Justiniano Chagas, a Brazilian physician and researcher who discovered the disease in 1909. Chagas disease presents in two phases. The initial acute phase lasts for about two months after infection. During the acute phase, a high number of parasites circulate in the blood, but in most cases, symptoms are absent or mild and unspecific. In less than 50% of people bitten by a triatomine bug, characteristic first visible signs can be a skin lesion or a purplish swelling of the lids of one eye. Additionally, they can present with fever, headache, enlarged lymph glands, pallor, muscle pain, difficulty in breathing, swelling, and abdominal or chest pain. During the chronic phase, the parasites are hidden mainly in the heart and digestive muscle. One to three decades later, up to 30% of patients suffer from cardiac disorders and up to 10% suffer from digestive (typically enlargement of the oesophagus or colon), neurological or mixed alterations. In later years the infection in those patients can cause the destruction of the heart muscle and nervous system, consequent cardiac arrhythmias or progressive heart failure and sudden death.

While Chagas disease was once entirely confined to the South Americas, in recent decades the epidemiological pattern of the disease changed from a rural to a mostly urban disease, mainly due to population mobility, urbanization and emigration. As a consequence, increased number of cases have been detected in Canada and the United States of America, and in many European and some African, Eastern Mediterranean and Western Pacific countries. Due to the high number of people who remain undiagnosed or untreated, in 2018 the WHO estimated that 75 million people were at risk of infection, see Figure 2.1[236].

BNZ was originally registered as a treatment for Chagas disease by Roche (Hoffman-LaRoche) in the 1970s/80s and was licensed in Brazil, Argentina, Bolivia, Uruguay, Peru, Nicaragua, and Japan as either as Radanil®, Ragonil®, or Rochagan® (100 mg and 50 mg BNZ tablets). However, after donating all commercial rights and the technology to manufacture BNZ to the Brazilian government as a "generic"

version of Roche's product, Roche withdrew its registration. Latterly BNZ tablets were manufactured by Pernambuco State Pharmaceutical Laboratory (Laboratório Farmacêutico do Estado de Pernambuco; LAFEPE), which is a public laboratory in Brazil, with this formulation often referred to in the literature as the LAFEPE product[237].

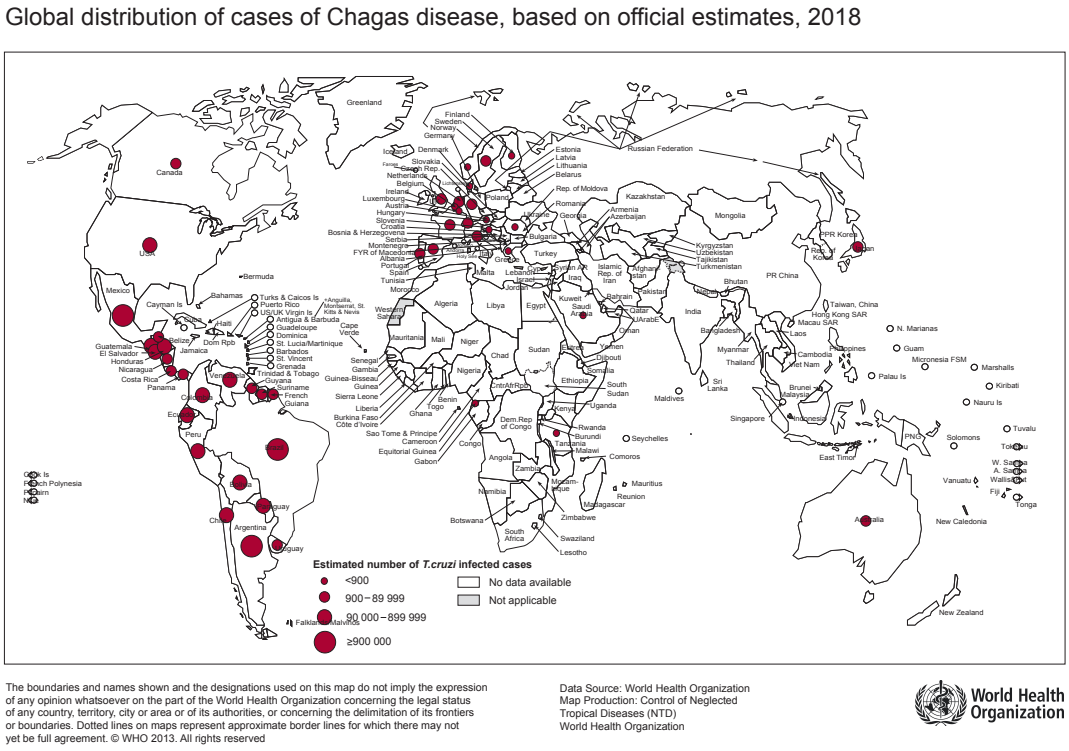

Figure 2.1: Estimated global distribution of chagas disease.

After the primary manufacturer, Hoffmann-La Roche, suspended production and transferred the technology and license to Lafepe Labs in Brazil in 2003, significant supply shortages of BNZ were seen. In 2011, a 12.5 mg paediatric dosage form (manufactured by Lafepe Labs and to not for profit organisation Drugs for Neglected Diseases initiative (DNDi)) was registered by the Brazilian Health Surveillance Agency to further improve the treatment of paediatric Chagas disease. Since 2012 Elea Laboratory in Argentina has been producing benznidazole and in 2014, Elea started a joint project with Liconsa labs (Chemo Group) in Spain.

More recently in 2017 Chemo Research, S.L. c/o Exeltis USA, Inc. were granted approval by the FDA (NDA 209570) to market their 100 mg and 12.5 mg BNZ tablets for the treatment of Chagas disease in paediatric patients 2 to 12 years of age, with the sponsor committing to conducting a prospective, single-arm, multicentre trial, with

historical controls, to evaluate safety, efficacy, and pharmacokinetics of benznidazole tablets for treatment of Chagas disease in children, with trial completion by the end of 2025. The current US paediatric dosing recommendations are a weight based total daily dose of 5 mg/kg to 8 mg/kg of orally administered BNZ given in two divided doses separated by approximately 12 hours for a duration of 60 days[238].

Wiens *et. al.* published the first meta-analysis of benznidazole PK studies in 2016 in an effort to improve estimates of the basic pharmacokinetic properties of benznidazole[239]. A total of 9 adult PK studies (healthy volunteers and patients) were included in their analysis. No single-dose BNZ PK studies in children were identified. Three studies contained individual patient-level data from adults following a single benznidazole dose of 100 mg, however only one was a published study[240]. Three studies contained limited individual patient-level data from multidose studies. Of these, only the 1980 study by Raaflaub[241] provided data pertinent to their primary analyses. One additional study contained some further high dose single-dose summary data. This was a study of a single dose of 25 mg/kg in oncology patients[242]. A further two studies evaluated benznidazole, using typical therapeutic doses, in a sample of patients with Chagas disease, of these only one was published[243]. Importantly Weins *et. al.* found that the primary oral PK parameters of interest, including AUC, Cmax, Tmax, kel, V/F, and CL/F, showed remarkable consistency between the studies evaluated. The overall across study estimates of CL/F, V/F and Ka were 2.04 L/h (95% credibility interval (CrI) 1.77 to 2.32 L/h), 39.19 L (95% CrI, 36.58 to 42.17 L) and 1.16 /hr (95% CrI, 0.59 to 1.76 /hr) respectively. Of note is that this consistency across studies is observed across adult populations (healthy vs patients) and also across the different suppliers of BNZ tablets which suggests absorption of BNZ is not significantly influenced by either BNZ solubility or dissolution rate. This observation is consistent with a lack of significant food effect on BNZ PK after dosing a single 100 mg tablet to health adult volunteers (n=18) under fasting and fed (high fat breakfast) conditions[244].

In 2017 Molina *et. al* evaluated the PK of Abarax® (100 mg BNZ tablets prepared by Laboratorio Elea, Argentina) in 8 health volunteers. Rich PK data was obtained and using NCA median CL/F was derived 2.07 L/hr (2.4 to 1.7 L/hr IQR). The publication paid significant attention to an apparent sex effect however the CL/F estimates for men versus women appear to have been incorrectly reported and the apparently higher AUC in women is likely to be entirely due to the sex differences in BW, mean BW was 81.15 kg and 57.25 kg in the male versus female volunteers respectively[245].

With respect to efficacy BNZ is highly effective in curing Chagas disease if given soon after infection (at the onset of the acute phase), including in cases of congenital transmission, however efficacy appears to diminish the longer a person has been infected and adverse reactions are known to be more frequent in older patient groups, with up to 40% of adults reporting unwanted side effects and consequently poor treatment compliance. Like other well known nitroheterocyclics (eg. metronidazole) BNZ requires bioactivation or enzymatic reduction of the nitro group to form the reactive species that exerts the desired antimicrobial effect, see Figure 2.2[246,247].

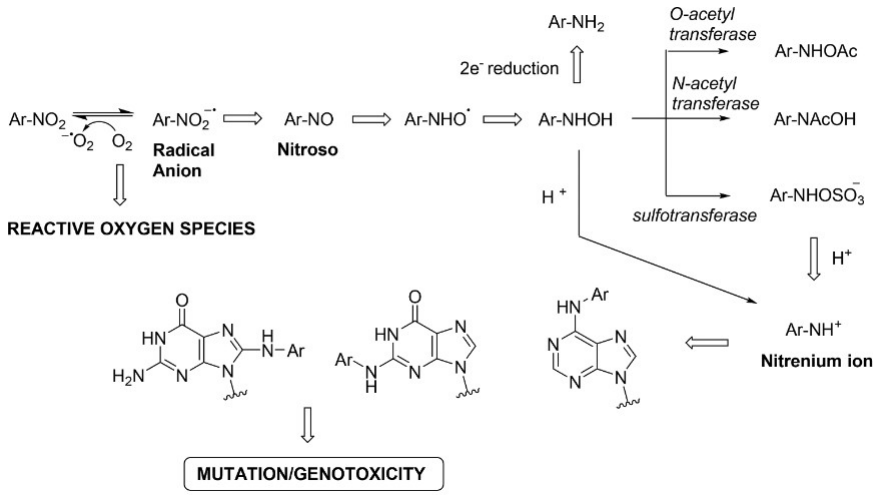

Figure 2.2: Mutagenic pathways of nitroheterocyclics, reproduced from Nepali et al 2019.

The recent BENDITA trial (which evaluated the efficacy and safety of new benznidazole monotherapy regimens and combinations with fosravuconazole in adult patients with chronic Chagas disease) concluded that BNZ induced effective antiparasitic response, regardless of treatment duration, dose, or combination with fosravuconazole, and proposed that shorter or reduced dose regimens of BNZ could substantially improve treatment tolerability and accessibility[248]. However, the conclusions did receive some criticism and requests for further analysis of the pharmacokinetic results (not presented) in the context of efficacy and safety[249].

While the exposure-response relationship for BNZ is not clearly defined or understood some have suggested that the lower than expected (based on allometric scaling) systemic exposure seen in children aged 2-12 years may be responsible for the reduced occurrence of side effects reported in paediatric patients on BNZ therapy. Sparse pharmacokinetic data collection from patients aged 2-12 years (clinical trial NCT00699387) was previously analysed using population PK methods by Altcheh

et. al[185]. This study collected at least 3 PK samples per child, with some children contributing levels after a single dose and some after repeat dosing of 5-9 mg/kg/day (using q12hr dosing frequency) of multiple and/or fractioned 100mg Radanil tablets. The paediatric PK dataset included 117 plasma concentrations from 38 children and was modelled alongside adult PK data extracted from the literature[240,241] using a one-compartment model with first order absorption. The final adult adjusted (assuming age is 40 years and WT 70 kg) estimates for Ka, V/F and CL/F were 0.294 /hr, 43.8 L and 1.61 L/hr. Inter-individual variability was estimated for all fixed effects and proportional residual error utilised; 246%, 27.1%, 43.4% and 27% respectively. Both age and weight were included in the model as covariates although somewhat unusual parameterisation was employed to scale for these effects, see Equations (2.1) to (2.2).

$$\mathrm{V/F_i} = -5.73 + 0.707 \times \mathrm{WT_i(kg)} \tag{2.1}$$

$$\mathrm{CL/F_i} = 0.418 + 0.0049 \times \mathrm{AGE_i(years)} + \left(\frac{\mathrm{WT_i}}{70}\right)^{0.0743} \tag{2.2}$$

If the adult BNZ CL estimated by Altcheh *et. al.* is scaled using simple allometric approaches using a fixed exponent of 0.75 then assuming F is not different between adults and children the CL/F in a 16kg, 3 year old would be predicted to be 0.53 L/hr however Altcheh's model, which appears to describe the paediatric PK, would predict a typical CL/F of 1.33 L/hr, approximately 2.5 fold higher than expected based of standard allometric scaling of size (BW) alone. Unfortunately, in the absence of IV BNZ PK data in either adults or children from this analysis it is difficult to delineate whether the age effect is due to differences in CL or oral F, which along with Fh (fraction surviving first pass metabolism) and Fg (fraction surviving gut wall metabolism) captures the fraction of drug absorbed into the enterocyte (Fa).

Unfortunately, there are a number of fundamental PK knowledge gaps that exist for BNZ which make understanding the reasons for this apparent disconnect between adult and paediatric exposure challenging. Firstly, no human IV PK has ever been published or filed with regulators which means human BNZ clearance in adults is not known and as a result human/adult F has never been determined. Secondly while a human 14C-BNZ ADME study (radiolabelled mass balance study) has been performed (clinical trial NCT03739541, completed in Nov 2018, sponsored by Exeltis)[250] and a finalized study report filed with the FDA in March 2019 (completion of this study was a requirement of the FDA approval; NDA209570 in 2017) the results are yet to appear in the scientific literature[251] or updated prescribing information[238].

Currently a fairly uninformative statement regarding excretion is made "Benznidazole and unknown metabolites are reported to be excreted in the urine and faeces". There is also no clinical trial data evaluating the impact of hepatic or renal impairment on BNZ PK and only until very recently there was a complete absence of any contemporary clinical drug-drug interaction studies.

While no human IV PK data is published for BNZ, this data is available for metronidazole, a structurally similar nitroimidazole. Houghton previously reported that in nine healthy females (average weight = 56 kg, average age = 30 years) metronidazole plasma AUC after a 500 mg IV dose was 151 ± 42 $mg * h/L$, therefore total clearance is 3.31 L/hr[252]. Estimating passive renal filtration based on the product of GFR (typical healthy adult GFR ~ 120 mL/s (7.2 L/hr)) and a fraction unbound in plasma of 0.89[253] renal clearance might be expected to be approximately 6.4 L/hr, which is ~2-fold higher than the total plasma clearance reported by Houghton *et. al.*. In fact Houghton reported that only 10% of the metronidazole dose was recovered unchanged in urine[252]. Since the observed total plasma clearance was approximately half the predicted renal clearance based on $Fup \cdot GFR$ even assuming that hepatic clearance is negligible this suggests a significant, ≥ 50%, of drug cleared by passive renal filtration appears to be re-absorbed from urine. In a subsequent metronidazole PK study to evaluate the impact of renal impairment on metronidazole clearance, Houghton *et, al,* reported total clearance in healthy male volunteers (n=9, average body weight = 75 kg, average age 32 years) to be 72 ± 16 mL/min (4.32 L/hr) and renal clearance to be 6.8 ± 2.5 mL/min (0.41 L/hr). Therefore, in that study hepatic clearance accounted for 91.4% of the total metronidazole clearance[254].

In 2021 Riberio *et. al.* report on the interaction between E1224 (a prodrug of ravuconazole) and BNZ after a single-oral dose of 2.5 mg/kg BNZ in 28 healthy male subjects. While they conclude there is no clinically relevant interaction the AUC_{inf} ratio is reduced to 0.83 in the presence on E1224 (90% CI 0.80-0.87)[255]. A similar 'not clinically relevant' (<20%) effect of coadministration of fosravuconazole on BNZ CL/F was also reported by Assmus *et. al.* in a recent conference abstract/poster[256]. It should be highlighted that this information on the 'DDI' between fosravuconazole and BNZ was obtained following PopPK analysis of sparse PK data taken during a combination arm of the BENDITA efficacy trial[248]. While these interactions are considered not 'clinically relevant' they may be potentially informative when trying to mechanistically understand BNZ's ADME properties. There are also older reports of drug-drug interactions between BNZ and other nitroimidazoles such as misonidazole (MISO), with nitrosoureas such as lomustine (historically referred to as CCNU

in the scientific literature), with BNZ pre-treatment being shown to increase CCNU exposure (plasma AUC) after 20 mg/kg ip dosing to mice by 4-7 fold[257] and to increase the half-life of CCNU and its active hydroxylated metabolites from 2.6 to 5.2 hours in 26 human cancer patients[242]. The authors Lee *et. al.*[257] link the extent of the DDI between the nitroimidazole analogue and CCNU to the lipophilicity of the nitroimidazole but this is more likely to be a result of either transporter or enzyme inhibition/induction by BNZ. BNZ is reported to be a P-gp substrate[238] however beyond this limited information exists regarding the involvement of transporters in BNZ disposition or on the specific metabolic pathways involved in BNZ clearance. While historically benznidazole pharmacokinetics were somewhat neglected, recent reports that BNZ related toxicities are less profound in children has prompted an increasing interest in understanding the age-related differences in BNZ oral bioavailability.

For compounds such as BNZ where only oral PK data is available and therefore there is uncertainty regarding the contribution of F and CL to systemic exposure following oral dosing, PBPK can be an extremely valuable tool as the extent of absorption or fraction of dose absorbed (Fa) is predicted based on inherent physical chemical properties such as pKa, lipophilicity, solubility and permeability. However, the process of PBPK model development requires collation of a diverse set of compound specific *in-vitro* and *in-vivo* pre-clinical and clinical ADME data, as it is this data that underpins model parameterisation.

2.2 Aims and objectives

The aim of this study was to use PopPK and PBPK modelling methods to develop and test a mechanistic hypothesis for the previously reported age-dependent changes in BNZ oral bioavailability (apparent clearance)[185]. Specific objectives can be split into 4 categories.

1. Quantify the effect of age on oral bioavailability (CL/F)

   1a. Conduct a population PK analysis of adult and paediatric benznidazole PK data using conventional allometric approaches, thereby allowing unambiguous delineation and quantification of the apparent effect of age on CL/F.

   1b. Interrogate the PopPK model to generate insight regarding the source of the age effect, oral absorption or clearance?

2. Define initial PBPK parameter estimates and modelling strategy.

   2a. Mine *in-vitro* physicochemical and ADME data from published scientific literature, US regulatory documentation and in-house Roche and DNDi data.

   2b. Conduct a retrospective analysis and PBPK modelling of published preclinical intravenous and oral dog[258] and rabbit[259] PK data.

   2c. Use ADMET Predictor (v10.4-05, developed by SimulationPlus[260]) to predict compound specific ADME properties based on the 2D chemical structure.

   2d. Predict human BNZ plasma clearance based on IVIVE and cross-species allometry.

   2e. Translate the non-pregnant PK-Sim IV Metronidazole (MNZ) model presented by Dallmann *et al.*[253] into GastroPlus.

3. Develop and verify an adult PBPK model

   3a. Develop an adult human PBPK model that describes single and multiple dose PK data over a dose range that tests the underlying model assumptions/mechanisms determining dose proportionality.

   3b. Verify the adult PBPK model using an 'external' BNZ PK dataset (one that was not used during objective 3a for parameter fitting).

4. Extrapolate the adult PBPK model to simulate paediatric PK.

   4a. Define a mechanistic hypothesis that can be implemented in the PBPK model to explain the apparent lower CL/F seen in children compared to adults.

   4b. Analyse the available paediatric PK data and define appropriate sub-populations based on age and weight.

   4c. For each paediatric sub-population scale the physiological settings in the adult PBPK model and simulate the paediatric PK.

   4d. Refine as necessary the paediatric physiological assumptions to reconcile the observed paediatric PK.

The modelling workflow is outlined in Figure 2.3.

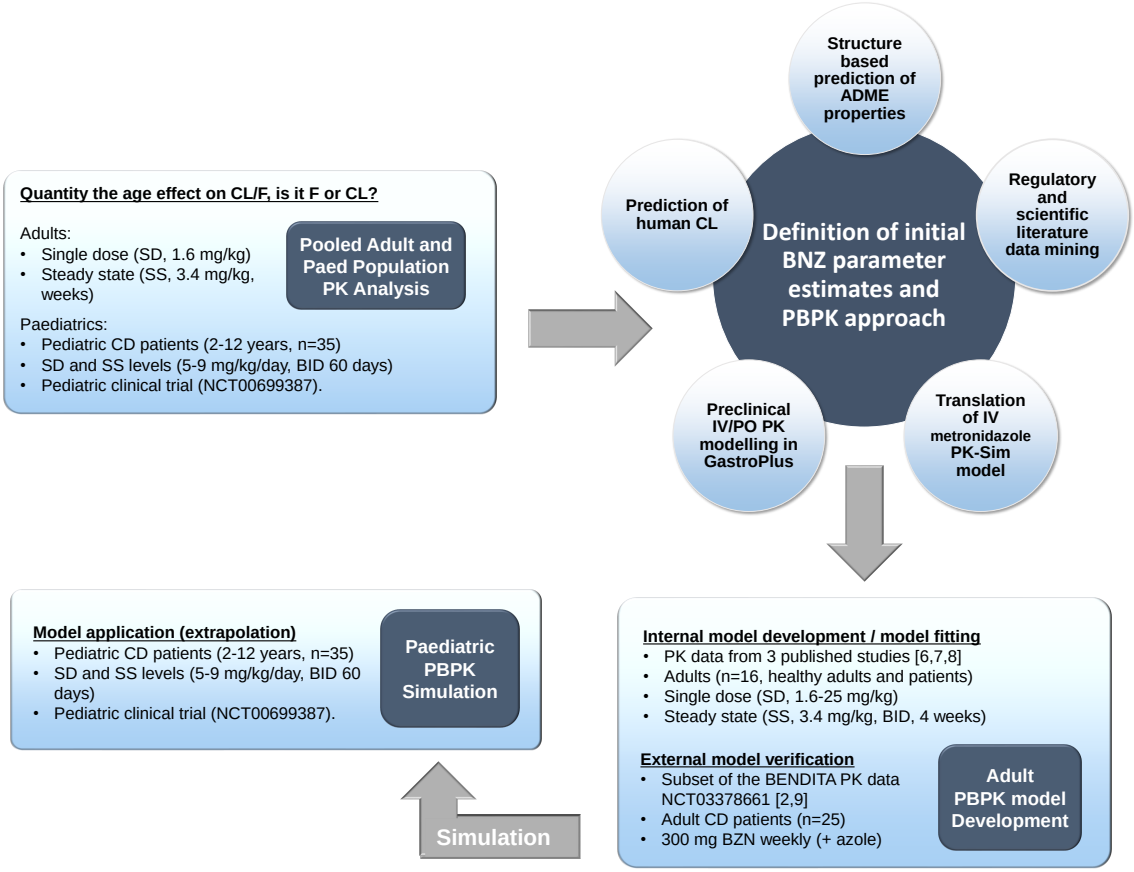

Figure 2.3: Overview of modelling workflow/strategy

2.3 Methods

2.3.1 Quantifying the effect of age (objective 1)

To quantify the age-dependent changes in CL/F, BZN plasma concentration-time data was pooled from children aged 2-12 years (Altcheh 2014, www.clinicaltrials.gov; NCT00699387)[185] with published PK data collected in adult populations (healthy volunteers and Chagas disease patients; Raaflaub 1979 and Raaflaub 1980)[240,241]. The pooled paediatric and adult BNZ PK data was then modelled using the population approach in NONMEM v7.4 (ICON Development Solutions, Ellicott City, MD)[212]. Both the adult and paediatric datasets include single dose and steady state PK data, and the study details are summarised in Table 2.1.

Table 2.1: Clinical BNZ PK data analysed using the poulation approach

Study	**Regimen**	**Dose (mg/kg)**[a]	**Population**	**WT/Age (kg)/(yrs)**[a]	**Subjects/ Samples**
Raaflaub 1979	single dose	1.66	Heathy Volunteers	60.5 / 23.0	6 / 62
Raaflaub 1980	repeat dose q12hr	3.50	Chagas patients	56.0 / 37.5	8 / 97
Altcheh 2014[b]	repeat dose q12hr	3.25	Chagas patients	22.0 / 5.8	35 / 109

[a] Median dose, weight and age.

[b] NCT00699387 individual subject data shared by C.Cruz and F.García-Bournissen.

The adult PK published by Raaflaub *et. al.* in 1 979[240] comprised single dose PK in six healthy volunteers, subjects received a single 100mg Radanil tablet. In the repeat dose study published by Raaflaub *et. al.* in 1 980[241] eight adult Chagas disease patients were dosed twice a day with a nominal 3.5 mg/kg per dose. In the paediatric study published by Altcheh *et. al.*[185] children were eligible for inclusion if they were diagnosed with Chagas disease and aged 2-12 years. The study design included single and multiple dose PK sampling following a regimen of 5-9 mg/kg BID dosing for 60 days. Children were randomised to either group A, B or C and at least 3 PK samples were collected from each child. In group A PK samples were taken at 0-2h, 2-6h and 6-12 h post the first d ose. In group B trough, 0-2h and 2-6h samples were taken on day 3-59 (steady state PK) and in group C PK samples were taken between 12-18h, 18-24h and 24-36h after the patient's last dose on day 60. The dosage form administered was the 100 mg Radanil tablet and tablet fractionation was necessary in some children. This paediatric dataset included single dose PK in 11 children (33 observations) and steady state PK data in 24 children (76 observations). The

baseline median [range] age and weight of children was 5.83 [2.1 - 12.0] years and 22.0 [11.5 - 50.0] kg and the median [range] dose administered was 3.25 [2.5 - 4.4] mg/kg. Visualization of the baseline age, weight and dose administered in the paediatric PK study published by Altcheh *et. al.* can be found in Figure 2.4.

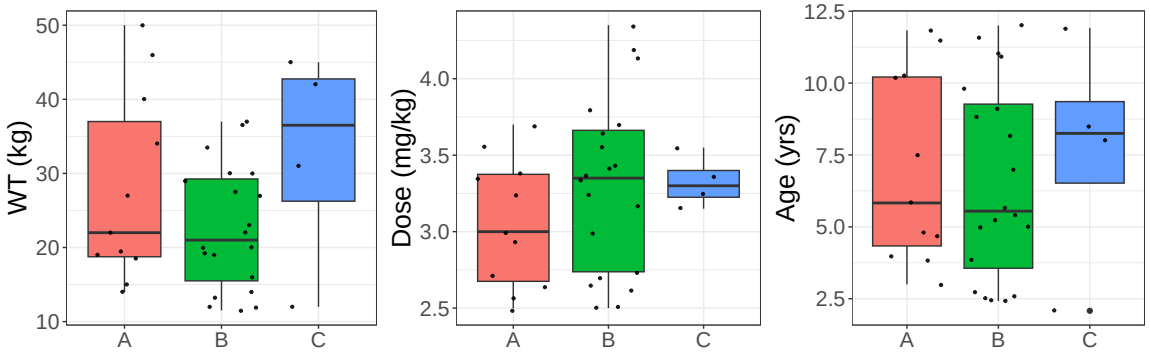

Figure 2.4: Visualisation of the baseline weight, age, and dose (mg/kg) administered in the paediatric PK study published by Altcheh 2014.

For the adult PK studies, NONMEM modelling datafiles were constructed using individual subject demographic, dose and concentration-time plasma levels transcribed from the original publications[240,241]. For the paediatric study, the raw dose history, demographic and bioanalytical data were shared by collaborators F.García-Bournissen and C.Cruz, the former of whom was the principal investigator on the original paediatric study (NCT00699387)[185].

The free statistical programming software R[217] was used to clean, visualise, and prepare the NONMEM modelling datafile. PSN and Xpose were used during PopPK data analysis[218].

To allow delineation of age effects on PK parameters, weight was included *a priori* on CL/F and V/F using fixed exponents of 0.75 for clearance and 1 for V/F, see Equation (2.3). All model parameters were centred on a mature adult weighing 58 kg as this was the median adult weight having pooled the two adult studies/populations[240,241].

$$\mathrm{CL_i} = \mathrm{CL_{std}} \times \left(\frac{\mathrm{WT_i}}{58}\right)^{0.75} \quad \text{and} \quad \mathrm{V_i} = \mathrm{V_{std}} \times \left(\frac{\mathrm{WT_i}}{58}\right) \tag{2.3}$$

The effects of age on CL/F were tested according to Equation (2.4). This maturation function estimates the fractional change in CL/F compared to adults at birth (θ_M)

and the rate of change in CL/F (θ_N).

$$\mathrm{CL_{mat}} = \theta_\mathrm{M} + (1 - \theta_\mathrm{M}) \times \left(1 - \mathrm{e}^{-\mathrm{AGE}\times\theta_\mathrm{N}}\right) \tag{2.4}$$

Age was also tested as a covariate on the population estimate of absorption rate (Ka) using a sigmoidal Hill function as shown in Equation (2.5), the Hill exponent (θp) and time to 50% mature (θ_q) are both estimated.

$$\mathrm{Ka_{mat}} = \frac{\mathrm{AGE_i}^{\theta_\mathrm{P}}}{({\theta_\mathrm{q}}^{\theta_\mathrm{P}} + \mathrm{AGE_i}^{\theta_\mathrm{P}})} \tag{2.5}$$

2.3.2 Definition of initial PBPK parameter estimates and modelling strategy (objective 2)

The BNZ dose-exposure relationship is poorly understood, and knowledge gaps exist regarding BZN pharmacokinetic (PK) and ADME properties. Because of this and because no prior PBPK model has ever being presented for BNZ, definition of initial parameter estimates and the PBPK modelling strategy/approach incorporates evidence from several sources.

2.3.2.1 Published ADME data review (objective 2a)

Standard literature searching techniques were performed using PubMed and also using PKPDai. PKPDai is a new open source web-based tool (`https://pkpdai.com/`) developed to process PK literature through Natural Language Processing approaches[261]. PKPDai searches for the following terms: benznidazole, 2-nitroimidazole, and 5-nitroimidazole were performed. US regulatory information was accessed through `Drugs@FDA` (www.fda.gov/drugsatfda) which contains submission information for FDA approved drugs.

2.3.3.2 PBPK modelling of pre-clinical IV/PO PK (objective 2b)

The lack of human BNZ IV PK data means that in addition to human clearance, tissue distribution and oral bioavailability (F) are also unknown. PBPK modelling of published pre-clinical intravenous and oral PK data (rabbit[259] and dog[258]) was performed to inform initial estimates of intestinal effective permeability (Peff), and

importantly selection of an appropriate tissue/plasma partition coefficient (Kp) calculation method. For the rabbit PK study individual animal bioanalytical data (both plasma and urine) has been shared by M.Davanco[259]. The dog plasma-concentration time data was extracted from the source publication using a web-based application called WebPlotDigitizer version 4.5[262].

The intravenous and oral pre-clinical PK datasets analysed in this part of the study are summarised in Table 2.2. NCA and data visualisation of this data was performed in R[217] and all physiologically based pharmacokinetic modelling (PBPK) was performed using GastroPlus v9.7 (Simulations Plus,Inc.)[263].

Table 2.2: Pre-clinical IV and PO PK data modelled using GastroPlus

Study Details	**Rabbit**	**Dog**
Route	IV / PO / PO	IV / PO
Dose (mg/kg)	3.3 / 4.2 / 33.2	5 / 25
Matrix	plasma and urine	plasma
No Animals	7	2 (crossover)
Weight Range (kg)	2.5 to 3.5	20, 28
Study	Davanco 2016[a]	Workman1984

[a] Individual animal dose information and bioanalytical data in plasma and urine was shared by M.Davanco

2.3.3.5 Structure based parameter predictions using ADMET Predictor (objective 2c)

ADMET (Absorption, Distribution, Metabolism, Elimination and Transporter) Predictor (AP) is a cheminformatics quantitative structure-activity relationship (QSAR) platform developed by Simulations Plus (version 10.4)[260]. Using classification and regression models that are established and available to users of the software it is possible to predict, based on just the chemical structure, physico-chemical, transporter and metabolism properties. This was done for BNZ and a selection of structurally similar 2- and 5- substituted nitroimidazoles, see Figure 2.5 for the 2D-chemical structures of the compounds that were characterised using ADMET Predictor.

The transporter classification models within ADMET Predictor were developed by SimulationPlus to predict whether a compound is a substrate for P-gp, BCRP, OATP1B1, OATP1B3, OAT1, OAT3, OCT1 and OCT2. If the prediction accuracy is $< 60\%$ this indicates the compound does not lie within the applicability domain of the model and *in-vitro* experimentation is recommended. The "Metabolism Module" in ADMET Predictor also provides substrate classification and site of metabolism

models for nine human CYPs (1A2, 2A6, 2B6, 2C8, 2C9, 2C19, 2D6, 2E1 and 3A4) and nine human UGT isoforms (UGTs 1A1, 1A3, 1A4, 1A6, 1A8, 1A9, 1A10, 2B7 and 2B15).

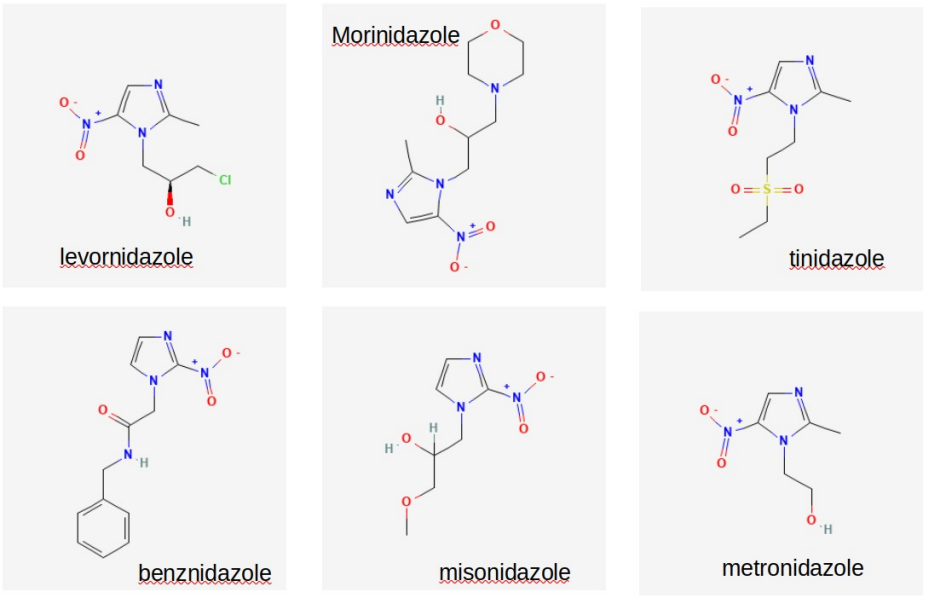

Figure 2.5: Nitroimidazoles; anti-cancer and anti-infective agents

ADMET Predictor includes artificial neural network ensemble based regression models that can predict the unbound *in-vitro* human microsomal (mic) and hepatocyte (hep) intrinsic clearance ($CLint_u$), see Figure B.3 in the Appendix for the associated GOF plots (observed versus predicted parameters). In the absence of measured *in-vitro* intrinsic clearance these can be scaled to *in-vivo* intrinsic liver clearance based on a human adult liver weight, and and either microsomal content or number of hepatocytes. AP predicted fraction unbound in plasma F_{up}, AP predicted blood to plasma ratio R_{bp} and an assumed human fasted liver blood flow (Q) are then incorporated using Equation (2.6) to predict *in-vivo* hepatic clearance CL_h . Where CL_h is the *in-vivo* hepatic plasma clearance, CL_b is *in-vivo* hepatic blood clearance, R_{bp} is the blood to plasma ratio, Q is liver blood flow, $CL_{int,u}$ is the *in-vivo* unbound intrinsic liver clearance and F_{up} is the fraction unbound in plasma.

$$\mathrm{CL_h} = \mathrm{R_{bp}} \times \mathrm{CL_b} = \mathrm{Q} \times \left[\frac{\mathrm{CL_{int,u}}}{\mathrm{CL_{int,u}} + \mathrm{Q} \times \frac{\mathrm{R_{bp}}}{\mathrm{F_{up}}}} \right] \tag{2.6}$$

AP also implements the Extended Clearance Classification System (ECCS) proposed by *Varma et al*[264] using predicted physicochemical properties and predicted passive

membrane permeability. The AP implementation of the ECCS was used to predict the predominant clearance mechanism for BNZ and the structurally similar analogues presented in Figure 2.5.

In addition to structure-based prediction of *in-vitro* microsomal and hepatocyte $CLint_u$, kinetic regression models that included prediction of Km, Vmax, and $CLint_u$ for the five major CYPs; 1A2, 2C9, 2C19, 2D6, 3A4 have been developed by SimulationsPlus. These models have been developed using data from in vitro metabolic studies in cloned virus infected cells expressing human enzyme-specific microsomes (recombinant CYP experiments; rCYPs). The visual GOF plots (observed versus predicted parameters) for the rCYP1A2 kinetic models included in ADMET Predictor are included in Appendix Figure B.4. These models were also used to predict CYP liabilities for BNZ and the structurally similar analogues presented in Figure 2.5.

2.3.3.3 Prediction of human clearance (objective 2d)

Estimating human BNZ clearance is a key requirement to developing a PBPK model. Due to the absence of human IV PK data, there are three methods available to predict BNZ human hepatic clearance (CL_h); *in-vitro/in-vivo* extrapolation (IVIVE) of either i) *in-vitro* measured or ii) *in-silico* predicted unbound intrinsic clearance ($CL_{int,u}$)) as described in Equation (2.6), and iii) cross-species allometry. The latter also requires assumptions about the hepatic:renal contribution to total clearance. These three methods were evaluated to define an initial estimate of hepatic clearance that was ultimately refined during PBPK model development (parameter fitting).

Extrapolation of measured *in-vitro* metabolic stability data (IVIVE) alongside measured *in-vivo* pre-clinical clearance (allometry) is widely accepted as the standard way to predict human metabolic clearance[265]. The *in-vitro* methods typically used to study hepatic metabolism include hepatocytes (isolated cells of liver) or microsomal preparations which are extracted from liver homogenates. A compound is incubated with hepatocytes (or microsomes) and the disappearance of the drug is monitored. This disappearance is called intrinsic clearance (CLint). The hepatocyte clearance or microsomal clearance can be converted to hepatic clearance with appropriate scaling factors, although there is often a disconnect between predicted human clearance based on human liver microsomes (HLM) and human hepatocyte (HH) $CL_{int,u}$. Published BNZ turnover data as measured in *in-vitro* human microsomal or hepatocyte based assays are also evaluated.

Finally cross-species allometric scaling[266,267] of total plasma clearance as measured in four pre-clinical species; mouse, rat, rabbit and dog[258,259,268] was performed. The dog, rat and mouse IV PK data was extracted from the respective publications using the web-based graph digitiser tool (Webplot digitiser)[262], the individual rabbit PK data was shared by M.Davanco[@ 259]. See Table 2.3 for a summary of the pre-clinical IV studies that were included in the cross-species allometric prediction of human clearance. Individual data is presented for n=2 dogs but for rat and mouse only an

Table 2.3: Published pre-Clinical IV PK data utilised in cross-species allometric scaling to predict human BNZ clearance

	Mouse	**Rat**	**Rabbit**	**Dog**
Route	IV	IV	IV	IV
Dose (mg/kg)	65 / 32.5	0.2	3.3	5.0
Matrix	plasma	blood	plasma	plasma
No Animals	NS	4	7	2
Weight Range (kg)	0.02 to 0.035	0.18 to 0.25	2.5 to 3.5	20, 28
Study	Workman 1984	Morilla 2004	Davanco 2016	Workman1984

average Cp-time profile is presented. The mouse IV PK study does not specify (NS) the number of animals used, while the rat study utilized 4 animals; group1 generated the data out to T=4hr and group 2 post T=4 hrs which accounts for the unusual PK profile s hape. In the rat, BNZ concentrations are reported in blood as opposed to plasma, blood to plasma ratio (Rbp) is assumed to be 1 as reported for human[240].

Based on the findings of Tang *et. al.*[269] the measured pre-clinical clearance was corrected for species differences in the fraction of BNZ unbound in plasma (Fup). In Equations (2.7) and (2.8) CL_u is the unbound plasma clearance and the terms 'a' and 'b' represent the intercept and slope of the linearised relationship between weight (WT) and CLp_u.

$$\mathrm{CLp_u} = \frac{\mathrm{CLp}}{\mathrm{F_{up}}} \tag{2.7}$$

$$\mathrm{CLp_u} = \mathrm{aWT^b} \quad \text{and} \quad \log_{10}\mathrm{CLp_u} = \log_{10}\mathrm{a} + \mathrm{b} \times \log_{10}\mathrm{WT} \tag{2.8}$$

Initial estimates of human BNZ renal clearance CL_r assumed that this is a passive process and can be estimated from the product of Fup and glomerular filtration rate (GFR). GFR is a system/physiological parameter within a PBPK model that is calculated based on the body weight, age, and ethnicity.

2.3.3.4 Translation of PK-Sim IV metronidazole model (objective 2e)

While human IV PK data is lacking for BNZ it is available for metronidazole: a 5-substituted nitoimidazole with similar physico-chemical properties to BNZ[252]. PBPK modelling of IV metronidazole PK data has previously been reported by Dallmann *et. al.* using the PKSim platform[253]. The IV plasma and urine PK data from the original publication[252] was extracted and modelled using GastroPlus to quantify the relative contribution of CLh and CLr to metronidazole elimination.

2.3.3 Adult PBPK model development (objective 3)

2.3.3.1 Internal PBPK model validation / parameter fitting (objective 3a)

Three clinical BNZ PK datasets from published studies were used in this way to develop the human PBPK model (internal validation/parameter fitting). These include the two adult datasets modelled using PopPK methods in Chapter 2.3.1 (Raaflaub 1979 and Raaflaub 1980)[240,241], along with a third high dose PK study published by Roberts *et. al.*[242].

During human PBPK model development some drug-specific parameters were optimised by fitting the simulated/predicted plasma concentration–time (Cp-time) curve to measured human PK data.

In a PBPK model physiological/system parameters depend on the age, weight and ethnicity of the virtual body that is created for use in simulations. For each BNZ dataset a virtual body was created that matched the median demographics of the *in-vivo* study group, see Table 2.4. Where this data is lacking[242] a body weight of 65 kg and age of 30 years were assumed. Only data from subjects that did not receive fractionated tablets in the Raaflaub repeat dose study were utilised in PBPK model development to minimise errors associated with dosing inaccuracies[241].

Due to a lack of data regarding the specific enzymes responsible for the metabolism of BNZ, a lumped (non enzyme specific) unbound in-vivo hepatic intrinsic clearance was employed. In GastroPlus hepatic intrinsic clearance is not defined per gram of liver tissue, or per kg of body weight, and it needs to be scaled across different populations ($_p$) by the user. In this study in-vivo $CL_{int,u,p}$ has been centred on a 65kg body weight and scaled across populations based on Equation (2.9).

$$\mathrm{CLh_{int,u,p}} = \mathrm{CLh_{int,u,std}} \times \left(\frac{\mathrm{WT_i}}{65}\right)^{0.75} \tag{2.9}$$

Pharmacokinetic predictions were evaluated using visual/graphical checks of model

performance by i) superimposing predicted plasma Cp-time profiles on *in-vivo* data, ii) linear regression of observed vs. predicted plasma concentrations and iii) evaluation of the percentage prediction error (PE) with time and concentration.

$$\% \text{ Prediction Error } = \frac{(\hat{y}_t - y_t)}{y_t} \times 100 \tag{2.10}$$

Table 2.4: Clinical BNZ PK data utilised in PBPK (GastroPlus) model development, verification and extrapolation.

Study	Regimen	Dose (mg/kg)[a]	Population	WT/Age (kg)/(yrs)[a]	Subjects/ Samples
Model Development					
Raaflaub 1979	single dose	1.66	Heathy Volunteers	60.5 / 23	6 / 62
Raaflaub 1980	repeat dose q12hr	3.45	Chagas Patients	58 / 32	5 / 59
Roberts 1984	single dose	25	Oncology Patients	Adults[b]	5 / 45
Houghton 1985[c]	single dose	8.93	Healthy Volunteers	56 / 30	9 / 144
Model Verification					
Torrico 2021[d]	repeat dose q12hr	2.31	Chagas patients	65 / 34	25 / 73
Model Extrapolation					
Altcheh 2014[e]	repeat dose q12hr	3.25	Chagas patients	22.0 / 5.8	35 / 109

[a] Median dose, weight and age.

[b] Weight and age of patients not reported.

[c] 500mg IV metronidazole PK study, 9 healthy females, 144 plasma samples, 45 urine samples.

[d] NCT03378661 individual subject dose information and bioanalytical data for treatment group 6 shared by F.Assmus.

[e] NCT00699387 individual subject dose information and bioanalytical data shared by C.Cruz and F.García-Bournissen.

Individual *in-vivo* concentrations were used to calculate geometric mean Cp-time profiles and the observed mean concentrations were plotted against predicted concentrations. For the Roberts 1984 dataset[242] individual PK data was not available therefore the average concentration-time profile was extracted/digitized from the original publication.

In addition to visual/graphical checks of model performance the best model was selected based on an analysis of the root mean square error (RMSE), coefficient of determination (R^2) and associated intercept, average fold error (AFE) and absolute fold error (AAFE)[270]. Where y_t is the observed average plasma plasma concentration at time t, $\hat{y}_t$ is the predicted average plasma concentration at time t, and $\bar{y}$ is the average plasma concentration. If predicted plasma concentrations match exactly observed concentrations, then RMSE and the linear regression intercept will equal zero,

while R^2, AFE, and AAFE will all equal 1.0.

$$\mathrm{RMSE} = \sqrt{\mathrm{MSE}} = \sqrt{\frac{1}{\mathrm{n}}\sum_{\mathrm{i}=1}^{\mathrm{n}}(\mathrm{y_t} - \hat{\mathrm{y}}_\mathrm{t})^2} \tag{2.11}$$

$$\mathrm{R}^2 = 1 - \frac{\sum(\mathrm{y_t} - \hat{\mathrm{y}}_\mathrm{t})^2}{\sum(\mathrm{y_t} - \bar{\mathrm{y}})^2} \tag{2.12}$$

$$\mathrm{AFE} = 10^{\frac{1}{\mathrm{N}}\sum \log_{10}\left(\frac{\hat{\mathrm{y}}_\mathrm{t}}{\mathrm{y_t}}\right)} \quad \text{and} \quad \mathrm{AAFE} = 10^{\frac{1}{\mathrm{N}}\sum\left|\log_{10}\left(\frac{\hat{\mathrm{y}}_\mathrm{t}}{\mathrm{y_t}}\right)\right|} \tag{2.13}$$

Parameter sensitivity analysis was performed using the final PBPK model. The impact of varying Fup, Rbp, Peff, CLh, Aq solubility, P-gp Vmax, and renal transporter Vmax on; F, AUC_{inf}, Cmax and Tmax was simulated.

2.3.3.2 External model verification (objective 3b)

A subset of benznidazole PK data collected in Chagas patients as part of the DNDi funded BENDITA clinical trial (NCT03378661) was utilised for external model verification[248]. The data was shared by collaborators who were responsible for the PopPK/PD analysis of the BENDITA trial data. The PK data was collected in treatment group 6 of the trial in which 150mg BNZ was administered BID once every seven days in conjunction with fosravuconazole (FOS). Fosravuconazole was administered orally at a loading dose of 300 mg once daily for 3 days, followed by 300 mg once per week. While combination dosing was a potential complicating factor compared to monotherapy, this arm of the study employed the most informative PK sampling schedule post the initial BNZ dose and data collected out to 72 hrs post the first dose was included.

Bioanalysis of PK samples in the BENDITA trial utilised a dried blood spot assay method[248]. These concentrations were converted to plasma concentrations using the correlation published by Bedor *et. al.*[271], and the final adult estimate of $CLh_{int,u}$ was increased by 14% to account for the effect of fosravuconazole on BNZ CL/F reported by Frauke *et. al.*[256].

Using the final adult PBPK model parameter sensitivity analysis was performed and used to select which parameters to vary in the model verification population simulation. The observed BNZ plasma concentrations were compared to the 95% confidence interval calculated using the simulated data.

2.3.4 Paediatric PBPK model extrapolation (objective 4)

Based on the findings from objectives 1-3 of this study a hypothesis for the effect of age on BNZ CL/F was defined and implemented in the PBPK paediatric simulations.

Hypothesis: Renal reabsorption of BZN is assumed to be transporter mediated and expression in children aged 2-6yrs is less than half the expression in adult populations.

The same paediatric BNZ PK data (clinical trial NCT00699387)[185] that was modeled using population PK methods to achieve objective 1 of this study, was simulated using the final PBPK model develop in objective 3 of this study.

Because the paediatric PK data is highly variable, sparse and unbalanced, PBPK modelling of average concentration-time profiles was not an option, therefore the data were divided into single dose or steady state groups, and then pooled using the following age groupings; 2-4, 4-6, 6-9.5 and 9.5-12years. As per the clinical protocol steady state was assumed to have been reached by day three, this relies on the half-life in children being at most 10 hours. In total this dataset included 109 observations from 35 children however once divided there was only a small amount of data within each paediatric sub-population, see Table 2.5.

Table 2.5: Paediatric sub-population information: Number of observations (plasma concentrations) and children included in each sub-population and the median: weight, age and dose administered in each paediatric sub-population

	Number of		Median		
Group	**Observations**	**Children**	**Weight (kg)**	**Age (yrs)**	**Dose (mg/kg)**
Single Dose					
Group 1	9	3	15	3.8	3.4
Group 2	9	3	19	4.8	2.6
Group 3	3	1	27	7.5	3.7
Group 4	12	4	43	10.9	3
Steady State					
Group 1	21	7	12	2.5	3.8
Group 2	15	5	20	5.2	2.6
Group 3	20	6	31	8.5	3.4
Group 4	20	6	33.5	11.6	3.5

[a] Group 1: 2-4 years. Group 2: 4-6 years. Group 3: 6-9.6 years. Group 4: 9.5-12 years.

Looking at Figure 2.6 there is no obvious trend for higher exposure in older children after single BNZ doses, this trend seems to only manifest at steady state, however

caution is required when interpreting Figure 2.6 as dose varies between individuals from 2.5 to 4.4 mg/kg. The observation that the age effect becomes more obvious at steady state is taken as further evidence that age is affecting a systemic clearance mechanism, resulting in a longer half-life in older children and therefore greater accumulation. Because of this and because the steady state dataset is double the size of the single dose data; 76 versus 33 observations respectively, the main focus of this part of the study concerned simulating the steady state paediatric data.

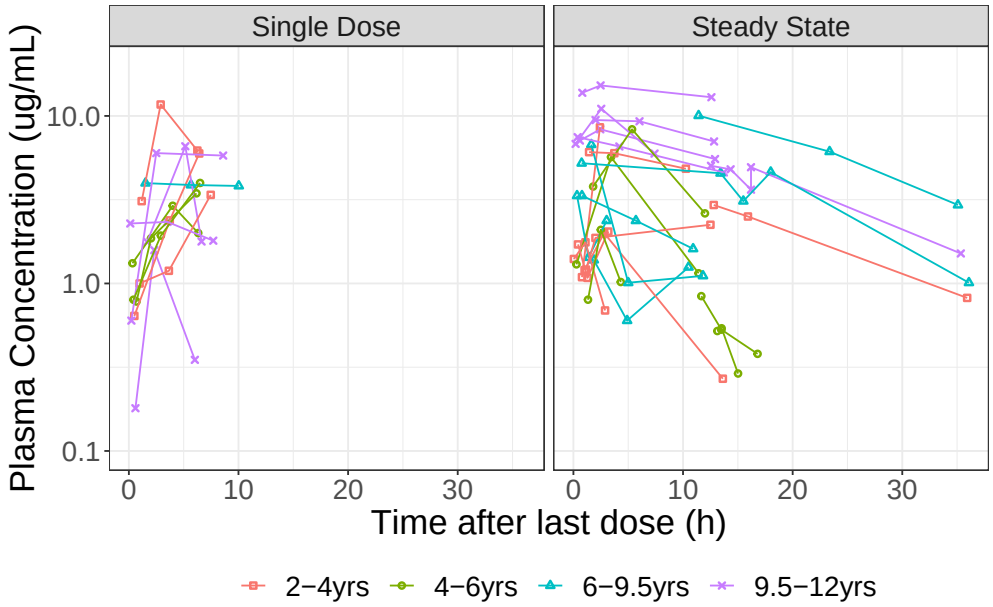

Figure 2.6: Measured paediatric plasma PK, pooled based on age. Red: Group 1 (2-4 yrs). Green: Group 2 (4-6 yrs). Blue: Group 3 (6-9.5 yrs). Purple: Group 4 (9.5-12 yrs).

For each paediatric group the median age, weight and dose as outlined in Table 2.5 were implemented in the PBPK model and subsequently all the 'system/body' parameters were scaled by the PBPK software. The adult *in-vivo* unbound CLint of 2.31 L/hr/65kg is also scaled based on these median body weights as previously described in Equation (2.9). Finally, in the 2-6 year old sub-populations fed state dosing was implemented (medium calorie/medium fat) to reflect the slower Ka observed in younger children, see Chapter 2.4.1.

When extrapolating to paediatrics within GastroPlus length and radius of the intestinal compartments are scaled by body weight. Intestinal volumes are calculated from length and radius, and transit times are derived from the literature, however no quantitative data is available to inform surface area enhancement factor (SEF) values in paediatrics. Therefore, by default SEFs remain at fitted adult levels when

performing paediatric simulations. This results in the paediatric absorption scale factors (ASFs) being greater than those implemented in adults. With respect to regional expression/abundance of transporters within the intestine, the default approach in GastroPlus is to reduce the P-gp distribution factors (DFs) according to BW. The DF is a fractional term (can vary from 0 to 1) and adjusts the transporter Vmax regionally throughout the intestinal compartments and acts as a surrogate for modifying Pgp expression.

2.4 Results

2.4.1 Quantifying the effect of age (objective 1)

BNZ PK data from three clinical studies, two adult[240,241] and one paediatric[185] study were pooled and a population PK analysis performed to quantify the effect of age on BNZ PK parameters. Data cleaning, visualisation and preparation of the NONMEM modelling dataset was performed and the pooled measured plasma concentrations versus calculated time after last dose for the three studies is presented in Figure 2.7.

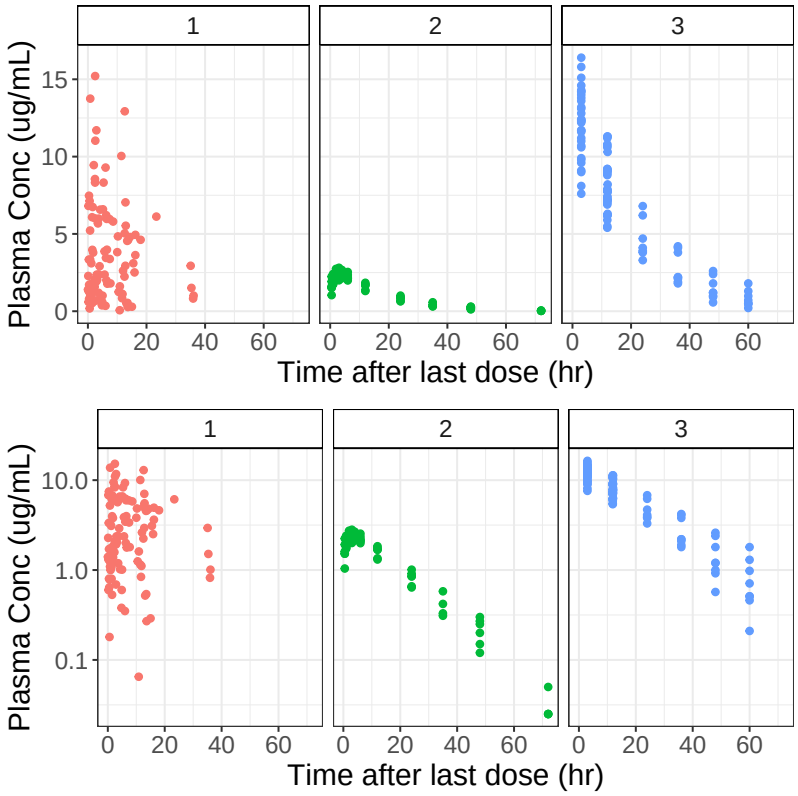

Figure 2.7: Visualisation of the NONMEM modelling dataset (measured concentration versus time after last dose) for the pooled paediatric and adult BNZ PK data. Red circles: Paediatric Chagas disease study 5-9 mg/kg BID single and multiple dose PK (Altcheh 2014). Green circles: Adult single dose 1.6mg/kg in healthy volunteers (Raaflaub 1979). Blue circles: Adult multiple dose PK 3.5 mg/kg BID in Chagas patients. Facets: Left; Altchech 2014. Middle; Raaflaub 1979. Right; Raaflaub 1980. Rows: Top; Linear y-axis. Bottom; Log y-axis.

The base model was a one-compartment distribution and elimination model with first order absorption. OMEGA block was supported by the data, so IIV was es-

timated for all fixed effects. Greater variability was seen in the paediatric data as compared to the adult data so separate residual error terms were estimated for children and adults. A proportional error model was selected for both adults and children. The base model parameter estimates are presented in Table 2.6 and individual η's on CL/F, V/F and Ka are shown in Figure 2.8. Figure 2.8 clearly shows that before adding age as a covariate individual CL/F and Ka estimates are affected by age; CL/F reduces while Ka increases with age. The relationship between V/F and age is more ambiguous, but based on visual assessment of Figure 2.8B, it was concluded to not be significant, and not tested during model development. The absence of an effect of age on V/F, but presence for CL/F, is considered to be evidence that age influences BNZ exposure through a clearance mechanism that does not influence F, i.e. not Fa, Fg or Fh.

Table 2.6: Base model parameter estimates. Clearance and volume estimates were centred on a 58 kg adult.

Parameter	**Estimate (%RSE)**	**IIV %CV (%RSE)**
CL/F (L/hr/58kg)	2.75 (11.0)	65 (26.1)
V/F (L/58 kg)	34.84 (7.1)	21 (93.7)
Ka_{tab} (/hr)	0.65 (30.1)	134 (38.2)
Prop Err Paed (%)	42 (32.1)	-
Prop Err Adult (%)	11 (19.1)	-
OFV	176.2	-

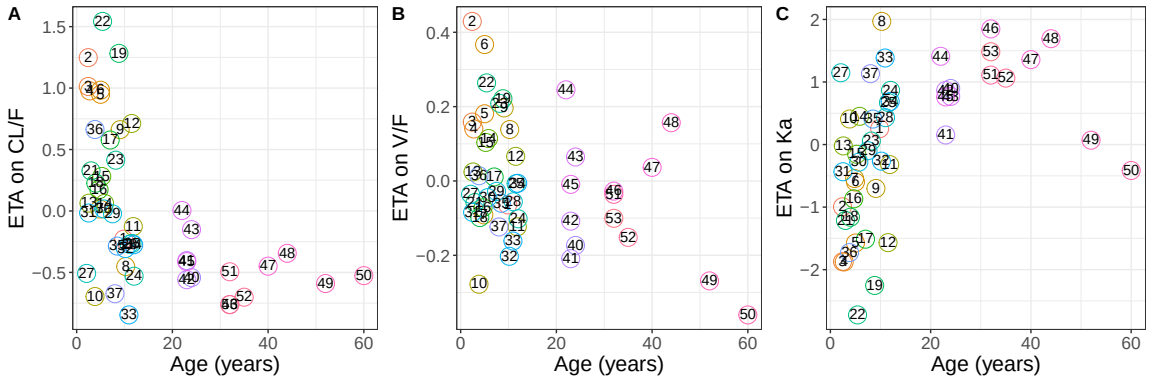

Figure 2.8: ETA plots constructed using the base BNZ population PK model. Shrinkage on the IIV terms was 5.4%, 21.9% and 16.1% for CL/F, V and Ka respectively. For the residual error terms shrinkage was 12.6% and 10.2% for children and adults.

GOF and VPC plots for the final model are presented in Figure 2.9 and 2.10,and show that the model describes the data well. In Figure 2.9 the observed data are evenly distributed around the line of unity in the DV vs iPRED plot (left) and also around y=0 in the CWRES vs PRED plot (right) with all conditional weighted residual (CWRES) lying within ± 4.

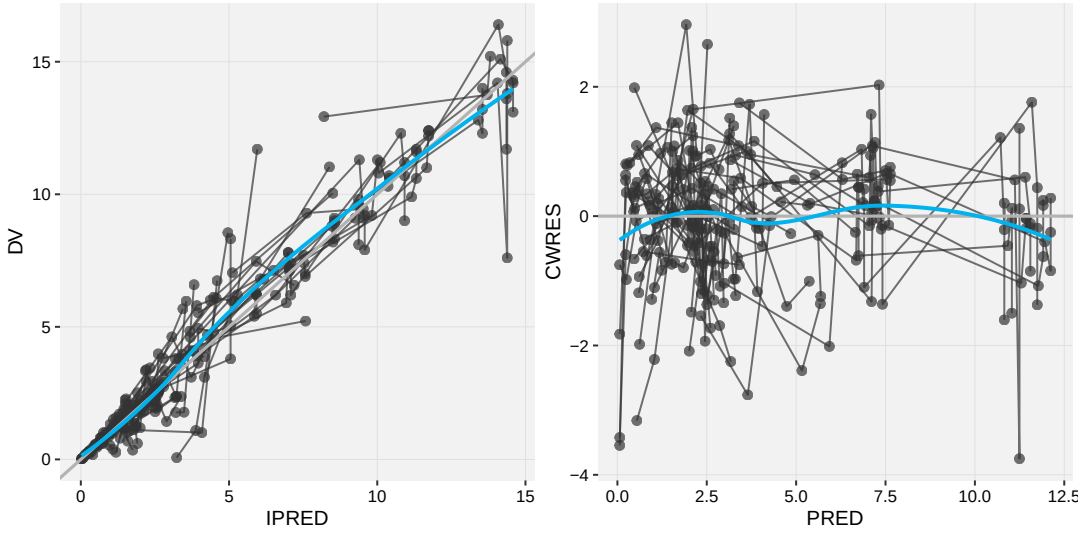

Figure 2.9: Final BNZ PopPK model GOF plots. Left; observed BNZ plasma concentration vs individual predicted plasma concentration (μg/mL). Right; conditional weighted residual vs population predicted BNZ plasma concentration (μg/mL).

The VPC plots for the final model (Figure 2.10 show that the model predicts the paediatric PK data well; the observed data is falling within the simulated prediction interval (PI; shaded area) for all percentiles (2.5th, 50th and 97.5th) and the width of each PI captures the variability in the observed data (Figure 2.10, STDY=1). However for the adult datasets (Figure 2.10, STDY=2 and STDY=3) the model is over-predicting the PK variability at the upper and lower percentiles (blue shaded areas) and these are clearly wider than the observed data. This could potentially be improved by estimating IIV for paedatric and adult populations separately, however because the observed 50th percentile (solid black line) lies centrally within the grey shaded area, the model was considered fit for quantifying the effect of age at a population level, and suitable for estimating the magnitude of the average trend prior to performing the mechanistic (PBPK) modelling.

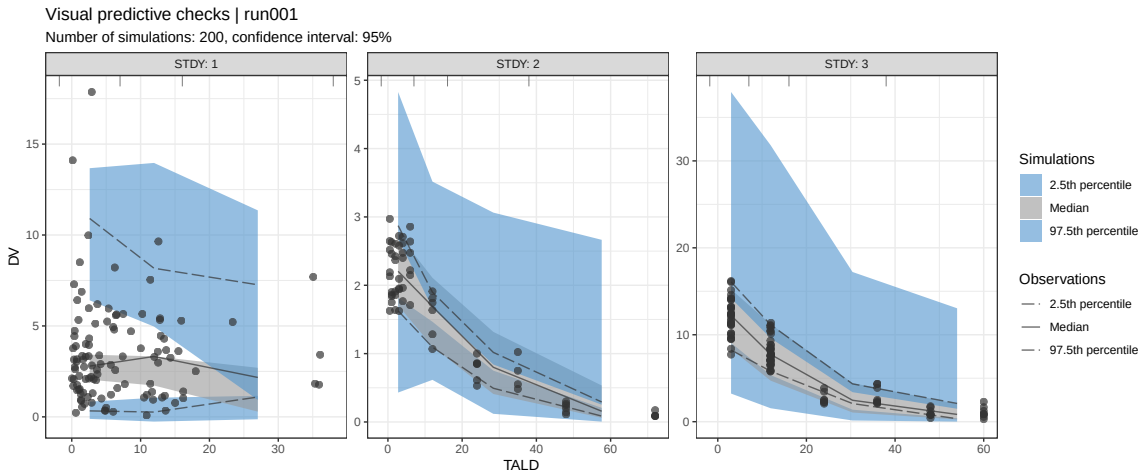

Figure 2.10: Final BNZ PopPK model VPCs. Left to Right; Paediatric Study NCT00699387, Raaflaub 1979, Raaflaub 1980. Key: DV; BNZ plasma concentration μg/mL. TALD; time after last dose (hr). Black circles; measured BNZ plasma concentrations.

The final model includes age as a covariate on CL/F and age as a covariate on Ka according to Equations (2.4) and (2.5) in Methods. Inclusion of maturation on CL/F and on Ka introduced four additional fixed effects and reduces the OFV by 28.98 points ($p < 0.01$), and the age functions estimated on CL/F and Ka are visualized in Figure 2.11. The final model parameters are presented in Table 2.7.

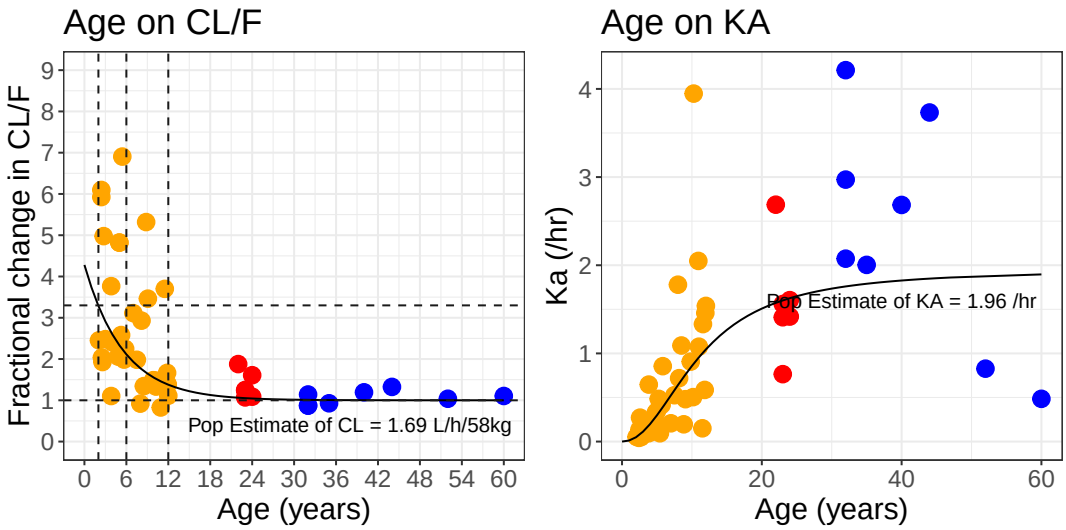

Figure 2.11: Visualisation of the effect of age on BNZ apparent clearance (CL/F) and absorption rate constant (Ka). Key: Yellow circles; paediatric study NCT00699387. Red circles; Raaflaub 1979. Blue circles; Raaflaub 1980. Solid black lines; model estimated maturation functions.

Table 2.7: Final BNZ PopPK model parameter estimates. Clearance and volume estimates were centred on a 58 kg adult.

Parameter	**Estimate (%RSE)**	**IIV %CV (%RSE)**
CL/F (L/hr/58kg)	1.69 (8.5)	47 (38.9)
V/F (L/58kg)	32.83 (4.5)	20 (37.1)
Ka_{tab} (/hr)	1.95 (42.0)	90 (56.8)
θ_p on k_a	2.12 (27.9)	-
θ_q on k_a (years)	11.21 (48.6)	-
θ_M on CL/F	4.28 (54.1)	-
θ_N on CL/F (/year)	0.18 (77.3)	-
Prop Err Paed (%)	44 (21.8)	-
Prop Err Adult (%)	11 (18.8)	-
OFV	147.3	-

Note: CL/F, apparent total plasma clearance; V/F, apparent volume of distribution; Ka_{tab}, tablet absorption rate constant; θ_p, the maturation exponent on the absorption rate constant; θ_q, time to 50% maturation on the absorption rate constant; θ_M, the fraction change in CL/F compared to adults at birth; θ_N, the rate of change in CL/F; %RSE, asymptotic standard error; %CV, coefficient of variation; IIV, interindividual variability.

2.4.2 Definition of initial PBPK parameter estimates and modelling strategy (objective 2)

The process of PBPK model development requires collation of a diverse set of compound specific *in-vitro* and *in-vivo*, pre-clinical and clinical ADME data, as it is this data that underpins model parameterisation.

2.4.2.1 Published ADME data review (objective 2a)

In-vitro physicochemical and ADME data were collected through review of published scientific literature, US regulatory documentation and in-house Roche and DNDi data have also been evaluated. Results from PKPDai searches for the following terms: benznidazole, 2-nitroimidazole, 5-nitroimidazole are tabulated in Appendix B.1, these search terms returned 39, 74 and 15 hits respectively.

Metabolic stability and clearance mechanisms:

No *in-vitro* metabolic stability data for benznidazole was identified in published scientific literature however data was obtained from internal DNDI study reports

that were made available by collaborators working at the Mahidol-Oxford Tropical Medicine Research Unit (MORU) in Thailand. The study report reference is 'CDCO_DNDi_09_026_Met', it is dated 02nd July 2009 and was issued to DNDI by the Centre for Drug Candidate Optimisation Monash Institute of Pharmaceutical Sciences. The stability of BNZ and other drug candidates were tested in mouse and human liver microsomes and the authors reported that after incubation at 1 μM EPL-BS0063 (i.e. Benznidazole) was slowly degraded in human and mouse liver microsomes, and would be expected to be subject to low hepatic clearance in both species. In fact the lack of BNZ degradation in-vitro meant that a intrinsic clearance could not be accurately calculated and all that could be concluded was that Eh (hepatic extraction ratio) was predicted to be < 0.2 and that no metabolites were detectable.

The same picture of low metabolic turnover of BNZ was painted by data submitted to the FDA as part of a new drug application (NDA-209570) filled by Chemo Research S.L in 2017 [244]. The sponsors reported that after incubation of BNZ (10 μM) in hepatocyte suspensions collected from male CD1 mouse, Han-Wistar rat, New Zealand white rabbit and human (pool of 10 donors) for 120 minutes BNZ was metabolically stable, and all t1/2 values were above 120 minutes. BNZ incubation with mouse or rabbit hepatocytes did produce some metabolic degradation, 7.3 and 11.7% respectively, whereas no metabolic degradation was observed in rat or human hepatocytes. However clearly some metabolism of BNZ does occur in humans as Marson et. al. have previously identified two BZN metabolites (N-amine-BZN and N-hydoxy-amine-BZN) in human urine samples[272].

Regarding other therapeutic nitro-imidazoles there are some reports of human clearance in the literature. For example, in 2018 Lombardo *et. al.* published a trend analysis of human intravenous pharmacokinetic data on a data set of 1352 drugs, 4 of which are the nitro-imidazoles; metronidazole, morinidazole, ornidazole and tindazole. In this order the human clearances were reported as 0.85, 1.60, 1.08 and 0.60 mL/min/kg, (ranged from 6.7 to 2.5 L/hr assuming a 70kg BW), Fup was not reported for morinidazole but was 0.96, 0.88 and 0.8 for the other three nitro-imidazoles respectively[273].

Transporter interactions:

For many drugs transporters play an important role in intestinal absorption and hepatic and/or renal clearance.

Renal clearance (CLr), fup and transporter interaction data were collated for

157 drugs by Scotcher *et. al.*, two of these compounds were the nitroimidazoles; metronidazole and tindazole [274]. The authors reported an overall weighted mean CLr for metronidazole and tinidazole in healthy adult populations of 9.6 and 11.3 mL/min (0.576 and 0.678 L/hr), which given the high fraction unbound (the authors report for these two drugs; 0.98 and 0.94 respectively), indicates significant renal reabsorption occurs. The authors made significant efforts to ensure the potential impact of renal transporter mediated secretion of drugs was factored into their predictions of renal reabsorption but for these two drugs no information regarding whether either drug is a substrate for renal drug transporters was identified.

Morinidazole is a novel 5-nitroimidazole antimicrobial drug that undergoes extensive phase-2 metabolism in humans. Zhong *et. al.* wanted to assess the effects of renal impairment on the pharmacokinetics of 500mg IV morinidazole and to elucidate the potential mechanisms. *In-vitro* transporter studies revealed that while the main metabolites of morinidazole are substrates for organic anion transporter 1 (OAT1) and OAT3, morinidazole itself was not found to be a substrate for the transporter-transfected cells examined (OAT1, OAT3 and OCT2). Total clearance and renal clearance of morinidazole was reported to be 8.5 $\pm$ 1.79 L/hr and 1.28 $\pm$ 0.47 L/hr respectively in healthy subjects (n=10), while in patients with serve renal impairment this reduced to 5.75 $\pm$ 1.31 L/hr and 0.35 $\pm$ 0.16 L/hr (n=10). The healthy subjects were required to have a CLCR of $>$ 90 mL/min and were matched to patients with severe renal impairment for sex, age (within 5 years), and body mass index (within 15%)[275].

Tinidazole, morinidazole and metronidazole are included in a later review of renal transporters and their role in drug-drug interactions published by Ivanyuk *et. al.* in 2017[276]. In this review morinidazole is identified as a substrate for OAT1 and OAT3 however this appears to be an incorrect representation of the work performed by Zhong et. al.[275]. As in Scotchers 2016 review[274] no new evidence suggesting that either metronidazole or tinidazole are substrates for any renal drug transporters was identified, however data is still lacking for a number of important renal transporters. To support the new drug application filed with the FDA by Chemo Research in 2017 (NDA: 209570) *in-vitro* transporter studies in immortalised human embryonic kidney cells (HEK293 cells) were performed. These studies found that BNZ was not a substrate for the renal transporters typically implicated in renal secretion; OAT1 or OAT3, OCT1, OCT2, OATP1B1*1a or OATP1B3, however the data suggests that BNZ may be an inhibitor of OAT3 with a mean IC_{50} of 34 uM. In this same filing data from bi-directional transport studies using Caco-2 cells are presented. Three BNZ

concentrations were tested 1, 10 and 100 uM and the apical to basolateral apparent permeability ranged from 172 ± 28 to 208 ± 31 nm/s and an efflux ratio ranging from 1.7 to 2.0 was observed. Efflux was completely inhibited by treatment with both 100uM cyclosporine A and 100 uM quinidine which was taken as evidence by the agency that BNZ is a substrate for P-gp. However, the FDA reviewers make efforts to highlight that monolayer integrity in this study is questionable due to unusually high lucifer yellow Papps (10x higher than expected). Lucifer yellow is an EMA approved zero permeability marker compound[238]. Other researchers have also suggested P-gp involvement in BNZ disposition[277,278]

Permeability:

The ADMET (structural prediction) of effective human jejunal permeability (Peff) as shown in Table 2.15 is predicted to 0.98x10-4 cm/s, which would be considered as moderate permeability (Fa 50-84%) according to the relationship established by Lennernas *et. al.*[279]. The regulatory cut off for low or high permeability is ideally defined based on a clinically determined fraction absorbed (Fa). For a drug to be considered high permeability, Fa needs to be $\geq$ 85% according to the EMA[280] or $>$ 90% according to the FDA[281]. In Europe a claim of high permeability to support a biowaiver can be based on *in-vitro* Caco-2 data but the compound in question must be evaluated against five known low (Fa<50%), moderate (Fa 50-84%) and high (Fa >=85%) permeability marker compounds[280].

In-house data generated by DNDI as part of their on-going activities to develop new drugs to treat Chagas Disease was made available through our collaborators at MURO in Bangkok. Apparent permeability data generated on Benznidazole in the PAMPA assay[282] provides evidence supporting a low permeability classification for BNZ. The maximum estimated BNZ Papp was 0.8x10-6 cm/s and the low perm marker compound Nadolol (Nadolol is classified by the EMA as low permeability (Fa $<$ 50%)[280]) had a Papp of 1.0x10-6 cm/s. While any marker data is very valuable the lack of a lab specific Papp to Peff correlation[283] does make this data of limited direct use for model parameterisation.

Physical chemical properties and solubility:

In the original human PK papers published by Roche BNZ is described as an uncharged molecule devoid of acid or base functional groups in the pH range of physiological interest (pH 1-8) with a partition co-efficient of the drug between organic solvents and water of 7.0 in 1-octanol/pH 7.4 aq buffer and 5.1 in chloroform/pH 7.4 aq buffer at room temperature[240]. It is more conventional today to compare lipophilicity

using a Log_{10} scale, and at pH 7.4 it can be said that the Log D of BNZ was found by Raaflaub et. al. to be 0.85[240]. This estimate of lipophilicity is in good agreement with the values reported more recently by Maximiano et. al, here BNZ partitioning between 1-octanol and different aqueous media (water, simulated gastric media and simulated intestinal media) ranged from 0.76 to 0.78.

BNZ aqueous solubility at 37°C was reported by Raaflaub *et. al.* to be 0.4 mg/mL[240]. More recently solubility in simulated gastric and intestinal media has been evaluated and solubility is reported to be 0.236 and 0.244 mg/mL, however these studies were only performed at room temperature[284]. Other researchers have explored the solid-state chemistry of BNZ and characterised the impact that polymorphic form (crystal structure) has on BNZ solubility. Three polymorphs of BNZ were characterised and solubility was not sensitive to the crystal habit with solubility ranging from 0.22 to 0.25 mg/mL in water. Temperature in these solubility studies was not specified[285]. Because of the absence of a pKa between pH's 1-8 BNZ is not thought to show pH-dependent solubility in the gastro-intestinal tract.

Blood to plasma ratio and fraction unbound in plasma:

Blood to plasma ratio (Rbp) and the fraction of drug unbound in plasma (Fup) are important species dependent parameters that influence clearance and tissue distribution in a PBPK model. BNZ blood to plasma ratio in humans using blood from healthy subjects is reported to be 1.0[240]. In mouse it is reported to be 1.16 ± 0.04 (n=16). For the fraction unbound in plasma more data are available. Fup has been reported in the literature to range from 0.61 - 0.62 in mouse[258] and additional in-house DNDI funded studies have found mouse Fup to be 0.68. In dog Fup is reported to range from 0.41 to 0.48, values as low as 0.26-0.28 are reported following IV dosing but the increase in binding was attributed to vehicle effects[258]. In humans Fup has been found to be variable, in plasma from healthy subjects values of 0.56 ± 0.14 (n=5)[240] and 0.42 ± 0.12 (n=5)[286] were reported in two separate studies. In cancer patients Roberts et. al. found Fup to be 0.40 ± 0.1 (n=24)[242]. Internal DNDI funded studies find human Fup to be 0.53.

2.4.2.2 PBPK modelling of pre-clinical IV/PO PK: Dog (objective 2b)

The observed dog plasma PK reported by Workman *et. al.*[258] is presented in Figure 2.12. In this study two dogs received benznidazole following both intravenous and oral administration using a cross-over study design. The oral dose was administered at 25 mg/kg which was 5-fold higher than the 5 mg/kg intravenous dose. The oral

formulation is this study was simply unformulated drug substance packed into soft gelatine capsules. The results following NCA of the individual dog PK data (n=2 dogs) is presented in Table 2.8. Total plasma clearance of BNZ in dog is low ranging across the two dogs from 0.74 to 1.63 L/hr, which if dog liver blood flow is assumed to equal 35.75 L/hr (9.93 mL/s in a 24kg dog) equates to only 2.5 to 3.9% of liver blood flow. Oral bioavailability at 25 mg/kg (500 mg to dog D and 700 mg to dog C) ranged from 1.11 to 1.55. A bioavailability in excess of 1.0 is indicative of two things, a high fraction absorbed and potentially a non-linear clearance mechanism.

Table 2.8: Dog NCA results summary

ID	WT (kg)	Dose (mg/kg)	Route	Cmax (μg/mL)	AUCinf (μg*h/mL)	Extrapolation (%)	CL (L/h)	F	Fraction of LBF (%)
C	28	5	IV	8.49	85.72	7.27	1.63	NA	3.91
D	20	5	IV	12.90	135.56	13.38	0.74	NA	2.49
C	28	25	PO	39.30	664.18	18.55	NA	1.55	NA
D	20	25	PO	46.20	753.10	24.10	NA	1.11	NA

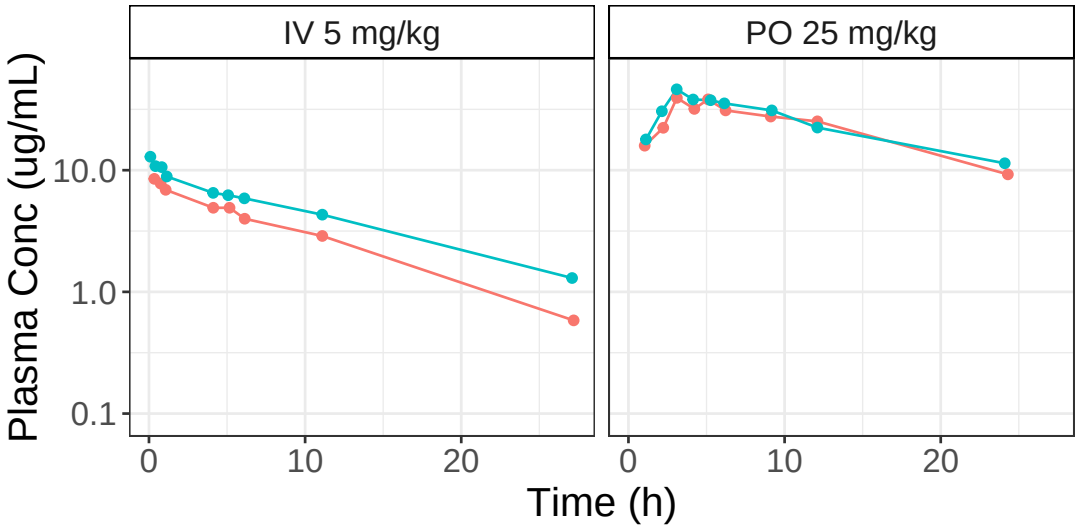

Figure 2.12: Measured dog PK (Workman 1984, n=2 dogs).

The GastroPlus parameters used in the dog PBPK simulations are presented in Table 2.9. Observed versus simulated concentration-time profiles are compared in Figure 2.13, and the PBPK simulation results are shown in Table 2.10.

Table 2.9: Summary of PBPK model parameters used to simulate benznidazole IV and PO plasma PK in dog. PO1-PO5 are sequential dog PK simulations illustrating the evolution of the modeling approach/parameter estimates.

Property	**Units**	**IV**	**PO1**	**PO2**	**PO3**	**PO4**	**PO5**
Dose	mg	120	600	600	600	600	600
Species		Dog	Dog	Dog	Dog	Dog	Dog
Weight	kg	24	24	24	24	24	24
Physico-Chemical							
pKa	-	none	none	none	none	none	none
Log P	-	0.75	0.75	0.75	0.75	0.75	0.75
Fup	(%)	44	44	44	44	44	44
Rbp	-	1	1	1	1	1	1
Permeability							
Human Peff	X10^{-4}cm/s	0.98	0.98	0.98	1.78	1.78	1.78
Tissue Distribution							
Kp Calculation Method [160]		Berezovsky	Berezovsky	Berezovsky	Berezovsky	Berezovsky	Berezovsky
Tissue Model		Perfusion	Perfusion	Perfusion	Perfusion	Perfusion	Perfusion
Clearance							
Lumped Liver $Clint_u$	L/hr	2.594	2.594	2.594	2.594	2.594	1.87
Liver Blood Flow (Q)	mL/s	9.93	9.93	9.93	9.93	9.93	9.93
CL_h	L/hr	1.1	1.1	0.55	1.1	1.1	0.8
GFR	mL/s	0.13	0.13	0.13	0.13	0.13	0.13
CL_r	L/hr	0	0	0	0	0	0
Systemic CL ($CL_h + CL_r$)	L/hr	1.1	1.1	0.55	1.1	1.1	0.8
Solubility and Dissolution							
Aq Solubility at 37°	mg/mL	na	0.25	0.25	0.25	0.25	0.25
Particle Radius (um)	μm	na	25	25	25	25	25
Bile Salt Solubilisation		487	487	487	487	487	487
Dissolution Model [282, 283]		na	Johnson	Johnson	Johnson	Johnson	Johnson
Gut Physiology							
Fed Status		na	fasted	fasted	fasted	fed	fed

Notes: Simulations used average body weight. Fup; fraction unbound in plasma. Rbp; blood to plasma ratio. CL_h; in-vivo hepatic clearance. CL_r; in-vivo renal clearance. GFR; glomerular filtration rate. Aq; aqueous.

The IV plasma PK profiles are well described using the parameters outlined in Table 2.9. The fraction unbound in dog plasma of 44% falls within the range of values reported by Workman et al[258]. There is no pKa in the model which is consistent with the reported lack of ionisation across physiologically relevant pH ranges[240]. As a measure of benznidazole blood to plasma ratio in dog has not been identified in published literature, the value reported for humans has been used[240]. The Berezhkovskiy Kp calculation method[169] was found to best describe tissue distribution and the shape of the IV plasma concentration time profile. A total plasma clearance of 1.1 L/hr was employed in the IV simulation presented in Table 2.10 and Figure 2.13. All clearance in this simulation is assumed to be metabolic and placed in the liver using a lumped unbound liver CLint of 2.594 L/hr.

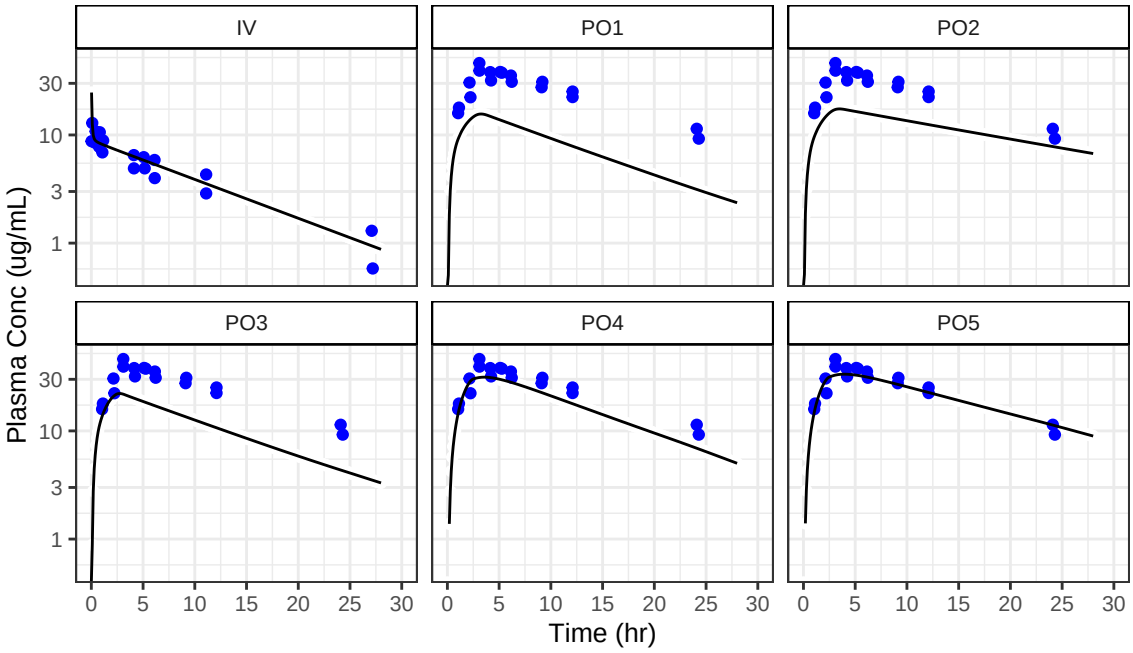

Figure 2.13: Dog GastroPlus modelling. Blue filled circles represent observed data, black solid line the predicted plasma concentration profile.

A total plasma clearance of 1.1 L/hr is consistent with the clearance determined by NCA of IV dog PK data, see Table 2.8. Since passive renal filtration predicted according to Fup*GFR is 1.62 L/hr, significant under-prediction of plasma AUCinf was avoided by fixing renal clearance to zero. No urine levels or total amount extracted in urine is reported by Workman et. al.[258].

Regarding the oral dog PK modelling. The parameters that were implemented in the sequential PO simulations are also presented in Table 2.9 PO1 to PO5. In all

the oral simulations in-vivo dissolution was described dynamically using the Johnson model[287,288], and particle size was unchanged from the default parameter value of 25 μm. Other initial absorption parameter estimates were based on the *in-vitro* data summarised previously in Section 2.4.2.1. Aqueous solubility at pH 7.4 was set to 0.25 mg/mL, human effective permeability was set to 0.98x10^{-4} cm/s, and in simulations P01-P03 the default fasted state gut system parameters were utilised.

However, these initial estimates of BNZ permeability and solubility only resulted in 45% of the oral dose being absorbed, and as shown in Table 2.10 this led to a significant underprediction of total exposure (AUCinf). This remained the case even following a 50% reduction in total plasma clearance as in PO2. The observed oral dog PK could only be reconciled by increasing the effective human permeability estimate from 0.98x10^{-4} cm/s to 1.78x10^{-4} cm/s and assuming the dogs were dosed in the fed state, which through a small increase in intestinal solubility (bile salt solubilisation increased solubility from 0.25 to 0.284 mg/mL) and an extended absorption window (increased gastric transit time in the fed state) increased the fraction absorbed to 96% and with a small reduction in CL_h; from 1.1 L/hr (as used in IV01) to 0.8 L/hr, the observed oral AUCinf was reproduced in simulation PO5.

Table 2.10: Dog PBPK simulation results

	Dose	Tmax (h)		Cmax (μg/mL)		AUCinf (μg.h/mL)					
ID	(mg/kg)	Pred	Obs	Pred	Obs	Pred	Obs	Fa (%)	F (%)	RMSE	R^2
IV	5	0.0	0.09	83.3	10.8	119.9	109.0	na	na	3.88	0.45
PO1	25	3.3	3.10	15.6	42.8	241.2	713.7	44.9	43.3	18.57	0.74
PO2	25	3.5	3.10	17.4	42.8	494.6	713.7	44.7	43.8	16.14	0.88
PO3	25	2.7	3.10	22.2	42.8	334.6	713.7	62	59.9	14.33	0.64
PO4	25	3.6	3.10	31.4	42.8	509.8	713.7	96.3	93.4	6.61	0.82
PO5	25	3.9	3.10	33.4	42.8	706.6	713.7	96.3	94.1	4.77	0.84

Notes: See Table 2.8 for the model parameters used in each simulation.

As well as summarising the observed and predicted summary statistics; AUC, Cmax and Tmax, Table 2.10 presents the goodness of fit statistics RMSE and R^2, and as a final visual diagnostic, GOF plots comparing the predicted BNZ plasma concentrations to the observed BNZ plasma concentrations are presented in Figure 2.14A, and precentage prediction error versus observed plasma concentration are presented in Figure 2.14B. Both clearly show that the parameter estimates utilised in simulation PO5 provide the best description of the observed oral dog PK.

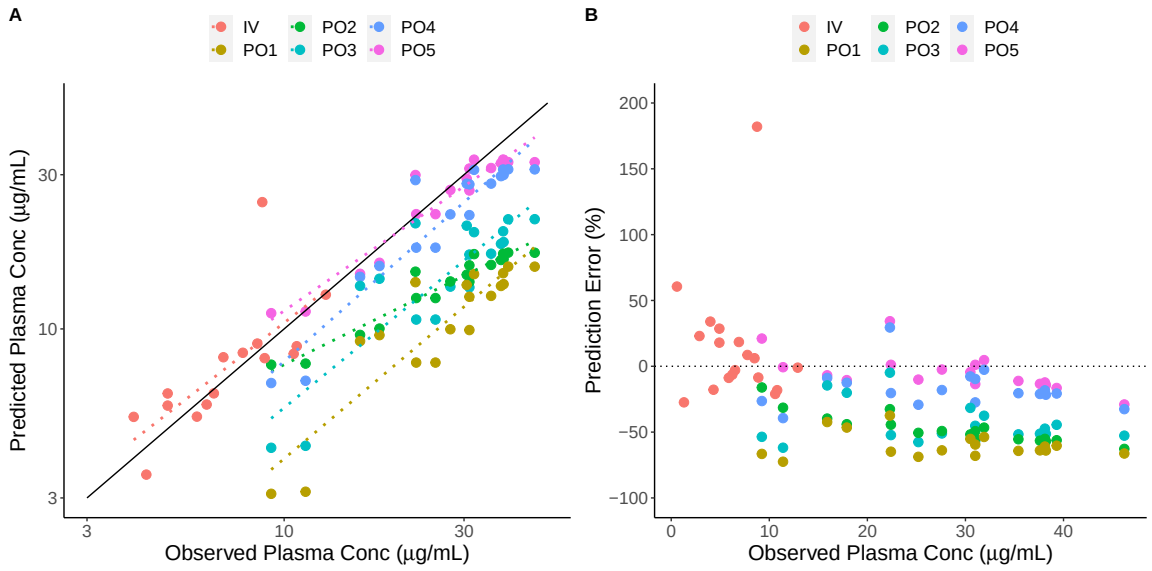

Figure 2.14: Dog IV/PO PBPK modelling GOF plots. A) Predicted plasma concentration versus observed plasma concentrations. B) Percentage prediction error versus observed plasma concentrations.

2.4.2.3 PBPK modelling of pre-clinical IV/PO PK: Rabbit (objective 2b)

The rich PK data published by Davanco *et. al.* was generated in n=7 rabbits in each arm of the study, however the study was not crossover in design, and while individual rabbit bioanalytical plasma and urine data was made available for PBPK modelling, individual animal body weights were not.

As shown in Table 2.11 geometric mean total plasma clearance is 1.74 L/hr (580 mL/h/kg assuming a 3kg rabbit) which agrees well with the clearance reported by Davanco *et. al.* of 511 (95% CI; 390-632) mL/h/kg. The observed rabbit plasma concentration-time data reported by Davanco *et. al.*[259] are presented in Figure 2.15 and the cumulative amount excreted in urine are presented in Figure 2.16.

Table 2.11: Geometric mean plasma PK parameters calculated from NCA of individual rabbit PK data (Davanco 2016).

Regimen	**Tmax / CV** **hours / %**	**Cmax / CV** **µg/mL / %**	**AUCinf / CV** **µg.h/mL / %**	**Extrap** **%**	**CL** L/hr	**F** **%**
IV 10mg	NA / NA	2.99 / 63.96	5.76 / 23.37	9.36	1.74	NA
IR 12.5mg	2.2 / 29.32	0.82 / 31.1	3.4 / 39.07	17.32	NA	47.15
IR 100mg	5.57 / 41.05	8.06 / 31.83	82.51 / 33.77	2.39	NA	143.18

Notes: Extrap: Extrapolated AUC. PO; per oral. IV; intravenous.

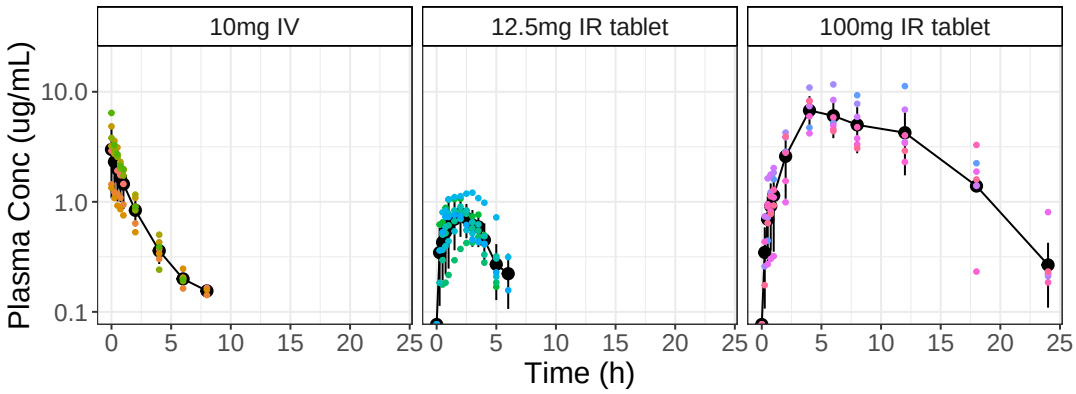

Figure 2.15: Individual rabbit plasma PK data, black solid line is the geometric mean Cp-time profile. (Davanco 2016)

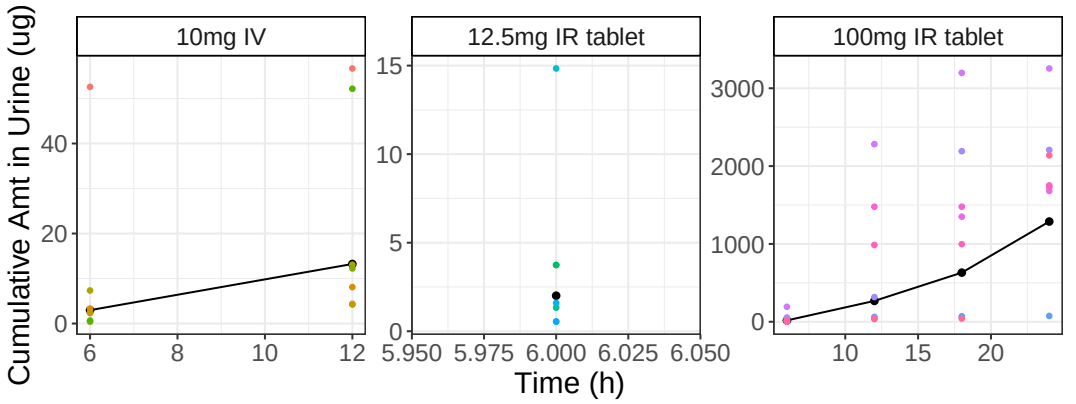

Figure 2.16: Individual rabbit urine PK data (cumulative amount excreted in urine), black solid line is the geometric mean amount-time profile. (Davanco 2016)

Comparing the geometric mean AUC_{inf} for the 3 regimens, absolute bioavailability is estimated to be 47% at the lower 12.5 mg dose and 143% at the higher 100mg dose. An absolute bioavailability >100% is indicative of non-linear clearance and while this may completely account for the almost three fold increase in F% when comparing oral exposures after 12.5 and 100 mg, there may also be a dose dependent increase in Fa occurring (higher Fa at higher doses).

The PBPK model parameters used to simulate the rabbit intravenous (IV01-IV05) and oral (PO1-PO2) PK data are presented in Table 2.12. The predicted plasma concentration-time profiles and predicted cumulative amount of unchanged BNZ excreted in urine are shown in Figure 2.17 for the IV simulations and Figure 2.19 for the oral PK simulations. PBPK simulation results (predicted versus observed PK parameters; Tmax, Cmax and AUC∞, Fa, F, and numeric goodness of fit measures)

are presented in Table 2.13 and Table 2.14 for the IV and PO simulations respectively and GOF plots are presented in Figure 2.20.

Building on from the dog PBPK modelling results the same estimates of Log P (0.75) and the same tissue partition co-efficient calculation method (Berezovsky[169] with perfusion limited tissues) was utilised. No measured blood to plasma ratio or plasma protein binding data has been previously reported in the literature for rabbit. Blood to plasma ratio was therefore fixed to 1.0 (as in dog) and the fraction unbound in plasma was fitted using the rabbit IV PK data and consideration of the fraction unbound reported in mouse, dog and human plasma which ranges from 0.40 to 0.68[240,242,258,286]. These parameters (LogP, Rbp and Fup) and the Berezovsky tissue partition coefficient method estimate rabbit Vss to be 2.0L/3kg rabbit. Regarding intestinal permeability the structure-based prediction of human Peff (0.98 x10^{-4} cm/s) was used as an input into the model and converted using the software's inbuilt species correlation, to a rabbit Peff of 2.24 x10^{-4} cm/s

In intravenous simulation IV01 renal clearance was estimated by multiplying the fraction of BNZ unbound in plasma by rabbit glomerular filtration rate (CLr = 0.328 L/hr/3kg rabbit). A broadly comparable amount of hepatic clearance was also included (0.29 L/hr/3kg rabbit). However, this total clearance of 0.62 L/hr/3kg rabbit (~ one third of the clearance calculated by NCA) resulted in a more than two-fold over prediction of plasma AUCinf and almost one hundred fold over-prediction of the amount of BNZ excreted in urine. This shows that significant renal reabsorption of BNZ is occurring and that potentially BNZ is being cleared from the systemic circulation by an additional mechanism other than hepatic metabolism. In simulation IV02 renal clearance was reduced and fixed to 0.003 L/hr/3kg rabbit which reduces the amount of BNZ predicted to be excreted in urine from ~5000ug to ~80ug in 12 hours, see Figure 2.17B versus Figure 2.17C. While this brings the urine simulation more in line with the measured amount in urine it only worsens the over-prediction of the plasma PK; in IV02 AUC∞ is five fold over-predicted. In IV03 hepatic clearance (CLh) is increased to 1.48 L/hr/3kg rabbit (see Table 2.12 for the change in model parameters) and plasma levels are captured out to 4 hours post dose, however levels at T_6 and T_8 are still under-predicted, see Figure 2.17A. Because P-gp has previously been implicated in BNZ disposition[278] inclusion of intestinal efflux was evaluated in the model as an additional route of elimination (intestinal secretion) in simulation IV04 and IV05, see Table 2.12 for the model parameters.

Table 2.12: Summary of PBPK model parameters used to simulate rabbit IV and PO benznidazole PK (plasma and urine). IV1-IV5 and PO1-PO2 are sequential rabbit PK simulations illustrating the evolution of the modeling approach/parameter estimates.

Property	**Units**	**IV01**	**IV02**	**IV03**	**IV04**	**IV05**	**PO1**	**PO2**
Dose	mg	10	10	10	10	10	12.5 / 100	12.5 / 100
Species		Rabbit	Rabbit	Rabbit	Rabbit	Rabbit	Rabbit	Rabbit
Weight	kg	3	3	3	3	3	3	3
Physico-Chemical								
pKa	-	none	none	none	none	none	none	none
Log P	-	0.75	0.75	0.75	0.75	0.75	0.75	0.75
Fup	(%)	70	70	70	70	70	70	70
Rbp	-	1	1	1	1	1	1	1
Permeability								
Human Peff	X10^{-4}cm/s	0.98	0.98	0.98	0.98	0.98	0.98	0.98
P-gp Km	ug/L	na	na	na	20	400	20	20
P-gp Vmax	ug/s	na	na	na	2	1	2	2
Tissue Distribution								
Kp Calculation Method [160]		Berezovsky	Berezovsky	Berezovsky	Berezovsky	Berezovsky	Berezovsky	Berezovsky
Tissue Model		Perfusion	Perfusion	Perfusion	Perfusion	Perfusion	Perfusion	Perfusion
Clearance								
Lumped Liver $Clint_u$	L/hr	0.437	0.437	2.6	1.2	1.7	1.2	2.4
Liver Blood Flow (Q)	mL/s	2.43	2.43	2.43	2.43	2.43	2.43	2.43
CL_h	L/hr	0.29	0.29	1.48	0.75	1.03	0.75	1.38
GFR	mL/s	0.13	0.13	0.13	0.13	0.13	0.13	0.13
CL_r	L/hr	0.328	0.003	0.003	0.003	0.003	0.003	0.003
Systemic CL ($CL_h + CL_r$)	L/hr	0.62	0.29	1.48	0.75	1.03	0.75	1.39
Solubility and Dissolution								
Aq Solubility at 37°	mg/mL	na	na	na	na	na	0.4	0.4
Particle Radius	μm	na	na	na	na	na	25 / 300	25 / 300
Bile Salt Solubilisation		na	na	na	na	na	487	487
Dissolution Model		na	na	na	na	na	Johnson	Johnson

Notes: Simulations used average body weight. Fup; fraction unbound in plasma. Rbp; blood to plasma ratio. CL_h; in-vivo hepatic clearance. CL_r; in-vivo renal clearance. GFR; glomerular filtration rate. Aq; aqueous. For details of the Johnson dissolution model see Refs [282, 283].

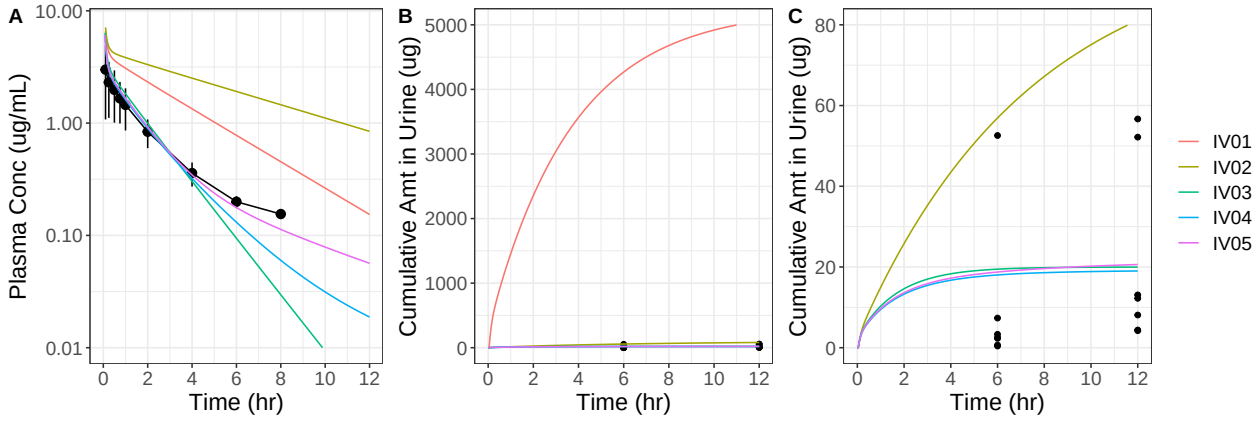

Figure 2.17: GastroPlus Rabbit IV PK simulations IV01 to IV05. IVO1-IV05 are sequential rabbit PK simulations illustrating the evolution of the modeling approach/parameter estimates.

As shown in Figure 2.17A inclusion of intestinal efflux in the model can have a significant impact on the shape of the predicted IV plasma concentration-time profile; compare the terminal phase of simulations IV03, IV04 and IV05. While it is not possible to confidently estimate P-gp kinetic terms (Vmax and Km) from a single IV dose, IV04 and IV05 illustrate how these parameters are predicted to alter the amount of drug lost from systemic circulation through intestinal secretion even following intravenous administration, see Figure 2.18.

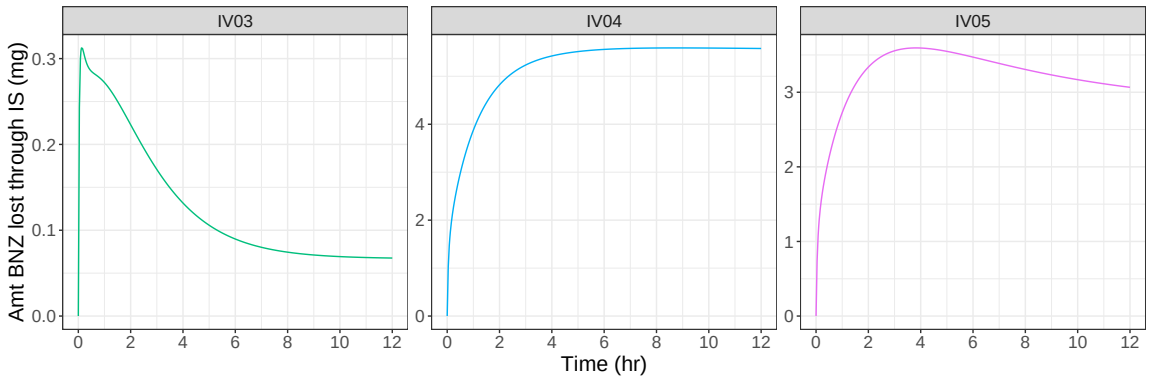

Figure 2.18: Predicted amount of BNZ lost from systemic circulation (into the gut) following IV administration as a result of P-gp mediated intestinal secretion (IS). For the model parameters used in simulations IV03, IV04 and IV05 see Table 2.11.

The numerical goodness of fit measures presented in Table 2.13 show that the parameters used in IV03, IV04 and IV05 can all recover the observed AUC∞; the prediction errors (see Equation (2.10)) are 2.1, -0.6 and 11.2 % respectively. However

based on the lowest AUC prediction error, and the RMSE, the IV parameters used in simulation IV4 were carried forward to model the oral rabbit PK data, where plasma levels following a 12.5mg low dose (LD) tablet, and 100mg high dose (HD) tablet are available. Building on the findings from PBPK modelling of intravenous

Table 2.13: Rabbit IV PBPK simulation results

ID	Dose (mg/kg)	Tmax (h) Obs	Tmax (h) Pred	Cmax (μg/mL) Obs	Cmax (μg/mL) Pred	AUCinf (μg.h/mL) Obs	AUCinf (μg.h/mL) Pred	Fa (%)	F (%)	RMSE	R^2
IV01	3.33	0.1	0.1	2.99	6.60	6.58	15.97	98.2	98.3	1.78	0.96
IV02	3.33	0.1	0.1	2.99	7.11	6.58	33.17	96.1	96.2	2.46	0.93
IV03	3.33	0.1	0.1	2.99	5.42	6.58	6.72	99.3	99.4	0.91	0.96
IV04	3.33	0.1	0.1	2.99	5.05	6.58	6.53	44.2	49.0	0.73	0.95
IV05	3.33	0.1	0.1	2.99	5.14	6.58	7.32	69.3	72.9	0.77	0.95

and oral benznidazole PK in dog, where a reference/aqueous benznidazole solubility of 0.275 mg/mL[284,285] was found to underpredict the extent of absorption unless the dogs were assumed to be in the fed state, a reference solubility of 0.4 mg/mL[240] has been used in the rabbit oral PBPK modelling. The same theoretical (Log P based) bile salt solubilisation ratio (BSSR = 487) as utilised in dog has also been implemented in the rabbit simulations. Drug dissolution has again been simulated using the Johnson model[287] and a mono-disperse particle radius of 25 um and 300 um used when simulating *in-vivo* dissolution of the low 12.5mg and high 100mg tablet doses respectively (see Table 2.12 for a summary of model parameters).

Moving from PO1 to PO2 the total systemic/plasma clearance is increased 2-fold from 0.75 to 1.39 L/hr/3kg rabbit, 0.75 L/hr/3kg being the systemic clearance used in intravenous simulation IV04. As shown in Figure 2.19A the plasma levels at the higher 100mg dose are best described in simulation PO1, while at the 8-fold lower oral dose (12.5mg) the 2-fold higher CL of the PO2 simulation better describes the observed plasma PK, see Table 2.14. At 12.5mg the Cmax and AUC prediction errors in simulation PO1 are 23.1% and 66.2% but reduce to -7.7% and 8.8% in simulation PO2. RMSE decreases from 0.23 to 0.09 and R^2 increases from 0.76 to 0.85 moving from simulation PO1 to PO2 respectively. However, for the 100mg oral dose, the numerical measures of model performance are improved in PO1 as compared to PO2. Cmax and AUC prediction errors in PO2 are -29.0% and -42.0% and in PO1 are 17.0% and 10.0%. RMSE decreases from 1.28 to 1.06 and Rsq increases from 0.81 to 0.93. The need for both intestinal efflux and dose dependent plasma CL to reconcile the 12.5 and 100mg oral rabbit PK may be evidence that the P-gp kinetics defined using only the IV PK data are miss-specified, or that another non-linear clearance

mechanism is contributing to BNZ disposition.

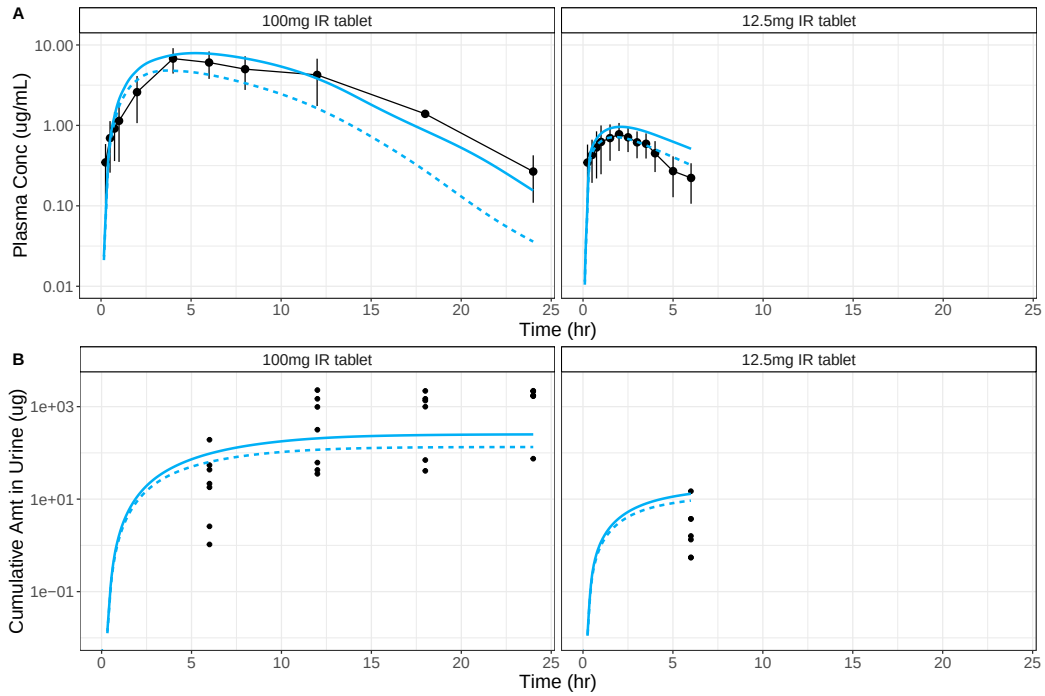

Figure 2.19: GastroPlus Rabbit PO PK simulations. PO1: solid blue line. PO2: dashed blue line.

Table 2.14: Rabbit PO PBPK simulation results

ID	Dose (mg/kg)	Tmax (h) Obs	Tmax (h) Pred	Cmax (μg/mL) Obs	Cmax (μg/mL) Pred	AUCinf (μg.h/mL) Obs	AUCinf (μg.h/mL) Pred	Fa (%)	F (%)	RMSE	R^2
PO1LD	4.17	2	2.1	0.78	0.96	4.12	6.83	38.3	35.0	0.23	0.76
PO2LD	4.17	2	1.8	0.78	0.72	4.12	4.47	47.4	39.9	0.09	0.85
PO1HD	33.30	4	5.3	6.77	7.92	77.08	84.08	69.2	63.3	1.06	0.93
PO2HD	33.30	4	3.6	6.77	4.81	77.08	44.69	73.4	61.8	1.28	0.81

Notes: LD; low dose (12.5mg). HD; high dose (100mg).

For simplicity in the rabbit simulations subsequent to IV1 total plasma clearance has been modified using hepatic clearance; (changes made to the lumped unbound liver CLint) however considering the model's ability to describe the observed urine PK data following oral dosing, see Figure 2.19B, it may be that the extent of renal re-absorption (and therefore renal clearance) is in fact a concentration dependent/saturable mechanism. For example, the fixed renal clearance of 0.003 L/hr/3kg rabbit underpredicts the mean amount of BNZ excreted in urine at Tlast by -86.4% at 100mg (PO1), while at 12.5mg the mean amount excreted in urine at Tlast is overpredicted by 220.6% (PO2). However, the lack of PK (plasma and urine) data beyond

six hours post dose at 12.5mg makes it difficult to confidently draw conclusions about the non-linearity of renal clearance.

As a final visual diagnostic, GOF plots comparing the predicted to the observed BNZ plasma concentrations are presented in Figure 2.20A and Figure 2.20C for the IV and PO simulations respectively. In Figure 2.20B and Figure 2.20D the percentage prediction error is compared to the observed plasma concentration for the IV and PO simulations respectively. These clearly show that the parameters used in IV03, IV04 and IV05 result in very similar predictive performance with some small improvement in the underprediction of the lowest concentrations in IV05. IV01 and IV02 result in a significant overprediction of plasma concentrations across all observations. For the oral data the best agreement with the observed data is achieved with the parameters used in PO1 for the high dose (HD; 100mg), but for the low dose (LD; 12.5mg) the parameters in PO2 are more predictive of the observed PK.

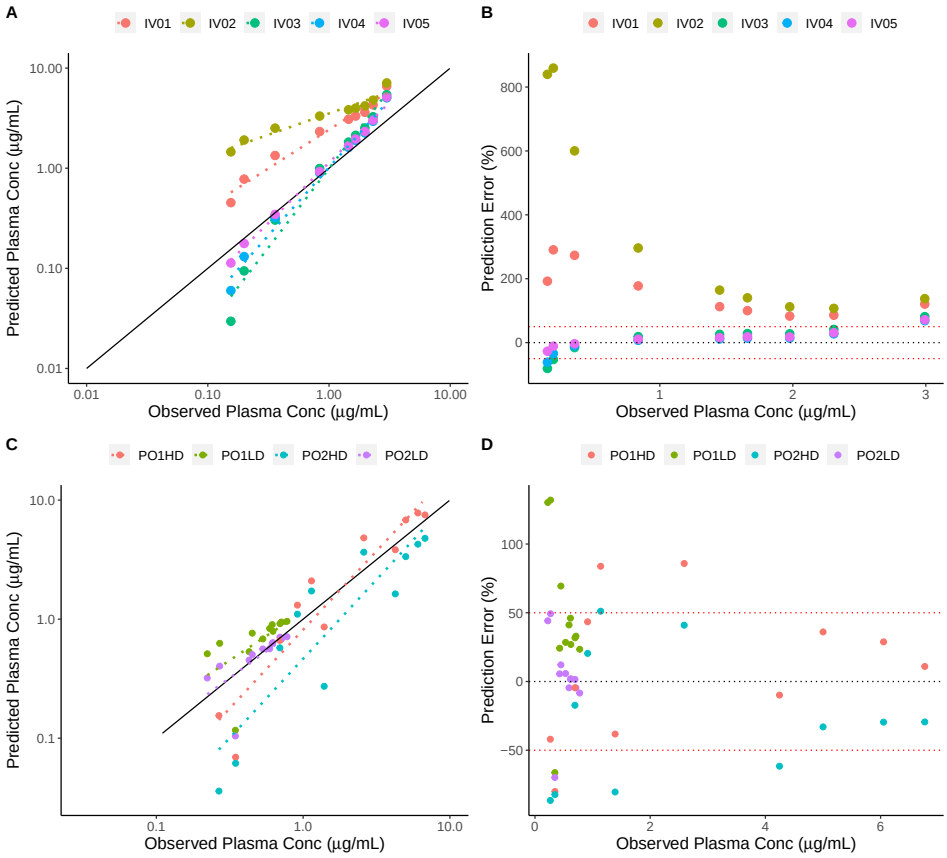

Figure 2.20: Rabbit IV and PO PBPK modelling GOF plots. A) and C) Predicted plasma concentrations versus observed plasma concentration for IV and PO simulations respectively. B) and D) Percentage prediction error versus observed plasma concentration for IV and PO simulations respectively.

2.4.2.6 Structure based parameter predictions using ADMET Predictor (objective 2c)

The physico-chemical, transporter and clearance properties predicted using ADMET Predictor[260] from 2D-structure of BNZ and selected structural analogues are presented in Table 2.15, Table 2.16 and Table 2.17 respectively. For additional information a comparison between benznidazole and metronidazole ionisation states is included in Appendix Figure B.1 and B.2. While the basic centre in metronidazole has a pKa approximately 2.5 log units higher then benznidazole both compounds are predicted to exist in their neutral forms when dissolved in solutions of pH 4 and above. There is however still delocalised charge associated with the nitrogen and oxygen atoms of the nitro group. As presented in Table 2.16 benznidazole is

Table 2.15: Physico-chemical Properties Predicted from 2D-Structure

							Fraction Unbound (%)			Blood to Plasma (%)		
Identifier	**Mw**	**Basic pKa**	**Log P**	**Log D**	**Peff**	**Sw**	**Human**	**Rat**	**Mouse**	**Human**	**Rat**	**Mouse**
metronidazole	171.157	2.41	-0.334	-0.334	2.535	13.419	83.113	80.445	81.634	1.112	0.878	0.895
misonidazole	201.183	-0.71	-0.195	-0.195	1.699	13.066	78.327	80.505	65.094	0.991	0.818	0.825
levornidazole	219.629	2.23	0.193	0.193	2.750	2.245	73.028	70.500	51.380	1.005	0.831	0.980
tinidazole	247.274	1.84	-0.282	-0.282	2.496	1.359	80.596	67.636	56.373	0.968	0.885	0.841
benznidazole	260.254	-0.87	0.749	0.749	0.979	0.333	38.272	27.738	26.585	0.756	0.960	0.893
morinidazole	270.290	6.39; 2.04	-0.298	-0.337	1.853	9.102	80.215	79.561	61.562	0.940	0.922	0.874

[1] Mw; molecular weight (g/mol)
[2] Peff; human effective permeability (x10-4 cm/s)
[3] Sw; solubility in water (mg/mL)

not predicted to be a substrate for P-gp, BCRP, OATP1B1, OATP1B3, OAT1, or OCT2 however all of these classifications are predicted with a low accuracy score (shown in parenthesis) $\leq 66\%$. Benznidazole is predicted to be a substrate for OCT1, but again the confidence in the prediction is low (54%), and also to be a substrate for OAT3 where uniquely the prediction accuracy is estimated to be high (94%). Benznidazole is predicted with $\geq 84\%$ confidence to not be a substrate for alde-

Table 2.16: Transporter Substrate Classification and Km Predictions from 2D-Structure.

Identifier	**P-gp**	**OAT1**	**OAT1 Km^2**	**OAT3**	**OAT3 Km^2**	**OCT1**	**OCT1 Km^2**	**OCT2**	**OCT2 Km^2**
metronidazole	No (51)	Yes (95)	45	Yes (94)	231.3	Yes (85)	761.3	Yes (56)	1135.6
misonidazole	No (45)	Yes (95)	12.7	Yes (75)	137.1	Yes (85)	790.6	Yes (53)	245.6
levornidazole	No (60)	Yes (83)	138.4	Yes (58)	209.3	Yes (85)	444.3	No (59)	NS[3]
tinidazole	No (56)	Yes (87)	228.3	Yes (99)	219.6	No (47)	NS[3]	Yes (56)	362.1
benznidazole	No (45)	No (50)	NS[3]	Yes (94)	25.8	Yes (54)	124.6	No (66)	NS
morinidazole	Yes (66)	Yes (65)	8	Yes (78)	87.1	Yes (76)	356.6	No (49)	NS

[1] prediction accuracy shown in parenthesis is expressed as a percentage.
[2] Km expressed in uM.
[3] NS; non-substrate.

hyde oxidase (AOX), CYP2B6, CYP2C9, CYP2D6, UGT1A1, UGT1A10, UGT1A3,

UGT1A4 and UGT1A6. The enzymes that are predicted to metabolise benznidazole are CYP1A2, CYP2A6, CYP2C8, CYP2E1, UGT1A8, UGT2B7 and UGT2B15. Only the UGT2B7 prediction is associated with $\geq 90\%$ confidence, the other positive substrate classifications are all associated with low prediction confidence (46-62%). Finally, benznidazole is not predicted to be a substrate for CYP2C19, CYP3A4 or UGT1A9 but again these are low confidence predictions (46-64%). For information the ADMET Predictor predicted metabolic pathways and metabolite structures are presented in 2.21 and Figure 2.22.

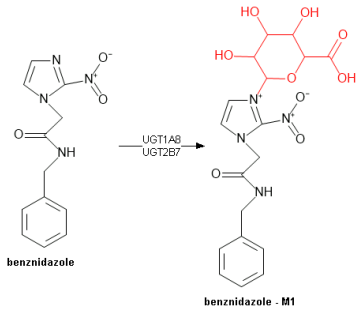

Figure 2.21: UGT mediated metabolic pathways predicted by ADMET Predictor software

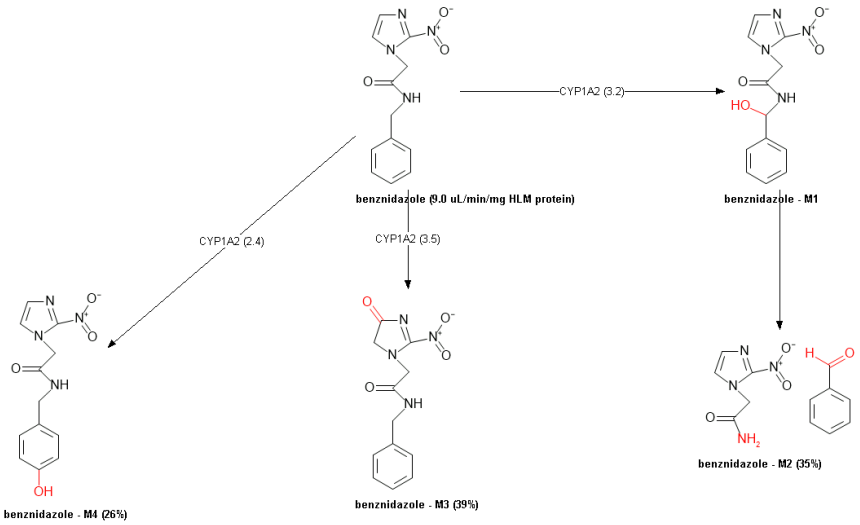

Figure 2.22: CYP mediated metabolic pathways predicted by ADMET Predictor software

Based on the AP implementation of the ECCS[264] the predominant clearance pathway for BNZ (and all the nitroimidazole analogues evaluated) is predicted to

be metabolism (99% prediction confidence) and not hepatic uptake or renal excretion. Out of the recombinant CYP kinetic models available in ADMET Predictor (CYP1A2, 2C9, 2C19, 2D6 and 3A4), AP only found benznidazole to be a substrate for CYP1A2. Table 2.17 presents the ADMET Predictor pre-dicted unbound human microsomal, and hepatocyte intrinsic clearance, alongside the predicted CYP1A2 kinetic parameters. As a comparison the metabolic substrate

Table 2.17: ADMET Predictor (AP) in-vitro intrinsic clearance and CYP specific Km/Vmax predictions from 2D-Structure

Identifier	AP Weight	CYP1A2 CLint[1]	CYP1A2 Km[2]	CYP1A2 Vmax[3]	CYP Sum CLint[1]	MIC CLint[1]	HEP CLint[4]
metronidazole	171.2[1]	12.7	88.1	21.4	12.7	14.7	4
misonidazole	201.2	130.1	8	19.9	130.1	14.8	5
levornidazole	219.6	70.2	24.1	32.6	70.2	14.4	4.9
tinidazole	247.3	1.8	117.4	4.1	2.8	12.5	4.7
benznidazole	260.3	9	170.3	29.6	9	25.7	12.2
morinidazole	270.3	NonSubstrate	NonSubstrate	NonSubstrate	0	8.2	5.6

[1] uL/min/mg HLM protein
[2] uM
[3] nmol/min/nmol enzyme
[4] uL/min/10E6 cells

classification models within ADMET Predictor found metronidazole to be a substrate for CYPs 2E1 (82%), 2A6 (82%) and 1A2 (79%). For UGTS 2B7 (93%), 1A9 (61%) and 1A8 (57%) are suggested. For comparison Pearce *et. al.* suggest that CYP2A6 is the primary catalyst responsible for the 2-hydroxylation of metronidazole; Km = 0.383 mM in pooled human liver microsomes (n=2) and 0.289 mM in rCYP2A6[289]. Unfortunately, kinetic models for CYP2A6 are not yet available in ADMET predictor.

2.4.2.4 Prediction of human clearance (objective 2d)

As discussed in Section 2.4.2.1 it has not been possible for others to establish an in-vitro BNZ intrinsic clearance in either human hepatocytes or human microsomes, as such it was not possible to perform IVIVE based predictions of human BNZ liver clearance based on measured *in-vitro* $CL_{int,u}$. Two alternative approaches remained i) IVIVE using the ADMET Predictor predicted $CL_{int,u}$ estimates, ii) cross species allometry.

ADMET Predictor based IVIVE

Scaling the ADMET Predictor predicted microsomal and hepatocyte unbound in-vitro intrinsic clearance ($CL_{int,u}$) using the Equation (2.6), predicted that BNZ hepatic liver clearance was 20.6 L/hr/70 kg and 26.4 L/hr/70 kg respectively.

Allometry

Several pre-clinical IV BNZ PK studies were identified[258,259,268]. The Dog PK reported by Workman *et. al.* and the rabbit PK reported by Davanco *et. al.* also report oral PK data and these two datasets have already been discussed and evaluated extensively using PBPK modelling, see Chapter 2.4.2.4 and Chapter 2.4.2.5 respectively.

Table 2.3 summarises the key study information for the four pre-clinical IV PK studies that were evaluated to generate an multi-species allometry based prediction of human BNZ clearance. Total plasma clearance was calculated by NCA and the results are presented in Table 2.18.

Because the rabbit PK data presented by Davanco *et. al.* was potentially highly informative (plasma and urine PK, IV and two oral dose levels) the individual rabbit plasma and urine PK data (n=35 animals, 7 in each arm) was requested from the authors for use in PBPK model development and therefore as with dog, it was possible to calculate CL at the individual level. However, a nominal rabbit BW of 3 kg was used as this information was not available. Nominal BWs are also used for rat and mouse as only the range in BW is detailed in the source publications. The total clearance from all four pre-clinical species was used to allometrically predict human BNZ clearance.

The pre-clinical IV PK profiles analysed and the resulting allometric relationship are presented in Figure 2.23. The tabulated data used to construct Figure 2.23B is included for reference in the Appendix B.5.

Using Equations (2.7) and (2.8), and assuming an average human Fup of 0.48[240,242], a 70 kg adult is predicted to have a total BNZ plasma clearance of 11 L/hr based on the relationship between BW and clearance presented in Figure 2.23B. If benznidazole excretion is mediated entirely by liver metabolism this would represent approximately 12% first pass extraction (assuming human liver blood flow is 90 L/hr).

Table 2.18: Pre-Clinical Pharmacokinetic Study Information

ID	Species	BW (kg)	Dose (mg/kg)	Cmax (ug/mL)	Tlast (h)	AUClast (ug*h/mL)	AUCinf (ug*h/mL)	Extrap %	CL (L/h)	LBF (L/hr)	FPE (%)
Mean	Mouse	0.028	32.5	25.962	5	61.377	73.994	17.1	0.012	0.148	8.1
Mean	Mouse	0.028	65	114.601	7	122.878	143.716	14.5	0.012	0.148	8.3
Mean	Rat	0.215	0.2	1.678	9	9.257	9.831	5.8	0.004	1.096	0.4
1	Rabbit	3	3.33	2.913	8	5.532	6.006	7.9	1.665	12.6	13.2
2	Rabbit	3	3.33	1.441	8	3.672	4.129	11.1	2.422	12.6	19.2
3	Rabbit	3	3.33	1.342	8	3.477	4.286	18.9	2.333	12.6	18.5
4	Rabbit	3	3.33	4.845	6	6.754	7.245	6.8	1.38	12.6	11
5	Rabbit	3	3.33	3.216	6	6.467	6.912	6.4	1.447	12.6	11.5
6	Rabbit	3	3.33	3.806	6	5.378	5.739	6.3	1.742	12.6	13.8
7	Rabbit	3	3.33	6.427	6	6.391	6.909	7.5	1.447	12.6	11.5
C	Dog	28	5	8.49	27.2	79.491	85.72	7.3	1.633	41.664	3.9
D	Dog	20	5	12.9	27.1	117.417	135.558	13.4	0.738	29.76	2.5

[1] LBF; Liver Blood Flow
[2] FPE; First Pass Extraction

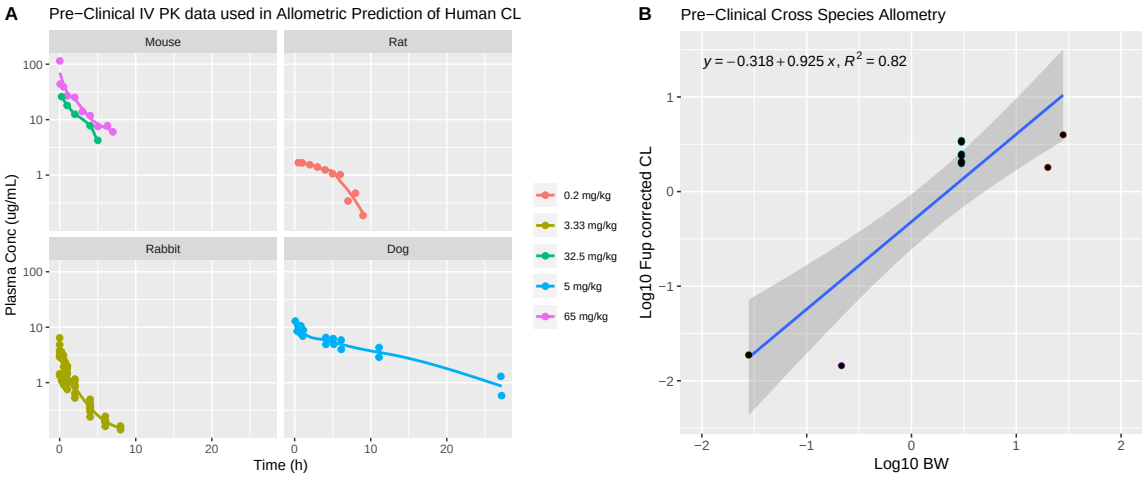

Figure 2.23: A) Pre-clinical IV PK data and B) Cross species allometry (confidence intervals: slope 0.62 to 1.23, intercept -0.61 to -0.03).

2.4.2.5 Translation of PK-Sim IV metronidazole model (objective 2e)

As discussed in the introduction there is evidence for the renal reabsorption (total $CL_p < Fup \cdot GFR$) of metronidazole, a compound that is structurally very similar to BNZ[252,253]. The metronidazole IV PK published by Houghton *et. al.*[252] was modelled in GastroPlus using insights from the PK-Sim model published by Dallmann *et. al.*[253] to investigate the balance between hepatic and renal clearance.

The model parameters used to simulate the IV metronidazole PK (plasma and urine) shown in Figure 2.24 are summarised in Table 2.19. Figure 2.24 presents predicted plasma concentration-time profiles and predicted cumulative amount of drug excreted into urine following a 500mg IV dose of metronidazole and compares

to the published measured concentrations/amounts[252].

In 'simulation 1' metronidazole plasma and urine PK are predicted using the physico-chemical and distribution parameters outlined by Dallmann et. al.[253], the model assumes no hepatic metabolism and passive renal filtration is estimated based on the product of $GFR \cdot F\,up$. The under-prediction of plasma levels and over-prediction of the amount of metronidazole excreted unchanged into urine is clear.

In 'simulation 2' (Figure 2.24, right facet) the only difference made to the model was the introduction of 2.65 L/hr hepatic clearance (CLh) and a permeability term (PSTc; permeability surface area product) on the apical side of the kidney, thereby increasing the amount of drug that is renally reabsorbed from the urine back into the systemic circulation via passive diffusion. In this second simulation 93.2% of metronidazole that is being cleared into urine through renal filtration ($F\,up * GFR$) is being re-absorbed, and the IV metronidazole plasma and urine PK are now well described. Using the simulated plasma and urine PK profiles from simulation no.2 the renal clearance (CL_r is calculated to be 0.31 L/hr ($CL_r = Ae_t/AUC_t$), therefore the relative contribution of hepatic and renal clearance to metronidazole elimination is 0.895:0.105 (CLh:CLr). In Table 2.19 the model parameters used in metronidazole PK simulation 1 and 2 are presented.

Benznidazole physico-chemical properties are very similar to metronidazole's, both are substituted nitro-imidazoles and like metronidazole renal excretion of unchanged benznidazole into urine is, given benznidazole's relatively low molecular weight and polar nature, surprisingly low (6%)[242]. Based on the findings from this metronidazole PBPK modelling, increasing apical permeability in the kidney as a means to increase the amount of renal reabsorption of benznidazole was also evaluated during benznidazole human PBPK model development.

Table 2.19: Summary of PBPK model parameters used to simulate Metronidazole IV plasma and urine PK shown in Figure 2.21

Property	Units	Simulation 1	Simulation 2
Dosing Information			
Dose	mg	500	500
Infusion Time	hr	0.33	0.33
Population Information			
Sex		female	female
Age	years	30	30
Weight	kg	56	56
Ethnicity		white American	white American
Physico-Chemical			
pKa	-	2.49 (B^a)	2.49 (B^a)
Log P	-	-0.02	-0.02
Fup	(%)	89	89
Rbp	-	1	1
Tissue Distribution			
Kp Calculation Method		Rogers and Rowland	Rogers and Rowland
Clearance			
Lumped Liver $Clint_u$	L/hr	0	3.102
Liver Blood Flow (Q)	mL/s	20.93	20.93
CL_h	L/hr	0	2.65
GFR	mL/s	2.0051	2.0051
CL_r	L/hr	6.42	0.31
Kidney Apical PSTc	mL/s	0	0.45
Systemic CL ($CL_h + CL_r$)	L/hr	6.42	2.96

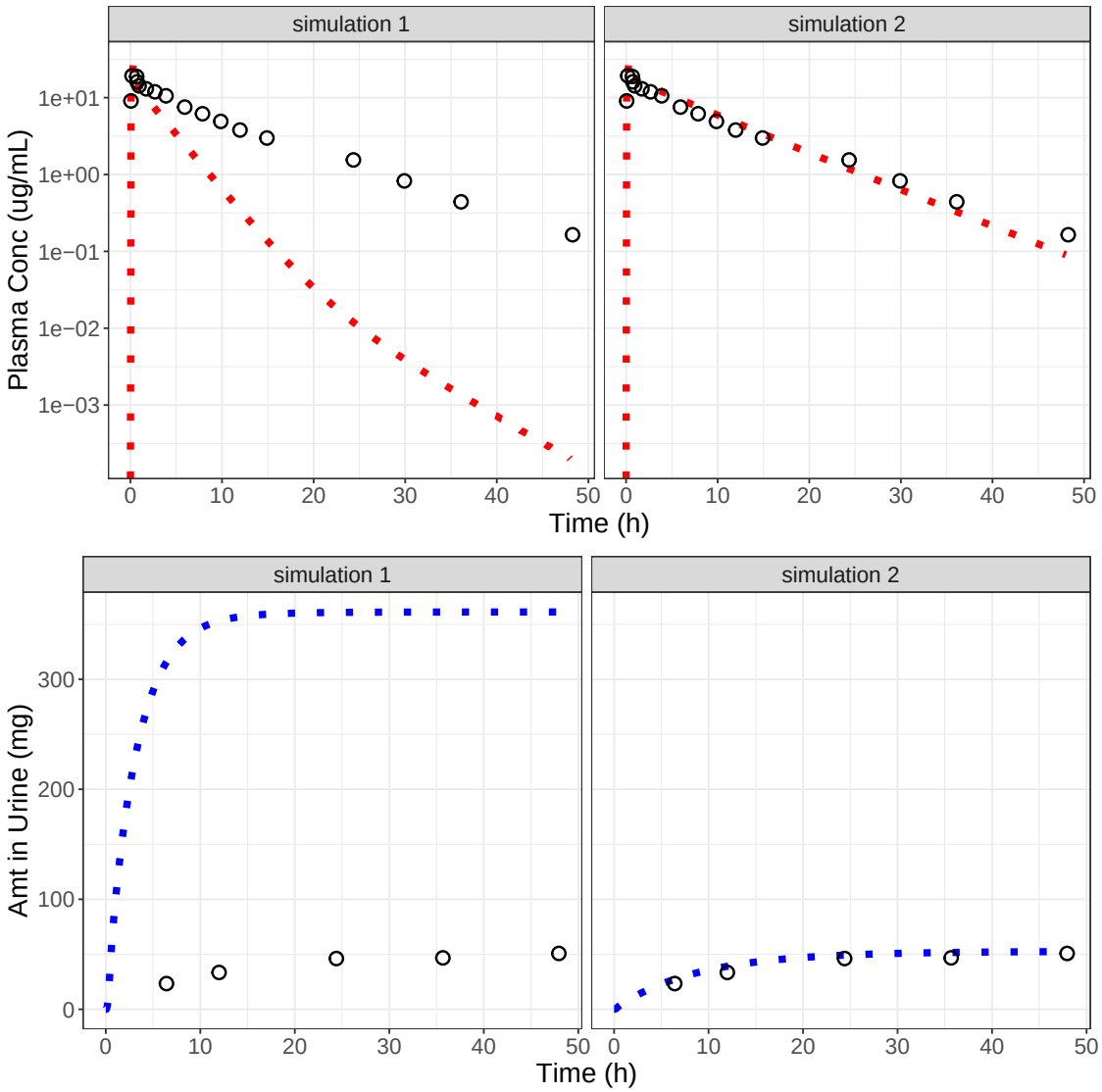

Figure 2.24: GastroPlus Metronidazole Simulations, 500mg IV. Top: Plasma PK. Bottom: Urine PK. Simulation 1: utilises a renal clearance predicted based on Fup*GFR (6.42 L/hr). Simulation 2: Implements increased renal reabsorption, thereby reducing overall renal clearance to 0.31 L/hr

2.4.2.7 Summary of BNZ PBPK properties and Initial parameter estimates

Table 2.20 summarizes and compares the results from the structure-based property predictions, the pre-clinical PBPK modelling and the human metronidazole PBPK modelling that has been performed. In Table 2.20 the ADMET predictions of species dependent properties that are shown (e.g. Fup and Rbp) are just the 'human' BNZ predictions. Table 2.20 also outlines the initial BNZ parameter estimates taken forward into physiologically based modelling of human BNZ PK data described in Chapter 2.4.3.

Table 2.20: Summary of Benznidazole ADME properties; platform of evidence for initial human BNZ PBPK parameter estimates

Property	Units	ADMET Predictor	Pre-Clinical BNZ PBPK Dog	Rabbit	IV MNZ PBPK	Initial Human Est. (sim 1)
Physico-Chemical						
pKa	-	-0.87 (B)	none	none	2.49 (B)	none
Log P	-	0.75	0.75	0.75	-0.02	0.75
Fup	%	38.27	44	70	89 (H)	56 (H)
Rbp	-	0.76	1	1	1 (H)	1 (H)
Permeability						
Human Peff $\times 10^{-4}$	cm/s	0.98	1.78	0.98	-	1.3 (H)
P-gp Km	ug/L	-	-	20	-	-
P-gp Vmax	ug/s	-	-	2	-	-
Solubility and Dissolution						
Aq solubility	mg/mL	0.33[f]	0.25	0.4	-	0.4
Particle Radius	um	-	25	25, 300	-	25
BSSR		487	487	487	-	487
Clearance						
In-vitro MIC $Clint_u$		25.7	-	-	-	-
In-vitro HEP $Clint_u$		12.2	-	-	-	-
In-vivo CL_h	L/hr	20.6[b] 26.4[c]	0.8 – 1.1	0.75 - 1.38	2.65	0
In-vivo CL_r	L/hr	2.8314	fix 0	0.003	0.31	3.698
Kidney Apical Pstc	mL/s	NA	NA	NA	0.45	-
Tissue Distribution						
Kp Method [160]		-	Berezovsky	Berezovsky	Rog and Row	Berezovsky
Tissue Model		-	perfusion	perfusion	perfusion	perfusion

[a] MNZ; metronidazole, B; base, R; rabbit, D; dog, BSSR; bile salt solubilisation, H; human, MIC; microsomal, HEP; hepatocyte

[b] In-vitro MIC CLint units; uL/min/mg protein

[c] In-vitro HEP CLint units; uL/min/10E6 cells

[d] Metronidazole simulation 2 parameters; Table 2.8

[e] Dog simulation PO5 parameters; Table 2.10

[f] Rabbit simulation IV05, LDPO2 and HDPO1; Table 2.13

2.4.3 Adult PBPK model development (Part 3)

2.4.3.1 PBPK model/parameter fitting (objective 3a)

While effort was made to inform starting estimates for compound related model parameter, see Figure 2.3 and Table 2.20, there still remains some uncertainty regarding BNZ permeability and clearance. As such these parameters have been further refined/fitted using adult clinical PK data sets.

Clinical PK data from three separate studies were used in development of the human PBPK model, the PK data is presented in Figure 2.25 and relevant study information is summarised in Table 2.4.

Combined these studies included PK data from 16 adults and includes 172 plasma levels pooled from both healthy volunteers and patients. All studies included in this dataset administered the original Roche 100mg benznidazole tablet (Radanil), however only data from 5 of the 8 subjects dosed in the Raaflaub 1980 repeat dose study[241] have been included here for calculation of the average concentration time profile as the remaining subjects all received fractionated tablets including tablets broken in halves and/or quarters. Multiple 100mg tablets were administered to achieve the very high mg/kg dose level evaluated by Robert *et. al.*[242] however subject body weight (and age) are not reported in the original publication. Plasma concentrations range from 0.025 to 29.61 ug/mL in this dataset.

As shown by Figure 2.25B overall exposure (AUC_{inf}) appears dose proportional when comparing the single dose Raaflaub 1979[240] (1.6 mg/kg) and single dose Roberts 1984[242] (25 mg/kg) PK data, while there is an approximately 20% increase in average dose normalised AUC when comparing the AUC_{inf} from the lower single dose Raaflaub study[240] (1.6 mg/kg) to the AUC_{τ}s after 3.4 mg/kg BID from the Raaflaub 1980[241] study; 29.63 to 36.61 $\mu g \cdot h/mL$ per mg/kg. While only 5 subjects received 2x100mg tablets BID in the multiple dose study, peak (3hrs post dose) and trough levels (C_{12}) were analysed on four occasions (day 10,15,20 and 25), and on 15 occasions both peak and trough levels were available on the same day hence 15 individual AUC_{τ}s are presented. While calculating an AUC from just a peak and trough level may be questionable for some compounds, given the mono-exponential decline in BNZ PK and the Tmax observed in the richly sampled single dose study (ranged from 3-4 hours)[240] this is considered a reasonable comparison to make.

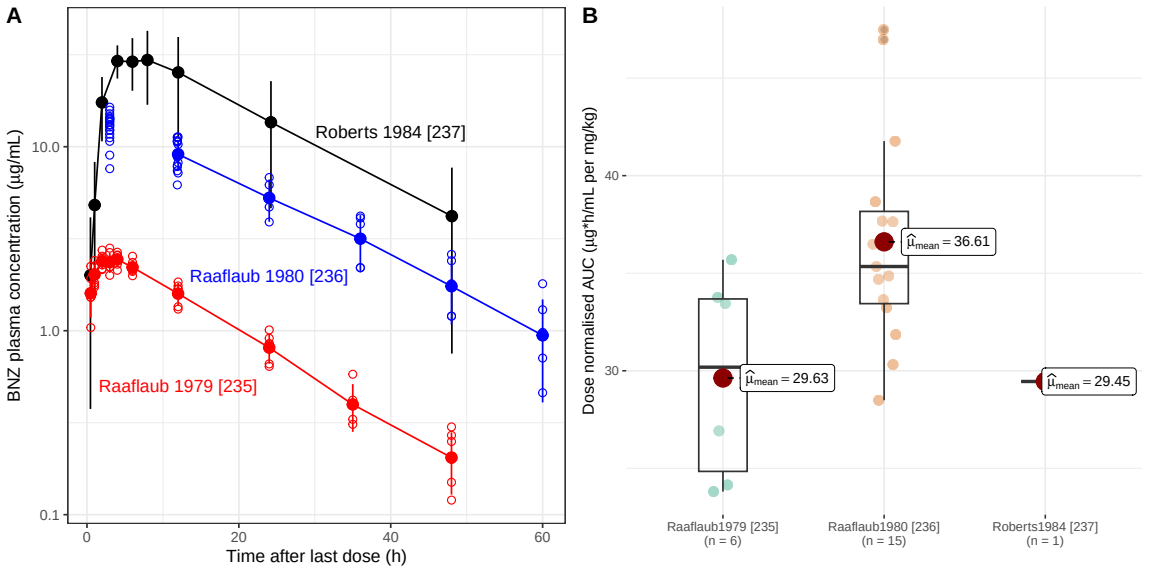

Figure 2.25: Summary of the adult benznidazole plasma PK data available for model development. Left: A) Red: 100mg single dose Radanil tablet PK in healthy volunteers, Ref [235] B) Blue: 2x100mg Radanil tablet PK at steady state after q12hr dosing in adult Chagas patients, Ref [236] C) Black: 25 mg/kg single dose PK in cancer patients using multiple Radanil tablets, Ref [237]. Filled circles and solid lines represent the calculated average (geometric mean) concentration-time profiles. Vertical error bars represent the geometric coefficient of variation (%CV) Right: Comparison of dose (mg/kg) normalised AUCs for the individuals in each study, for Roberts et. al. only the average cp-time profile is available.

Initial human PBPK simulations use the model parameters defined based on the knowledge generated in Section 2.4.2, and is summarised in Table 2.20. PK profiles simulated using these 'initial' model parameters are referred to as 'simulation 1' in Figure 2.26 and Table 2.21.

In the initial human simulations (the base human model; simulation 1) no liver metabolism was incorporated and renal clearance of BNZ is predicted based solely on $Fup * GFR$. As illustrated graphically in Figure 2.26 and by the negative linear regression intercept values (-0.398, -1.341, -0.401) and average fold errors (AFEs) which are all well below 1.0 (0.387, 0.179, 0.458) the initial human model significantly under predicts human exposure across all 3 regimens/studies. In simulation 1 Bioavailability (F) is predicted to be >95% for both Raaflaub regimens, so clearly total plasma clearance needs to be less than the 2.9-3.9 L/hr predicted by $Fup * GFR$.

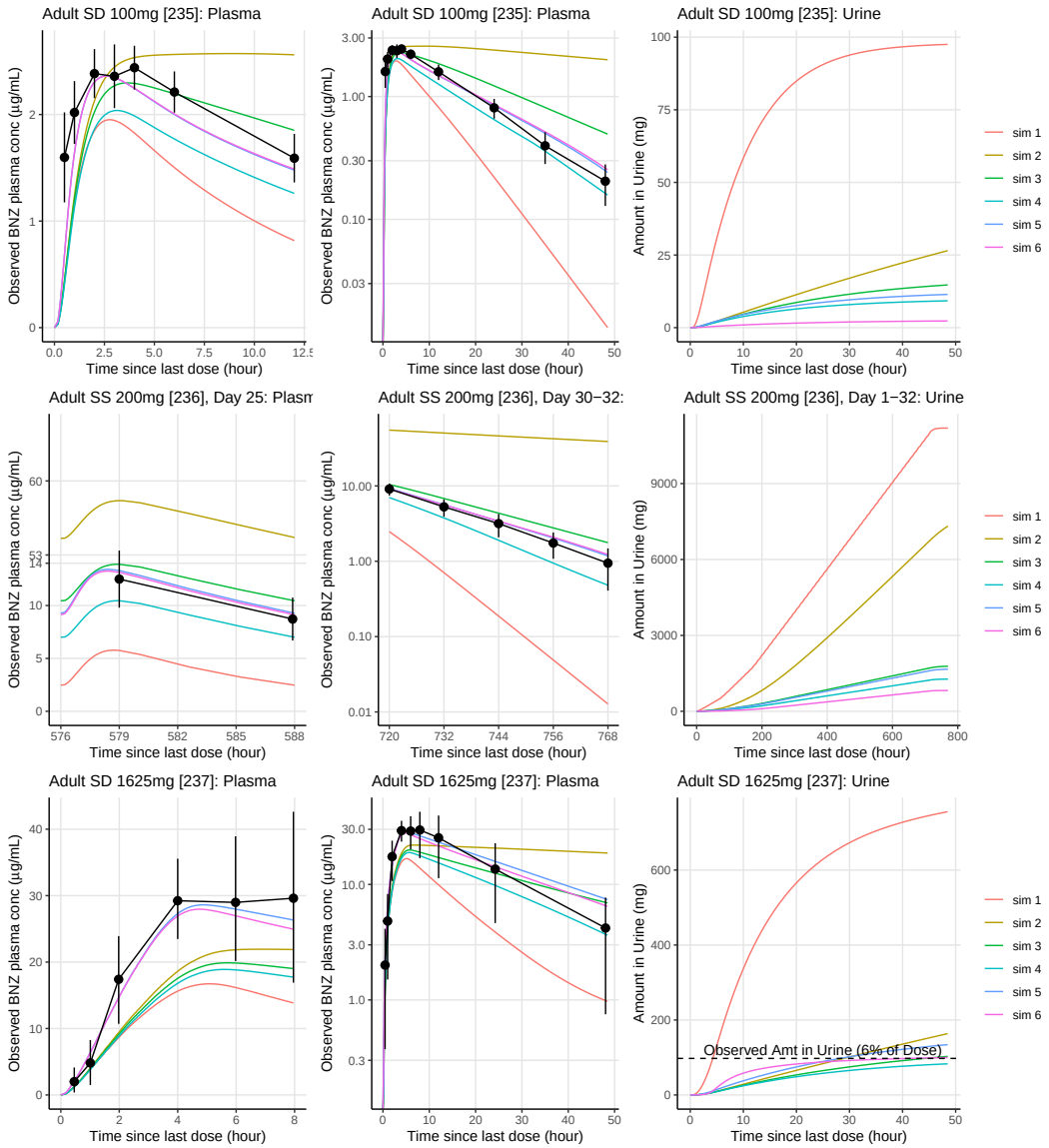

Figure 2.26: Model development predicted versus observed concentration-time profiles. Top row: Raaflaub 1979 [235] - 100mg tablet to healthy volunteers. Middle row: Raaflaub 1980 [236] - 200mg tablet q12hr to adult Chagas patients. Bottom row: Roberts 1984 [237] - 25 mg/kg to adult oncology patients. Columns 1 and 2 present plasma concentrations on a linear and log scale y-axis. Column 3 presents the predicted cumulative amount of unchanged BNZ excreted into urine, which is reported in the Roberts study [237] to be six percent of the total dose.

Table 2.21: PBPK model development simulation results and numerical measures of model performance/GOF

	Predicted			Numerical GOF Measures			
Simulation	Fa %	F %	Fe %	R^2 , Intercept	RMSE	AFE	AAFE
Raaflaub 1979 [235]							
1	96.8	96.8	97.5	0.892 , -0.398	0.673	0.387	2.585
2	94.3	93.8	26.5	0.004 , 1.964	1.099	1.476	2.151
3	95.9	94.5	14.7	0.615 , 0.393	0.518	1.009	1.533
4	55	54.3	9.2	0.814 , -0.084	0.561	0.7	1.429
5	69.8	68.8	11.4	0.876 , 0.01	0.331	0.916	1.201
6	69.5	68.4	2.3	0.873 , 0.026	0.331	0.925	1.211
Raaflabu 1980 [236]							
1	95.4	95.4	102.9	0.893 , -1.341	5.905	0.179	5.587
2	78.5	78.4	67.3	0.262 , 42.664	41.373	7.403	7.403
3	93.5	92.3	16.4	0.974 , 1.36	1.351	1.228	1.236
4	65.9	65	11.7	0.977 , -0.476	2.053	0.72	1.388
5	86.3	85.2	15.3	0.977 , 0.365	0.684	1.059	1.082
6	96.4	85.1	7.6	0.979 , 0.417	0.631	1.056	1.08
Roberts 1984 [237]							
1	48.3	48.1	46.5	0.921 , -0.401	10.642	0.458	2.182
2	46.3	46	10.1	0.504 , 6.681	7.918	0.942	1.625
3	47.3	46.7	6.3	0.921 , 2.038	7.301	0.747	1.499
4	34.3	34	5.1	0.976 , 0.72	8.09	0.65	1.539
5	58.4	57.8	8.3	0.976 , 2.237	2.271	1.066	1.186
6	58.7	57.9	6.1	0.981 , 1.916	2.633	1.016	1.178

Notes: Fa; fraction of dose absorbed into the enterocyte. F; Fraction of dose systemically available (bioavailability). Fe; Fraction of dose excreted as unchanged BNZ into urine

In simulation 2 renal clearance was significantly reduced by increasing the permeability on the apical side of the kidney compartment (urine facing) to allow more BNZ to be reabsorbed, this is clearly shown by the significant drop in the amount of unchanged BNZ predicted to be excreted into urine when comparing simulation 1 and 2. This has been achieved by increasing the apical permeability surface area product (PSTc) in the kidney compartment from 0 to 0.4 mL/s. The effect is essentially a PK simulation with minimal clearance hence for all regimens all plasma levels post Cmax are significantly overpredicted, the R^2 values are the worst out of all the simulations (0.004, 0.262, 0.504) and the intercepts the highest (1.964,42.664, 6.681) for all the three regimens. However, it is noteworthy that the Cmax for the high dose study

(Roberts 1984)[242] is still underpredicted, which suggests that the simulation 2 model is not correctly describing the relationship between dose and Fa.

In simulation 3 a small amount of hepatic clearance was introduced by incorporation of an unbound hepatic intrinsic clearance of 1.9 L/hr. Apical kidney PSTc is held at 0.4 mL/s. All 3 regimens show a significant improvement in R^2. However, the requirement for incorporation of additional non-linearity into the model (in addition to solubility effects on Fa) becomes apparent. Moving from simulation 2 to 3 the RMSE improves for the steady state[241] and single dose[240] Raaflaub datasets; 41.373 to 1.351, and 1.099 to 0.518 respectively, but stays roughly the same for the Roberts study[242] (7.918 to 7.301). Considering also the AFE, this indicates reasonably precise prediction of the single dose Raaflaub data[240] (AFE 1.009) slightly more over prediction of the SS Raaflaub data[241] (AFE 1.228) but predominantly under prediction of the Roberts[242] plasma levels (AFE 0.747). Moreover, the shape of the Roberts[242] PK profile is so poorly captured that even though there is a general trend for underprediction the intercept from the linear regression (observed versus predicted levels) is still > 0 (Intercept = 2.038). Again in simulation 3 there is also a significant difference between Fa for the two Raaflaub regimens[240,241] and the Roberts[242] regimen; 95.9, 93.5 and 47.3 respectively.

Since a contribution of P-glycoprotein (MDR1) efflux to BNZ disposition has previously been suggested[238,278] incorporation of intestinal efflux into the model was evaluated in simulation 4. P-gp Km and Vmax parameters were fitted using the clinical model development datasets. The parameter values used in simulation 4 (and the final model) are 20 $\mu g/L$ (76.8 nM) and 0.5 $\mu g/s$ for Km and Vmax respectively. Default software settings were used to define regional P-gp expression in the intestine. Inclusion of P-gp had a significant effect on the Fa predicted for the lowest dose levels, reducing Fa from 96% to 55% (single dose Raaflaub regimen, 100mg[240]). Fa reduced from 94% to 66% for the steady state Raaflaub regimen, 200mg[241] and from 47% to 34% for the high single dose Roberts study, 25 mg/kg[242]. The result across the entire data set is that rather than under-prediction of just the high single dose study[242], all the regimens were now under-predicted, AFE = 0.7, 0.72 and 0.65.

Simulation 5 corrected this general under-prediction through an increase in the initial estimate of effective jejunal permeability (Peff) from 1.3 to 2.2 x 10^{-4} cm/s. Across the three studies in order of increasing dose Fa was now predicted to be; 70%, 86% and 58%. RMSE and AFE were improved for each regimen; RMSE in simulation 5 is; 0.331, 0.684 and 2.271, down from; 0.561, 2.053 and 8.09 in simulation 4. AFE in simulation 5 is; 0.916, 1.059 and 1.066, which was up from; 0.7, 0.72 and 0.65 in

simulation 4.

The final change to the model relates to the switch from passive renal reabsorption achieved through the apical PStc term in the kidney, to inclusion of an apical influx transporter in the kidney instead. This change to the model was not made to improve the fit to the adult data which was already good as seen in simulation 5 but to facilitate testing of the hypothesis that it is the extent of renal reabsorption that is reduced in children aged 2-6 years, see Chapter 2.4.4. In simulation 6 a generic apical influx transporter was added to the kidney and expression set at a level comparable to other renal transporters; 28 $\mu g/g$-tissue. Hepatic clearance is increased slightly by raising the unbound *in-vivo* liver Clint to 2.31 L/hr/65kg and scaling this across the three study populations. The final *in-vivo* renal transporter kinetics are fitted using the clinical PK data; Km = 10 $\mu g/mL$ (38.4 μM) and Vmax = 2 $\mu g/s/mg$-transporter. Given the expression level that has been defined (28 μg-protein/gram-tissue) this *in-vivo* Vmax would convert to an unbound *in-vitro* Vmax of 0.11 nmol/min/mg protein.

2.4.3.2 PBPK final adult model (objective 3a)

The final adult PBPK model parameters are presented in Table 2.22, they are presented for each of the datasets/studies evaluated during model development. This highlights the differences between the PBPK parameters used to simulate the observed PK in the three studies. These include the body weight and age of the *in-silico* physiology and the dose/regimen implemented in the simulation.

Where measured data were available for the fraction of drug bound to plasma proteins in a given population/study then this has been used as it has a significant impact on the calculated tissue partition coefficients (the predicted Vss) and therefore levels of drug observed in plasma. Plasma protein binding (PPB) in five healthy female subjects is reported by Raaflaub et. al. to be 44.1 % ± 1.39[240]. This data is not reported for the Chagas patient population used by Raaflaub to evaluate the multiple dose kinetics of BNZ[241]. In the final BNZ PBPK model human Fup is assumed to be 56 % unless study/population specific measured data is available, such as in the population studied by Roberts *et. al.*[242] where they report PPB to be 60 % ± 1 (n=24)[242]. Within Gastroplus a contribution of drug binding to lipids present in plasma is incorporated through an 'adjustment' of Fup which is a calculation based on a compounds lipophilicity. Since BNZ is a relatively hydrophilic compound (low Log P) this results in only a small adjustment; an Fup of 56% is 'adjusted' to 54.95 when considering protein and lipid binding.

Table 2.22: Adult PBPK model: Final Parameters

Parameter	Units	Raaflaub 1979	Raaflaub 1980	Roberts 1984	Source
Population					
Age	years	23	36	34	Study
Weight	kg	61	58.5	65	Study
Dose	mg/kg	1.64	3.42	25	Study
Regimen		Radanil SD	Radanil q12hr SS	Radanil SD	Study
Physico-Chemical					
pKa		none	none	none	Measured
Log P		0.75	0.75	0.75	Measured/AP
Adjusted Fup	%	54.95	54.95	39.46	Measured
Rbp		1	1	1	Measured
Permeability					
Human Peff	x10^{-4}cm/s	2.2	2.2	2.2	Optimised
P-gp Km	$\mu g/L$	20	20	20	Optimised
P-gp Vmax	$\mu g/s$	0.5	0.5	0.5	Optimised
Solubility and Dissolution					
Aq solubility at 37°C	mg/mL	0.4	0.4	0.4	Measured
Particle Radius (um)	μm	25	25	25	Default
Bile Salt Solubilisation		487	487	487	Calculated
Dissolution Model [282, 283]		Johnson	Johnson	Johnson	Default
Gut System Parameters (ACAT)					
Asc Colon P-gp DF		1	1	1	Default
Duodenum P-gp DF		0.538	0.538	0.538	Default
Stomach Transit Time	hr	0.5	0.5	0.5	Optimised
Clearance					
Systemic Clh	L/hr	1.19	1.153	0.901	Calculated
$Clh_{int,u}$	L/hr	2.2	2.13	2.31	Optimised
Liver Blood Flow (Q)	L/hr	78.22	76.53	81.03	System
Clr_{filt}	L/hr	4.14	3.87	2.81	System
Renal T K_m	$\mu g/mL$	10	10	10	Optimised
Renal T V_{max}	$\mu g/s/mg$	2	2	2	Optimised
Renal T Expression	$\mu g/g$	28	28	28	Optimised
Tissue Distribution					
Kp Method [160]		Berezovsky	Berezovsky	Berezovsky	Rat and Dog
Tissue Model		Perfusion	Perfusion	Perfusion	Rat and Dog

Notes: SD; single dose. SS; steady state. DF; regional gut distribution factor. AP; ADMET Predictor. References; Raaflaub 1979 [235], Raaflaub 1980 [236], Roberts 1984 [237].

Finally, the majority of gut physiology (ACAT) parameters; regional intestinal length, radius, volume, villi density, P-gp expression have been unmodified from the default values that are calculated by the PBPK software based on the user defined weight of the *in-silico* 'body'. Stomach transit time was increased from the default 0.25hr typically used in the fasted state for an IR tablet, to 0.5hr. Absorption scale factors (ASFs) are a set of parameters that are both 'system' and 'compound' derived

and are how, within GastroPlus, regional differences in intestinal permeability can be accounted for. Figure 2.27 presents the average adult values for these predominantly 'system' derived absorption parameters, they do vary slightly between the three adult datasets/study because of the small differences in median body weights utilised in the predictions. To see study specific parameters see Appendix Table B.6

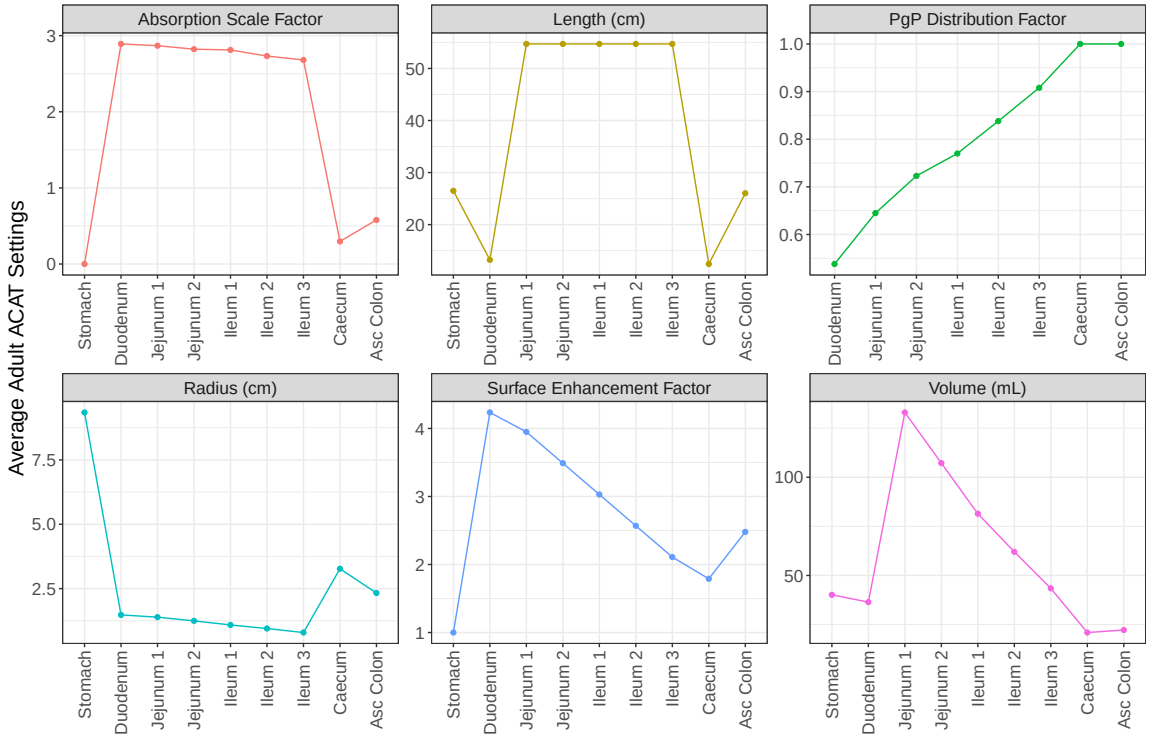

Figure 2.27: Adult Advanced Compartmental Absorption and Transit (ACAT) Settings

In Figure 2.28 the predicted relationship between dose and fraction absorbed (Fa, expressed as a percentage) is compared using the final model (the Raaflaub 1979 physiology/system parameters were utilized) and the 'bottom up' model, which refers to a model that uses the 'initial' parameter estimates as presented in Table 2.20. The ver-tical reference lines highlight the doses administered in the three model development datasets. The 'initial' model predicts that solubility will reduce the Fa at doses above ~300mg, while the dose versus Fa relationship described by the final model, involves supra-proportional increases in Fa up to around 400 mg followed by reductions in Fa due to solubility limitations.

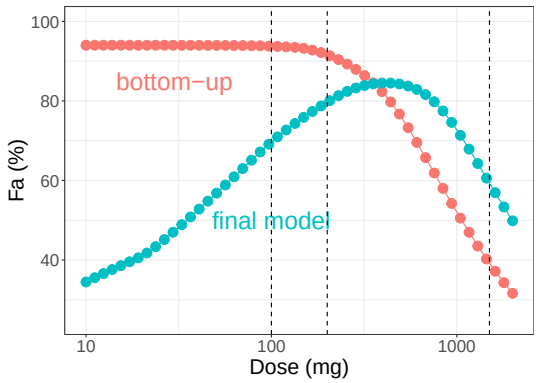

Figure 2.28: The predicted effect of dose on fraction absorbed (Fa, expressed as a percentage). A comparison between 'bottom-up' and final model predictions. Vertical reference lines highlight dose levels in the model development datasets.

Figure 2.29 evaluates the final model performance by comparing the predicted and observed geometric mean plasma cp-time profiles (first y-axis) and the cumulative amount excreted into urine (second y-axis). In the Roberts 1984[242] study, 6% of the administered BNZ dose was excreted unchanged in the urine. Assuming a median BW of 65kg, this equates to approx 98 mg BNZ excreted unchanged into urine, see the blue horizontal dashed reference line in Figure 2.29C. The final PBPK model predicts 99.7 mg which is in good agreement.

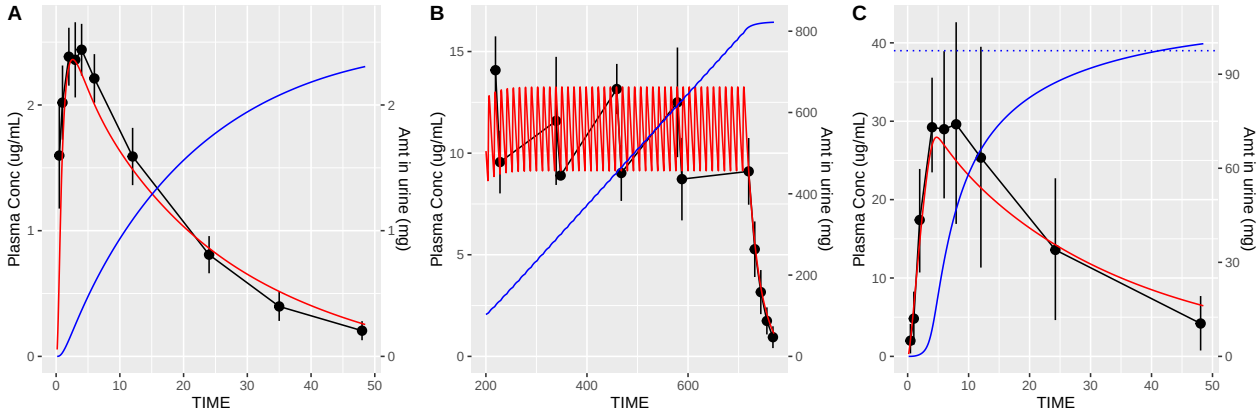

Figure 2.29: Final adult PBPK model performance; predictions versus observed data. First y-axis; BNZ plasma concentration. Second y-axis; amount in urine. Red lines; model predicted plasma concentration-time profile. Blue line; model predicted cumulative amount in urine. Black circles and lines; observed geometric mean plasma-concentration profiles. Facets: A) Raaflaub 1979 - 100mg tablet to healthy volunteers [235]. B) Raaflaub 1980: 200mg tablet q12hr to adult Chagas patients [236]. C) Roberts 1984 - 25 mg/kg to adult oncology patients [237].

Evaluating the GOF plots presented in Figure 2.30, all predicted plasma concentrations are within ± 60% of the observed geometric mean concentrations (84% were within +/-25%) for the three studies used during model development: internal model validation.

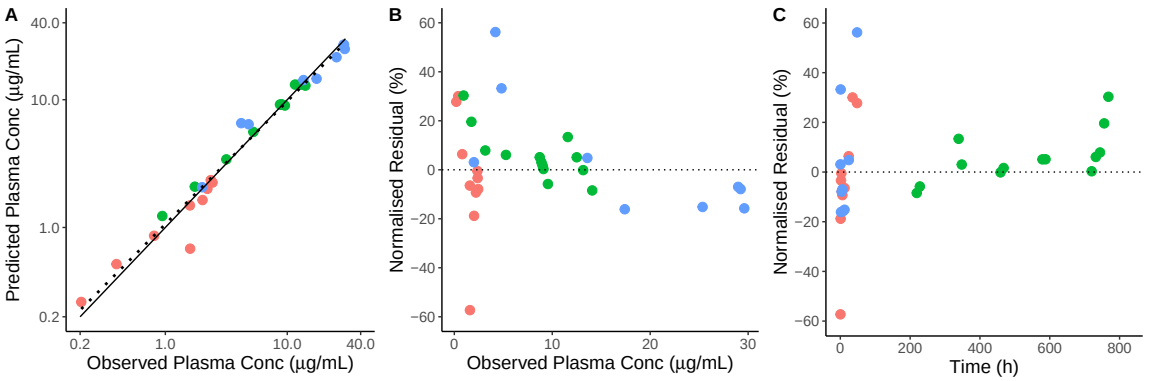

Figure 2.30: Final adult PBPK model GOF plots. A) Predicted vs observed geometric mean plasma concentrations. B) Percentage prediction error vs observed geometric mean plasma concentrations. C) Percentage prediction error vs time since first dose. Blue: Roberts 1984 [237]. Green: Raaflaud 1980 [236]. Red: Raaflaub 1979 [235].

The predicted PK parameters for the internal model validation datasets[240–242] are presented in Table 2.23.

Table 2.23: PK predictions for the internal validation datasets

Parameter	**Raaflaub 1979**	**Raaflaub 1980**	**Roberts 1984**
Fa	0.697	0.865	0.587
F	0.685	0.852	0.579
AUCinf/AUCtau ($\mu gh/mL$)	52.6	135	911.2
Cmax ($\mu g/mL$)	2.4	13.3	27.9
Tmax (h)	2.6	2.4	4.8
Total CLp (L/h)	1.302	1.262	1.033
CLr (L/h)	0.048	0.102	0.139
Renal Reabs	0.989	0.974	0.951
Fe (%)	2.298	7.529	6.056
Fm:Fr	0.96:0.04	0.92:0.08	0.86:0.14

[a] SD; single dose. SS; steady state

The impact of varying Fup, Rbp, Peff, CLh, aqueous solubility and transporter Vmax (P-gp and the renal apical influx transporter) on F, AUC_{inf}, Cmax and Tmax is presented in Figure 2.31.

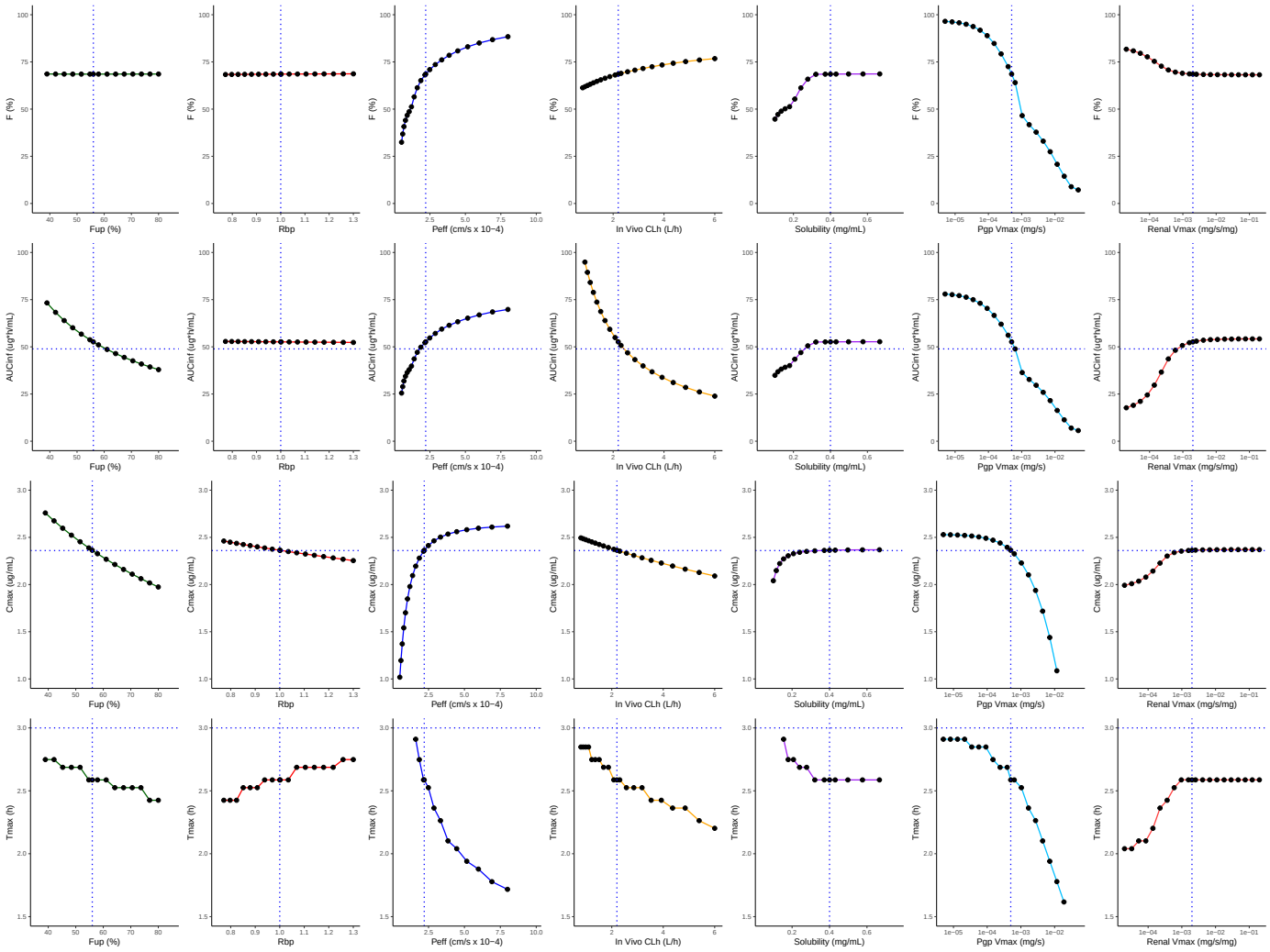

Figure 2.31: Parameter sensitivity analysis with the final adult BNZ PBPK model

This analysis showed that F% (because of the impact on Fa) is highly sensitive to Peff and P-gp Vmax and further *in-vitro* permeability studies are highly recommended to increase confidence in the model estimates. AUC and Cmax can vary by 50% as Fup is varied from 40 to 80% and measuring PPB in future clinical trials that have PK end points would also be valuable.

2.4.3.3 External model verification (objective 3b)

A subset of the BENDITA trial[248] BNZ PK data was simulated as 'external' verification of the final adult model parameters.

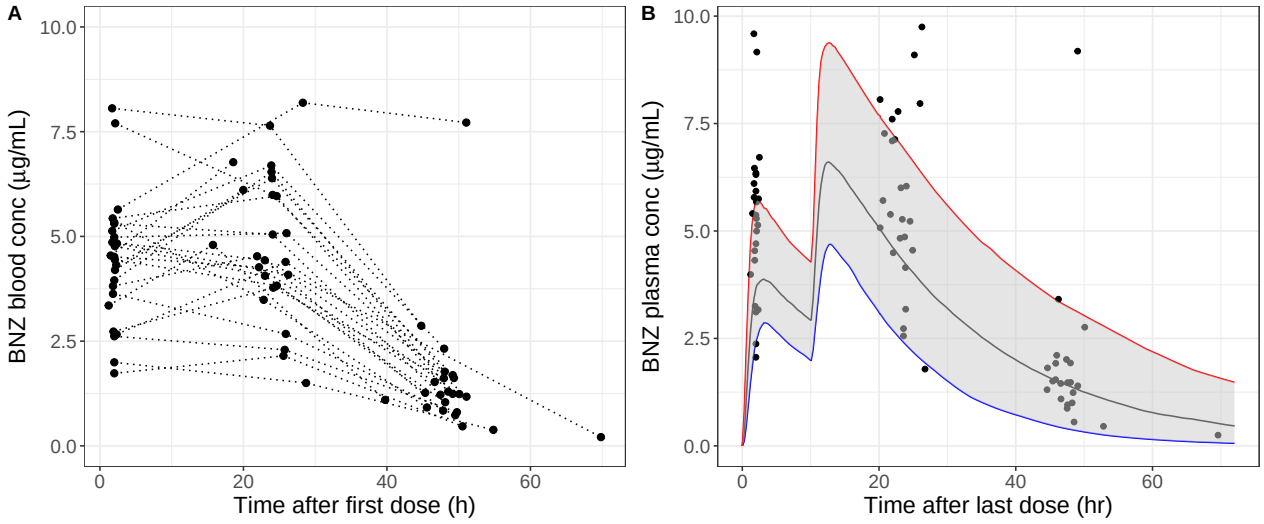

Figure 2.32: Adult PBPK model verification using BNZ PK data from the BENDITA trial (treatment group 6) [243]. Left - BNZ concentrations following day 1 dosing, determined using the dried blood spot assay. Right - Population simulation results, n=300 simulations, blood levels were converted to plasma levels using the correlation published by Bedor et. al. (2018) [266]. Key: Black circles; measured BNZ concentrations in blood (Fig 2.31A) and in plasma (Fig 2.31B). Dashed black lines; connect measured BNZ concentrations from a given individual patient. Grey shaded area; 95% prediction interval from n=300 PBPK simulations. Blue solid line; 2.5th percentile of the simulated plasma profiles. Black solid line; 50th percentile of the simulated plasma profiles. Red solid line; 95th percentile of the simulated plasma profiles.

The BNZ blood concentrations as quantified by a dried blood spot assay in the BENDITA trial[248] are presented in Figure 2.32A. In Figure 2.32B BNZ plasma concentrations are compared with the 2.5th, 50th and 97.5th percentile from a population simulation (n=300 simulations) using the final adult PBPK model. In Figure 2.32B,

78% of measured BNZ concentrations fall within the 95% prediction interval, this shows acceptable performance of the adult PBPK model and it's ability to predict BNZ PK data that was not used during model development/parameter fitting.

2.4.4 Paediatric PBPK model extrapolation (Part 4)

Figure 2.33 and Table 2.24 compare the paediatric simulation results that were achieved using extrapolation of the final adult model in three different ways; simulations 1 to 3 (sims1, sim2 and sim3).

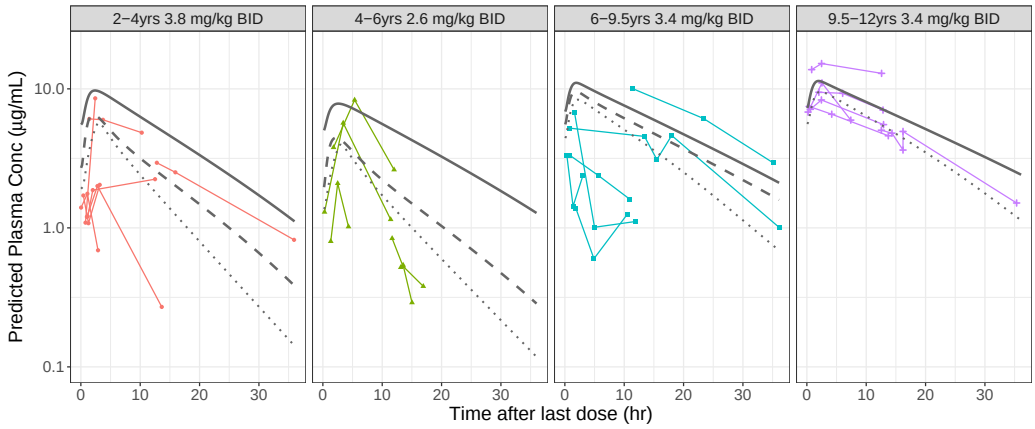

Figure 2.33: Paediatric PBPK predictions compared to measured steady state plasma levels. Solid black line: Simulation 1 (sim1): implements the final adult PBPK model scaled for only paediatric age, weight, and dose. Dashed black line: Simulation 2 (sim2) as in sim1 plus reduced renal transporter expression in children < 9.5 years. Dotted black line: Simulation 3 (sim3) as in sim2 plus modification to the default ACAT setting to further reduce predicted paediatric Fa.

The differences in approach in simulations 1-3 were as follows:

- **Simulation 1 (sim1)**: Utilised the final adult model scaled only for paediatric age, weight and dose.
- **Simulation 2 (sim2)**: Utilised the final adult model scaled for paediatric age, weight and dose, and used age based reduction of renal transporter abundance; reduced to between 20-40%, 70% and 100% of adult levels in the 2-6, 6-9.5 and 9.5-12 year age groups respectively
- **Simulation 3 (sim3)**: Utilised the final adult model scaled for paediatric age, weight and dose, and used age based reduction of renal transporter abundance;

reduced to between 20-40%, 70% and 100% of adult levels in the 2-6, 6-9.5 and 9.5-12 year age groups respectively. Plus modifications to the default ACAT (gut physiology) settings.

Table 2.24: PBPK predicted paediatric exposure: AUCtau and fraction absorbed (Fa) at Steady State. Paediatric sub-populations: Group1: 2-4 years. Group 2: 4-6 years. Group 3: 6-9.5 years. Group 4: 9.5-12 years.

	AUCtau (μg.hr/mL)			**% Fa**		
Age (yrs)	**sim1**[a]	**sim2**[b]	**sim3**[c]	**sim1**[a]	**sim2**[b]	**sim3**[c]
2-4	90.4	52.2	42.2	91.7	92.4	60.6
4-6	75.8	36.5	29.8	88.8	90.2	62.7
6-9.5	104.7	87.9	77.2	90.4	90.7	67.6
9.5-12	109.2	109.2	93.2	90.3	90.3	68.5

[a] sim1: implements the final adult PBPK model scaled for only age, weight, and dose.
[b] sim2: 'sim1' approach plus reduced renal transporter expression in children < 9.5 years.
[c] sim3: 'sim2' approach plus modification to the default ACAT settings to further reduce Fa.

In the younger children the 'default' approach to scaling the ACAT 'gut/system' parameters may be contributing to an over-prediction of Fa, see Table 2.24 and Figure 2.33. In paediatric simulation 3 the surface area enhancement factors (SEFs) have been manually modified to achieve absorption scale factors (ASFs) consistent with those in the adult model, and the Pgp distribution factors (DFs) have also been matched to those used in the final adult model. This results in Fa in the steady state paediatric groups reducing from 89-92% in simulations 1 and 2 to 61-69% in simulation 3.

In Figures 2.34 and 2.35 the gut specific 'system' parameters (the ACAT parameters) are compared between the final adult ACAT model and the paediatric simulations; simulations 1 and 2 in Figure 2.34 and simulation 3 in Figure 2.35. Paediatric simulations 1 and 2 use the default ACAT setting as defined by the software based on the specified paediatric age and weight.

A visual comparison of the relative renal transporter expression levels employed in paediatric simulations 2 and 3 are presented alongside the OCT1 ontogeny data reported by Cheung *et. al.* in the Appendix Figure B.5. In simulation 3 the same renal transporter expression levels as used in simulation 2 are employed plus modifications to the default ACAT/gut settings have been made to further reduce Fa in the paediatric simulations. All paediatric PBPK parameters used in Simulation 3 are outlined in Table 2.25 and the simulation 3 results summarised in table 2.26.

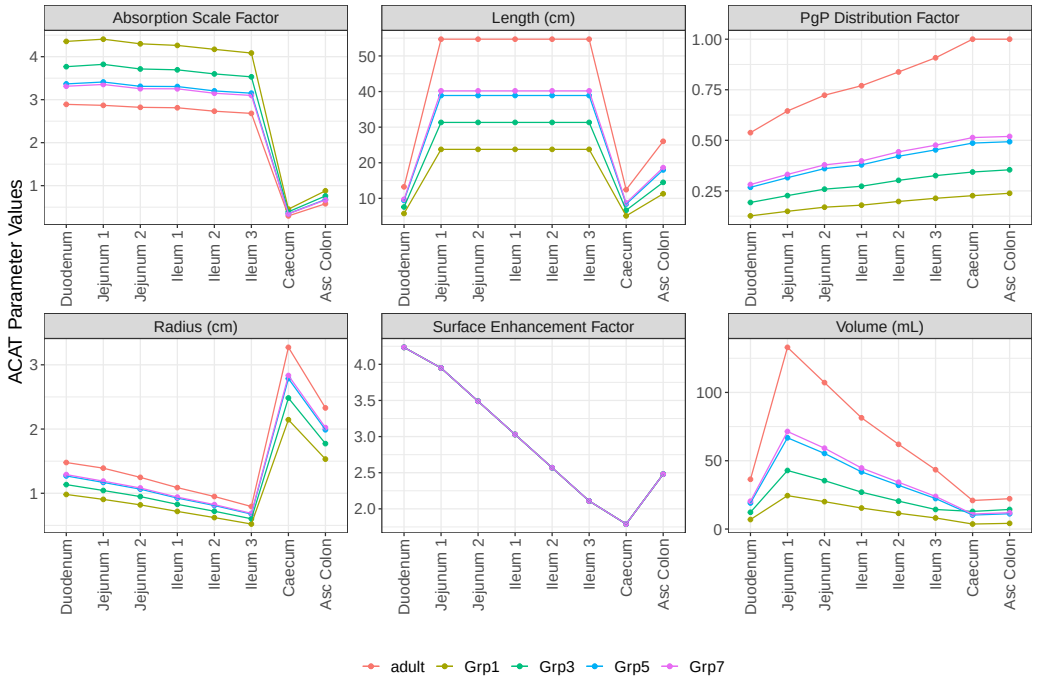

Figure 2.34: Comparison between the default adult and default paediatric ACAT settings used in paediatric simulations 1 and 2. Key: Grp1; 2-4 years. Grp3; 4-6 years. Grp5; 6-9.5 years. Grp7; 9.5-12 years.

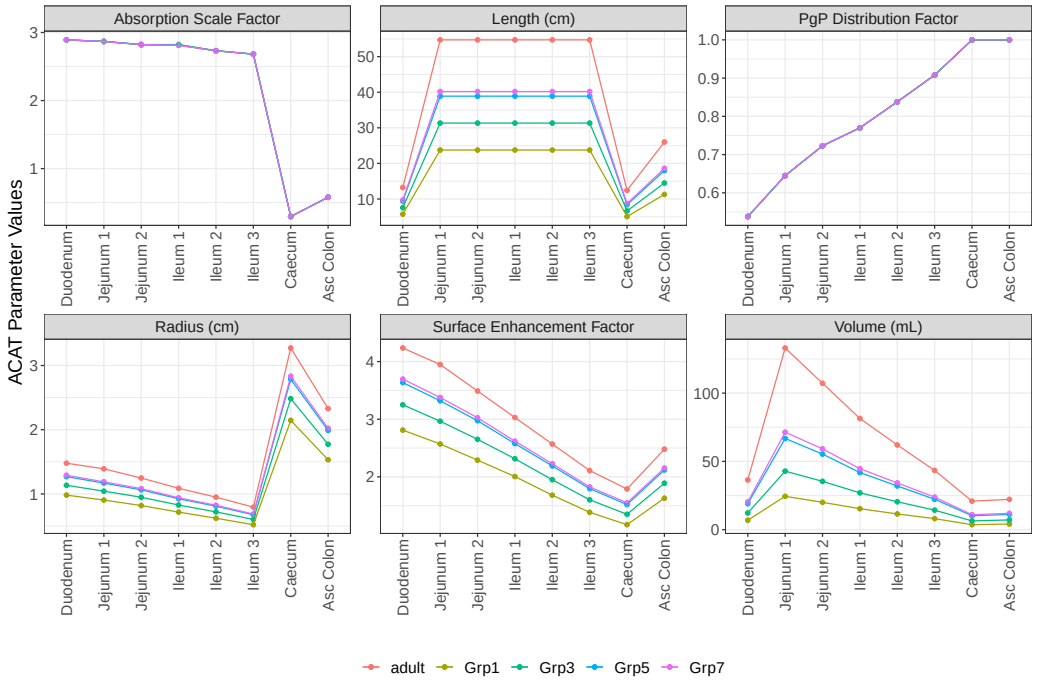

Figure 2.35: Comparison between the default adult and modified paediatric ACAT settings used in paediatric simulation 3. Key: Grp1; 2-4 years. Grp3; 4-6 years. Grp5; 6-9.5 years. Grp7; 9.5-12 years.

Table 2.25: Paediatric PBPK parameters used in Simulation 3

		Age Groups			
PBPK Model Parameters	**Units**	**2-4yrs**	**4-6yrs**	**6-9.5yrs**	**9.5-12yrs**
Age	years	3	5	8	11
Weight	kg	12	20	30	32
Dose	mg/kg	3.8	2.6	3.4	3.38
Physico-Chemical					
LogP		0.75	0.75	0.75	0.75
Fup	Fup (%)	57.2548	56.7835	56.0909	55.415
Rbp		1	1	1	1
Permeability					
Human Peff	x10^{04}cm/s	2.2	2.2	2.2	2.2
P-gp Km	μg/L	0.02	0.02	0.02	0.02
P-gp Vmax	μg/s	0.0005	0.0005	0.0005	0.0005
Solubility and Dissolution					
Aq Solubility at 37°	mg/mL	0.4	0.4	0.4	0.4
Particle Radius	μm	25	25	25	25
BSSR		487	487	487	487
Dissolution Model [282, 283]		Johnson	Johnson	Johnson	Johnson
Gut/System Parameters (ACAT)					
Asc Colon P-gp DF		1	1	1	1
Duodenum P-gp DF		0.538	0.538	0.538	0.538
Stomach Transit Time	hr	2.7	2.7	0.5	0.5
Clearance					
Systemic CL_h	L/hr	0.431	0.533	0.712	0.74
$Clh_{int,u}$	L/hr	0.65	0.953	1.292	1.356
Liver Blood Flow (Q)	L/hr	25.5145	34.12087	41.70564	48.10716
Clr_{filt}	L/hr	1.7096	2.12919	2.83544	3.3712
Renal T Km	μg/mL	10	10	10	10
Renal T Vmax	μg/s/mg	0.002	0.002	0.002	0.002
Renal T Expression	μg/g	0.0112	0.006	0.0196	0.028
Tissue Distribution					
Kp Method [160]		Berezovsky	Berezovsky	Berezovsky	Berezovsky
Tissue Model		Perfusion	Perfusion	Perfusion	Perfusion

Notes: DF; regional gut distribution factor. Kp; tissue/plasma partition coefficient. Absorption scale factors (ASFs) manually fixed to average adult values.

Table 2.26: Predicted paediatric steady state PK using the 'Simulation 3' approach.

	Age Groups (years)			
PK Parameters	**2-4**	**4-6**	**6-9.5**	**9.5-12**
Dose (mg/kg)	3.8	2.6	3.4	3.38
Fa	0.61	0.63	0.68	0.69
F	0.6	0.62	0.66	0.67
AUCtau ($\mu g \cdot h$/mL)	42.17	29.82	77.15	93.23
Cmax (μg/mL)	5.7	3.97	8.36	9.54
Tmax (h)	2.99	2.98	2.2	2.33
Total CLp (L/h)	0.65	1.08	0.88	0.78
Renal Reabs	0.85	0.76	0.94	0.98
Fe (%)	24.9	30.35	12.38	5.18
Fm:Fr	0.58:0.40	0.52:0.48	0.81:0.19	0.92:0.08

2.5 Discussion

The objective of this study was to develop for the first time a PBPK model for benznidazole and to use it alongside population PK methods to develop and test a mechanistic hypothesis for reportedly higher CL/F seen in children aged 2-6 years as compared to in adult populations[185], see Figure 2.11. This study has shown that significant renal reabosorption of BNZ from urine is occurring and age-related changes in transporter mediated renal reabsorption is proposed as the mechanism driving the difference in BNZ exposure in children aged 2-6yrs as compared to in adults. The paediatric BNZ PK data evaluated in this study is highly variable, and sparse, which makes it difficult to analyse using PBPK methods. However, in addition to age-related changes in renal reabsorption, it appears that the lack of quantitative data to inform "surface area enhancement factor" (SEF) estimates in the paediatric ACAT model, may be resulting in an over-estimation of the fraction of BNZ absorbed from the gastrointestinal tract, especially in the younger children.

In the first part of this study PopPK methods were used to analyse oral BNZ PK data pooled from studies in paediatric and adult populations. Allometric scaling of CL/F and V/F using fixed exponents was included in the model *a priori* to allow delineation of the effect of age on PK parameters. For two of the three PK datasets that were pooled for this analysis (paediatric PK; Altcheh 2014[185]), and adult steady state PK; Raaflaub 1980[241]) the PK data was sparse in nature (and unbalanced for the paediatric study) and the population approach is therefore the best way to quantify the effect of age on exposure. This study found age to be a significant covariate on both CL/F and Ka reducing the OFV by 28.98 for the addition of four fixed effects (see Equations (2.4) and (2.5)). Having accounted for size *a priori* the maturation function on CL/F estimated that at 6 years CL/F is 2.11 fold higher than in a typical adult and at 2 years of age it was 3.29 fold higher. The precision associated with the estimates θ_M and θ_N are 54.1 and 77.3% respectively. The final population PK model also found the absorption rate constant (Ka) to be slower in younger children. The adult population estimate of Ka was 1.95 /hr (42.0% RSE). In children aged 6 years this was reduced to be 0.41 /hr and in children aged 2 years it was only predicted to be 0.05 /hr. The precision associated with θ_p and θ_q are 27.9 and 11.2% respectively.

Finally, one of the most important observations that came from the population PK analysis, and shaped subsequent thinking concerning which aspect of BNZ pharmacokinetics is altered in children, was the analysis of the individual η's estimated using the base PopPK model. As shown in Figure 2.8 CL/F is correlating with age

but V/F is not. The interpretation of this finding is that the age effect is not associated with factors that influence F, i.e. the fraction absorbed into the enterocyte, the fraction metabolized in the gut, or first pass metabolism in the liver. Instead that a systemic clearance mechanism is altered in children as compared to adults.

The lack of intravenous human PK data for BNZ introduces additional complexity to this work. IVIVE based prediction of human BNZ clearance has not been possible due to the fact that there is insufficient turnover of BNZ in either microsomes or hepatocytes to be able to estimate an *in-vitro* CLint. Essentially in both *in-vitro* systems BNZ appears to be metabolically very stable. *In-silico* QSAR models (ADMET Predictor version 10.4) have been evaluated and predict human BNZ hepatic clearance to be 20.6 or 26.4 L/hr/70 kg depending on the model used, while cross-species allometric scaling predicts that human total plasma clearance will be 11 L/hr/70kg.

In the final adult PBPK model presented here, CLh and CLr as determined by NCA of the simulated plasma and urine Cp-time profiles, range from 1.03 to 1.30 L/hr and 0.048 to 0.139 L/hr respectively. Across the model development study populations median body weight ranged from 58-65 kg. Factoring in the oral bioavailability (F) predicted by the final model; 0.579 to 0.852 depending on dose, these CL estimates agree well with the 2.04 L/hr estimate of CL/F (95% credibility interval 1.77 to 2.32 L/h) reported by Weins *et. al.* in their systematic review of BNZ PK data[239]. Comparisons with metronidazole as a structurally similar nitro-imidazole may also be of value as both plasma and urine PK data following IV administration are available[252]. PBPK modelling of the plasma and urine metronidazole PK data following a 500mg IV dose presented as part of this work, estimates that metronidazole CLh is 2.65 L/hr/56kg and CLr is 0.31 L/hr/56kg and based on a Fup of 0.89[253] 93.2% of the metronidazole that is being cleared into urine through renal filtration is being reabsorbed.

Renal reabsorption of drug from urine is also a feature of the final BNZ PBPK model. Models using both passive and active renal reabsorption have been presented (simulation 5; passive and simulation 6; active in Figure 2.26 and Table 2.21). Both passive and active renal reabsorption can be used to describe the model development datasets with minimal variation between the numerical GOF measures. Unfortunately, the only human PK study identified to report the amount of unchanged BNZ excreted into urine is the study published by Roberts *et. al*, where the authors report 6% of the BNZ dose is excreted into urine as unchanged drug[242]. Irrespective of whether passive or active renal reabsorption is implemented the PBPK model prediction of the fraction of dose excreted in urine (Fe) for the Roberts 1984[242] regimen is

in good agreement: 8.3% with passive renal reabsorption, or 6.1% with active renal reabsorption. The primary driver for selecting active reabsorption in the final model was to facilitate testing of the proposed hypothesis for increased CL/F in children compared to adults. The final PBPK model utilised an apical uptake transporter in the kidney with influx described by a Km of 10 ug/mL (38.4 uM) and a Vmax of 2 ug/s/mg-protien, which given the expression level that has been defined (0.028 mg-protein/gram-tissue) converts to an unbound *in-vitro* Vmax of 0.11 nmol/min/mg protein.

During human PBPK model development it was observed that the physico-chemical properties, solubility, and passive permeability of BNZ (as estimated from *in-silico, in-vitro* and pre-clinical IV/oral modelling) resulted in poor prediction of the observed dose-proportionality in adults. Since BNZ is reported to be a MDR1 P-glycoprotein (P-gp; ABCB1) substrate, intestinal efflux was incorporated into the adult model using the default software settings for regional P-gp expression. The adult model development PK datasets[240–242]) were used to fit the P-gp kinetic terms. The final model describes P-gp intestinal efflux via a Km of 20 ug/L (76.8 nM) and Vmax of 0.5 ug/s. Having incorporated intestinal efflux into the model the dose/Fa relationship is altered (see Figure 2.28) and the apparent dose proportionality between the Raaflaub 1979 and Roberts 1984 datasets and the approx. 20% higher CL/F seen in Raaflaub1979[240] study compared to the Raaflaub 1980[241] study (see Figure 2.25B) is now captured. However, further work to characterise the interaction between BNZ and P-gp would be highly desirable.

The final PBPK model has been verified using PK data collected in adults aged 18-50 years with a confirmed diagnosis of *T. cruzi* infection. The data is a subset of the PK data collected in the BENDITA trial[248]. The richest PK sampling was performed on day1 of the final treatment regimen in which patients received Benznidazole 300 mg once per week (150mg at T=0 and T=12 hr on day 1, 7, 14 etc) for 8 weeks plus fosravuconazole (n=30). Whilst correction of the whole blood PK data[271] and co-administration of fosravuconazole (FOS) increased BZN clearance by 14.5% ($p \leq 0.001$)[256]) had to be accounted for, a population simulation using the final PBPK model was still able to capture 78% of observations within the 95% PI (n=300).

Having defined an adult PBPK model, before extrapolation to a paediatric population can be performed consideration of relevant enzyme and transporter ontogeny is required. Since *in-vitro* stability data in the presence of specific isoenzyme (phenotyping) is lacking there is uncertainty regarding the enzymes responsible for BNZ metabolism. However, ontogeny data has been evaluated based on the structural pre-

diction of CYP and UGT liabilities in which CYP1A2, UGT1A8 and UGT2B7 are proposed. CYP1A2 is not highly expressed in the gut[290,291] and ontogeny of hepatic CYP1A2 is well characterised. While there are significant increases in CYP1A2 microsomal expression in the first 2 years of life, which would undoubtedly limit the applicability of allometric based clearance scaling in children <2 years, after 15 months postnatal age Song *et. al.* conclude that any developmental changes in CYP1A2 activity would be modest and likely depend on exogenous factors[292]. Data concerning maturation of UGT expression in the intestine and liver is more limited but recent data presented by Kiss *et. al.* does indicated higher expression of UGT1A1 in adult (n=8) compared to paediatric (n=10) jejunums ($p< 0.033$) and also in adult (n=8) and paediatric (n=48) illeums ($p<0.000067$)[293].

Regarding intestinal P-gp ontogeny, all pre 2015 studies that investigate developmental changes in P-gp intestinal expression have reported large inter-individual variation and mostly report that the overall developmental pattern of P-gp expression in the intestine revealed a consistent change from undetectable expression in the first trimester of foetal life to present and apparently stable P-gp expression from approximately 12 weeks of gestation onwards[294]. In a more recent study (Kiss *et. al.*) an age-related increase of MDR1 protein abundance in the ileum is observed although significance was not retained after false discovery rate correction on a continuous scale[293].

This study has shown that significant renal reabosorption of BNZ from urine is likely occurring (as is the case for metronidazole[252]) and age-related changes in transporter mediated renal reabsorption is proposed as the mechanism driving the difference in BNZ exposure in children aged 2-6yrs compared to in adults. Cheung *et. al.* analysed both mRNA and protein abundance of several renal transporters in postmortem frozen renal cortical tissues (preterm newborns to adults) and found that expression of P-gp, URAT1, OAT1, OAT3 and, OCT2 increased with age. The authors highlight the different rates and patterns of maturation exhibited by renal transporters, but several are associated with slow maturation (incomplete maturation by the age of 2 years). Using OAT1 as an example, children older than 2 years of age (PNA > 102 weeks) had highly variable expression levels, while the typical 2 year old (Hill function: $TM_{50} = 19.71$ [7.81, 36.95] weeks, Hill exponent = 0.43 [0.27, 0.61]) is predicted to only have 67% of adult protein abundance[77]. Regarding the interaction of BNZ with renal transporters there is evidence that BNZ is not a substrate for OAT1, OAT3, or OCT2, however these are all secretory renal transporters (basolateral influx transporters)[238]. PEPT1 however, is an apical uptake transporter found in both the

intestinal epithelia and kidney proximal tubules[294] and recent studies have found a significant association of PEPT1 expression in the illeum with age[293]. PEPT1 (SLC15A1) is associated with the transport of zwitterionic ammino acids typically in the form of di- and tri- peptides so there may also be some recognition of benznidazoles nitro group. *In-vitro* studies to determine whether BNZ is a substrate for PEPT1 are recommended to test this hypothesis.

In the absence of further *in-vitro* renal transporter data the final BNZ PBPK model presented here utilises a generic apical uptake transporter in kidney. In adult simulations expression of this transporter is set to 0.028 mg-enzyme/g-kidney. In the paediatric PBPK simulations that have been presented discrete expression levels are defined for each paediatric group. A visual comparison of the relative renal transporter expression levels employed in the paediatric simulations presented here alongside the OAT1 ontogeny data reported by Cheung *et. al.* is included in the Appendix Figure B.5. In the paediatric simulations reduced expression of the apical renal influx transporter results in less renal reabsorption in younger children and therefore a shift in the fraction of drug cleared by metabolism versus renal excretion and increase in total plasma clearance. While the low renal clearance of BNZ makes determination of the amount of BNZ excreted into urine challenging, incorporating urine analysis into future paediatric and adult BNZ PK studies would be desirable to be able to test this model with plasma and urine PK data in both adult and paediatric populations.

Finally, while agreement between the observed and simulated paediatric PK is significantly improved in the 2-6 year age groups by reducing expression of the renal transporter in the model there are some individuals who still achieve significantly lower plasma levels than the PBPK model adjusted only for BW, age and renal transporter expression predicts; refer to simulation 2 predictions in Chapter 2.4.4. And while the paediatric PK is highly variable, it does appears that the default scaling of the gut physiology, and lack of quantitative data to inform "surface area enhancement factor" (SEF) values in paediatrics may be resulting in an over-estimation of the fraction of drug absorbed, especially in the younger children. The final paediatric predictions (simulation 3) that are presented in Chapter 2.4.4 utilise a model in which refinements to the default paediatric gut physiologies have been made, the goal being to further reduce the predicted Fa (and consequently F). This aspect of the work may highlight misspecification in the BNZ model that has been developed, the need for individual paediatric PBPK simulation rather than a pooled approach, or it may provide valuable insights concerning paediatric extrapolation of the ACAT model.

Chapter 3

Posaconazole - Oral bioavailability in children

3.1 Introduction

Invasive fungal infections (IFIs) are a serious problem for immunocompromised patients undergoing both solid organ and stem cell transplantation. Posaconazole was first approved for use in adults by the EMA in 2005, with Merck Sharp and Dohme (MSD) initially launching the oral suspension, followed in 2013/2014 by the gastro-resistant/delayed release tablet and a solution for infusion. Finally in May 2021 MSD received regulatory approval from the FDA for a 'new' oral suspension referred to as the PowderMix for delayed-release oral suspension. In the US this 'new' posaconazole suspension is licensed for use in children above 2 years old weighing less than 40 kg[295]. In Europe however paediatric posaconazole dosing is still performed off-label and as such there is an urgent need for greater understanding of posaconazole PK in children.

Posaconazole is a lipophilic (logP=4.6), dibasic, poorly soluble, and highly plasma protein bound (97-99% mainly to albumin) small molecule[296].

Previously published rich PK data after IV dose escalation (50 – 300mg) to healthy adult volunteers shows posaconazole PK follows bi-exponential distribution and elimination, and exhibits more than dose-proportional increases in exposure up to 200mg, then exposure increases in a dose-proportional manner between 200 to 300 mg[297]. The mean volume of distribution of posaconazole was 261 L and ranged from 226-295 L across dose levels. With decreasing CL on dose escalation, half-life increased from 19 hrs at 50 mg to 25 hours at 300 mg [297,298]. Inter-individual variability in AUC_{∞} following the IV solution in this study was only 32%[297].

Posaconazole undergoes (limited) metabolism in healthy adults, primarily mediated by uridine 5'-diphospho-glucuronosyltransferase (UGT) enzymes (especially UGT1A4), with elimination predominantly through faecal excretion with only trace amounts of posaconazole measured in urine. Posaconazole is a substrate for P-gp efflux, and biliary and intestinal secretion are thought to be likely[299,300].

The pharmacokinetics (PK) of posaconazole oral suspension have been extensively studied in both healthy volunteers and patients at risk for IFI [301–305]. The bioavailability of posaconazole oral suspension is significantly enhanced when coadministered with food, particularly a high-fat meal, and the posaconazole label recommends that the oral suspension be administered with food or a nutritional supplement to ensure that adequate plasma concentrations are attained. [301,306]. However, those at high risk for IFI, such as neutropenic patients undergoing chemotherapy and recipients of allogeneic hematopoietic stem cell transplants, may be unable to eat because of

mucositis, nausea, or neutropenic enterocolitis. In patients unable to eat, the absorption of posaconazole oral suspension may be enhanced by dividing the posaconazole doses (200 mg 4 times daily) or by administering the drug with a liquid nutritional supplement or acidic beverage such as ginger ale[301,303]. The PK of posaconazole oral suspension has been studied in combination with esomeprazole, which increases gastric pH, and metoclopramide, which increases gastric motility[301]. The administration of 400mg of posaconazole oral suspension to healthy volunteers under conditions of increased gastric pH (coadministered esomeprazole) decreased posaconazole exposures (mean AUC) by 32% and 21% under fasting conditions and in the presence of an acidic carbonated beverage, respectively. Furthermore, administration of 400 mg of posaconazole oral suspension under conditions of increased gastric motility (coadministered metoclopramide) decreased posaconazole exposure (mean AUC) by 19% (geometric mean ratio, 0.81, 90% confidence interval 0.72 to 0.91). Previous population PK analysis of paediatric posaconazole TDM data has confirmed that in children exposure following suspension posaconazole dosing does not increase in a dose proportional manner. This is thought to be due to a reduction in the fraction of dose absorbed with escalating dose, due to the poor intestinal solubility of posaconazole. Thus leading to sub-proportional increases in exposure as suspension dose is escalated[307].

The delayed release/gastro-resistant tablet formulation[1] that was approved in the EU in 2014 is a substantially different oral formulation compared to the older 40 mg/mL oral suspension product. The posaconazole tablet was developed to produce an oral posaconazole formulation that would improve exposure and avoid the requirement for multiple dosing taken with a high fat meal, which was recognized to pose problems in the target population. The tablet was designed to inhibit the release of the active ingredient until the drug reaches the small intestine, where release of the entire dose of solubilised posaconazole is triggered by the higher luminal pH, thereby maximizing systemic absorption. The tablet delayed release/gastro-resistant effect is achieved through use of a pH-sensitive polymer; hypromellose acetate succinate (HPMCAS) and solubilisation of posaconazole via hot-melt extrusion which produces an amorphous solid dispersion of posaconazole[308]. This results in substantially improved exposure (~3 fold) compared with that for the oral suspension in healthy adults in the fasting state[309]. This attribute of posaconazole tablets may be beneficial in patients with poor food intake or a limited ability to take the medication with a high-fat meal. Time to steady state for the tablet is reported to take between 6-8

[1]Simply referred to from here on as the tablet formulation

days, the half-life is reported as 26hr however the accumulation ratio is higher than expected with an accumulation factor of approximately 3. The reasons for this at the time of the European regulatory filing were stated as unclear but possibly related to changes in food intake or auto-inhibition[310]. Absolute bioavailability of the tablet has been assessed and the mean value is reported to be 0.54 (31.9 %CV) when a 300mg tablet is compared in a crossover study to 300mg IV, however this study appears not to have been published in the scientific literature but is referred to in regulatory documentation (internal MSD study number P07783). See Appendix Figure C.1 for a copy of the study results as reported to the EMEA[310]. An absolute bioavailability study in healthy Chinese subjects has been published recently[311] which tells a similar story to studies in Western subjects. After 300mg IV/oral crossover in n=18 subjects the fasted state the geometric mean F of the tablet is 42.2%, Tmax 4.0 hour (range; 2-6) and $T_{1/2}$ 25.2 hour (%CV 24.3) and intravenous CL was 5.0 L/hr (confidence interval 4.3-5.8 L/hr), with a 2 fold increase in F in the fed state (87.1%). In terms of tablet dose proportionality this is established for the tablet between 200-400mg (2.9 to 5.7 mg/kg) in a Phase I study reported by Krishna *et. al.*[312]. While there are publications presenting no, or minimal food effect (FE) following posaconazole tablet dosing[309], these studies used 'development/prototype' tablets not the final commercial tablet and the tablet prescribing information still recommends taking posaconazole tablets with food since the absolute bioavailability of the commercial tablet formulation does indicate incomplete absorption[299,313]. When posaconazole tablet PK is compared between healthy adults versus adult patients, exposures are reported to be approximately 25% lower in patient groups, and this has been attributed to factors associated with the underlying acute illness influencing posaconazole absorption and steady state exposure. While a number of studies have modelled suspension posaconazole PK data[314–319], there is limited evidence on the best way to describe the absorption profile following administration of the tablet. In 2021 Bentley *et. al.* estimated a tablet absorption rate constant in children with cystic fibrosis as 0.16 /hr but went on to use a value of 0.588 /hr in PTA simulations[320]. The tablet Ka was also fixed to 0.588 /hr by Boonsathorn *et. al.* in their 2019 posaconazole Population PK modelling paper, where they analyse paediatric posaconazole TDM data that comprised 95% suspension and 5% tablet plasma levels. The estimate of 0.588 /hr for the tablet Ka originally came from the PopPK analysis of adult TDM data published by Petitcollin *et. al.*[318].

Recent work published in 2021[321] used the PBPK tool Simcyp™ to describe the drug-drug interaction (DDI) between posaconazole and venetoclax, a targeted

anticancer agent approved for the treatment of chronic lymphocytic leukemia and acute myeloid leukemia. Interestingly this work avoided the issue of non-linearity in posaconazole clearance by defining posaconazole clearance as a constant 6.54 L/hr based on only the 200mg IV data published by Kersemaekers *et. al.*, however, they do go on to successfully predict the observed exposure ratio for midazolam, simvastatin and venetoclax after oral dosing of posaconazole, where posaconazole doses range from 100-200 mg QD with the suspension and 300 mg QD for the tablet. Important to note from this work is that to enable the improved F of the tablet (compared to the suspension) the intrinsic solubility used when simulating tablet PK was 16.6 times higher than when simulating suspension PK (increased from $9.81\text{x}10^{-4}$) to $1.63\text{x}10^{-2}$ mg/mL). More-over the model-predicted Tmax was underpredicted; this was more significant for the tablet, attributed to the complex super-saturation and precipitation of posaconazole in the gut and was concluded to have no significance on the primary objective of the work which was to predict DDIs[321].

A significant (~ 2 fold) positive effect of food on tablet bioavailability was also very recently confirmed by Chen *et. al.* when simultaneous modelling of rich IV/tablet/suspension PK data from healthy adult subjects (data curated from multiple phase I studies) estimated tablet F to increase from 53.2-63.2% (CI) in the fasted state to 99.5%[2] in the fed state[322].

In 2020 Groll *et. al.* reported results from a non-randomised, open-label, sequential dose-escalation, phase 1b trial that evaluated the PK and safety of posaconazole IV and PFS (a novel powder for oral suspension)[3] in children aged 2 to 17 years with documented or expected neutropenia (ClinicalTrials.gov, NCT02452034; MSD protocol number, MK-5592-P097)[323]. In this study children received IV posaconazole at doses of 3.5, 4.5 or 6.0 mg/kg/d for $\geq$ 10 days, with an option to switch to posaconazole PFS at the identical dose for $\leq$ 18 days. PK sampling was performed between days 7 and 10 and six PK samples were taken within the 24hr dosing interval. CL and CL/F were estimated using AUC_{τ} calculated by NCA for children aged 2 to <7 years and 7 to 17 years old. For the younger children geometric mean CL (geometric %CV) is estimated to be 3.39 (52.8%), 2.97 (36.2%) and 3.27 (49.3%) L/hr at 3.5, 4.5 and 6.0 mg/kg/d respectively. In the older children CL was reported to be 6.64 (29.1%), 6.69 (37.3%) and 4.76 L/hr. Unfortunately, no body weight information is reported in the original article but this likely explains the apparent higher clearance in the older children. Regarding evidence of non-linearity in clearance, from the data

[2]Although tablet F in the fed state was fixed not estimated due to boundary problems

[3]The previously mentioned 'new' suspension

presented it would appear that at the doses evaluated ($\geq$ 3.5 mg/kg, q24hr, steady state) clearance is linear which is consistent with the findings in healthy adults[297]. After 7 days of dosing 4.5 and 6.0 mg/kg once daily ~90% of participants achieved a $C_{avg} \geq 500$ ng/mL[323]. While CL/F for the PFS/'new' suspension is reported in this work the authors do not report F of the oral formulation which ranges from 0.68 to 0.85 in the younger children to 0.57 to 0.87 in the older children[323]. It is unclear whether dosing of the PFS formulation was conducted in the fed or fasted state in this study[323].

In this chapter real world posaconazole PK from therapeutic drug monitoring in hospitalised children receiving intravenous, tablet and oral suspension is presented. The key novelty of this work concerns evaluation of real world IV posaconazole PK data in children and thereby simultaneous estimation of oral bioavailability for the suspension and tablet. Since IV dosing is only performed in a hospital setting the analysis is focused on modelling in-patient TDM levels. Because published intravenous posaconazole pharmacokinetic data clearly demonstrates that in healthy adults over a dose range of 50 to 300mg (~ 0.7 to 4.3 mg/kg assuming a 70 kg body weight) clearance decreases from 10.9 to 6.9 L/hr (determined using NCA)[297] the decision was made to evaluate modelling the paediatric TDM data using both linear and non-linear clearance. To inform paediatric model parameters rich adult PK following tablet[324] and IV dosing[297] has also been modelled.

3.2 Aims and objectives

The overall aim of this study was to perform a population PK analysis of real world posaconazole TDM data from hospitalised children and estimate oral bioavailability of the suspension and tablet formulations routinely used off-label in Europe. Specific objectives can be split into three categories:

1. Model posaconazole IV and tablet PK using rich adult data from healthy volunteers to understand likely structural requirements for the paediatric posaconazole PK model.

   1a. Identify and extract rich adult IV and tablet PK from the literature.

   1b. Fit a population PK model to the adult IV and tablet PK data.

   1c. Explore non-linearity in CL using the IV data.

1d. Evaluate whether a simple first order absorption process (a single Ka) can be used to describe tablet absorption.

2. To develop a population pharmacokinetic model of posaconazole in hospitalised children that can estimate the oral bioavailability of the tablet and suspension formulation routinely used off-label in Europe.

   2a. Extract posaconazole in-patient dose history information, posaconazole TDM plasma concentrations and relevant patient covariate data from the GOSH digital research environment (DRIVE)[325] via the Arhidia platform[326].

   2b. Clean and merge the source data to prepare a PK modelling datafile.

   2c. Fit a population PK model to IV paediatric TDM data, explore non-linearity in CL and compare with published adult IV data.

   2d. Incorporate the oral paediatric TDM data to estimate the suspension and tablet bioavailablity.

3. Provide dosing guidelines for posaconazole in hospitalised children.

   3a. Generate a demographic dataset including covariates representative of the target patient population.

   3b. Simulate a range of doses using the developed PK model.

   3c. Evaluate PK simulations in the context of established PD targets.

3.3 Methods

3.3.1 Modelling of published adult intravenous and tablet posaconazole PK (objective 1)

Average IV concentration time profiles were extracted from a dose es-calation study previously published by Kersemaekers *et. al.*[297]. The study evaluated posaconazole PK following intravenous doses of: 50, 100, 200, 250 and 300mg (n=9 healthy males in each cohort). The study found clearance (by NCA) to be linear between 200 to 300 mg, however exposure increased in a greater than proportional manner between 50 - 200 mg, as illustrated by a reduction in CL from 10.9 to 6.5 L/hr[297]. The data from this study was modelled to i) ensure appropriate NONMEM coding of saturable clearance prior to evaluating non-linear clearance using the GOSH paediatric TDM data and ii) to estimate CLsat and Km in a healthy adult population.

One and two compartmental models with first order absorption and either linear or non-linear clearance from the central compartment were evaluated during model development. Non-linear clearance was accounted for using a parameterisation derived from the Michaelis-Menten equation, Equation (3.1)[327,328].

$$\mathrm{CL} = \frac{\mathrm{CL_{sat}[C]}}{\mathrm{K_m} + \mathrm{[C]}} \tag{3.1}$$

This allows clearance to vary depending on the concentration C in plasma based on two parameters CL_{sat}, the maximum (or saturated) rate of clearance and K_m, the concentration at which clearance is half its maximal value. In order to confirm appropriate parameterisation of saturable clearance in the NM model file the adult IV PK data published by Kersemaseker *et. al.* was extracted from the original publication[297] and modelled prior to modelling of the paediatric TDM dataset. Only average concentration-time profiles were available in the original Kersemaekers *et. al.* publication[297] so while the PK modelling was performed using first-order conditional estimation method with interaction (FOCEI) in NONMEM version 7.4.3[212], IIV was not estimated for any model parameters.

NONMEM is designed to estimate the amount of drug in any given compartment rather than estimate the concentration. Several different parameterisations of non-linear clearance were evaluated but the parameterisation shown in Equation (3.3) was selected. This is same parameterisation of saturable clearance described by Dennis Fisher and Steven Shafer in the 2007 NONMEM Workshop entitled "Pharmacokinetic and Pharmacodynamic Analysis with NONMEM, Basic Concepts"[329]. Here C_i is the concentration of drug in compartment i, A_i is the amount of drug, V_i the compartment volume and k the elimination rate constant. K_m and CL_{sat} are defined above.

$$\mathrm{C_i} = \frac{\mathrm{A_i}}{\mathrm{V_i}} \quad \text{and} \quad \mathrm{k} = \frac{\mathrm{CL_{sat}}}{\mathrm{V_i}} \tag{3.2}$$

$$\frac{\mathrm{dA_i}}{\mathrm{dt}} = \frac{-\mathrm{kA_i}}{\left(1 + \frac{\mathrm{C_i}}{\mathrm{K_m}}\right)} \tag{3.3}$$

To inform the absorption modelling approach for the posaconazole tablet formulation data from the control arm of a 5-way crossover study looking into the effects of gastric pH and motility on posaconazole PK following a single 400 mg tablet dose (4 x 100mg delayed release tablets) was extracted from the publication by Kraft.W *et. al.*[324]. Only the average concentration time profiles were available in the publication, but the data represents rich PK sampling from 20 fasted healthy adults, (86% were male,

62% were black or African American), median weight was 78.2 kg (range; 52.5-105.1 kg) and median age 38 years (range; 24-53 years). NCA results from the paper report that the median tablet Tmax occurred at 4 hours (range: 2-8 hr), and arithmetic mean $T_{1/2}$ was 27.3 hours (37% CV)[324].

Extraction of the IV PK data published by Kersemaekers *et. al.*[297] was performed using a web-based application called WebPlotDigitizer version 4.5[262].

3.3.2 Paediatric real-world TDM data (objective 2a and 2b)

A retrospective analysis of posaconazole therapeutic drug monitoring (TDM) data captured by the electronic patient record system (EPRS) at a single specialist paediatric hospital between Jan 2017 and 2nd July 2021 was performed. This time period was selected as the data prior to this had been previously analysed and published by Boonsathorn *et. al.*[307]. In that work[307] the dataset did not include any IV data and only 5% of levels followed tablet posaconazole dosing.

Since this study was a retrospective analysis of posaconazole TDM data captured by a single specialist pediatric hospital's EPRS it was restricted to retrospective de-identified data. As such patients or their parents were not required to provide informed consent. The study was approved by the London and South East Research Ethics Committee under reference no. 21/LO/0646.

The raw TDM data was transferred from the GOSH digital research environment (DRIVE)[325] via the Arhidia platform[326] (project workspace: re23-im-stmcell-res). Separate datafiles containing; patient demographic information, patient biochemical data, posaconazole dosing information (formulation type, dose, route of administration, dose frequency and importantly the dose date/time), and posaconazole plasma concentration data that had been collected as part of routine therapeutic drug monitoring (TDM), were all combined to build the PK modelling datafile. All data cleaning, modelling datafile preparation, and data visualisation was performed using R (ver 4.1)[217,330].

The time-varying covariate data incorporated into the modelling datafile included age, weight, proton-pump (PPI) co-administration, occurrence of diarrhoea, concentration in blood of the liver function biomarker alanine aminotransferase (ALT) and the plasma protein albumin (ALB). Unfortunately, information regarding the timing of posaconazole dosing in relation to food was not available. Because of the time period over which this analysis has been performed data comes from both the legacy hospital patient records database and from the newer data capture system 'Epic'[331]

which went live at the hospital in April 2019.

During NONMEM datafile preparation any posaconazole TDM levels that were reported as less than the LOQ were replaced with 1/2 the associated LOQ in the observation column, commonly referred to as the M6 method[332,333].

Information regarding episodes of diarrhoea were manually collated by Iek Cheng (a GOSH clinical pharmacist) from patient records.

As advised by members of the clinical project team who have practical ward experience of TDM blood sampling, where a plasma level had a calculated time after last dose (TALD) of < 0.5hr the time of the sample collection was manually modified so that in the modelling data file the level was seen as a trough sample rather than a post dose sample. In practice TDM levels that are taken around the time of a dosing event are typically drawn just prior to dosing but the bar code scanner that assigns the time of sampling is located at the nurses station not by the patient bedside, so typically the nurse will finish dealing with the patient and then return to the nursing station to scan the blood sample tube.

TDM plasma levels were retained in the final dataset if the time after last dose (TALD) calculated using in-patient dosing information was within 150% of the specified dosing interval.

In acknowledgment of some uncertainty regarding the time to reach steady state in this population following IV and oral dosing, an analysis of the number of days of in-patient posaconazole dosing preceding each level in the modelling dataset was performed.

3.3.3 Paediatric population PK modelling (objective 2c and 2d)

Population pharmacokinetic modelling was undertaken using first-order conditional estimation method with interaction (FOCEI) in NONMEM version 7.4.3[212]. Prior to modelling the paediatric TDM data from IV and oral data simultaneously, the IV TDM levels were modelled separately.

During model building any sample with a conditional weighted residual (CWRES)[150] value of >6 was investigated further. It was planned to remove these samples and re-run the model to check for differences ($>15\%$ change) in parameter estimates.

Due to the wide ranging body weights of the children in the study population, allometric scaling was included *a priori* using a fixed exponent of 0.75 on clearance

terms and linear scaling on volume terms see Equation (3.4). A standard weight of 70 kg was used to allow comparison of parameter estimates with previous studies.

$$\mathrm{CL_i} = \mathrm{CL_{std}} \times \left(\frac{\mathrm{WT_i}}{70}\right)^{0.75} \quad \text{and} \quad \mathrm{V_i} = \mathrm{V_{std}} \times \left(\frac{\mathrm{WT_i}}{70}\right) \tag{3.4}$$

Continuous covariate effects were modelled using a power function centred on the median value see Equation (3.5) and categorical covariates evaluated by estimation of their fractional change of any given fixed effect see Equation (3.5).

$$\mathrm{COV_{continuous}} = \left(\frac{\mathrm{COV_i}}{\mathrm{COV_{median}}}\right)^{\theta} \quad \text{and} \quad \mathrm{COV_{catagorical}} = (1-\theta) \tag{3.5}$$

The function described by Boonsathorn *et. al.*[307] was used to account for the effect of dose on suspension bioavailability, see Equation (3.6), where D is the dose in mg/m^2 and D_{50} is the dose at which F is 0.5. In Boonsathorn's work the D_{50} term was referred to as β_{dose} and was calculated relative to the tablet bioavailability (Ftab) however as we include IV data in this analysis this term becomes one.

$$\mathrm{F_{sus}} = 1 - \frac{\mathrm{D}}{\mathrm{D} + \mathrm{D_{50}}} \tag{3.6}$$

To calculate dose per body surface area (BSA) we used the Boyd method, as shown in Equation (3.7) to estimate BSA based solely on body weight (BW)[334,335].

$$\mathrm{BSA} = 4.688 \times \mathrm{BW}^{(0.8168 - 0.0154 \cdot \log(\mathrm{BW}))} \tag{3.7}$$

Covariate effects were evaluated for dose, concomitant diarrhoea, and PPI dosing as these have previously been reported to be significant determinants of suspension F%[307,320], and were tested for effects on both tablet and suspension F. Because posaconazole is known to undergo phase 2 metabolism[300] and to be highly plasma protein bound[296] the influence of alanine aminotransferase (ALT) and albumin (ALB) concentrations in the blood were also tested on CL and V respectively. In the PopPK analysis of predominately suspension TDM levels from immunocompromised children published by Boonsathorn *et al*, allometric scaling of absorption rate constants was included in the final model, the utility of this was also be tested using a fixed exponent of -0.25, see (3.8).

$$\mathrm{Ka_i} = \mathrm{Ka_{std}} \times \left(\frac{\mathrm{WT_i}}{70}\right)^{-0.25} \tag{3.8}$$

In regard to IV dosing the nominal posaconazole infusion time used in adults is 90 minutes and the same is specified in internal GOSH clinical dosing guidance for use in children. This nominal infusion time was used to calculate infusion rate (mg/hr).

With regard to estimating residual error the strategy was to evaluate a combined additive and proportional error model and only if estimates tended to zero or if a zero gradient occured was a single residual error term utilised.

Significance was tested for hierarchical models using the χ^2 distribution and likelihood ratio test (LRT). For univariate forward selection covariates were included if $p<0.05$ but removed from the combined covariate model if $p>0.01$ on backward elimination. The final PopPK model was selected based on the likelihood ratio test, goodness of fit (GOF) plots[217] and visual predictive checks (VPC). A non-parametric bootstrap (n=1000) was performed on the final model to test parameter robustness and derive parameter uncertainty. Perl-speaks-NONMEM (PsN)[218] was used for the bootstrap analysis and to produce the VPC, which was visualized using Xpose4[219]. Auto-binning was used in construction of the VPC plot for the IV and tablet data, while manual binning was used for the suspension. Covariate effects were visualised to aid interpretation of the final model.

3.3.4 PK simulations and probability of target attainment (objective 3)

Using the observed baseline demographic information for the children included in the final modelling dataset (n=104) the variance-covariance matrix was calculated between log transformed age and weight. From this n=10,000 hypothetical children were simulated and categorized into age based groups; 0.5-2, 2-4, 4-6, 6-9, 9-12, 12-16 years. Hypothetical individuals created with an age less than 0.5 years or older than 16.0 years were not used. From the hypothetical weight the Boyd method[334,335] was used to calculate the individuals body surface area as when simulating suspension F_{sus}, dose must be specified in mg/m^2 as per Equation (3.6). ALT was included in the simulation dataset for each hypothetical subject by randomly generating a normal distribution (rnorm()) based on the observed distribution of the log transformed ALT data. (n=10857 observations, mean=3.967 U/L, standard deviation=0.758 U/L). PPI co-administration was either specified as with or without when simulating suspension PK.

Tablet simulations were performed at 100, 200, 300, 400 and 500 mg QD, IV simulations at 1, 2.5, 5, 7.5 and 10 mg/kg QD and suspension simulations at 1, 5,

10, 20 and 30 mg/kg TID both with and without concomitant PPI. In addition QD tablet simulations were also performed at 5 mg/kg to enable a comparison between all formulations; IV, tablet, and suspension, at an equivalent dose. Finally based on the observed dosing regimens for each formulation a 'typical' IV, tablet and suspension regimen was defined and steady state simulations performed.

Full PK time course simulations were performed using NONMEM for 8 days (Tlast = 192 hours) and AUC_{24} and C_{min} from the last 24 hour period were used in calculation of the probability of target attainment (PTA) using previously published PD targets; a steady state $AUC_{24} \geq 30$ mg.hr/L[336], a steady state C_{min} greater than 1 mg/L[336] and a steady state C_{avg} greater than 500 ng/mL (which is equivalent to a $AUC_{24} \geq 12$ mg.hr/L, assuming q24hr dosing)[323].

3.4 Results

3.4.1 Modelling of published adult intravenous and tablet posaconazole PK (objective 1)

Table 3.1 presents the OFV and minimisation details achieved when modelling the previously published IV posaconazole PK data in healthy adults[297]. A two compartment distribution model is clearly better at describing the rich IV PK data than a 1-compartment model (Run 2 compared to Run1, ΔOFV - 24.95 for two degrees of freedom) and saturable clearance improves the model further (Run 3 versus Run 2, ΔOFV - 34.82 for one additional degrees of freedom). Parameter estimates for Runs

Table 3.1: Summary of the models tested to describe the rich intravenous posaconazole PK data in healthy adults published previously by Kersemaekers in 2015 [295]. Table includes the objective function value (OFV) and minimisation details.

Run	Description	OFV	cov.step	Min.Succes	zero.grads
1	1 comp Adult IV Dose Escalation, prop error, linear CL	-113.85	yes	yes	no
2	2 comp Adult IV Dose Escalation, prop error, linear CL	-138.81	yes	yes	no
3	2comp Adult IV Dose Escalation, prop error, nonlinear CL	-173.62	yes	yes	no

1-3 (as shown in Table3.1) are summarised in Figure 3.1. The clearance estimated when using a linear clearance model (Run1: 6.53 L/hr and Run2: 6.68 L/hr) are consistent with the clearance reported by Kersemaekers *et al.* at the highest IV doses (200 mg; 6.68 L/hr and 300 mg: 6.90 L/hr). The CLsat estimated in Run3 (12.11 L/hr) is in good agreement with the Kersemaekers *et al.* clearance by NCA at the

lowest 50 mg dose (10.9 L/hr). The total volume of distribution (Vss = V1 + V2) in Run 2 and Run 3 are 250.3 and 260.2 L respectively which are also consistent with the steady state volume reported by Kersemaekers *et al.*; Vz ranged from 226 to 294 L. Finally, the Km estimated in Run 3 is 0.49 mg/L and the impact of plasma concentration on clearance is presented in Figure 3.3.

Parameter	Estimate (%RSE)
CL (L/h)	6.53(11)
V (L)	202.37(9.6)
Prop Error	38%(16.6)
Run	Run 1

Parameter	Estimate (%RSE)
CL (L/h)	6.68(10.5)
V1 (L)	100.74(14.9)
Q (L/hr)	48.06(16.6)
V2 (L)	149.61(8.8)
Prop Error	28%(29.2)
Run	Run 2

Parameter	Estimate (%RSE)
CLsat (L/h)	12.11(4.5)
Km (mg/L)	0.49(13.3)
V1 (L)	96.8(11.2)
Q (L/hr)	47.84(12.2)
V2 (L)	163.37(7.6)
Prop Error	18%(23.8)
Run	Run 3

Figure 3.1: Parameter estimates from Runs 1-3. Modelling the adult IV dose escalation data published by Kersemaekers in 2015 [295].

The concentration-time plots in Figure 3.2 compare the observed average Cp-time data extracted from the Kersemaekers publication[297] compared to the model predicted Cp-time profiles. Figure 3.2 clearly shows how using linear clearance (Figure 3.2B) results in over-prediction of the terminal phase plasma concentrations at lower doses/concentrations, and under-prediction at higher doses/concentrations.

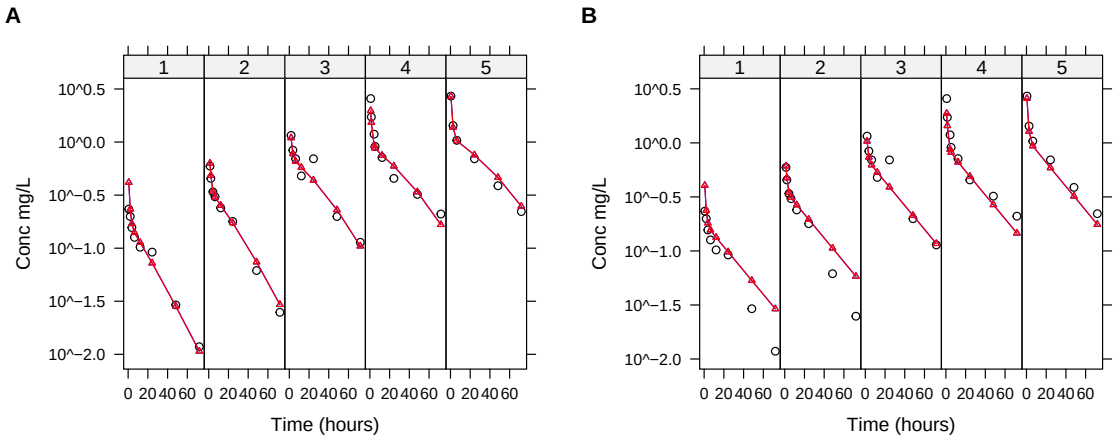

Figure 3.2: Adult IV dose escalation modelling, observed [295] average plasma concentrations versus model predicted Cp-time profiles. A) Run 3 (non-linear CL). B) Run 2 (linear CL). Facets number 1 to 5 correspond to the dose groups; 50, 100, 150, 200 and 300 mg respectively.

With saturable clearance, as in Run 3, the predicted versus observed Cp-time profiles are more aligned across the all dose levels (facets 1-5). The model estimated impact of posaconazole concentration on clearance is visualised in Figure 3.3.

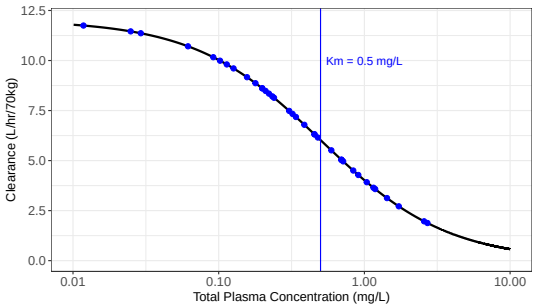

Figure 3.3: Model estimated impact of posaconazole concentration on posaconazole clearance using parameters estimated in Run 3. Blue circles: Plasma concentrations extracted from Kersemaekers.2015 [295].

The conditional weighted residual vs population prediction (CWRES-PRED) plot presented in Figure 3.4 also illustrates the over-prediction of plasma concentrations at lower doses/concentrations and under-prediction at higher doses/concentrations when using a model that implements linear clearance (Run 2, Figure 3.4B).

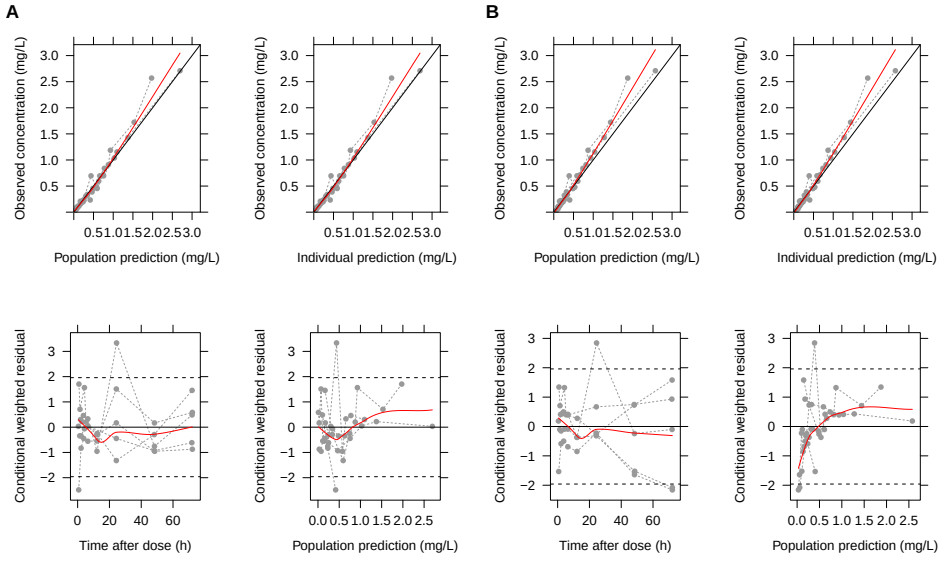

Figure 3.4: Adult IV dose escalation modelling, GOF plots. A) Run 3 (non-linear CL). B) Run 2 (linear CL). The red solid line is the LOESS regression (span 0.75). Black solid line is the line of unity in the top row and y=0 in the bottom row.

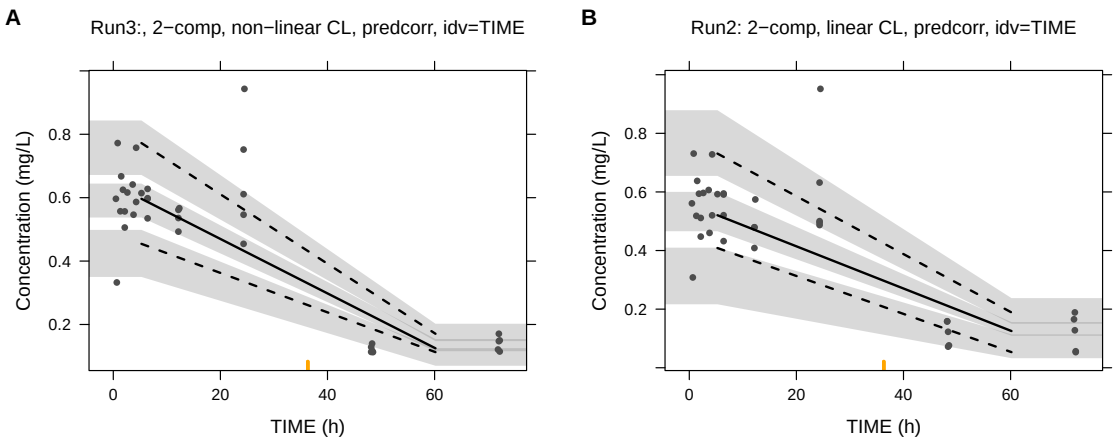

Figure 3.5: Adult IV dose escalation modelling, visual predictive check (VPC). A) Run 3 (non-linear CL). B) Run 2 (linear CL).

A comparison between prediction corrected VPCs (n=200 simulations) are shown in Figure 3.5A and Figure 3.5B, for Run 3 (non-linear clearance) and Run 2 (linear clearance) respectively. While both models generate acceptable VPCs, the lower residual error in Run 3 results in more precise (narrower) prediction intervals.

Table 3.2 summarises modelling approaches tested to estimate Ka and F using previously published rich adult IV[297] and tablet[324] PK data. All runs utilise a 2

Table 3.2: Summary of the models tested to describe the rich intravenous and oral posaconazole PK data in healthy adults published previously by Kersemaekers in 2015 [295] and Kraft in 2014 [322]. Table includes the objective function value (OFV) and minimisation details.

Run	Description	OFV	cov.step	Min.Succes	zero.grads
1	Adult IV and Tablet - All parameters estimated	-196.04	yes	yes	no
2	Adult IV and Tablet - only Ka and F estimated	-190.44	yes	yes	no
3	Adult IV and Tablet - Ka fixed to 0.588 and F estimated	-168.79	yes	yes	no

compartment distribution model with first order absorption and non-linear clearance and both an additive and proportional error term are included. In Run 1 in Table 3.2 all parameters were estimated, in Run 2 all clearance and volume terms were fixed to the values estimated from modelling just the adult IV dose escalation data and in Run 3 only F is estimated with Ka fixed to 0.588 /hr. Parameter estimates for these three runs are summarised in Figure 3.6. Accepting that between doses of 200 - 400 mg in healthy adults (without regard to food) tablet PK is reported to be dose proportional[312], the closest estimate of F to the reported tablet bioavailability of 0.54

(31.9 %CV)[310] is achieved with a Ka of 0.588 /hr (Run 3). Lower estimates of Ka as in Run 1 and Run 2 result in tablet F% being estimated between 0.72 and 0.75.

Parameter	Estimate (%RSE)
CLsat (L/h)	11.64(12.9)
Km (mg/L)	0.51(27.7)
V1 (L)	120.04(18.7)
Q (L/hr)	31.79(35.2)
V2 (L)	181.05(15.8)
Ka (/hr)	0.16(7.7)
Ftab	0.72(7.1)
Add Error (mg/L)	0.01 (166.7)
Prop Error (%)	27 %(44.8)
OFV	−196.037
Run	Run 1

Parameter	Estimate (%RSE)
CLsat (L/h)	12.11 (fixed)
Km (mg/L)	0.49 (fixed)
V1 (L)	96.8 (fixed)
Q (L/hr)	47.84 (fixed)
V2 (L)	163.37 (fixed)
Ka (/hr)	0.15(4.3)
Ftab	0.75(4.4)
Add Error (mg/L)	0.01 (98)
Prop Error (%)	27 %(45)
OFV	−190.444
Run	Run 2

Parameter	Estimate (%RSE)
CLsat (L/h)	12.11 (fixed)
Km (mg/L)	0.49 (fixed)
V1 (L)	96.8 (fixed)
Q (L/hr)	47.84 (fixed)
V2 (L)	163.37 (fixed)
Ka (/hr)	0.59 (fixed)
Ftab	0.59(5.8)
Add Error (mg/L)	0.02 (95.7)
Prop Error (%)	29 %(50.4)
OFV	−168.785
Run	Run 3

Figure 3.6: Adult IV dose escalation (Kersemaekers.2015) and 400mg tablet (Kraft.2014) parameter estimates

Figure 3.7 and Figure 3.8 compares the predicted and observed average plasma concentration time profiles from Run 2 (left) and Run 3 (right). Figure 3.7 is on a linear scale on the y-axis and the x-axis is modified to allow assessment of the model's ability to capture Cmax and Tmax.

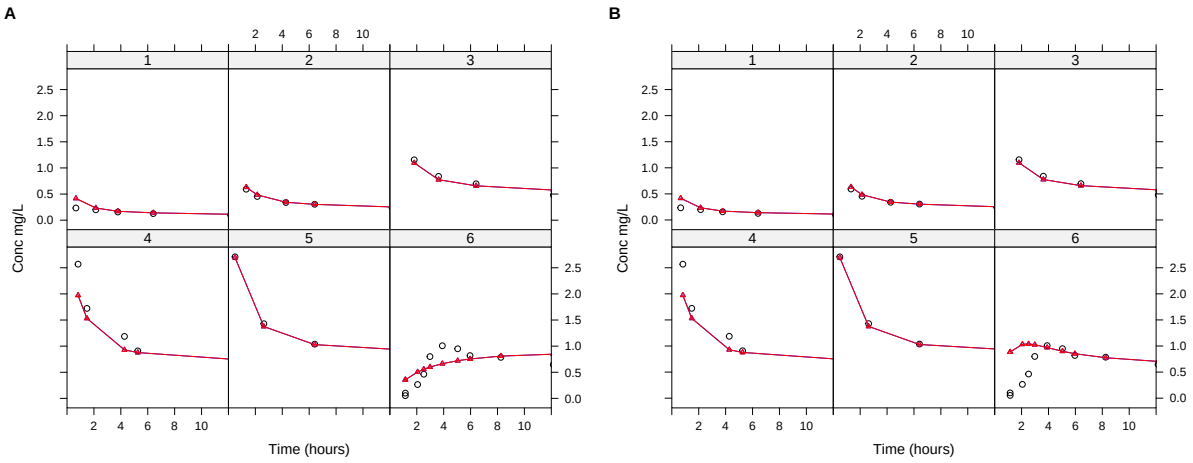

Figure 3.7: Adult IV dose escalation (Kersemaekers.2015) and 400mg tablet (Kraft.2014) observed v's predicted concentration time plots. A) Run 2. B) Run 3. Linear y-axis to evaluate tablet Tmax/Cmax.

Figure 3.8 has a log scale on the y-axis and shows the full time course on the x-axis to allow assessment of the ability to describe overall Cp-time profile and tablet half-life. Panels 1-5 in each plot show the IV dose escalation data[297], while panel 6 is the 400mg tablet PK data[324].

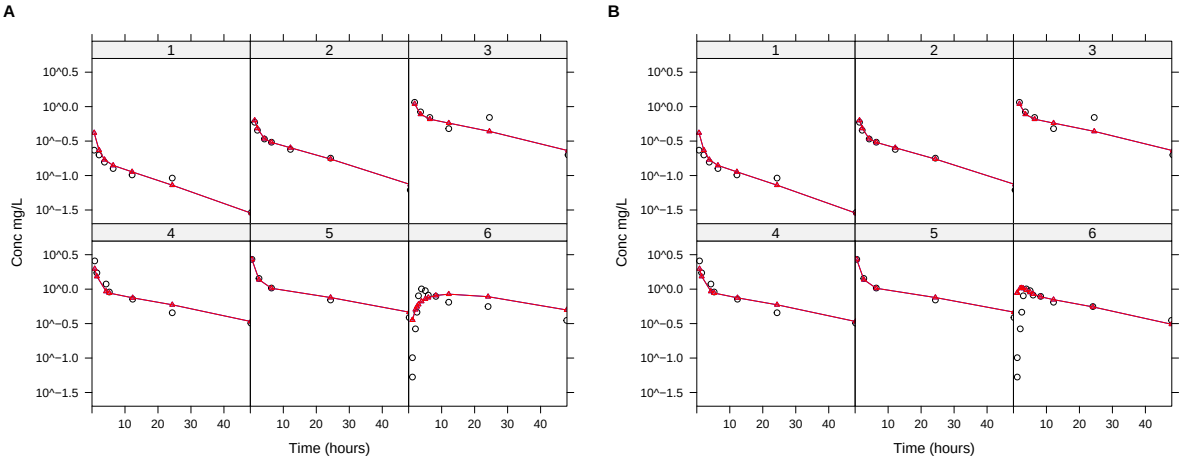

Figure 3.8: Adult IV dose escalation (Kersemaekers.2015) and 400mg Tablet (Kraft.2014) observed v's predicted concentration time plots. A) Run 2. B) Run 3. Log y-axis to evaluate tablet half-life.

3.4.2 Paediatric real-world TDM data (objective 2a and 2b)

This dataset was curated using all posaconazole TDM levels and in-patient posaconazole dose history information captured by the EPRS systems at GOSH between 1st Jan 2017 and 2nd July 2021. The data was made available through the Arhidia platform in Sep 2021. The start date of Jan 2017 was selected as posaconazole TDM data prior to this was previously analysed and published (95% suspension, 5% tablet data)[307].

Dose history plots were constructed to help easily identify which subjects had crossover data (IV and PO levels) and also where there was evidence of outpatient posaconazole dosing during periods between hospital stays. Examples of the dose history plots including periods of hospital stays (grey shaded areas) are shown for all the patients for which IV data is included in the final NM dataset, see Figure 3.9. Equivalent plots for all subjects included in the final NM dataset can be found in Appendix Figure C.2 to Figure C.6.

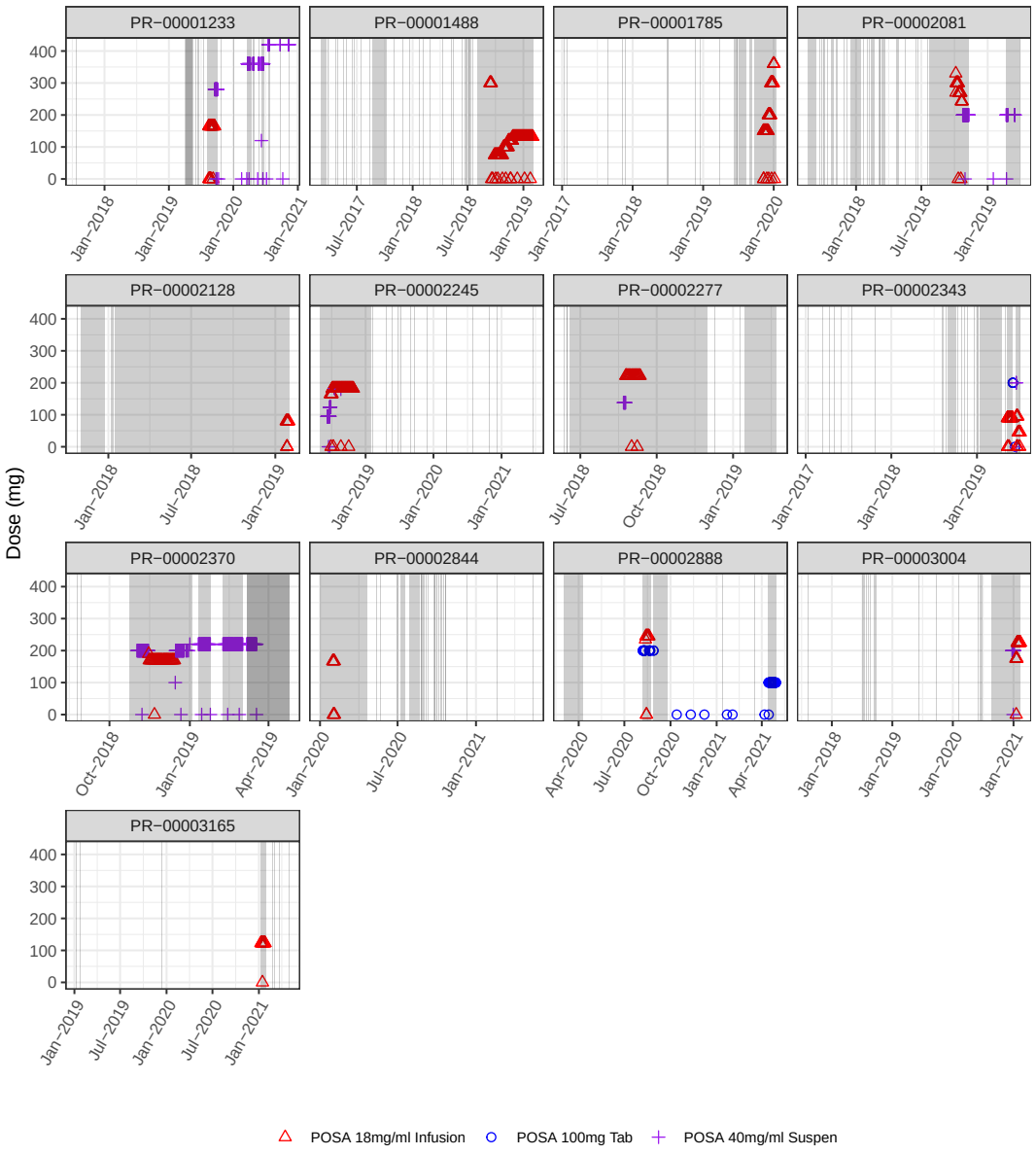

Figure 3.9: In-patient dose history plots showing periods of posaconazole (POSA) dosing in individuals who had IV plasma levels included in the final modelling dataset. Grey shaded areas represent periods of hospital stays. Symbols on the y=0 line indicate blood sampling times for posaconazole, when this is observed outside a grey shaded area, this is evidence that out-patient posaconazole dosing was occuring at that time.

Figure 3.10A presents the raw posaconazole PK data (posaconazole dose and plasma levels) analysed while Figure 3.10B looks at the reason stated for posaconazole prescribing, unfortunately this information on indication was only located using datafiles from the legacy GOSH EPRS system (stopped in April 2019) but is likely

representative of posaconazole usage to date. In Figure 3.10A the grey open circles are plasma levels that were not included in the final modelling data set as they could not be accounted for by in-patient dosing (49.5% of the TDM levels). In Figure 3.10B 'other' was attributed to 16.5% of all doses but to this additional groups that accounted for $< 1\%$ of the doses captured have been included increasing the proportion of 'other' doses to 19.8%. The non-surgical prophylaxis group at 43.7% accounts for the majority of posaconazole in-patient dosing. This group included posaconazole dosing to haematopoietic stem cell transplantation (HSTC) patients (pre and post conditioning).

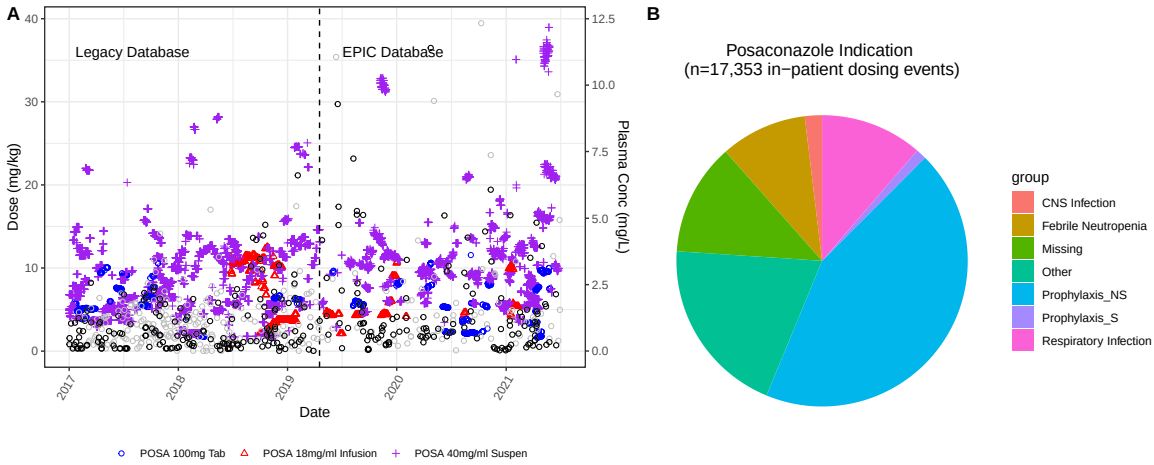

Figure 3.10: A) Posaconazole in-patient dose (mg/kg) and TDM plasma concentrations (mg/L) versus time (years). Vertical line indicates transition from the legacy to Epic EPRS system. Doses are described by the first y-axis. Plasma concentrations are described by second y-axis. Red triangles are IV doses. Blue circles are tablet doses. Purple plus are suspension doses. Black circles are plasma levels retained in the final modelling dataset. Grey circles are plasma levels that were not included in the final modelling data set as they could not be accounted for by in-patient dosing (49.5% of the TDM levels). B) Posaconazole indication 1st Jan 2017 to 18th April 2019. Key: NS; non-surgical, S; surgical.

The posaconazole PK data analysed here were sparse and unbalanced with sample times not optimised for PK modelling. Two hundred and ninety eight plasma levels from 104 children were included in the final PK modelling dataset. Plasma concentrations ranged from 10 to 11,400 ng/L. Ten children contributed crossover data so the total number of children contributing IV, tablet and suspension data was 13, 18, 83 respectively. The interquartile range (IQR) was 2.6-10.6 years (median 6.2 years) and

12.6-34.5 kg (median 19.5 kg) for age and weight respectively. See Figure 3.11 for the correlation between age and weight in all 104 children at baseline in this population, and for histograms showing the distribution of age and weight in all 104 children at baseline. As can be seen in Table 3.3 and Figure 3.12 the age and body weight of patients were not matched across the different posaconazole formulations due to the fact that the suspension prepared at 40 mg/mL allowed greater dose flexibility and utility in younger children whereas the less flexible (fixed unit dose of 100 mg) tablet had, in this data set, only been used in children greater than 8.9 years of age.

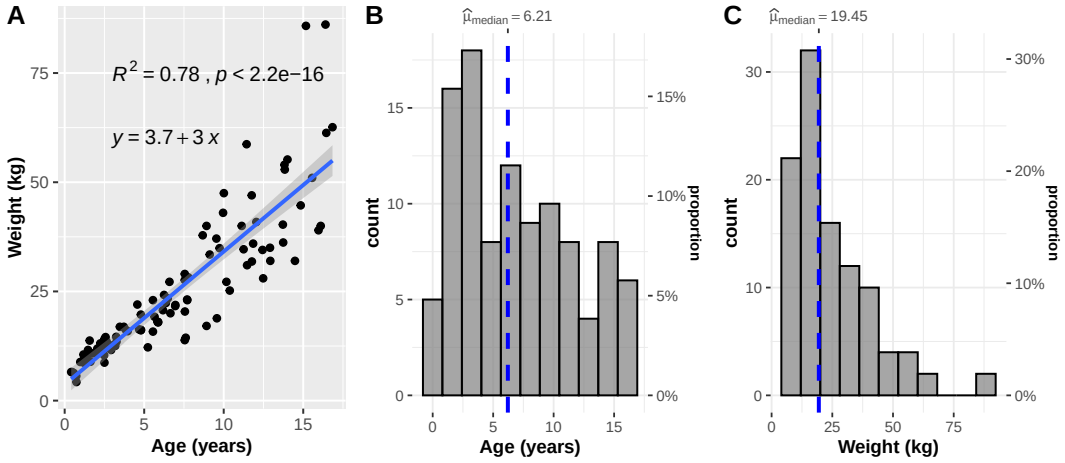

Figure 3.11: Baseline patient age and weight information. A) Corre-lation between age and weight. B) Observed distribution in age. C) Observed distribution in weight.

Table 3.3: Age and weight summary statistics for the paediatric posaconazole population. The number of patients contributing IV, tablet and suspension data to the final modelling dataset are 13, 18, and 83 respectively. Ten children contribute crossover data, and the total number of children in the final modelling dataset is 104.

variable	N	mean	sd	median	min	max	Formulation
Age (years)	13	8.87	3.78	9.57	2.84	13.84	IV
Weight (kg)	13	29.52	12.46	34.90	12.00	52.90	IV
Age (years)	18	13.40	2.44	13.78	8.92	16.84	Tablet
Weight (kg)	18	49.14	17.38	43.95	26.80	86.10	Tablet
Age (years)	83	5.62	4.03	4.79	0.41	16.45	Suspension
Weight (kg)	83	19.99	11.55	16.25	4.26	61.30	Suspension
Age (years)	104	6.92	4.73	6.22	0.41	16.84	Combined
Weight (kg)	104	24.75	16.33	19.45	4.26	86.10	Combined

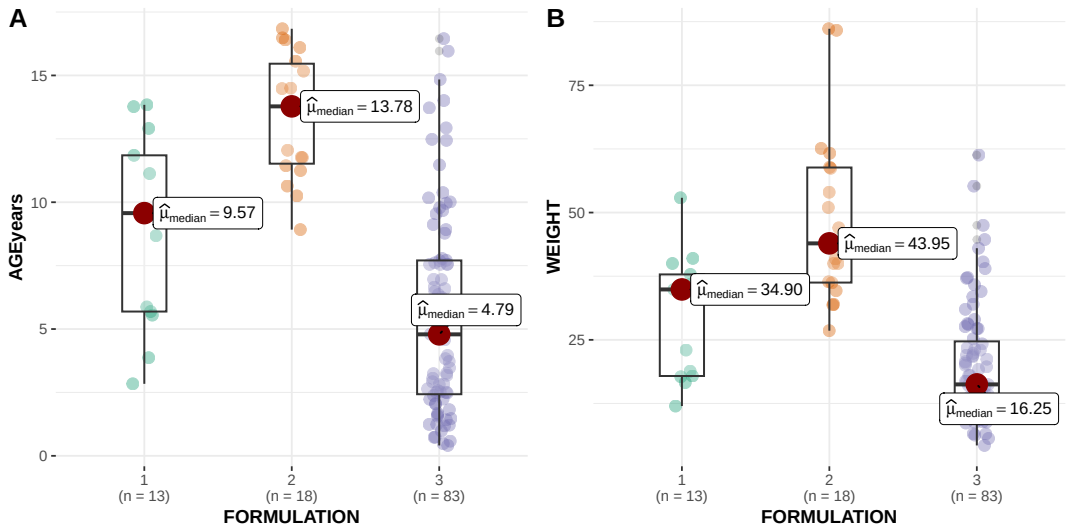

Figure 3.12: Baseline patient age and weight comparison stratified by formulation. A) Age comparison. B) Weight comparison. 104 children are included in the modelling dataset but crossover data is available in 10 children. Boxplot legend: IV/green, tablet/orange, suspension/purple.

The relative proportion of IV:Tablet:Suspension plasma concentrations is 16:13:71 (n=47/39/211 iv/tablet/suspension). Dose frequency varied between the formulations/routes, as illustrated in Figure 3.13 and doses ranged from 2.0 to 11.5, 1.6 to 10.6, 1.8 to 35.5 mg/kg for the IV, tablet and suspension formulations respectively. Summary statistics comparing doses administered (immediately prior to) and plasma concentrations achieved (in the final modelling data set, n=297) with the different posaconazole formulations are presented in Table 3.4.

Sixty nine percent of the plasma levels were collected during periods of concomitant PPI administration and 49% of levels during a period of diarrhoea.

None of the posaconazole levels record in Epic (up until Aug 2021) were reported as BLOQ, and the lowest posaconazole concentration reported was 0.03 mg/L. However, regarding the post Jan 2017 posaconazole TDM levels captured in the legacy system 49 levels (of which 18 were included in this modelling dataset; 4 tablet levels, 14 suspension levels) were reported as BLOQ and the LOQ for these levels ranged from 0.02 to 0.3 mg/L. To recap in the modelling datafile used in this analysis levels reported as BLOQ are included but the concentration was set to half the reported LOQ.

Summary statistics for dose, dose frequency and plasma concentration using the different posaconazole formulations are presented in Table 3.4 and Figure 3.13.

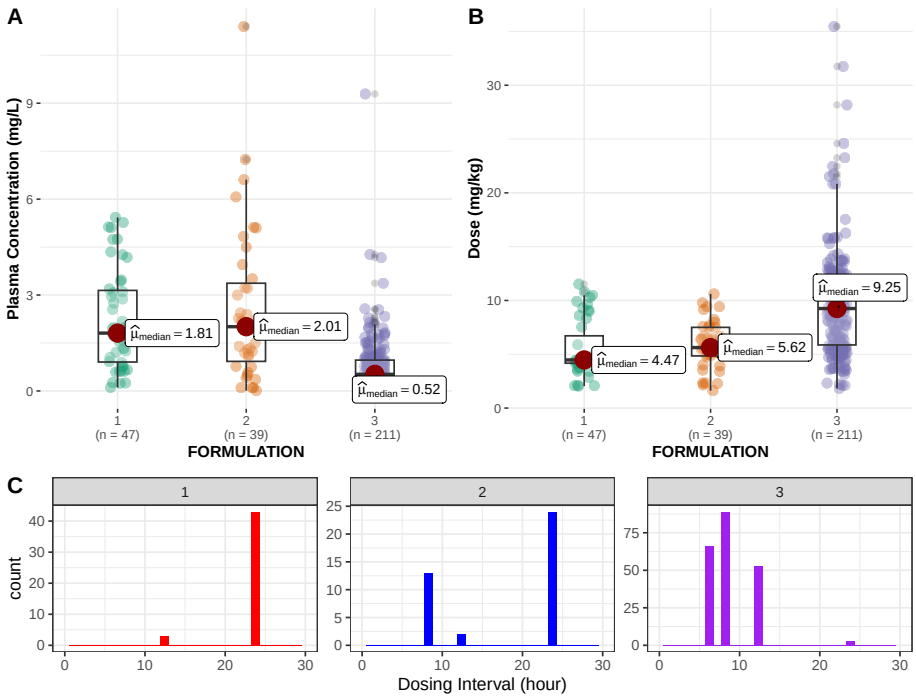

Figure 3.13: Comparison of A) plasma concentrations, B) doses administered, and C) dosing frequency utilised with the different posaconazole formulations. Boxplot legend: IV/green, tablet/orange, suspension/purple. Frequency plot legend: IV/red, tablet/blue, suspension/purple

Table 3.4: Dose and plasma concentration summary statistics[1,2]

variable	N	mean	sd	median	min	max	Formulation
Dose (mg/kg)	47	5.45	2.60	4.47	2.04	11.52	IV
Dose (mg/BSA)	47	150.92	62.26	128.46	54.88	272.73	IV
Daily Dose (mg/kg)	47	5.64	2.84	4.48	0.11	11.52	IV
Plasma Conc (μg/mL)	47	2.22	1.56	1.81	0.11	5.43	IV
Dose (mg/kg)	39	5.88	2.24	5.62	1.62	10.61	Tablet
Dose (mg/BSA)	39	188.93	63.00	187.50	58.82	333.33	Tablet
Daily Dose (mg/kg)	39	9.44	6.21	6.84	3.53	31.83	Tablet
Plasma Conc (μg/mL)	39	2.54	2.40	2.01	0.01	11.40	Tablet
Dose (mg/kg)	211	9.57	4.94	9.25	1.82	35.46	Suspension
Dose (mg/BSA)	211	223.35	94.77	226.80	62.50	625.00	Suspension
Daily Dose (mg/kg)	211	28.96	16.96	23.79	3.64	106.38	Suspension
Plasma Conc (μg/mL)	211	0.74	0.91	0.52	0.01	9.29	Suspension
Dose (mg/kg)	297	8.44	4.71	7.77	1.62	35.46	Combined
Dose (mg/BSA)	297	207.37	90.65	203.39	54.88	625.00	Combined
Daily Dose (mg/kg)	297	22.71	17.54	19.58	0.11	106.38	Combined
Plasma Conc (μg/mL)	297	1.21	1.50	0.72	0.01	11.40	Combined

[1] Evaluates the dose immediately prior to the plasma levels

[2] n=297 doses and plasma levels

Albumin (ALB) and alanine transaminase (ALT) blood concentrations were extracted from the EPRS and incorporated into the final NM modelling dataset to allow them to be investigated during covariate selection/model development. These biomarker concentrations were incorporated into the modelling dataset for every event (doses and observations, n=10857) and examples of the raw data are presented in Figure 3.14. For ALT in particular very large fluctuations in concentration in blood can be observed over time; the horizontal reference lines show the expected concentration range for each protein and the red markers (filled red circles) on y=0 show the timing of plasma levels included in the final dataset. The median ALT and ALB concentrations in blood were 49 U/L and 33 g/L respectively and 94.3% of the ALT concentrations and 98.3% of the ALB concentrations were measured within 24 hours of a given posaconazole TDM plasma level.

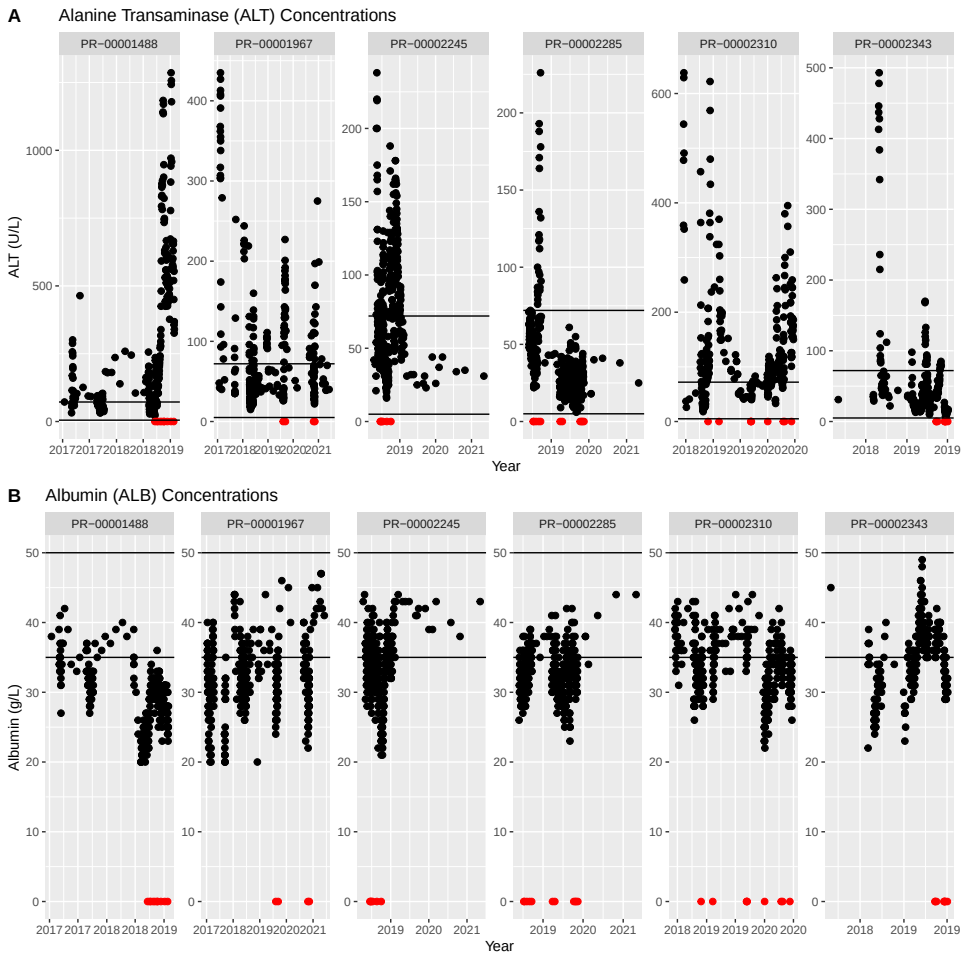

Figure 3.14: ALT and ALB time series data for six individuals. Red filled circles at y=0 show the timing of plasma levels in the final modelling dataset.

The measured plasma concentrations faceted by formulation/route of administration and compared to the calculated TALD are presented in Figure 3.15. This plot represents the final PK modelling dataset. The solid coloured lines are a linear regression through the final modelling dataset. The black dashed line represents the linear regression through each dataset having removed the BLOQ values from the dataset. As shown by the middle facet of Figure 3.15 the regression line for the tablet is the most affected by removal of BLOQ levels.

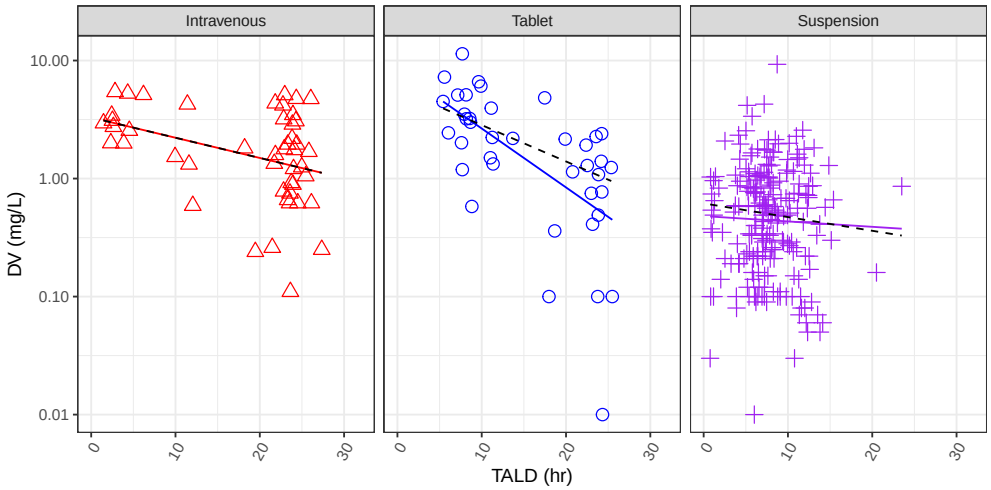

Figure 3.15: Pooled plasma concentrations (TDM levels) versus calculated time after last dose (TALD) included in the final modelling dataset. Facets from left to right represent the IV, tablet and suspension data. Solid coloured lines; linear regression through the observed data. Dashed black line; linear regression when BLOQ levels are removed; n=279 (47/35/197; iv/tablet/suspension).

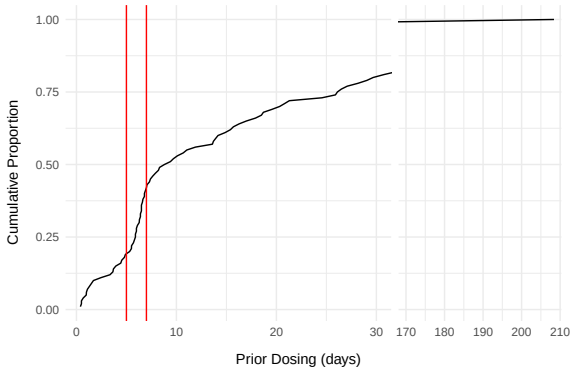

Figure 3.16: Cumulative proportion of in-patient dosing days preceding all plasma levels included in the final NM dataset. Red vertical reference lines highlight 5 and 7 days of prior inpatient dosing.

Analysis of the number of in-patient dosing days that precede a given plasma level is summarised in Figure 3.16 and just over half (56.7%) of all the levels included in the final dataset are preceded by > 7 days of in-patient dosing.

3.4.3 Paediatric population PK modelling (objective 2c and 2d)

Standalone IV Modelling

The paediatric IV dataset included 47 plasma levels collected after IV dosing in 13 patients. The pooled plasma concentrations versus calculated TALD were presented previously in Figure 3.15, and this same data is presented for each subject in Figure C.7. Cross over data (plasma levels following oral and IV dosing) is available for 7 of the 13 subjects: IDs 1233, 2081, 2245, 2343, 2370, 2888, 3004. The dose history plots for these subjects are presented below in Figure 3.17. As can be seen in Figure 3.17 some IV levels are preceded by oral dosing and the models presented below were evaluated both with and without inclusion of these levels, but this made no significant difference to the modelling conclusions so only the results obtained using all 47 concentrations are presented here.

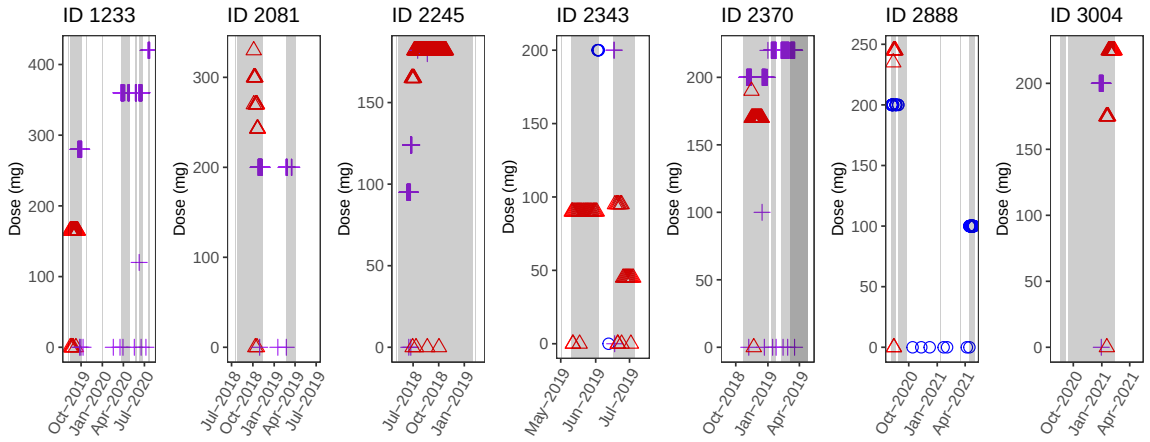

Figure 3.17: Dose history plots for subjects with IV and oral crossover data. Grey areas represent periods of hospital admission. Red triangles; IV dose. Blue circles; tablet doses. Purple cross; suspension doses. A circle, triangle or cross on the y=0 line represents a TDM (PK sample time) event. All TDM sampling times are included in these plots as a useful flag for periods of outpatient dosing

The age and weights recorded for the subjects with IV levels at the date/time closest to the TDM observation, not just the baseline age and weight, are presented in Figure 3.18. Whilst by no means a large IV dataset it does include data from children

aged 2.8 to 13.8 years, weighing 12 to 53 kg. Posaconazole plasma concentrations following IV dosing ranged from 0.1 to 5.4 mg/L.

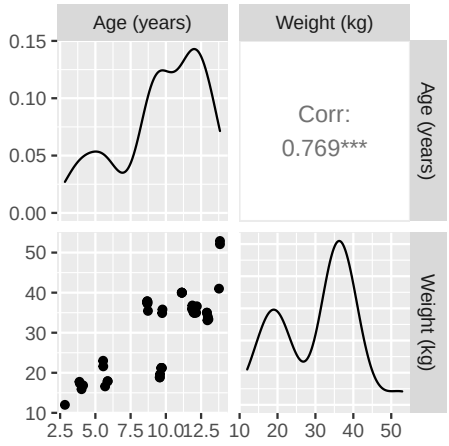

Figure 3.18: Correlation and distribution of age and weight in the IV PK paediatric population.

Figure 3.19 is an updated version of Figure 3.3 previously presented in Chapter 3.4.1. It compares the paediatric IV plasma concentrations (shown in red) with the previously modelled adult IV plasma concentrations (shown in blue). The paediatric TDM levels are within a concentration range where (assuming the same transporters and enzymes responsible for posaconazole elimination are present in our population) a model that incorporates saturable clearance would be expected to be superior to one that does not.

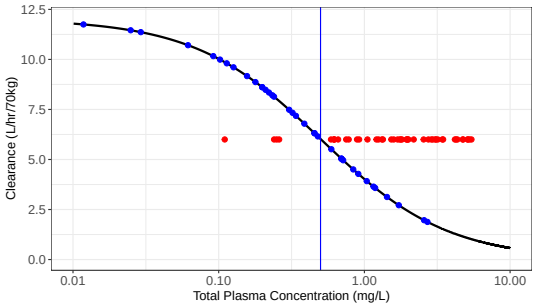

Figure 3.19: Comparison between posaconazole paediatric TDM plasma concentrations and those reported by Kersemaekers et. al. following IV dosing and the impact on clearance as estimated in Chapter 3.4.1. Blue: Adult plasma levels. Red: IV paediatric posaconazole concentrations.

In Figure 3.19 the clearance associated with the GOSH TDM levels has been arbitrarily set to 6 L/hr/70kg for plotting purposes. It is of interest to note that

paediatric TDM plasma levels are being observed in excess of the peak concentration achieved after a 300 mg single dose to a healthy adult volunteer: 5.43 versus 2.71 mg/L.

Modelling the IV plasma PK data separately from any oral PK data allowed clearance and distribution parameters to be estimated with confidence, however this IV dataset in isolation (minus the oral levels) is relatively small and the nature of TDM data means PK sampling is not specifically designed to ensure precise estimation of PK parameters. That said, during the modelling of this data no sample with a conditional weighted residual (CWRES) of 6 or more was identified and therefore no subjects or individual plasma levels were removed as outliers.

Table 3.5 presents model details for runs in which the IV paediatric TDM data were modelled using **linear** clearance. After adding IIV on CL the covariance step was

Table 3.5: IV paediatric TDM modelling: Linear Clearance

Run	Description	OFV	cov.step	Min.Succes	zero.grads
1	1comp, no IIV, add & prop error	77.47	no	yes	yes
2	1comp, IIV on CL, add & prop error	72.45	no	yes	yes
3	1comp, IIV on CL, add error only	72.45	yes	yes	no
4	1comp, IIV on CL, prop error only	84.22	yes	yes	no
5	1comp, IIV on CL and V, add and prop error	72.45	no	yes	yes
6	1comp, IIV on CL and V, add error only	72.45	no	yes	yes
7	1comp, IIV on CL and V, prop error only	84.22	no	yes	yes
8	2comp, IIV on CL, add and prop error	72.42	no	yes	no
9	2comp, IIV on CL, add error only	72.42	no	yes	no
10	2comp, IIV on CL, prop error only	82.87	yes	yes	no

only achieved if either an additive (Run3) or proportional (Run4) residual error was incorporated. Estimation of IIV on V was not possible with linear clearance (Runs 5-7). Addition of a second peripheral compartment as in Runs 8-10 did not result in a significant reduction in the OFV; Comparing Run 10 with Run4 p=0.509 (-Δ OFV 1.35). The IV TDM data is likely not rich enough to allow the bi-phasic distribution and elimination observed in adults to be detected therefore only a one-compartment distribution/elimination was taken forward to the combined IV/PO paediatric PK modelling.

Run 4 (proportional error and IIV on CL) was selected as the 'best' IV model using linear clearance. While Run3 (additive error and IIV on CL) gave a lower OFV (Run 3 versus Run 4 -Δ OFV 11.8) a comparison of the VPC's suggests better overall performance of a proportional residual error model. GOF plots, a VPC and parameter estimates for Run 4 are summarised in Figure 3.20. For information the

equivalent figure is presented for Run 3 in the Appendix: Figure C.13.

Parameter	Estimate (%RSE)	IIV %CV (%RSE)
CL (L/h/70kg)	5.67 (15)	55% (34.8)
V (L/70kg)	143.2 (8.5)	–
Prop Error (%)	57 (44.9)	–
OFV	84.22	–
Run	Run 4	–

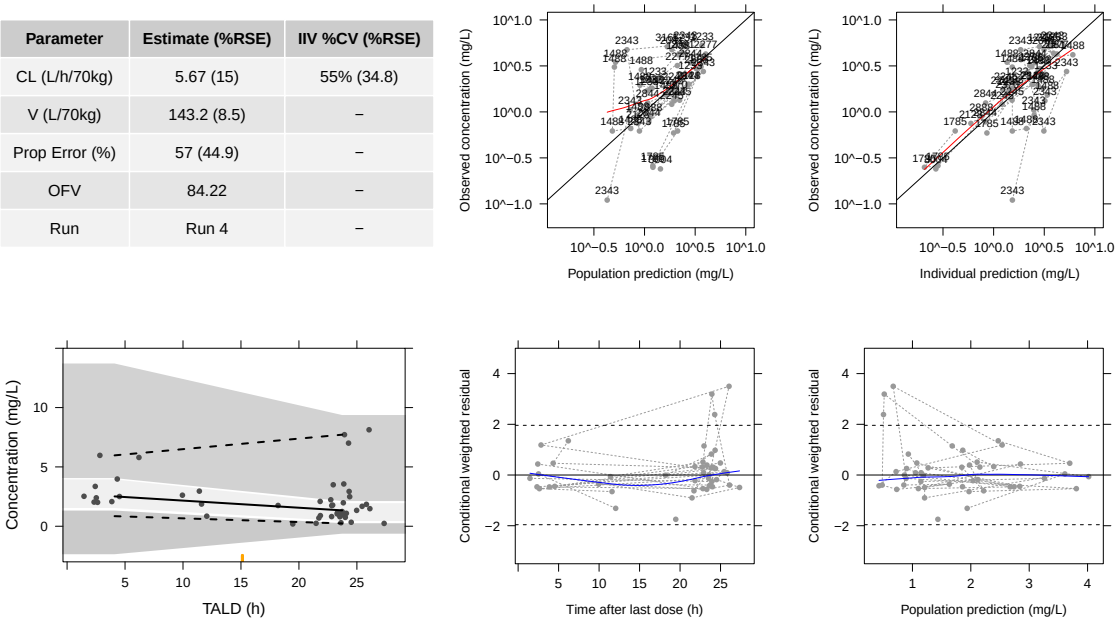

Figure 3.20: Parameter estimates and GOF plots for the best linear CL model. IIV on CL and proportional residual error (Run4: paediatric IV only modelling)

Model details for runs performed using **saturable/non-linear clearance** are described in Table 3.6. With non-linear clearance and IIV only on CLmax a combined

Table 3.6: IV paediatric TDM modelling: Non-Linear Clearance

Run	Description	OFV	cov.step	Min.Succes	zero.grads
NL-1	1comp, Km FIX 0.5, IIV on CLmax, add & prop error	113.15	yes	yes	no
NL-2	1comp, Km FIX 0.5, IIV on CLmax, add error only	108.85	-	no	-
NL-3	1comp, Km FIX 0.5, IIV on CLmax, prop error only	116.72	yes	yes	no
NL-4	1comp, Km FIX 2.0, IIV on CLmax, prop error only	105.46	yes	yes	no
NL-5	1comp, Km FIX 0.5, IIV on CLmax and V, add & prop error	106.92	no	yes	yes
NL-6	1comp, Km FIX 2.0, IIV on CLmax and V, add & prop error	90.60	-	no	-
NL-7	1comp, Km FIX 2.0, IIV on CLmax and V, add error only	90.60	-	no	-
NL-8	1comp, Km FIX 2.0, IIV on CLmax and V, prop error only	98.73	yes	yes	no
NL-9	1comp, Km FIX 2.0, IIV on CLmax and V with OMEGA BLOCK, prop error only	97.28	yes	yes	no
NL-10	As in Run 9 but CLmax and V FIXED to adult estimates	110.67	yes	yes	no

additive plus proportional residual error model is preferable (Run NL-1 compared to Runs NL-2 and NL-3). Initially Km was fixed to 0.5 mg/L; the value estimated from modelling adult IV dose escalation data, see Chapter 3.4.1. However, during model development, parameter sensitivity (OFV profiling) regarding the impact of Km found that it was beneficial to increase the estimate by approximately four fold

from the adult estimate of 0.49 to 2.0 mg/L, reducing the OFV by -Δ 11.26 point in run NL-4 compared to run NL-3.

With non-linear clearance the paediatric IV data does support estimation of IIV on both CL_{max} and V if a proportional error model is used as in Run NL-8, reducing the OFV by -6.73 compared to Run NL-4. In Run NL-9 the correlation between eta1 and eta2 was also estimated using OMEGA block, the correlation coefficient was -0.585 with a shrinkage of 8.8% and 31.1% on ETA1 and ETA2 respectively. However, the imprecision (relative standard error) of the parameter estimates in Run NL-9 is high, ranging from 76.1 to 315.9%, see Appendix Figure C.14.

In Run NL-10 CLmax and V were fixed to the adult estimated values of 12.0 L/hr/70kg and 250 L/70kg (Run3, Figure 3.1, (V = V1 + V2)), the OFV increases to 110.67 but estimation precision was improved and therefore this was defined as the 'best' IV model using non-linear clearance.

The 'best' IV models using linear (Figure 3.20), and non-linear (Figure 3.21) clearance were taken forward for evaluation using the full IV and oral paediatric datasets, with CL and V estimates fixed. The residual error model was re-evaluated with the larger combined data set, but inclusion of IIV on clearance and/or volume terms was not revisited, this was defined based on the paediatric IV only modelling.

Parameter	Estimate (%RSE)	IIV %CV (%RSE)
CLsat (L/h/70kg)	12 (fixed)	44% (39.2)
Km (mg/L)	2(fixed)	–
V (L/70kg)	250 (fixed)	63% (116.9)
Prop Error (%)	67.15(46.8)	–
OFV	110.67	–
Run	Run NL−10	–

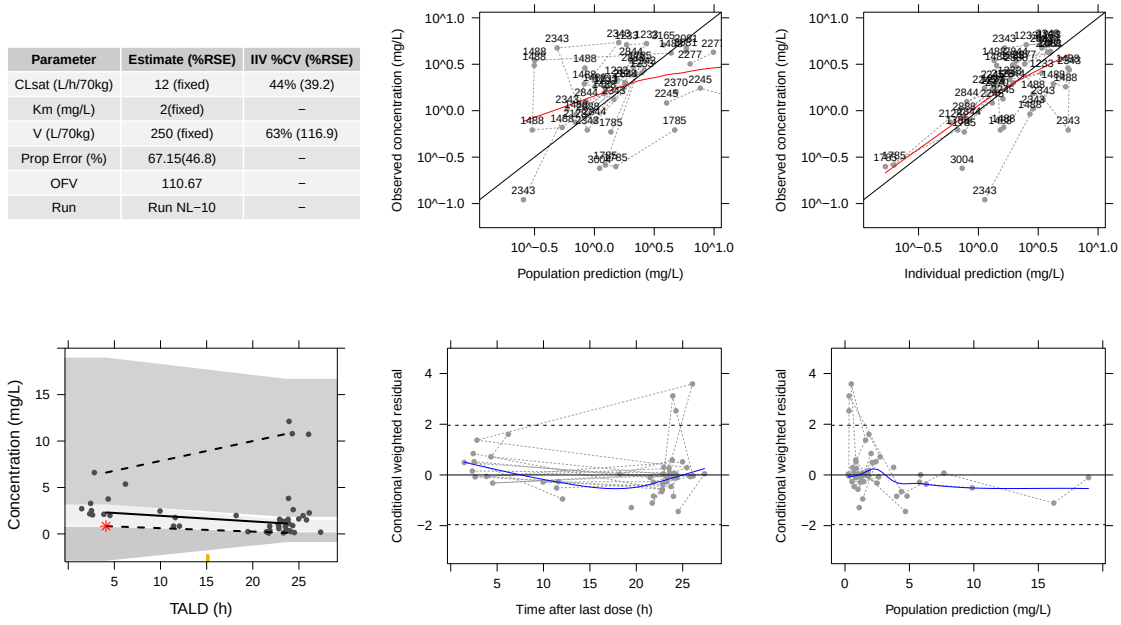

Figure 3.21: Parameter estimates and GOF plots for the best non-linear CL model. IIV on CL and V using OMEGA block with proportional residual error (Run NL-10: paediatric IV only modelling)

Combined IV Tablet and Suspension Modelling

As previously presented in Figure 3.17 the availability of IV/oral crossover data makes this a particularly informative dataset, however equally important to understanding posaconazole oral bioavailability in children is the tablet/suspension crossover data. Three subjects provided crossover tablet/suspension PK data; IDs 1933, 2310, 3145 and dose history plots for these individuals are presented in Figure 3.22.

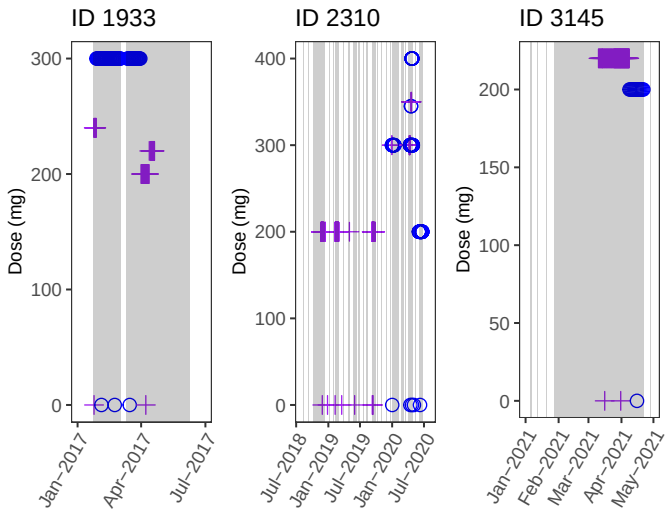

Figure 3.22: Dose history plots for subjects with tablet and suspension crossover data. Purple cross; suspension doses. Blue circle; tablet doses. Grey areas represent periods of hospital admission. A circle, or cross on the y=0 line represents a TDM (PK sample time) event. All TDM sampling times are included in these plots as a useful flag for periods of outpatient dosing.

Combined IV/PO Base Model Definition

Modelling of the suspension and tablet data alongside the IV data simultaneously required incorporation of 4 additional thetas; an absorption rate constant (Ka) and a bioavailability (F) term for each of the two oral formulations; tablet and suspension.

Incorporation of the oral data into the modelling dataset enable a combined residual error model to be estimated irrespective of whether a linear or non-linear clearance model was used. Tablet and suspension absorption rate constants were also fixed based on prior adult information[297,318,319]. Incorporation of IIV on both tablet and suspension bioavailability was tested but could not be supported by the data, therefore IIV was included only on the CL and V terms as identified during 'IV only' modelling (previous section). Shrinkage on η_1 in the linear clearance model was

32.4%. With the non-linear clearance model shrinkage on η_1 and η_2 were 21.4% and 43.6% respectively, the correlation coefficient between $\eta's$ was 0.484.

The combined IV and oral base models selected for use in covariate testing are presented in Figure 3.23.

A

Parameter	Estimate (%RSE)	IIV %CV (%RSE)
CL (L/h/70kg)	5.67 (fixed)	53% (47.3)
V (L/70kg)	143.2 (fixed)	–
Ktab (/hr)	0.59 (fixed)	–
Ksus (/hr)	0.2 (fixed)	–
Ftab	1.18(35.2)	–
Fsus	0.07(10.3)	–
Add Err (mg/L)	0.59(40.3)	–
Prop Error (%)	39.88(30.1)	–
OFV	215.93	–
Run	Base Linear	–

B

Parameter	Estimate (%RSE)	IIV %CV (%RSE)
CLsat (L/h/70kg)	12 (fixed)	58% (57.4)
Km (mg/L)	2 (fixed)	–
V (L/70kg)	250 (fixed)	140% (29.2)
Ka Tab (/hr)	0.59 (fixed)	–
Ka Sus (/hr)	0.2 (fixed)	–
F Tab	0.74(27.9)	–
F Sus	0.1(8.7)	–
Add Err (mg/L)	0.42(69.2)	–
Prop Error (%)	47.13(26.9)	–
OFV	226.33	–
Run	Base Non−Linear CL	–

Figure 3.23: Selected BASE models. A) Linear CL, B) Non-linear CL.

The difference in the OFV between the two BASE models is 10.40 points, this is slightly reduced compared to when modelling just the IV paediatric TDM data. The most significant difference between the two models presented in Figure 3.23 is the estimation of tablet bioavailability. Both models estimate tablet F with reasonable precision but when using linear clearance tablet bioavailability is estimated to be >1 (1.18, %RSE 35.2). With non-linear clearance this is reduced to a more plausible estimate of 0.74(27.9 %RSE). Parameter estimates using the base models and simultaneous estimation of clearance, volume and bioavailability terms are presented in Appendix Figure C.15.

Covariate Selection

Uni-variate covariate evaluation using the covariate functions outlined in Chapter 3.3.3 was performed. Table 3.7 presents the OFV and p-values associated with the addition or removal of individual covariates using the linear clearance BASE model and Table 3.8 the equivalent for the non-linear clearance BASE model. Dose and PPI on Fsus were found to be significant on forward selection ($p<0.05$) and remained

significant on backward elimination (p<0.01) for both BASE models (linear and non-linear clearance). In both BASE models the most significant reduction in the OFV by any one of the covariates tested was achieved through inclusion of dose on suspension bioavailability (Fsus); $-\Delta$OFV = 11.73 and 29.69 using the linear and non-linear CL respectively. Both PPI and Dose were also tested on tablet bioavailability. No effect was found when using non-linear clearance of either covariate. Some effect of dose on tablet bioavailability seemed to be found with linear clearance; - ΔOFV = 5.79 on forward selection. However, covariance was not achieved in run Lin-8 due to $D50_{tab}$ tending to the upper boundary of 1000 mg/BSA, as such dose on tablet bioavailability was not carried forward as a covariate. Diarrhoea (DIAR) was found

Table 3.7: Covariate selection: Linear CL model

Run	Description	OFV	deltaOFV	df	Pvalue
Base Lin	**Base Linear CL Model**	**218.24**	**na**	**na**	**na**
Lin-1	Dose on Fsus	206.51	-11.73	0	na
Lin-2	PPI on Fsus	208.61	-9.63	1	0.002
Lin-3	DIAR on Fsus	210.78	-7.46	1	0.006
Lin-4	DIAR and Dose on Fsus	199.07	-19.17	1	<0.001
Lin-5	Albumin on V	218.23	-0.01	1	0.92
Lin-6	ALT on CL	216.9	-1.34	1	0.247
Lin-7	PPI on Ftab	216.61	-1.63	1	0.202
Lin-8	Dose on Ftab	224.03	5.79	0	na
Lin-9	WT on Ka	216.66	-1.58	1	0.209
Lin-10	**Combined Covariates p<0.05**	**178.75**	**-39.49**	**2**	**<0.001**
Lin-11	minus DIAR on Fsus	188.64	9.89	1	0.002
Lin-12	minus PPI on Fsus	199.14	20.39	1	<0.001
Lin-13	minus Dose on Fsus	218.28	39.53	0	na

Note:
Run Lin-3 and Run Lin-8 no covariance step, covariate theta went to upper boundary.
Run Lin-13 no covariance step, PPI and DIAR terms went to upper boundary.
Red text highlights the covairates found to be significant, either forward or backward elim.
OFV; objective function value. Fsus; suspension bioavailability. Ftab; tablet bioavailability.
PPI; proton-pump inhibitor. DIAR; diarrhoea. ALT; alanine transaminase. CL; clearance
WT; weight. V; volume. Ka; absorption rate constant.

to be significant on forward selection using both BASE models but was only retained after backward elimination with linear clearance. It is worth highlighting that when using linear CL dose on Fsus was so important that the effect of diarrhoea could only be found if dose was also included, as in Run Lin-4 where $-\Delta$OFV was 19.17 for addition of both diarrhoea and dose.

Allometric scaling of absorption rate constants was tested as per Equation (3.8) but was not found to improve the model using either BASE model.

Neither ALB on volume or ALT on clearance were found to be significant covariates when tested using the linear clearance base model; run Lin-5 and Lin-6. However ALT on CL_{sat} was found to be significant on forward selection when using non-linear CL; run NL-5 p=0.002, however significance was not retained at p>0.01 on backward elimination therefore ALT was not included in the final non-linear clearance model.

Covariates in the final **linear** clearance model (Run Lin-10) include dose, diarrhoea, and concomitant administration of PPIs on suspension bioavailability, with no covariate effects on tablet bioavailability or clearance. Covariates in the final **saturable/non-linear** clearance model (Run NL-13) include dose and concomitant administration of PPIs on suspension bioavailability and ALT on CL_{sat}. Weight on

Table 3.8: Covariate selection: Saturable CL model

Run	Description	OFV	deltaOFV	df	Pvalue
Base NL	**Base Non-Linear CL Model**	**226.33**	**na**	**na**	**na**
NL-1	Dose on Fsus	196.64	-29.69	0	na
NL-2	PPI on Fsus	217.39	-8.94	1	0.003
NL-3	DIAR on Fsus	221.21	-5.12	1	0.024
NL-4	Albumin on V	225.82	-0.51	1	0.475
NL-5	ALT on CLsat	216.49	-9.84	1	0.002
NL-6	PPI on Ftab	223.75	-2.58	1	0.108
NL-7	Dose on Ftab	225.52	-0.81	0	na
NL-8	WT on Ka	225.76	-0.57	0	na
NL-9	Albumin on Km	226.31	-0.02	1	0.888
NL-10	**Combined Covariates p<0.05**	**173.64**	**-52.69**	**3**	**< 0.001**
NL-11	NL-10 minus DIAR on Fsus	178.84	5.2	1	0.023
NL-12	NL-10 minus ALT on Clsat	179.57	5.93	1	0.015
NL-13	**Combined PPI and Dose on Fsus**	**145.92**	**-80.41**	**1**	**< 0.001**
NL-14	NL-13 minus PPI on Fsus	196.64	50.72	1	< 0.001
NL-15	NL-13 minus Dose on Fsus	217.39	71.47	0	na

Note:
Run NL-3 and NL-4 minimisation terminated due to rounding errors.
Red text highlights the covairates found to be significant, either on forward or backward elim.
OFV; objective function value. Fsus; suspension bioavailability. Ftab; tablet bioavailability.
PPI; proton-pump inhibitor. DIAR; diarrhoea. ALT; alanine transaminase. CL; clearance
WT; weight. V; volume. Ka; absorption rate constant.

clearance and volume terms was included *a priori* in both models. In Run NL-13 additive error had reduced to 0.01 mg/L (105.8% RSE), see Appendix Figure C.16 for NL-13 parameter estimates. Therefore, additive error was removed in the final non-linear clearance model.

Final Linear and Non-Linear CL Models

Having selected which covariates to include, estimating clearance and volume terms was evaluated. With linear clearance this resulted in the estimate of clearance increasing from 5.67 (IV only modelling) to 9.03 L/hr/70kg and tablet bioavailability increasing from the linear clearance base model estimate of 1.18 to 1.51. While this run minimised successfully achieving an OFV of 109.2 the covariance step was not performed due to boundary issues with the estimation of volume (lower boundary set to 100 L/70kg). As such parameters in the final combined covariate model using linear clearance are estimated without estimating CL and V. However, with the combined covariate model and non-linear clearance estimating CL_{max} and V was possible. The resulting parameter estimates are compared in Table 3.9.

Table 3.9: Final model parameter estimates. Clearance and volume estimates are centred on a 70 kg adult.

Parameter	**Estimate (%RSE)**	**IIV %CV (%RSE)**
Linear Clearance		
CL (L/hr/70kg)	5.67 (fixed)	54 (39.5)
V (L/70 kg)	143.2 (fixed)	-
Ka_{tab} (/hr)	0.59 (fixed)	-
Ka_{sus} (/hr)	0.2 (fixed)	-
Tablet F	1.22 (31.1)	-
Suspension D_{50} (mg/BSA)	41.36 (53.8)	-
θ_{diar} on F_{sus}	-0.93 (64.4)	-
θ_{ppi} on F_{sus}	-0.54 (39.9)	-
Add Err (mg/L)	0.45 (51.4)	-
Prop Error (%)	47.65 (41.6)	-
OFV	178.75	-
Non-Linear Clearance		
CL_{sat} (L/hr/70kg)	13.47 (11.8)	57 (20.5)
K_m (mg/L)	2 (fixed)	-
V (L/70 kg)	186.01 (37.6)	120 (33.1)
Ka_{tab} (/hr)	0.59 (fixed)	-
Ka_{sus} (/hr)	0.2 (fixed)	-
Tablet F	0.66 (21.0)	-
Suspension D_{50} (mg/BSA)	43.25 (14.2)	-
θ_{ppi} on F_{sus}	-0.41 (27.5)	-
Prop Error (%)	63.0 (22.1)	-
OFV	138	-

The NONMEM code for the final linear CL and non-linear CL models (presented in Table 3.9) are included in Appendix C.1 and Appendix C.2 respectively.

With **linear clearance** tablet bioavailability (F) is estimated to be 1.22 (RSE 31.1%) and the dose at which Fsus is 50% was estimated to be 41.36 mg/m^2. The effect of concomitant PPI dosing is estimated to reduce Fsus by 54 % (FPPI = ($1+\theta_{ppi}$ = 0.54) compared to the population estimate, with only a major effect of diarrhoea: reducing Fsus by 93% = (FDIAR = $1+\theta_{diar}$) = 0.93). IIV on CL is estimated to be 54% (RSE 39.5%, shrinkage 28.2%). Additive and proportional error are estimated to be 0.45 mg/L (RSE 51.4%) and 47.65% (RSE 41.6%) respectively with shrinkage of the residual error calculated to be 8.66%.

With **non-linear clearance** tablet F is estimated to be 0.66 (21.0 %RSE), which is a significant reduction compared to that estimated using the linear clearance model. The dose at which suspension F is 50% is however estimated to be very similar; 43.25 mg/BSA (14.2 %RSE). The lowest suspension dose included in this dataset is 62.50 mg/BSA (see Table 3.4). Concomitant PPI administration is estimated to reduce suspension exposure (Fsus) by 41% (27.5 %RSE). IIV on CL_{sat} is estimated to be 57.0% (RSE 20.6%, shrinkage 12.0%) and IIV on V is estimated to be 120.0% (RSE 33.1%, shrinkage 46.2%), the correlation between η_1 and η_2 is 0.22. The residual/unexplained error is described using a proportional error model and is estimated to be 63% (RSE 22.1%).

Goodness of fit (GOF) plots and prediction corrected VPCs split by formulation (IV/tablet/suspension) are presented in Figure 3.24 for the final linear clearance model and in Figure 3.25 for the final non-linear clearance model. Combined GOF plots for each model can be found in Appendix C.17 and Appendix C.18. Because of the high variability in the data and therefore high remaining residual error (not unexpected for a retrospective analysis of TDM data) the lower prediction intervals calculated from VPC simulation were extending to include negative values so to prevent this a theoretical DV (TDV) was specified in the NONMEM model file. If a concentration was simulated at less than 0.08 mg/L, then it was then set to equal 0.08 mg/L.

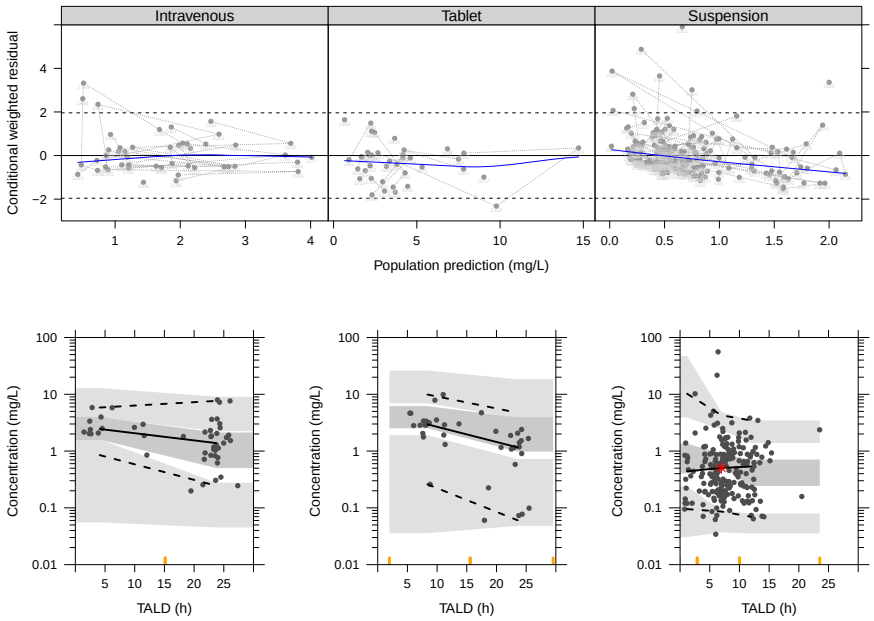

Figure 3.24: Linear CL model diagnostics. Top row; conditional weighted residuals versus population prediction. Bottom row; prediction corrected VPC plots. Faceted by formulation: Left; IV. Middle; tablet. Right; suspension. Key: TALD; time after last dose.

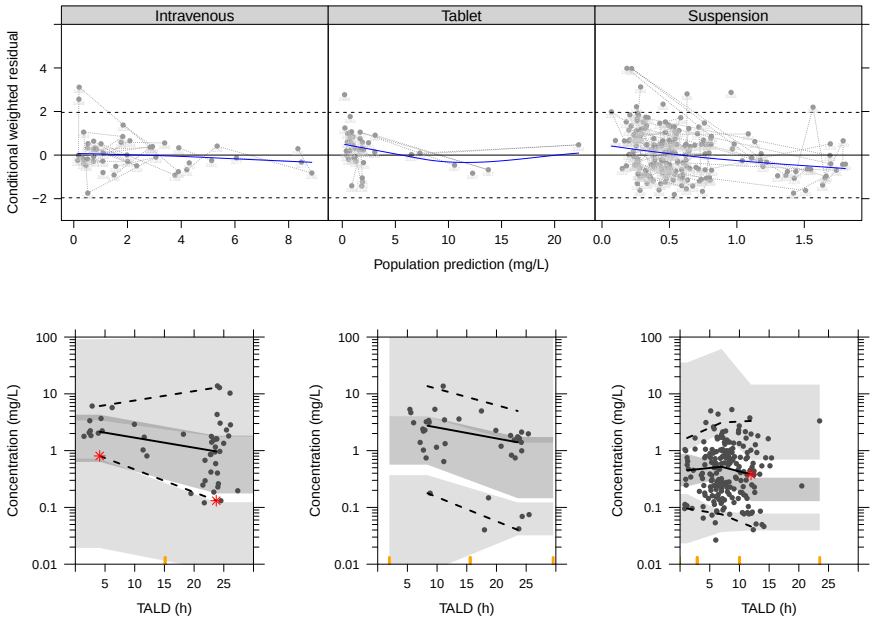

Figure 3.25: Non-linear CL model diagnostics. Top row; conditional weighted residuals versus population prediction. Bottom row; prediction corrected VPC plots. Faceted by formulation: Left; IV. Middle; tablet. Right; suspension. Key: TALD; time after last dose.

To further explore model performance individual η_i estimates on CL and CL_{sat} obtained with the final linear and non-linear clearance models were compared using Dunn's non-parametric all-pairs comparison test[330,337,338]. Figure 3.26 clearly shows a significant difference between individual estimates of clearance depending on the formulation/route when using linear clearance (Figure 3.26A); IV versus tablet p-value = 3.03e-09, IV versus suspension p-value = 6.95e-04, and tablet versus suspension p-value = 1.70e-05. When using the linear clearance model individuals contributing tablet levels typically had CL_i estimates significantly higher than those individuals contributing suspension or IV data. While there is still some formulation bias to individual η_i estimates with the final non-linear CL model, the effect is greatly reduced, and a significant difference is only found between IV and suspension η's (p-value = 9.43e-03).

The non-linear clearance model was selected as the 'best' overall model. The OFV is considerable lower; 138 compared to 179, the precision of the parameter estimates is greater for all parameters (lower RSE's) and the model allows simultaneous estimation of CL, V and F terms. Another key consideration in selection of the non-linear clearance model as the model with which to perform paediatric PK simulations that a tablet F greater than 1.0 is indicative of over simplification (miss-specification) of the linear clearance model.

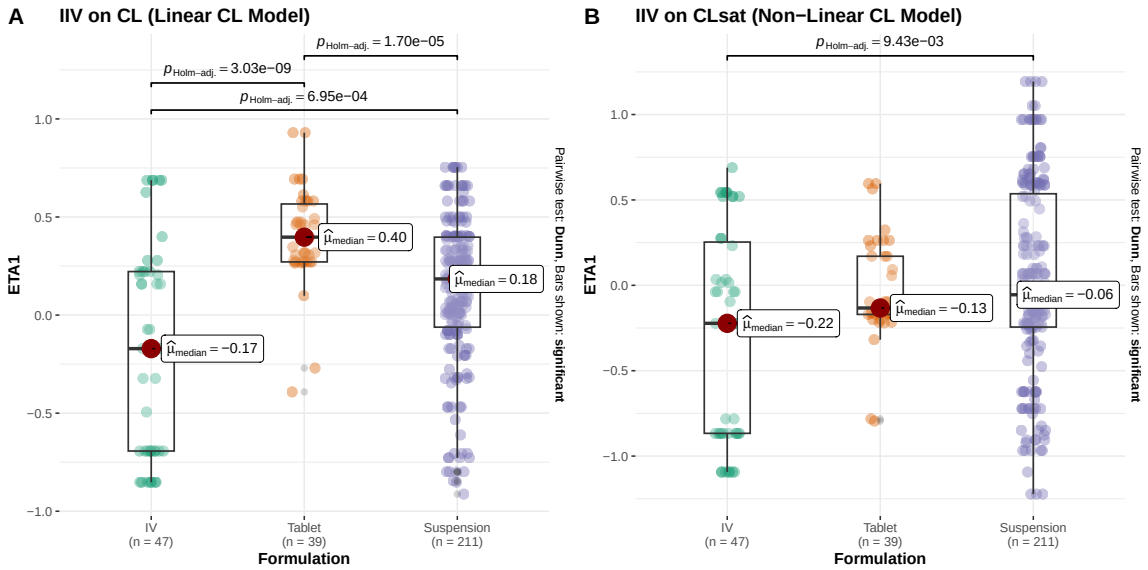

Figure 3.26: ETA on CL terms were compared for the final linear and non-linear clearance models across formulations. Pairwise comparisons were performed using the Dunn non-parametric all-pairs comparison test [328, 335, 336].

As the model selected for the execution of paediatric PK simulations, see Chapter 3.4.4, the **non-linear clearance** covariate effects; dose and concomitant PPI administration on F_{sus}, and plasma concentration on CL are visualised in Figure 3.27.

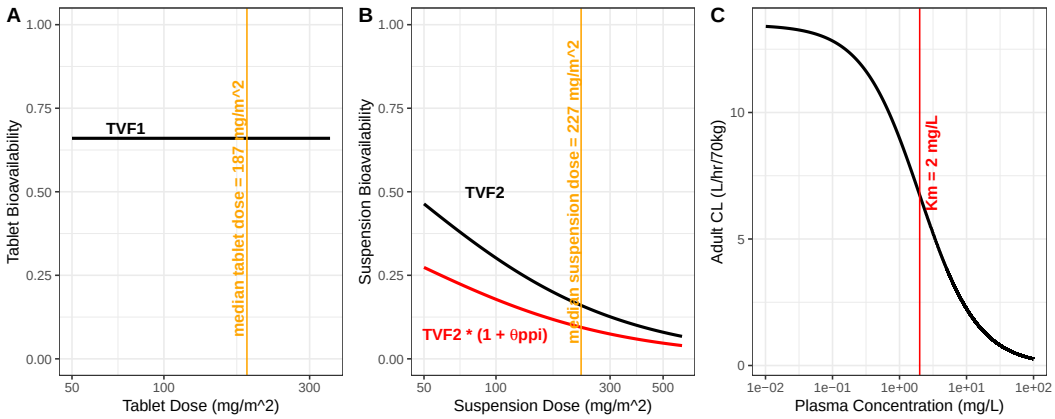

Figure 3.27: A) Effect of tablet dose on tablet F (F1). Black line; population estimate of F1. B) Effect of dose on suspension F (F2). Black line; population estimate of F2 without PPI, red line is F2 with PPI. C) Effect of plasma concentration on posaconazole clearance (centred on a 70kg adult).

The final model structure that has been used is visualised in Figure 3.28.

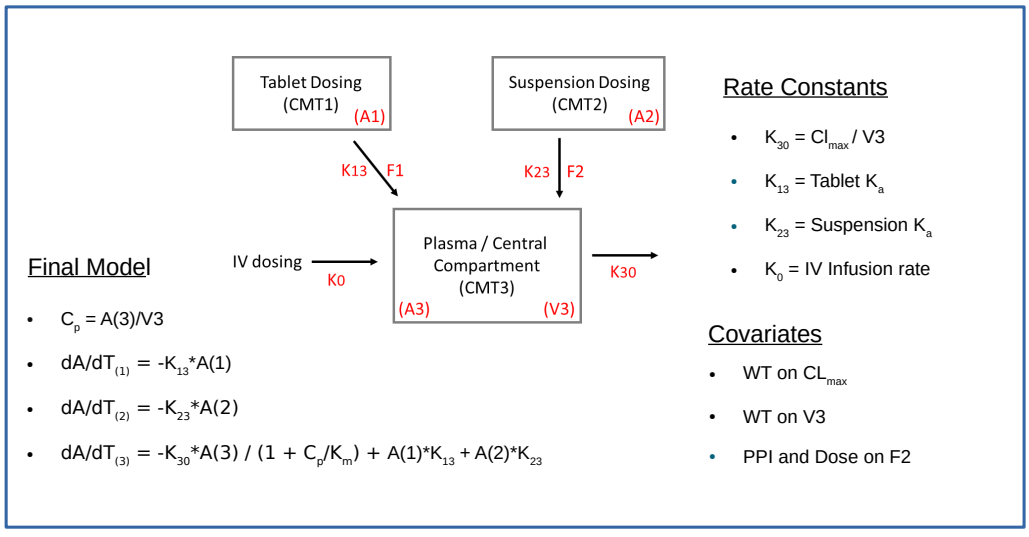

Figure 3.28: Final posaconazole PK model selected for use in paediatric PTA simulations. Key: K30; elimination rate constant. K13; first order absorption rate constant for the tablet. K23; first order absorption rate constant for the suspension. K0; intravenous infusion rate. F1; tablet bioavailability. F2; suspension bioavailability. WT; weight (continuous covariate). PPI; proton-pump inhibitor (catagorical covariate).

3.4.4 Paediatric simulations and PTA (objective 3)

Using previously published PD targets[336] the probability of target attainment in children using typical paediatric dosing regimens (IV, tablet and suspension) was evaluated using the final saturable clearance model as detailed in Table 3.9.

From a hypothetical population of n=10,000 children created for simulation purposes individuals were collected into groups by age: 0.5-2, 2-4, 4-6, 6-9, 9-12, 12-16 years. The number of hypothetical individuals within each of these groups was; 1489, 2489, 1697, 1657, 926, 687 (n=8943 in the final simulation population, the remaining 1057 were either younger than 0.5 years, or older than 16.0 years). The age and weight distributions of the full hypothetical population are presented in Figure 3.29A and Figure 3.29B respectively, the median age and weight are 4.5 years (range: 0.51 to 16.0 years) and 19.1 kg (range: 2.88 to 79.67 kg). Figure 3.29C compares the correlation between age and weight in the hypothetical paediatric population with the age and weight correlation observed in the real-world paediatric posaconazole population from this study, and the simulation population is considered to be a fair representation of the observed population.

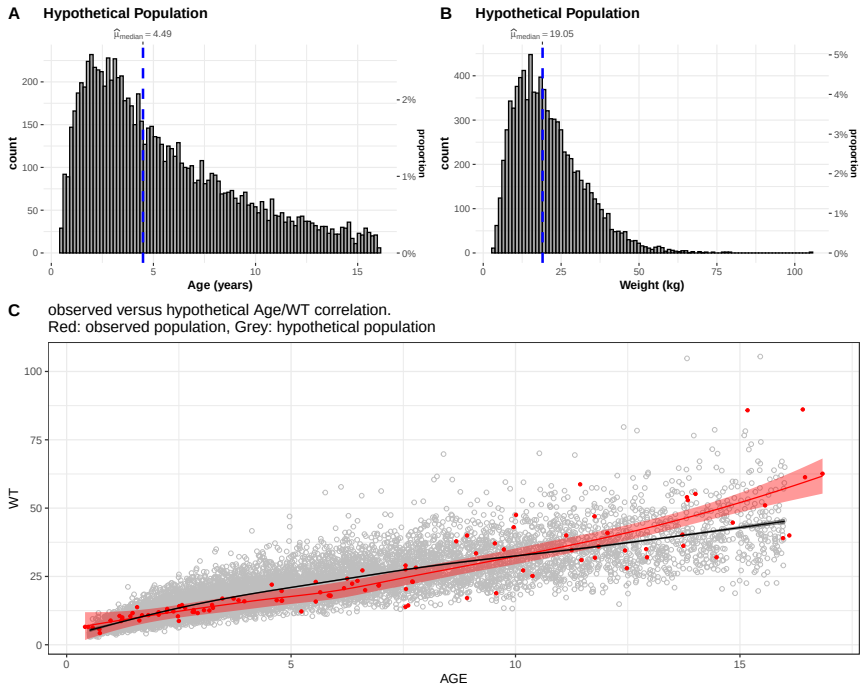

Figure 3.29: Hypothetical pardiatric population A) Age and B) weight distributions (n=10,000). C) Comparison between the observed (red) and hypothetical (grey circles and black line) age and weight correlations. The solid lines are smoothed conditional means and shaded areas are the associated 95% confidence intervals.

There is some deviation between the two correlations above approximately 12 years with the real children appearing to weigh more than represented in the hypothetical population, although this may simply be a result of the relatively small sample size; n=16 children > 12.5 years of age. The distributions and median age and weight in each hypothetical simulation group are presented in Figure 3.30.

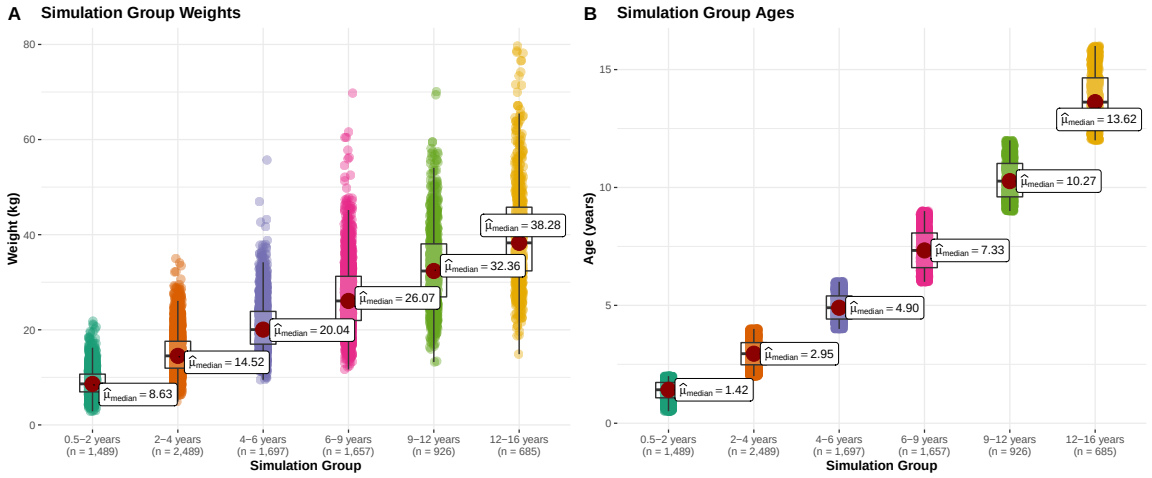

Figure 3.30: Distributions (and median) of the paediatric simulation sub-groups. A) Weight. B) Age.

Based on the dosing regimens observed in this paediatric posaconazole population, see Figure 3.13 and Table 3.4 in Section 3.4.2 for summary statistics, the 'typical' paediatric regimens were defined as 5 mg/kg QD for IV and tablet dosing and 10 mg/kg TID for suspension dosing. The median (50th percentile) concentration-time profiles for all age groups following 8 days of dosing using these 'typical' regimens are presented in Figure 3.31, while the 2.5th, 50th and 95th percentiles for each regimen in the 4-6 year old age group on day 8 of dosing are compared in Figure 3.32. One noticeable observation from Figure 3.31 is that the impact of BW/size on the simulated levels seems less significant after suspension dosing while they appear more important for IV and tablet dosing; the simulated Cp-time profiles vary more between the age groups for IV and tablet dosing compared to suspension. This is due to the covariate effect of dose (mg/BSA) on Fsus that is incorporated into the model. For example, in the 5mg/kg 0.5-2yr old simulation dataset, dose in mg/kg for those 1489 subjects varied from 4.993 to 5.007 mg/kg but dose in mg/BSA (BSA is calculated based on WT) varied from 68.48 to 129.17 mg/m^2 which will influence the estimate of F2 used when simulating the PK, the Fsus function is visualized in Figure 3.27. For example, following IV and tablet dosing across the different age groups, the

median Cmin on day eight ranged from 0.30 to 0.88 mg/L and 0.15 to 0.39 mg/L respectively. While following suspension dosing at 10 mg/kg TID without PPI the Cmin on day 8 ranged from 0.81 to 0.89 mg/L and with PPI from 0.41 to 0.43 mg/L.

While the youngest child in the model development dataset to receive tablet posaconazole was 8.9 years (see Table 3.3) the 4-6 year old age group was chosen as group that theoretically all formulations could be used in, although it is acknowledged that swallowing tablets may be challenging for most 4 year olds.

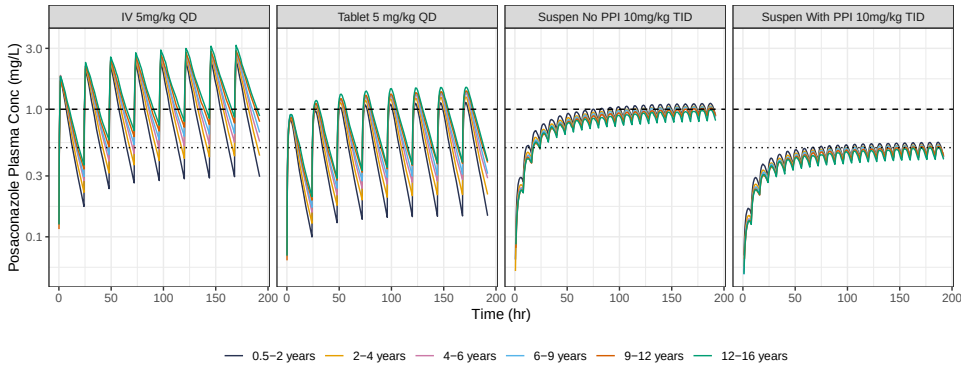

Figure 3.31: Simulated median Cp-time profiles, illustrating the predicted steady state levels and time to steady state using the 'typical' IV, tablet and suspension dosing regimens. Horizontal reference lines; Cmin > 1.0 mg/L [334], Cavg > 0.5 mg/L (500 ng/mL) [321]

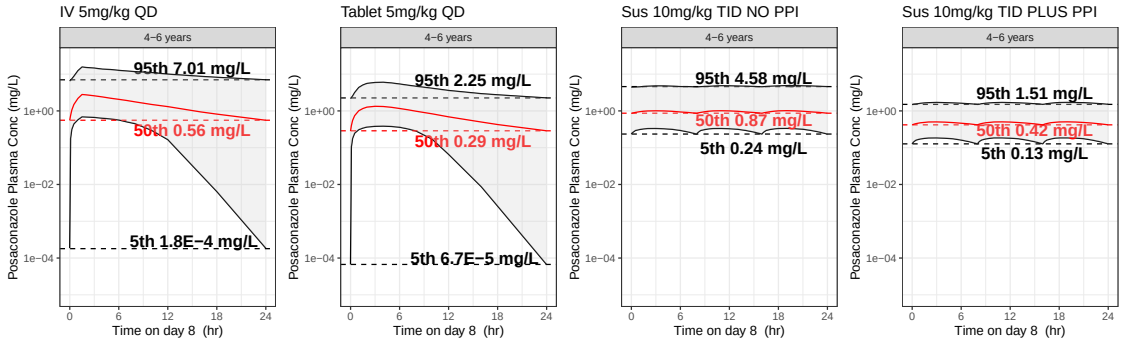

Figure 3.32: Cp-time population simulation result for children aged 4-6 years after eight days of dosing with 'typical' dosing regimens. QD; q24hr dosing. TID; q8hr dosing. PLUS PPI; with concomitant PPI

Figure 3.33 presents the probability of target attainment for all ages groups that have been calculated using the PK simulations performed in NONMEM. To aid comparisons the red circle highlights the probability of target attainment for the 4-6 year old group at a dose of 10 mg/kg which for this group would be equivalent to a 200 mg dose (median group BW = 20kg).

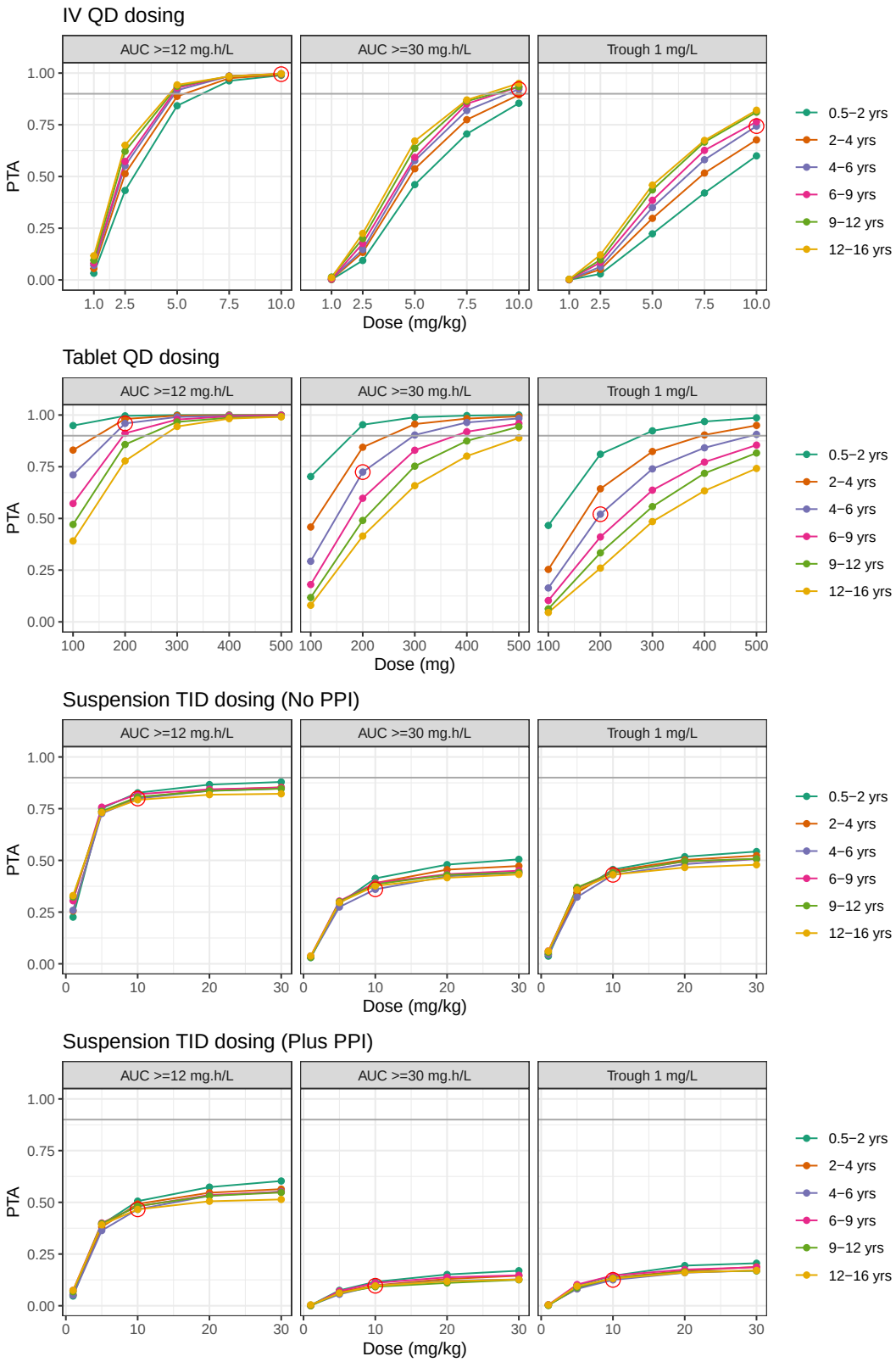

Figure 3.33: Probability of target attainment for all simulation age groups after eight days of QD dosing for IV and Tablet and TID dosing for suspension. QD; q24hr dosing. TID; q8hr dosing. Plus PPI; with concomitant PPI. Horizontal grey line represents 90% probability of target attainment

PTA following suspension TID dosing irrespective of concomitant PPI treatment shows little difference when applying the two targets previously described by Gastine et. al.[336]. Considering the 4-6 year age group; with PPI the PTA at steady state following a 10 mg/kg three times daily dosing regimen is 9.7 % and 12.5 % for the AUC and trough target respectively. For the lower C_{avg} target of $>$ 500 ng/mL ($AUC_{24} \geq 12$ mg.h/L) this increases to 46.6 %.

The probability of target attainment following tablet once daily dosing is described for multiples of the unit tablet strength (100 mg) rather than on a mg/kg basis as this was considered to be more useful to clinicians. However, to allow direct comparison to a suspension given at 10 mg/kg three times daily, and IV given at 10 mg/kg once daily, a 200mg tablet dose to the 4-6 year old group is highlighted as this equates to a 10 mg/kg once daily dose in a 20 kg child. Here, the probability of achieving a steady state $AUC_{24} \geq 30$ mg.h/L is 72.4 % and 52.0 % for exceeding a trough of 1 mg/L. If the AUC_{24} target is reduced to ≥ 12 mg.h/L the 4-6 year old age group is predicted to exceed 90 % PTA after 200 mg tablet once daily and all age groups are predicted to exceed 75 % PTA. Thus, tablet administration is more likely to reach adequate exposures compared to the suspension currently available in Europe.

Finally, following IV dosing the PTA results show that in contrast to the oral formulations, it is easier to achieve the AUC_{24} targets than the C_{min} target. Again, focusing on a typical 4-6 year old, 10 mg/kg once daily intravenous dosing is predicted to ensure 92.2 % of children achieve an $AUC_{24} \geq 30$ mg.h/L and 74.4 % would have a steady state trough $>$ 1 mg/L. However, while this regimen is predicted to result in 74.4 % of the population exceeding trough concentrations of 1 mg/L, it is also predicted that part of the population is at risk of high exposures; $Cavg_{ss}$'s greater than the upper limit of 2.5 mg/L proposed by Groll *et. al.*[323]. For example, the 95th percentile of trough concentrations after 7 days prior dosing of 10 mg/kg QD IV to 4-6 year olds, is predicted to be 51.6 mg/L, see Figure C.19. With a recommended C_{avg} below 2.5 mg/L used by Groll *et. al.*[323], this highlights the high inter-individual variability estimated by the underlying model.

3.5 Discussion

This study describes the first intravenous and oral population PK model based on real-world therapeutic drug monitoring data from immunocompromised children. This enabled the first joint estimation of posaconazole tablet and suspension oral bioavailability in children. It is also the first population PK model estimating the non-linear clearance previously reported by Kersemaekers *et. al.*[297], which has been key to a meaningful estimation of tablet bioavailability.

The starting point for model development was a one-compartment distribution and elimination model with linear clearance. Indeed, this model is used in most published posaconazole models irrespective of the underlying study population[314–319]. While an acceptable description of this sparse paediatric TDM dataset could be achieved with a model employing linear clearance, it did not allow meaningful estimation of both tablet and suspension bioavailability. Although this model was able to reconcile the low exposures seen following suspension dosing, the simultaneous description of IV, suspension and tablet levels was only possible if tablet bioavailability was not constrained to be ≤ 1. Thus, this analysis suggests, the poor exposure seen following suspension dosing, is not simply due to poor intestinal posaconazole solubility but is also compounded by a saturable clearance mechanism.

The reason non-linearity of posaconazole CL has not previously been found in suspension PK modelling is likely due to the fact that intestinal absorption is so poor that nonlinear clearance was masked. The enhanced solubility of posaconazole in the tablet combined with real world dosing, potentially in the fed state, means tablet F is estimated to be > 1 if clearance is assumed to be linear. Whilst this has not previously been reported in human PK models, it has however been seen preclinically in IV/tablet crossover studies in dog[339].

During model development attempts to estimate K_m and CL_{sat} using this paediatric dataset, resulted in K_m tending to the upper boundary and the model essentially collapsing clearance back to a linear process. A value of 2 mg/L for the paediatric K_m was identified through parameter sensitivity analysis and rationalised since between 97-99 % of posaconazole is reportedly bound to plasma proteins[296]. Therefore only a small difference in plasma protein binding, for example from 96% in healthy adults[297] (Km was estimated to be 0.5 mg/L using the healthy adult IV PK data published by Kersemaekers[297]), to 99% in this sick paediatric population, could lead to equivalent unbound posaconazole Km across the two populations (free Km would be 0.02 mg/L in both populations).

Tablet bioavailability estimated by this analysis was 66 % (22.1 % RSE). The fasted state tablet F reported to the EMEA as part of clinical development was 54 % (31.9 %CV)[310]. In addition, an absolute bioavailability study in healthy adult Chinese subjects has been published recently and after 300 mg IV/tablet crossover (n=18 Chinese subjects) in the fasted state the geometric mean F of the tablet was 42.2 %, Tmax 4.0 hours (range; 2-6 hours). The authors also found that tablet exposure increased 2-fold in the fed state (fed state F_{tab} = 87.1 %)[311]. Further evidence for the existence of a tablet food effect was recently presented by Chen *et. al.*. The authors performed a PopPK analysis of rich IV/tablet/suspension data from healthy adult subjects (multiple phase I studies) and clearly showed a positive food effect on tablet exposure. Tablet F confidence intervals were reported as 53.2-63.2% in the fasted state, but were fixed to 99.5% in the fed state; estimation in the fed state was not possible due to boundary problems[322]. Unfortunately for the real-world TDM data analysed during this study information on the patients fed or fasted status was unavailable.

The suspension D_{50} has been estimated previously by Boonsathorn et. al. at 99 mg/m^2[307]. Due to the lack of IV data availability at the time, this was estimated relative to the tablet CL/F and thus, was estimated relative to tablet exposure. Figure 3.27 shows how estimated suspension bioavailability evolves across the dose range evaluated in this study population. With IV data available for this analysis, suspension D_{50} was estimated relative to IV exposure to be 43.25 mg/m^2 (14.2 % RSE).

Concomitant PPI dosing is known to be an important covariate influencing suspension exposure (F_{sus}). This analysis was able to re-confirm this finding with concomitant PPI dosing on F_{sus} reducing suspension bioavailability by 41 % (27.5 % RSE). This agrees with the effect estimated by Boonsathorn et. al.; 42 % and the 45 % estimated by Dolton et. al. in healthy volunteers[307,314]. Figure 3.27 shows, that at the highest suspension dose evaluated (625 mg/m^2) only 3.8 % of the posaconazole given to the patient is estimated to reach the systemic circulation when administered alongside a PPI.

Some of the children/patients (probably <50% based on Figure 3.10) that contributed data to this dataset were receiving prophylactic posaconazole as part of undergoing HSCT and it is known that the conditioning required pre HSCT can influence gut integrity through both increased epithelial inflammation and reduced immunity[59]. Testing HSCT status as a covariate on bioavailability was not performed in this analysis but the impact of diarrhoea was evaluated during covariate testing and

because diarrhoea is associated with the GI problems typically seen in these patients it has been considered as a surrogate for HSCT status. While diarrhoea has previously been reported to be an important covariate on Fsus[307], in this analysis it was not retained when employing a 1 % level of significance in the backward elimination step. However curating information regarding the occurrence of diarrhoea is complex and also highly subjective relying on an individual's interpretation of diverse patient history notes. It should also be of note that the percentage of posaconazole levels in this modelling dataset identified as being collected during periods of diarrhoea was higher; 49 % as compared to the 20 % of samples identified in the Boonsathorn dataset. ALT was another covariate, like diarrhoea, that was found to be significant on forward selection ($p<0.05$) but was not included in the final model as $p>0.01$ on backward elimination. ALT has been previously identified as a important covariate on posaconazole CL in adults but was not included in the final model published by Petitcollin *et. al.* due to issues with model stability[318].

The final non-linear clearance population pharmacokinetic model presented in Table 3.9 has been used to simulate different dosing regimens for the three formulations administered to this study population, thereby allowing a side-by-side exposure comparison and evaluation against previously published PKPD indices. The results of this analysis are expressed through the probability of target attainment plots in Figure 3.33.

Pharmacodynamic target definition varies across literature. Jang *et. al.* published in 2010 on the posaconazole exposure-response relationship, which suggest C_{avg} of > 0.7 mg/L (700 ng/mL) yields adequate antifungal coverage[340]. Posaconazole efficacy in pre-clinical models by Gastine *et. al.* found an AUC_{24} of $\geq$ 30 mg.h/L or C_{min} > 1 mg/L to be relevant[336], While Groll *et. al.* reported intravenous/PO crossover PK data using the 'new' posaconazole suspension in children and a C_{avg} target exposure window of 0.5 to 2.5 mg/L (500 to 2500 ng/mL)[323]. Probability of target attainment was therefore performed for these indices: AUC_{24} of $\geq$ 30 mg.h/L[336]; C_{min} of >1 mg/L[336]; and C_{avg} of > 0.5 mg/L (which is equivalent to an AUC_{24} of $\geq$ 12 mg.h/L, since $C_{avg,ss} = AUC_{\tau}/\tau$, and assuming q24hr dosing)[323].

Because of the high inter-individual variability estimated by population PK modelling of this real-world paediatric data, therapeutic drug monitoring after posaconazole administration with subsequent dose adaptation appears to be warranted. From the PTA simulations and considering the AUC_{24} target of $\geq$ 12 mg.h/L (which is equivalent to a C_{avg} > 0.5 mg/L after q24hr dosing), all age groups are predicted to exceed 84.2 % PTA after q24hr IV doses of 5 mg/kg or above. This is in good

agreement with the paediatric IV PK study results reported by Groll *et. al.* where the authors found that after 7 days of dosing 4.5 and 6.0 mg/kg once daily, ~90 % of participants achieved a $C_{avg} > 0.5$ mg/L[323].

There are however limitations to our analysis that stem from the retrospective assessment of sparse real world TDM data combined with the relatively small number of patients contributing crossover intravenous and oral PK levels to the dataset. Because of this the dataset did not support estimation of Km and this parameter was fixed based on findings from modelling of adult IV data and parameter sensitivity analysis performed using the paediatric data.

Because of the decision to only include plasma levels in the modelling data set that are explained by in-patient dosing, the number of levels that have less than 5 days prior dose history (assumed time to steady state) has been evaluated. Of the 298 levels included in the final modelling dataset 19.5% are preceded by $\leq$ 5 days of in-patient dosing and these levels are tabulated in Table C.1. The information in Table C.1 along with the individual dose history plots, see Figures C.2 to C.6 can be used to identify levels that may in fact reflect steady state concentrations due to out-patient dosing and this may be something that can be incorporated as part of future model refinement work.

The FDA granted regulatory approval of a new suspension posaconazole product (Noxafil PowderMix delayed release oral suspension) to MSD in May 2021[295]. Regulatory approval and the ensuing routine clinical use of this 'new' suspension, which in the US is approved for use in children aged 2 years and older who weigh less than 40 kg, will likely bring increased focus on understanding the mechanisms behind posaconazole's saturable clearance. Until now this has been of limited clinical importance, masked by the poor, highly variable and dose dependent (decreasing with dose) fraction absorbed (fa) following paediatric dosing of the 'old' suspension formulation. While the tablet formulation has to a great extent removed the sub-proportional nature of posaconazole absorption on dose escalation, the lowest tablet strength available is 100 mg, equivalent to ~ 5 mg/kg to a typical 4-6 years old (assumes 20kg BW). However, the 'new' oral suspension combines the improved absorption characteristics of the tablet launched in 2014 with the added dosing flexibility of a typical paediatric liquid formulation and as it receives wider real world paediatric use it seems likely there will be increasing clinical observations of 'higher than expected' TDM levels, which may be of some concern since a clear safety exposure response relationship has, as yet never been established for posaconazole.

Conclusion

The research presented in this thesis has employed mixed effect (population PK) and mechanistic (physiologically based PK) models to estimate the oral bioavailability of three structurally diverse antimicrobials (fosfomycin, benznidazole and posaconazole) in three different paediatric patient populations (neonates with suspected sepsis, 2 to 12 year olds with Chagas Disease and 0.4 to 17 year olds at risk of invasive fungal infections).

The PK data analysed has come from prospective clinical trials and from retrospective analysis of real-world TDM data. Oral and intravenous PK data has been analysed for both fosfomycin and posaconazole and it has been possible to estimate paediatric oral bioavailability at a population level for both of these drugs. Thereby increasing our understanding of the dose-exposure relationship in children as compared to in adults, enabling simulation of paediatric PK and definition of paediatric dosing regimens that are optimised in consideration of known PD targets. Which at its core, is the purpose of model-informed drug development (MIDD) in the context of paediatric medicine[134–136].

This is the first study to report model-based estimation of oral bioavailability from cross-over data in a neonatal antibiotic study, and the first report of neonatal fosfomycin CSF penetration. PNA in addition to PMA was needed to describe immediate postnatal changes in CL distinct from gestational effects. We also establish a positive relationship between PR_i and CSF uptake of fosfomycin. Between subject variability and residual variability was higher following oral rather than intravenous fosfomycin, however no covariate effects were identified for bioavailability. Unfortunately, the oral PK data collected as part of the NeoFosfo study was not informative enough to allow estimation of between subject variability on Ka so it was not possible to evaluate if age was a significant covariate on the rate of absorption as has been shown for other drugs[66]. In any future neonatal oral/IV crossover studies consideration should be given to how more information during the absorption phase could be collected. However, considering fosfomycin's absorption properties the higher F

and csf/plasma ratio observed in this neonatal population, when compared to adults, is thought to provide further supporting evidence[62,63] of increased membrane permeability during the initial postnatal period, possibly due to increased paracellular permeation in neonatal epithelium. The model and target attainment simulations presented here can be used to aid selection of a neonatal IV dose based on an infant's PMA, PNA and WT and the oral step down dose personalised using likely pathogen MIC at 48 hours. Further *in vitro* work to better define target AUC/MIC ratios to achieve a 2 fold log kill against pathogens typically responsible for neonatal sepsis, alongside work to define relevant MIC breakpoints for bacteraemia and meningitis would be beneficial.

To quantify age-dependent changes in CL/F, benznidazole PK data was pooled from children aged 2-12 years and adult populations (healthy volunteers, CD patients) and a population PK analysis performed. This analysis clearly demonstrated an age effect on both CL/F and Ka. Building on these findings and utilising a platform of additional ADME evidence a PBPK model that describes benznidazole pharmacokinetics in adult populations has, for the first time, been presented. The model suggests incomplete oral absorption, low first pass extraction following oral dosing, and significant renal re-reabsorption. Extrapolation of the adult model to simulate paediatric PK has shown that the observed age dependent changes in CL/F can largely be accounted for through reduced renal absorption in children aged 2 to 6 years as compared to in adults, however further *in-vitro* transporter work with benznidazole is required to confirm the feasibility of this hypothesis. There is also some suggestion that the default age and weight based scaling of gut physiological parameters may be leading to an over estimation of Fa in younger children, this too needs further investigation, ideally with additional paediatric benznidazole PK data.

From real-world TDM data, more understanding of posaconazole PK in children has been generated. The model that has been presented successfully describes the bioavailability differences seen following tablet and suspension dosing in children. Key to this has been incorporation of saturable posaconazole clearance into the model. Due to the sparse nature of posaconazole TDM data extrapolation of PK in adult populations informed the base model and was used to inform and fix certain model parameters; Km, Ka_{tab} and Ka_{sus}. Covariate analysis confirmed previously reported dose-dependent decreases in suspension bioavailability, which are then further reduced by concomitant PPIs. The model has been used to evaluate typical paediatric IV, tablet and suspension dosing regimens using published PD targets. These simulations highlight that both IV and tablet formulations are capable of achieving

adequate posaconazole exposures across the paediatric population. However, for the original/old suspension formulation that is still widely used across Europe, escalation of dose beyond 10 mg/kg is essentially pointless and even with TID dosing many children are likely to be left with sub-therapeutic posaconazole exposures.

While incomplete absorption has been found for the three exemplar drugs evaluated, the ability to estimate between-subject variability in the extent (with assumptions F can be used to estimate Fa when CL is known) or the rate of oral absorption (Ka) has been a major challenge. Especially so with the real-world posaconazole TDM data where BSV on F could not be estimated and even the population estimates of absorption rate constants (Ka_{tab} and Ka_{sus}) had to be fixed to adult priors. This in turn makes it difficult to analyse and make conclusions concerning the effect of age within a paediatric population on rate and extent of oral absorption.

In the case of benznidazole where pharmacokinetics in humans has only ever been evaluated following oral administration PBPK modelling was utilised alongside population PK to try and delineate the underlying mechanisms responsible for the effect of age on CL/F and Ka. Future analysis of the fosfomycin and posaconazole datasets curated during this research using PBPK modelling would also be of interest as it may provide the PBPK research community with further verification of the underlying age dependent system parameters that underpin 'bottom-up' oral absorption predictions for children as more validatory evidence is still needed here[60,341,342].

Appendix A

Chapter 1

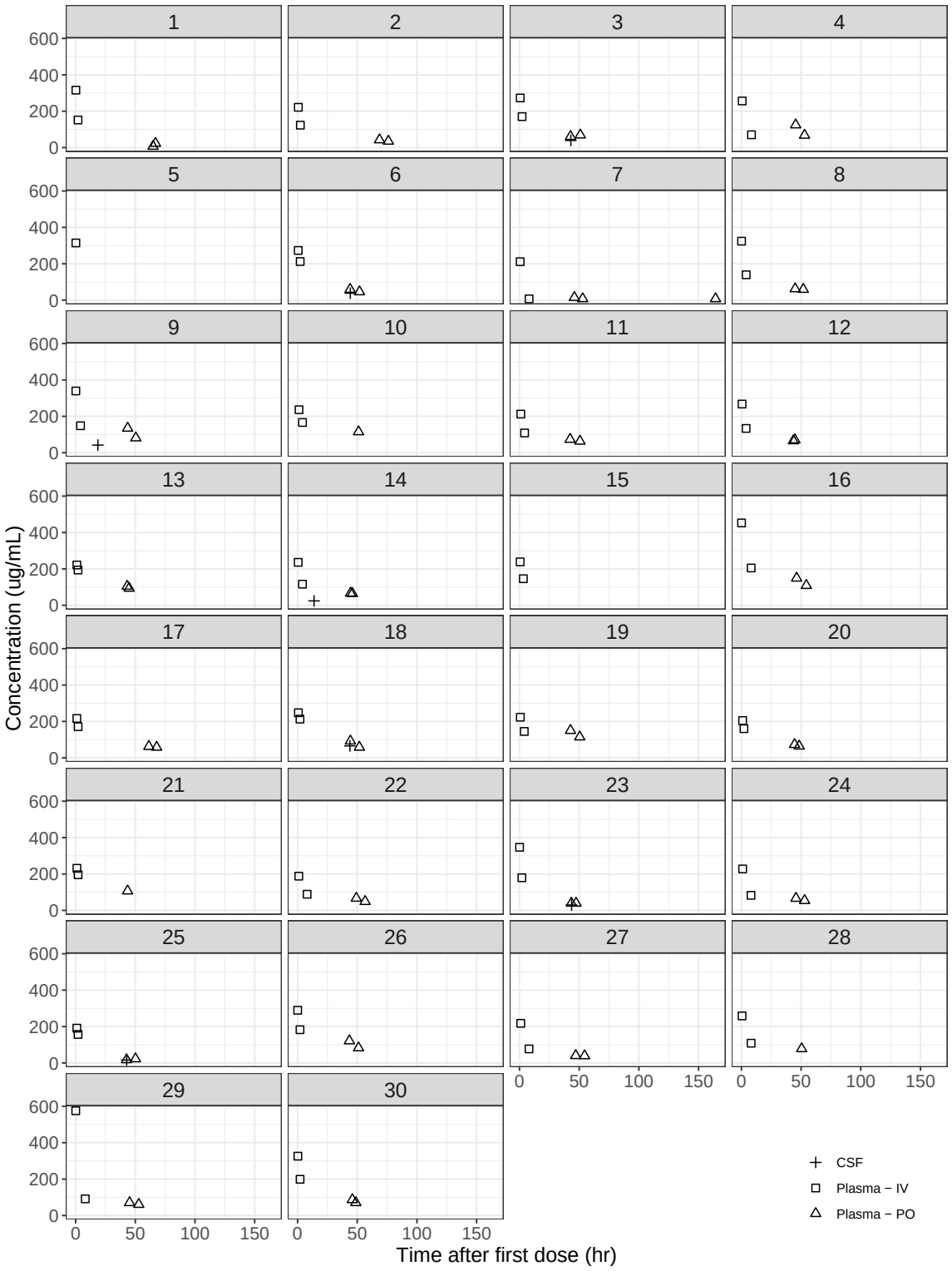

Figure A.1: Fosfomycin concentration versus time - Patient 1 to 30. Diamonds; IV plasma levels. Circles; PO plasma levels. Asterix; CSF levels.

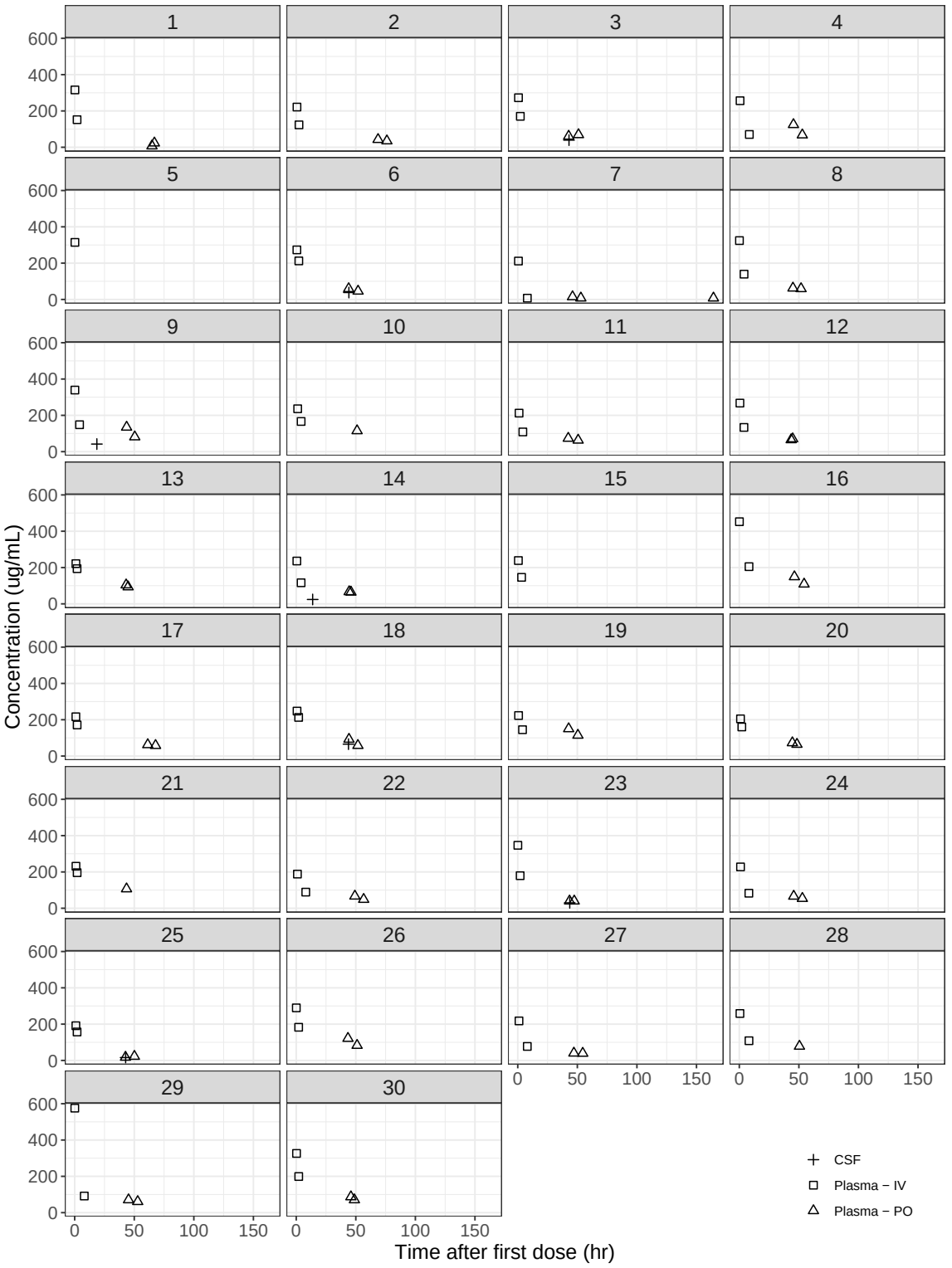

Figure A.2: Fosfomycin concentration versus time - Patient 31 to 60. Diamonds; IV plasma levels. Circles; PO plasma levels. Asterix; CSF levels.

A.1 Fosfomycin NONMEM model code

```
$PROBLEM    Fosfomycin neonatal pharmacokinetics
$INPUT      ID SEX GA AGE WT AMT TIME MATRIX DV PROTEIN MDV CMT ROUTE
            RATE TAD PNADAYS PNAYEARS TSCR PMAWEEKS SCR Na PNADAYS2
            PNASG PMA tCrea dCrea PNASGC flag
$DATA       neofosfo.pk.200208.csv  IGNORE=@
$SUBROUTINE ADVAN5 TRANS1
$MODEL      COMP(1) ; oral absorption
            COMP(2) ; central compartment
            COMP(3) ; peripheral compartment
            COMP(4) ; CSF compartment
$PK
;------ Covariate functions
 WTCL = (WT / 70000)**0.75   ; weight scaling for CL and Q terms
 WTV  = (WT / 70000)         ; weight scaling for volume terms
 MAT = PMA**3.4 / (47.7**3.4 + PMA**3.4 ;Rhodin 2008 GFR maturation
 CLPNA =  THETA(7) + (1 - THETA(7)) * (1 - EXP(-PNASGC * THETA(8)))
 ; CLPNA describes short term maturation of CL through PNA
;------ Typicl value of parameters
 TVCL = THETA(1)  ; clearance
 TVV2 = THETA(2)  ; central volume, allometrically scaled
 TVQ1 = THETA(3)  ; Inter compartmental clearance C2 to C3
 TVV3 = THETA(4)  ; Peripheral volume
 TVKA = THETA(5)  ; Absorption rate constant
 TVF1 = THETA(6)  ; Oral Bioavailability
 TVQ2 = THETA(9)  ; Inter-compartmental clearance between C2 and C4
 TVUP = THETA(10) ; Fraction uptake into CSF compartment
;------ MU modelling
 MU_1 = DLOG(TVCL)
 MU_2 = DLOG(TVV2)
;------ Individual parameters
 CL   = DEXP(MU_1 + ETA(1)) * WTCL * MAT * CLPNA
 V2   = DEXP(MU_2 + ETA(2)) * WTV
 Q1   = TVQ1 * WTCL
```

```
 Q2   = TVQ2 * WTCL   ; no eta on Q2 as not enough data
 V3   = TVV3 * WTV
 V4   = 0.15 * WTV    ; fixed to CSF volume in 70Kg adult
 KA   = TVKA
;----- Oral bioavailability logit
 BIO1 = DLOG(TVF1 / (1 - TVF1))       ; (-inf,inf)
 BIO2 = BIO1 + ETA(3)                 ; iiv now on normal scake
 F1   = 1 / (1 + DEXP(-BIO2))         ; back to (0, 1)
;------ CSF uptake fraction logit
 UPTK1 = DLOG(TVUP/(1 - TVUP))      ; (-inf,inf)
 UPTK2 = UPTK1 * (1 + THETA(11) * (PROTEIN - 0.94)) ; Median protein = 0.94
 UPTK  = 1 / (1 + DEXP(-UPTK2))     ; back to (0, 1)
;------ Rate constants
 K20 = CL/V2
 K23 = Q1/V2
 K32 = Q1/V3
 K24 = Q2*UPTK/V2
 K42 = Q2/V4
 K12 = KA
 S2  = V2
 S4  = V4

$ERROR
CP   = A(2) / V2
CCSF = A(4) / V4
;------ Plasma predictions
IF(CMT==2)   IPRED = CP
IF(ROUTE==1) Y = IPRED * (1 + EPS(1))
; EPS(1) is proportional residual error on IV
IF(ROUTE==2) Y = IPRED * (1 + EPS(2))
; EPS(2) is proportional residual error on PO
;------ CSF predictions
IF(CMT==4) IPRED = CCSF
IF(CMT==4) Y = IPRED + EPS(3)
; residual error term for csf, additive error model
;------ Calculate IWRES
```

```
 IRES  = DV-IPRED
 IF(ROUTE==1) SD = SQRT(SIGMA(1,1)) * IPRED ; IV
 IF(ROUTE==2) SD = SQRT(SIGMA(2,2)) * IPRED ; PO
 IF(CMT==4) SD   = SQRT(SIGMA(3,3))         ; CSF
 IF(SD==0)  SD   = 1
 IWRES = IRES/SD

;------ Final parameter estimates
 $THETA  8.94306     ; 1. TVCL
 $THETA  19.1087     ; 2. TVV2
 $THETA  8.00673     ; 3. TVQ1
 $THETA  7.53073     ; 4. TVV3
 $THETA  0.0987403   ; 5. TVKA
 $THETA  0.478167    ; 6. TVF1
 $THETA  0.449443    ; 7. M - frac of CL on day of birth
 $THETA  0.116786    ; 8. N - rate of maturation post birth
 $THETA  0.017 FIX   ; 9. Q2 clearance between C2 and C4
 $THETA  0.320868    ; 10. uptake into CSF, fractional
 $THETA  -0.952217   ; 11. protein covariate
;------ Interindividual parameter variability
 $OMEGA  0.0599312   ; variance for ETA(1)
 $OMEGA  0.0202154   ; variance for ETA(2)
 $OMEGA  0.269266    ; variance for ETA(3)
;------ Residual error
 $SIGMA  0.00592027  ; variance prop res error, IV plasma
 $SIGMA  0.0344364   ; variance prop res error, PO plasma
 $SIGMA  117.851     ; variance add res error, CSF

$ESTIMATION METHOD=1 INTER MAXEVAL=9999 PRINT=1 NOABORT
;------ standard error of estimate is calculated
$COVARIANCE
;------ Table output
$TABLE      ID TIME CMT TAD ROUTE MATRIX MDV IPRED IWRES CWRES NPDE
            ESAMPLE=300 NOPRINT ONEHEADER FILE=sdtab355
$TABLE      ID CL V2 V3 V4 Q1 Q2 KA F1 ETAS(1:3) NOPRINT NOAPPEND
            ONEHEADER FILE=patab355
```

```
$TABLE      ID GA AGE WT PROTEIN PNADAYS PNAYEARS TSCR PMAWEEKS SCR
            NOPRINT NOAPPEND ONEHEADER FILE=cotab355
$TABLE      ID SEX ROUTE NOPRINT NOAPPEND ONEHEADER FILE=catab355
```

Appendix B

Chapter 2

Table B.1: PKPDai Hits [259]: Benznidazole

Title	Publication.Year	Journal
Pharmacokinetics of Benznidazole in Healthy Volunteers and Implications in Future Clinical Trials.	2017	Antimicrob Agents Chemother
Preclinical pharmacokinetics of benznidazole-loaded interpolyelectrolyte complex-based delivery systems.	2018	Eur J Pharm Sci
Single-dose pharmacokinetics of the trypanosomicide benznidazole in man.	1979	Arzneimittelforschung
Population pharmacokinetic study of benznidazole in pediatric Chagas disease suggests efficacy despite lower plasma concentrations than in adults.	2014	PLoS Negl Trop Dis
Systematic Review and Meta-analysis of the Pharmacokinetics of Benznidazole in the Treatment of Chagas Disease.	2016	Antimicrob Agents Chemother
Preclinical pharmacokinetics of benznidazole.	1984	Br J Cancer
Population pharmacokinetics and biodistribution of benznidazole in mice.	2020	J Antimicrob Chemother
Pharmacokinetics and Tissue Distribution of Benznidazole after Oral Administration in Mice.	2017	Antimicrob Agents Chemother
Benznidazole Extended-Release Tablets for Improved Treatment of Chagas Disease: Preclinical Pharmacokinetic Study.	2016	Antimicrob Agents Chemother
Rapid and sensitive ultra-high-pressure liquid chromatography method for quantification of antichagasic benznidazole in plasma: application in a preclinical pharmacokinetic study.	2015	Biomed Chromatogr
Dried Blood Spot Technique-Based Liquid Chromatography-Tandem Mass Spectrometry Method as a Simple Alternative for Benznidazole Pharmacokinetic Assessment.	2018	Antimicrob Agents Chemother
Population pharmacokinetics of benznidazole in adult patients with Chagas disease.	2015	Antimicrob Agents Chemother
Preclinical monitoring of drug association in experimental chemotherapy of Chagas' disease by a new HPLC-UV method.	2012	Antimicrob Agents Chemother
Altered pharmacokinetics in the mechanism of chemosensitization: effects of nitroimidazoles and other chemical modifiers on the pharmacokinetics, antitumour activity and acute toxicity of selected nitrogen mustards.	1986	Cancer Chemother Pharmacol
Effects of benznidazole:cyclodextrin complexes on the drug bioavailability upon oral administration to rats.	2013	Int J Biol Macromol
A phase I study of the combination of benznidazole and CCNU in man.	1984	Int J Radiat Oncol Biol Phys
The pharmacokinetics in mice and dogs of nitroimidazole radiosensitizers and chemosensitizers more lipophilic than misonidazole.	1982	Int J Radiat Oncol Biol Phys
Pharmacokinetic and pharmacodynamic responses in adult patients with Chagas disease treated with a new formulation of benznidazole.	2016	Mem Inst Oswaldo Cruz
Antitrypanosomal activity of fexinidazole metabolites, potential new drug candidates for Chagas disease.	2014	Antimicrob Agents Chemother
An evaluation of benznidazole as a Chagas disease therapeutic.	2019	Expert Opin Pharmacother
Antitrypanosomal Treatment with Benznidazole Is Superior to Posaconazole Regimens in Mouse Models of Chagas Disease.	2015	Antimicrob Agents Chemother
Multiple-dose kinetics of the trypanosomicide benznidazole in man.	1980	Arzneimittelforschung
Successful Aspects of the Coadministration of Sterol 14alpha-Demethylase Inhibitor VFV and Benznidazole in Experimental Mouse Models of Chagas Disease Caused by the Drug-Resistant Strain of Trypanosoma cruzi.	2019	ACS Infect Dis
Misonidazole and benznidazole inhibit hydroxylation of CCNU by mouse liver microsomal cytochrome P-450 in vitro.	1987	Biochem Pharmacol
A Novel Prototype Device for Microencapsulation of Benznidazole: In Vitro/In Vivo Studies.	2020	AAPS PharmSciTech
Drug repurposing strategy against Trypanosoma cruzi infection: In vitro and in vivo assessment of the activity of metronidazole in mono- and combined therapy.	2017	Biochem Pharmacol
Modulation of biotransformation systems and ABC transporters by benznidazole in rats.	2013	Antimicrob Agents Chemother
New Class of Antitrypanosomal Agents Based on Imidazopyridines.	2017	ACS Med Chem Lett
Pharmacological characterization, structural studies, and in vivo activities of anti-Chagas disease lead compounds derived from tipifarnib.	2012	Antimicrob Agents Chemother
Ideal benznidazole dose regimen in chronic chagasic patients: a systematic review.	2020	Rev Inst Med Trop Sao Paulo
Efficacy and safety assessment of different dosage of benznidazol for the treatment of Chagas disease in chronic phase in adults (MULTIBENZ study): study protocol for a multicenter randomized Phase II non-inferiority clinical trial.	2020	Trials
Neolignans from leaves of Nectandra leucantha (Lauraceae) display in vitro antitrypanosomal activity via plasma membrane and mitochondrial damages.	2017	Chem Biol Interact
The activity of fexinidazole (HOE 239) against experimental infections with Trypanosoma cruzi, trichomonads and Entamoeba histolytica.	1983	Ann Trop Med Parasitol
8-Alkynyl-3-nitroimidazopyridines display potent antitrypanosomal activity against both T. b. brucei and cruzi.	2020	Eur J Med Chem
Benznidazole with CCNU: a clinical phase I toxicity study.	1985	Int J Radiat Oncol Biol Phys
Nitroimidazoles as modifiers of nitrosourea pharmacokinetics.	1984	Int J Radiat Oncol Biol Phys
Transbuccal delivery of benznidazole associated with monoterpenes: permeation studies and mechanistic insights.	2020	Eur J Pharm Sci
Limited infant exposure to benznidazole through breast milk during maternal treatment for Chagas disease.	2015	Arch Dis Child
A high-performance liquid chromatographic method for benznidazole quantitation in plasma of patients with Chagas disease.	2011	Clin Chem Lab Med

Table B.2: PKPDai Hits [259]: 2-nitroimidazole

Title	Publication.Year	Journal
Pharmacokinetics of tinidazole in male and female subjects.	1982	J Clin Pharmacol
Pharmacokinetics of ornidazole in patients with severe liver cirrhosis.	1986	Clin Pharmacol Ther
Modeling and Simulation of Pretomanid Pharmacokinetics in Pulmonary Tuberculosis Patients.	2018	Antimicrob Agents Chemother
PHARMACOKINETICS OF A SINGLE DOSE OF METRONIDAZOLE AFTER RECTAL ADMINISTRATION IN CAPTIVE ASIAN ELEPHANTS (ELEPHAS MAXIMUS).	2016	J Zoo Wildl Med
A clinical phase I toxicity study of Ro 03-8799: plasma, urine, tumour and normal brain pharmacokinetics.	1986	Br J Radiol
Virus-directed, enzyme prodrug therapy with nitroimidazole reductase: a phase I and pharmacokinetic study of its prodrug, CB1954.	2001	Clin Cancer Res
The pharmacokinetics, bioavailability and biodistribution in mice of a rationally designed 2-nitroimidazole hypoxia probe SR-4554.	1996	Anticancer Drug Des
Pharmacokinetics of Ro 03-8799 in mice bearing melanosarcoma: comparison with tumors without melanin.	1989	Int J Radiat Oncol Biol Phys
The effects of whole body hyperthermia on the pharmacokinetics and toxicity of the basic 2-nitroimidazole radiosensitizer Ro 03-8799 in mice.	1987	Br J Cancer
Pharmacokinetic studies using multiple administration of RO 03-8799, a 2-nitroimidazole radiosensitizer.	1982	Int J Radiat Oncol Biol Phys
Pharmacokinetics of ornidazole in patients with acute viral hepatitis, alcoholic cirrhosis, and extrahepatic cholestasis.	1989	Clin Pharmacol Ther
Pharmacokinetics of hypoxic cell radiosensitizers: a review.	1980	Cancer Clin Trials
Preclinical comprehensive physicochemical and pharmacokinetic profiling of novel nitroimidazole derivative IIIM-019 - A potential oral treatment for tuberculosis.	2016	Pulm Pharmacol Ther
Radiosensitizing activity and pharmacokinetics of multiple dose administered KU-2285 in peripheral nerve tissue in mice.	1994	Int J Radiat Oncol Biol Phys
Pharmacokinetics and Pharmacodynamics of the Nitroimidazole DNDI-0690 in Mouse Models of Cutaneous Leishmaniasis.	2019	Antimicrob Agents Chemother
In vivo efficacy and pharmacokinetics of a new hypoxic cell radiosensitizer doranidazole in SUIT-2 human pancreatic cancer xenografted in mouse pancreas.	2000	Oncol Rep
Pharmacokinetics of metronidazole in rat blood, brain and bile studied by microdialysis coupled to microbore liquid chromatography.	2003	J Chromatogr A
Dose-response relationships of FMISO between trace dose and various macro-doses in rat by ultra-performance liquid chromatography with mass spectrometry and radioactivity analysis.	2012	J Pharm Biomed Anal
Pharmacokinetics of EF5 [2-(2-nitro-1-H-imidazol-1-yl)-N-(2,2,3,3,3-pentafluoropropyl) acetamide] in human patients: implications for hypoxia measurements in vivo by 2-nitroimidazoles.	2001	Cancer Chemother Pharmacol
A phase I study of SR-2508 and cyclophosphamide administered by intravenous injection.	1991	Cancer Res
Enantioselective HPLC determination and pharmacokinetic study of secnidazole enantiomers in rats.	2014	J Chromatogr B Analyt Technol Biomed Life Sci
Pharmacokinetic and metabolic studies of the hypoxic cell radiosensitizer misonidazole.	1978	Xenobiotica
Clinical Pharmacokinetics of Levornidazole in Elderly Subjects and Dosing Regimen Evaluation Using Pharmacokinetic/Pharmacodynamic Analysis.	2017	Clin Ther
Plasma and skin blister fluid concentrations of metronidazole and its hydroxy metabolite after oral administration.	1996	Pol J Pharmacol
Bioequivalence assessment of Azomycin (Julphar, UAE) as compared to Zithromax (Pfizer, USA)–two brands of azithromycin–in healthy human volunteers.	2001	Biopharm Drug Dispos
Radiosensitizing, toxicological, and pharmacokinetic properties of hydroxamate analogues of nitroimidazoles as bifunctional radiosensitizers/chemical modifiers.	1992	Int J Radiat Oncol Biol Phys
Secnidazole concentrations in plasma and crevicular fluid after a single oral dose.	1993	J Clin Periodontol
Comparison of the fate of misonidazole (RO 07-0582) and its metabolite desmethylmisonidazole (RO 05-9963), two hypoxic cell radiosensitizers: penetration properties in tumor bearing rats.	1983	J Pharmacol
Phase I safety, pharmacokinetics, and pharmacogenetics study of the antituberculosis drug PA-824 with concomitant lopinavir-ritonavir, efavirenz, or rifampin.	2014	Antimicrob Agents Chemother
In vitro and in vivo activities of the nitroimidazole TBA-354 against Mycobacterium tuberculosis.	2015	Antimicrob Agents Chemother
Fluorinated 2-nitroimidazole derivative hypoxic cell radiosensitizers: radiosensitizing activities and pharmacokinetics.	1994	Int J Radiat Oncol Biol Phys
Pharmacokinetics of fluorinated 2-nitroimidazole hypoxic cell radiosensitizers in murine peripheral nervous tissue.	1992	Int J Radiat Biol
Lack of stereoselectivity in the pharmacokinetics and metabolism of the radiosensitizer Ro 03-8799 in man.	1991	Cancer Chemother Pharmacol
Pharmacokinetic considerations in testing hypoxic cell radiosensitizers in mouse tumours.	1979	Br J Cancer
The pharmacokinetics in mice and dogs of nitroimidazole radiosensitizers and chemosensitizers more lipophilic than misonidazole.	1982	Int J Radiat Oncol Biol Phys
Pharmacokinetic studies of amino acid analogues of 2-nitroimidazole, new hypoxic cell radiosensitizers.	1984	Int J Radiat Oncol Biol Phys
Enhanced binding of the hypoxic cell marker [3H]fluoromisonidazole in ischemic myocardium.	1989	J Nucl Med
KIH-802, an acetohydroxamic acid derivative of 2-nitroimidazole, as a new potent hypoxic cell radiosensitizer: radiosensitizing activity, acute toxicity, and pharmacokinetics.	1990	Cancer Chemother Pharmacol
Correlation of partitioning of nitroimidazoles in the n-octanol/saline and liposome systems with pharmacokinetic parameters and quantitative structure-activity relationships (QSAR).	1989	Pharm Res
Investigational new drug-directed toxicology and pharmacokinetic study of 4-[3-(2-nitro-1-imidazolyl)-propylamino]-7-chloroquinoline hydrochloride (NLCQ-1, NSC 709257) in Beagle dogs.	2010	Basic Clin Pharmacol Toxicol
Radiosensitization by a new potent nucleoside analog: 1-(1',3',4'-trihydroxy-2'-butoxy)methyl-2-nitroimidazole(RP-343).	1993	Int J Radiat Oncol Biol Phys
A phase I study of the hypoxic cell radiosensitizer Ro-03-8799.	1984	Int J Radiat Oncol Biol Phys
Comparative study of thermoradiosensitization by misonidazole and metronidazole in vivo: antitumour effect and pharmacokinetics.	1992	Int J Hyperthermia
Synthesis of new generation triazolyl- and isoxazolyl-containing 6-nitro-2,3-dihydroimidazooxazoles as anti-TB agents: in vitro, structure-activity relationship, pharmacokinetics and in vivo evaluation.	2015	Org Biomol Chem
Fexinidazole–a new oral nitroimidazole drug candidate entering clinical development for the treatment of sleeping sickness.	2010	PLoS Negl Trop Dis
[Radiosensitizing effects of nitroimidazole derivative, KIN-804].	1995	Nihon Igaku Hoshasen Gakkai Zasshi
Preclinical validation of the hypoxia tracer 2-(2-nitroimidazol-1-yl)- N-(3,3,3-[(18)F]trifluoropropyl)acetamide, [(18)F]EF3.	2004	Eur J Nucl Med Mol Imaging
Substituted carbamothioic amine-1-carbothioic thioanhydrides as novel trichomonicidal fungicides: Design, synthesis, and biology.	2018	Eur J Med Chem
A phase I study of the nitroimidazole hypoxia marker SR4554 using 19F magnetic resonance spectroscopy.	2009	Br J Cancer
[Plasma and tissues distribution of misonidazole (RO 07-0582) in the rat bearing a chimio induced tumor (author's transl)].	1981	J Pharmacol

Table B.3: PKPDai Hits [259]: 2-nitroimidazole ..continued

	Title	Publication.Year	Journal
51	In vitro and in vivo radiosensitizing effects of 2-nitroimidazole derivatives with sugar component.	1987	Strahlenther Onkol
52	Pentacyclic nitrofurans with in vivo efficacy and activity against nonreplicating Mycobacterium tuberculosis.	2014	PLoS One
53	Pharmacokinetics of 2-nitroimidazole hypoxic cell radiosensitizers in rodent peripheral nervous tissue.	1990	Int J Radiat Biol
54	[Clinical evaluation of ceftriaxone in severe infections in adults].	1986	Pathol Biol (Paris)
55	Biological characterization of novel nitroimidazole-peptide conjugates in vitro and in vivo.	2017	J Pept Sci
56	Hypoxic cell radiosensitizers in the treatment of high grade gliomas: a new direction using combined Ro 03-8799 (pimonidazole) and SR 2508 (etanidazole).	1988	Int J Radiat Oncol Biol Phys
57	Antitrypanosomal activity of fexinidazole, a new oral nitroimidazole drug candidate for treatment of sleeping sickness.	2011	Antimicrob Agents Chemother
58	Development and validation of a highly sensitive LC-MS/MS-ESI method for quantification of IIIM-019-A novel nitroimidazole derivative with promising action against Tuberculosis: Application to drug development.	2016	J Pharm Biomed Anal
59	In vivo radiosensitizing effect of nitroimidazole derivative KIN-804.	1994	Int J Radiat Oncol Biol Phys
60	Development and validation of a solid-phase extraction and high-performance liquid chromatographic assay for a novel fluorinated 2-nitroimidazole hypoxia probe (SR-4554) in Balb/c mouse plasma.	1995	J Chromatogr B Biomed Appl
61	In vitro and in vivo activities of ravuconazole on Trypanosoma cruzi, the causative agent of Chagas disease.	2003	Int J Antimicrob Agents
62	Initial results of a phase I trial of continuous infusion SR 2508 (etanidazole): a radiation therapy oncology group study.	1989	Int J Radiat Oncol Biol Phys
63	Nitroimidazoles as modifiers of nitrosourea pharmacokinetics.	1984	Int J Radiat Oncol Biol Phys
64	Treatment of bacterial vaginosis: a multicenter, double-blind, double-dummy, randomised phase III study comparing secnidazole and metronidazole.	2010	Infect Dis Obstet Gynecol
65	New antimetastatic hypoxic cell radiosensitizers: design, synthesis, and biological activities of 2-nitroimidazole-acetamide, TX-1877, and its analogues.	2001	Bioorg Med Chem
66	Evaluation of the radiosensitizing effects of RK28 intravenous, intraarterial, and intratumoral injections on the rabbit VX2 tumor system.	1996	Int J Radiat Oncol Biol Phys
67	Optical isomers of a new 2-nitroimidazole nucleoside analog (PR-350 series): radiosensitization efficiency and toxicity.	1995	Int J Radiat Oncol Biol Phys
68	Pharmacokinetics-pharmacodynamics analysis of bicyclic 4-nitroimidazole analogs in a murine model of tuberculosis.	2014	PLoS One
69	Electron-affinic compounds for labelling hypoxic cells: the synthesis and characterization of 1-[2-(2-iodophenoxy)-ethyl]-2-nitroimidazole.	1984	Nuklearmedizin
70	Carbon-14 radiolabeling and in vivo biodistribution of a potential anti-TB compound.	2015	J Labelled Comp Radiopharm
71	The combination of 5-fluorouracil with misonidazole in patients with advanced colorectal cancer.	1982	Int J Radiat Oncol Biol Phys
72	Assessment of a pretomanid analogue library for African trypanosomiasis: Hit-to-lead studies on 6-substituted 2-nitro-6,7-dihydro-5H-imidazo[2,1-b][1,3]thiazine 8-oxides.	2018	Bioorg Med Chem Lett
73	A comparison of tumor and normal tissue levels of acidic, basic and neutral 2-nitroimidazole radiosensitizers in mice.	1986	Int J Radiat Oncol Biol Phys

Table B.4: PKPDai Hits [259]: 5-nitroimidazole

Title	Publication.Year	Journal
Effects of renal impairment on the pharmacokinetics of morinidazole: uptake transporter-mediated renal clearance of the conjugated metabolites.	2014	Antimicrob Agents Chemother
Effects of rifampin and ketoconazole on pharmacokinetics of morinidazole in healthy chinese subjects.	2014	Antimicrob Agents Chemother
Metabolism and pharmacokinetics of morinidazole in humans: identification of diastereoisomeric morpholine N+-glucuronides catalyzed by UDP glucuronosyltransferase 1A9.	2012	Drug Metab Dispos
Disposition and metabolism of metronidazole in patients with liver failure.	1984	Hepatology
[Study of serum concentrations and urinary excretion of secnidazole after oral administration in man. Comparison with tinidazole].	1980	Pathol Biol (Paris)
Investigation of chiral inversion and pharmacokinetics of laevo-ornidazole by high-performance liquid chromatography.	2013	J Clin Pharm Ther
Studies on the disposition of a 5-nitroimidazole in laboratory animals.	1987	Eur J Drug Metab Pharmacokinet
Simultaneous determination of ornidazole and its main metabolites in human plasma by LC-MS/MS: application to a pharmacokinetic study.	2014	Bioanalysis
Secnidazole. A 5-nitroimidazole derivative with a long half-life.	1978	Br J Vener Dis
Antitrypanosomal activity of fexinidazole, a new oral nitroimidazole drug candidate for treatment of sleeping sickness.	2011	Antimicrob Agents Chemother
Susceptibility of Helicobacter pylori and pharmacokinetic properties in mice of new 5-nitroimidazole derivatives devoid of mutagenic activity in the Ames test.	1993	J Chemother
The activity of fexinidazole (HOE 239) against experimental infections with Trypanosoma cruzi, trichomonads and Entamoeba histolytica.	1983	Ann Trop Med Parasitol
A chiral high-performance liquid chromatography-tandem mass spectrometry method for the stereospecific determination of morinidazole in human plasma.	2014	J Chromatogr B Analyt Technol Biomed Life Sci
Simultaneous determination of morinidazole, its N-oxide, sulfate, and diastereoisomeric N(+)-glucuronides in human plasma by liquid chromatography-tandem mass spectrometry.	2012	J Chromatogr B Analyt Technol Biomed Life Sci
Determination of an optimal dosing regimen for fexinidazole, a novel oral drug for the treatment of human African trypanosomiasis: first-in-human studies.	2014	Clin Pharmacokinet

Table B.5: Pre-Clinical Cross Species Allometric Scaling

Species	BW (kg)	CL (L/hr)	Animal Fup	CLu (L/hr)	log10 BW	log10 CLu
Mouse	0.028	0.012	0.640	0.019	-1.553	-1.727
Mouse	0.028	0.012	0.640	0.019	-1.553	-1.727
Rat	0.215	0.004	0.277	0.014	-0.668	-1.840
Rabbit	3.000	1.665	0.700	2.379	0.477	0.376
Rabbit	3.000	2.422	0.700	3.460	0.477	0.539
Rabbit	3.000	2.333	0.700	3.333	0.477	0.523
Rabbit	3.000	1.380	0.700	1.971	0.477	0.295
Rabbit	3.000	1.447	0.700	2.067	0.477	0.315
Rabbit	3.000	1.742	0.700	2.489	0.477	0.396
Rabbit	3.000	1.447	0.700	2.067	0.477	0.315
Dog	28.000	1.633	0.410	3.983	1.447	0.600
Dog	20.000	0.738	0.410	1.800	1.301	0.255

[1] BW; body weight. CL; clearance. Fup; fraction inbound in plasma. CLu; unbound clearance.

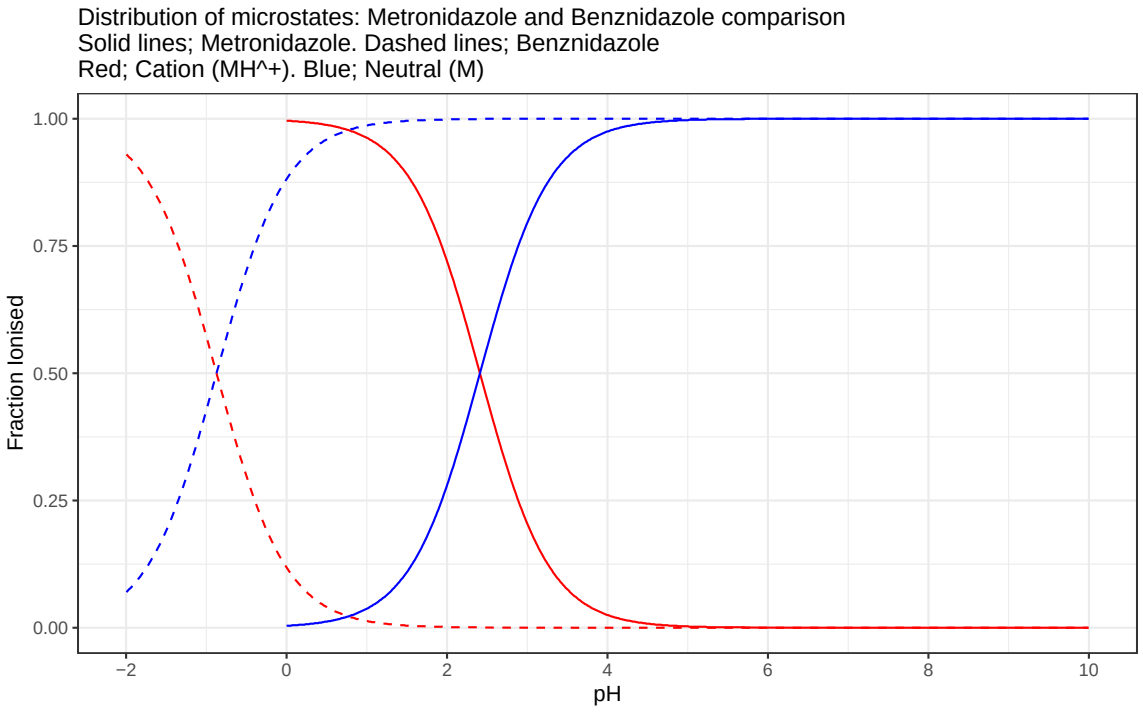

Figure B.1: Predicted effect of pH on the distribution of benznidazole and metronidazole micro/ionisation states.

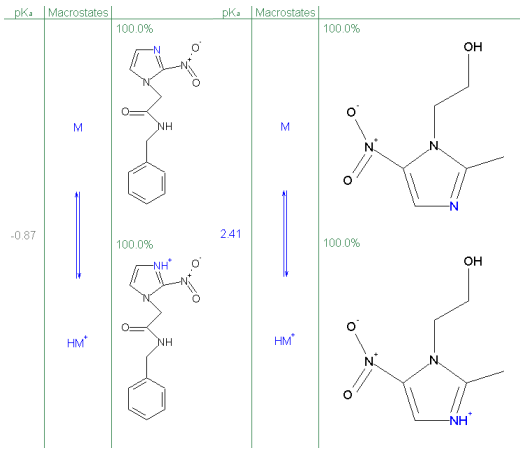

Figure B.2: Predicted ionisation/micro states of benznidazole and metronidazole. Predicted by AMDET Predictor ver 10.4 [258].

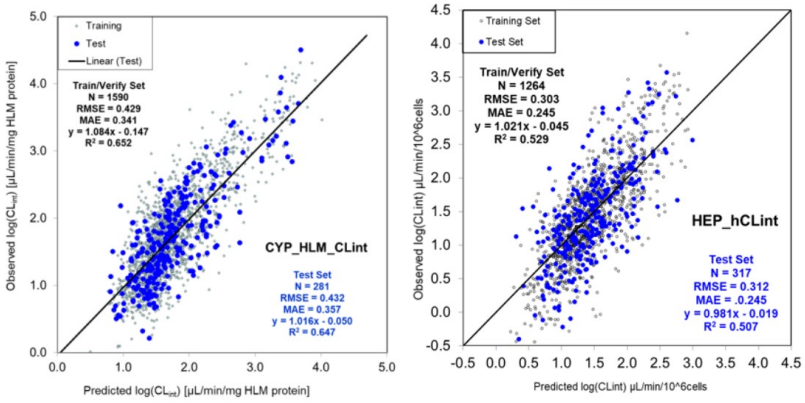

Figure B.3: Performance of ADMET Predictor liver microsomal (left) and hepatocyte (right) unbound CLint regression model. Reproduced from the AMDET Predictor user manual ver 10.4 [258].

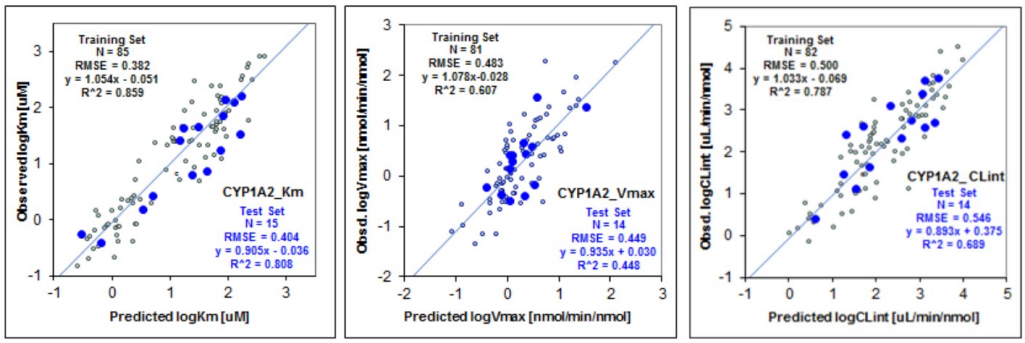

Figure B.4: Performance of ADMET Predictor rCYP1A2 kinetic model. Reproduced from the AMDET Predictor user manual ver 10.4 [258].

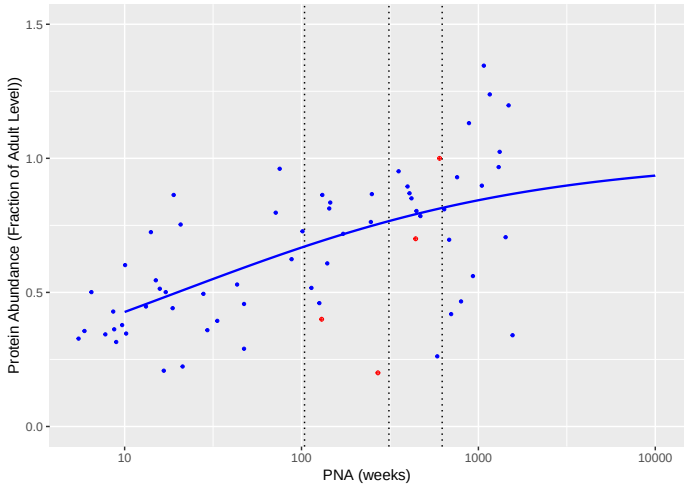

Figure B.5: OAT1 transporter ontogeny reported by Chenug 2019 [77]. Blue circles are the relative protein abundance of renal OAT1 reported by Cheung, blue solid line is the Hill maturation function estimated by Cheung. Red circles are the relative renal transporter expression levels applied in the BNZ paediatric PBPK simulations in this study. Vertical reference lines highlight ages 2, 6 and 12 years.

Table B.6: Adult Internal Validation ACAT Settings

Compartment	Raaflaub 1979 Healthy Volunteers	Raaflaub 1980 Chagas Patients	Roberts 1984 Cancer Patients	Adult Average
Transit Time (hr)				
Stomach	0.5	0.5	0.5	0.5
Duodenum	0.25286	0.2517	0.25463	0.253
Jejunum 1	0.91661	0.91242	0.92304	0.917
Jejunum 2	0.72697	0.72364	0.73207	0.728
Ileum 1	0.56893	0.56633	0.57292	0.569
Ileum 2	0.4109	0.40902	0.41378	0.411
Ileum 3	0.28447	0.28317	0.28646	0.285
Caecum	3.81388	3.70919	3.98138	3.835
Asc Colon	11.4416	11.1276	11.9441	11.504
Length (cm)				
Stomach	26.3894	25.8732	27.2207	26.494
Duodenum	13.1816	12.9244	13.5955	13.234
Jejunum 1	54.4886	53.4255	56.1997	54.705
Jejunum 2	54.4886	53.4255	56.1997	54.705
Ileum 1	54.4886	53.4255	56.1997	54.705
Ileum 2	54.4886	53.4255	56.1997	54.705
Ileum 3	54.4886	53.4255	56.1997	54.705
Caecum	12.3932	12.1445	12.7667	12.435
Asc Colon	25.9345	25.4215	26.7201	26.025
Radius (cm)				
Stomach	9.32171	9.23848	9.46481	9.342

Table B.6: Adult Internal Validation ACAT Settings *(continued)*

Compartment	Healthy Volunteers	Chagas Patients	Cancer Patients	Average
Duodenum	1.47624	1.46328	1.49838	1.479
Jejunum 1	1.38694	1.37167	1.41295	1.391
Jejunum 2	1.24591	1.23472	1.26467	1.248
Ileum 1	1.0852	1.07384	1.10493	1.088
Ileum 2	0.94788	0.93967	0.9615	0.95
Ileum 3	0.7927	0.78508	0.80566	0.794
Caecum	3.26473	3.23489	3.31493	3.272
Asc Colon	2.32477	2.30425	2.3592	2.329
Volume (mL)				
Stomach	39.7707	37.6116	43.0043	40.129
Duodenum	36.0988	34.7756	38.3572	36.411
Jejunum 1	131.713	126.316	140.993	133.007
Jejunum 2	106.288	102.352	112.953	107.198
Ileum 1	80.6365	77.4168	86.2204	81.425
Ileum 2	61.5205	59.2807	65.2895	62.03
Ileum 3	43.0262	41.3798	45.8404	43.415
Caecum	20.749	19.9626	22.0366	20.916
Asc Colon	22.0169	21.2021	23.3608	22.193
Surface Enhancement Factor				
Stomach	1	1	1	1
Duodenum	4.23464	4.23464	4.23464	4.235
Jejunum 1	3.949	3.949	3.949	3.949
Jejunum 2	3.489	3.489	3.489	3.489
Ileum 1	3.029	3.029	3.029	3.029
Ileum 2	2.569	2.569	2.569	2.569
Ileum 3	2.109	2.109	2.109	2.109
Caecum	1.79	1.79	1.79	1.79
Asc Colon	2.48	2.48	2.48	2.48
Absorption Scale Factor				
Stomach	0	0	0	0
Duodenum	2.89654	2.9222	2.85376	2.891
Jejunum 1	2.87509	2.90709	2.82216	2.868
Jejunum 2	2.82773	2.85333	2.78577	2.822
Ileum 1	2.81846	2.84828	2.76813	2.812
Ileum 2	2.73674	2.76063	2.69796	2.732
Ileum 3	2.68651	2.71258	2.64329	2.681
Caecum	0.29802	0.30077	0.29351	0.297
Asc Colon	0.57984	0.58501	0.57138	0.579
P-gp Distribution Factor				
Duodenum	0.538	0.538	0.538	0.538
Jejunum 1	0.645	0.645	0.645	0.645
Jejunum 2	0.723	0.723	0.723	0.723
Ileum 1	0.77	0.77	0.77	0.77
Ileum 2	0.838	0.838	0.838	0.838
Ileum 3	0.908	0.908	0.908	0.908
Caecum	1	1	1	1
Asc Colon	1	1	1	1

Appendix C

Chapter 3

Summary of Posaconazole Pharmacokinetic Parameters by Treatment, presented as mean (%CV) (P07783, Part I).

Parameter (unit)	POS 3x100 mg tablet D [a] N = 13	POS IV solution 300 mg [b] N = 13
Cmax (ng/mL)	613.8 (37.9)	4257.7 (19.1)
tmax (hr)[c]	5 (3-6)	0.5 (0.25-0.5)
t½ (hr)	28.1 (25.6)	28.8 (27.8)
AUC0-last (hr*ng/mL)	22721.9 (46)	42904.7 (30.7)
AUC0-∞ (hr*ng/mL)	23647.3 (47.8)	44380.4 (32.2)
CL (CL/F) (L/hr)[d]	15.44 (45.8)	7.61 (41.4)
Vz (Vz/F) (L)[e]	583.33 (36.0)	294.64 (24.8)

[a]Treatment A; [b]Treatment B;
[c]median (min – max);
[d]CL = Clearance: CL/F=Apparent clearance following oral administration;
[e]Vz = Volume of distribution during terminal phase;
[e]Vz/F = Apparent volume of distribution during terminal phase.

Figure C.1: Tablet absolute bioavailability study results reported to EMEA in February 2014. Study P07783, Part 1. (Merck Sharp and Dohme Corp, 2014)

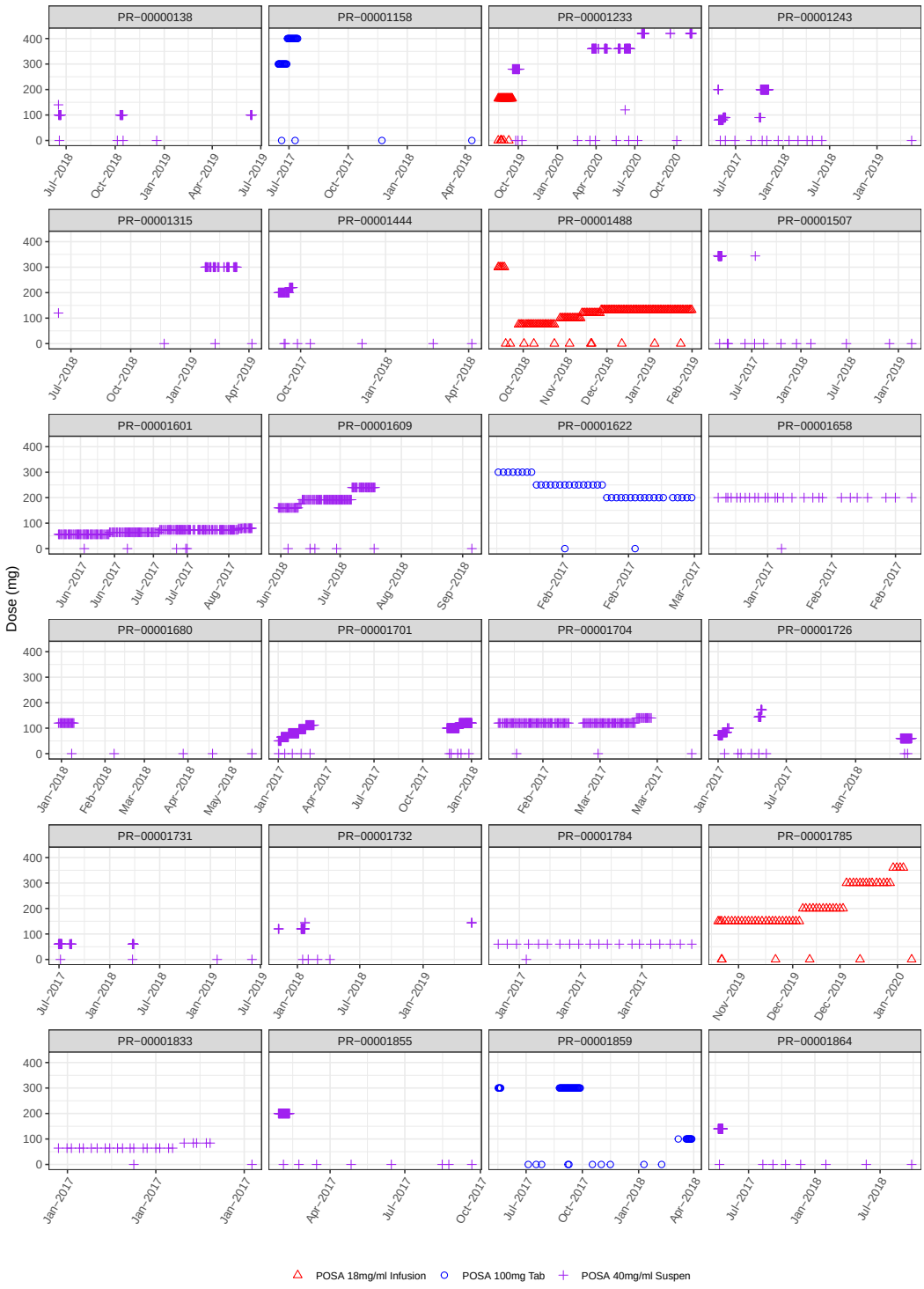

Figure C.2: Posaconazole in-patient dose history plots page 1/5. Red triangle; IV. Blue circle; tablet. Purple cross; suspension. Symbols on the y=0 line show when a TDM blood sample was taken.

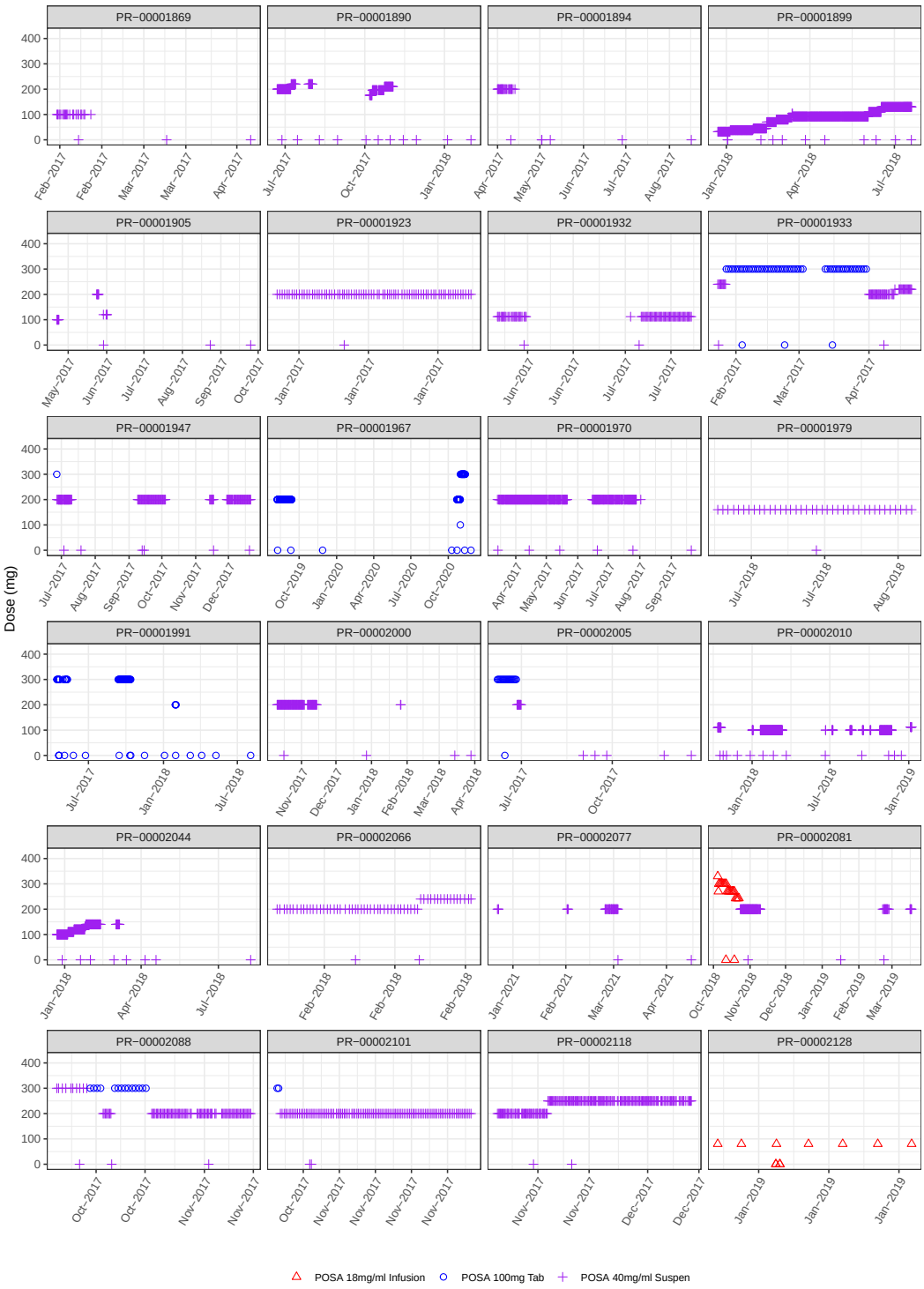

Figure C.3: Posaconazole in-patient dose history plots page 2/5. Red triangle; IV. Blue circle; tablet. Purple cross; suspension. Symbols on the y=0 line show when a TDM blood sample was taken.

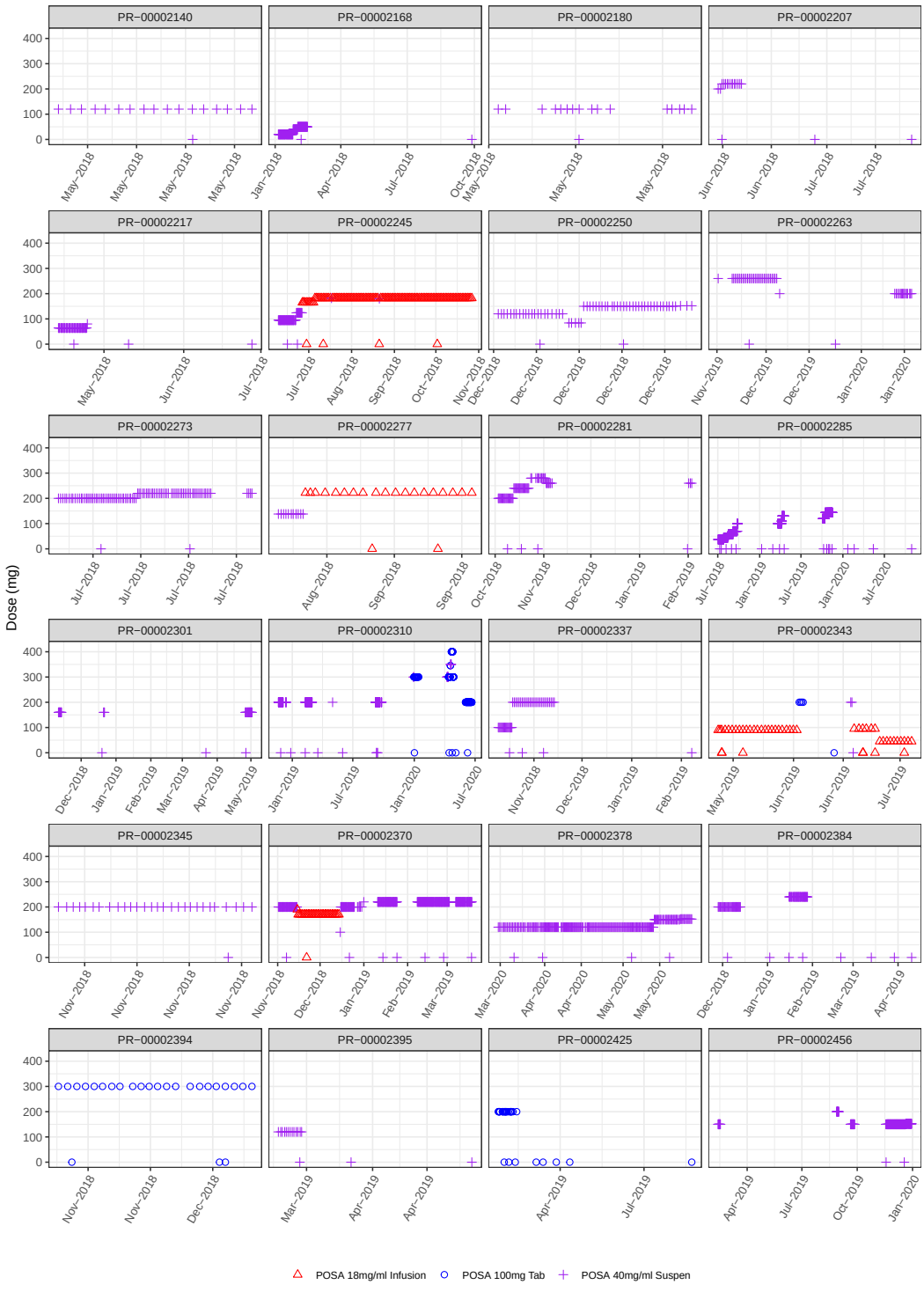

Figure C.4: Posaconazole in-patient dose history plots page 3/5. Red triangle; IV. Blue circle; tablet. Purple cross; suspension. Symbols on the y=0 line show when a TDM blood sample was taken.

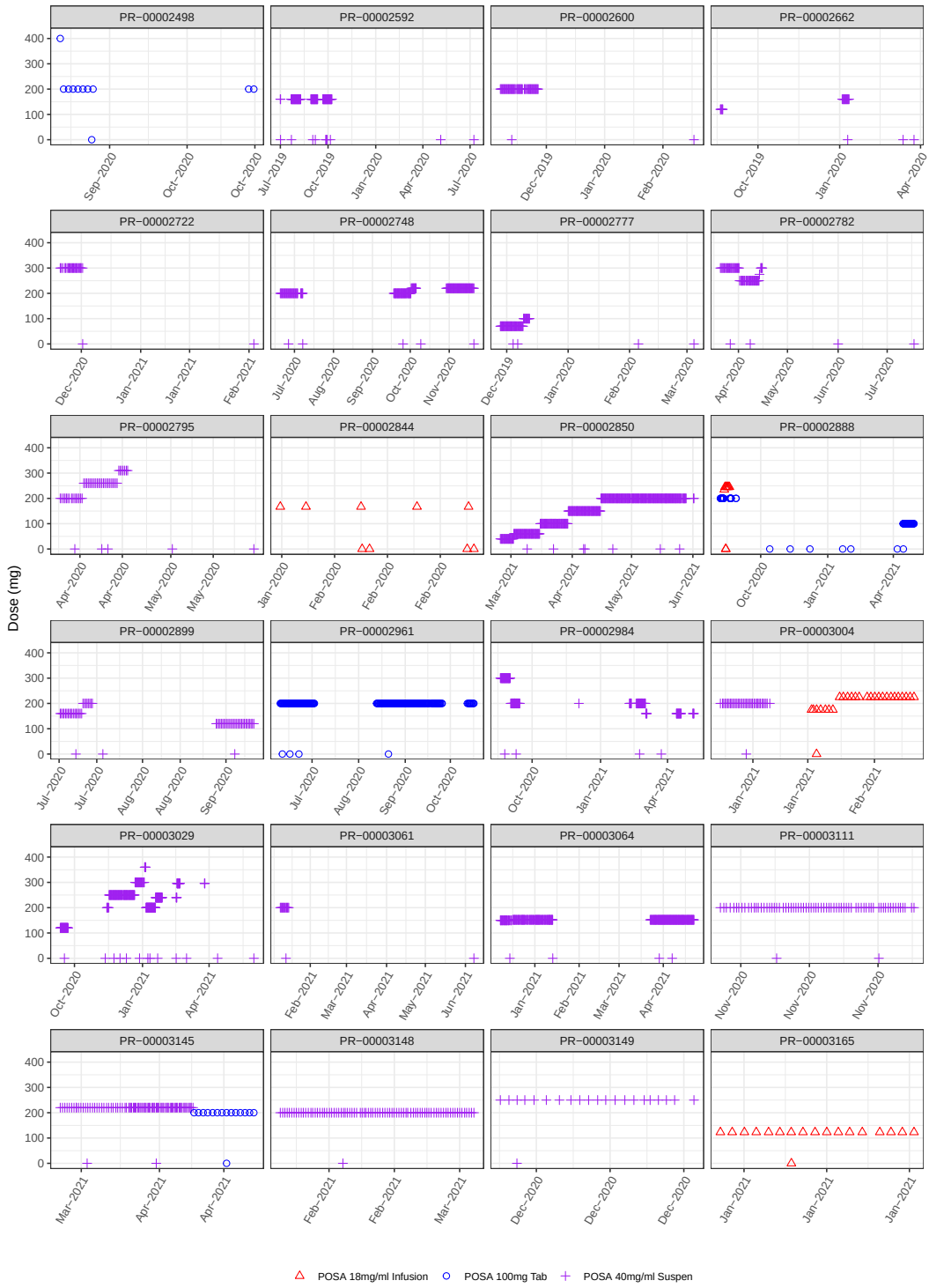

Figure C.5: Posaconazole in-patient dose history plots page 4/5. Red triangle; IV. Blue circle; tablet. Purple cross; suspension. Symbols on the y=0 line show when a TDM blood sample was taken.

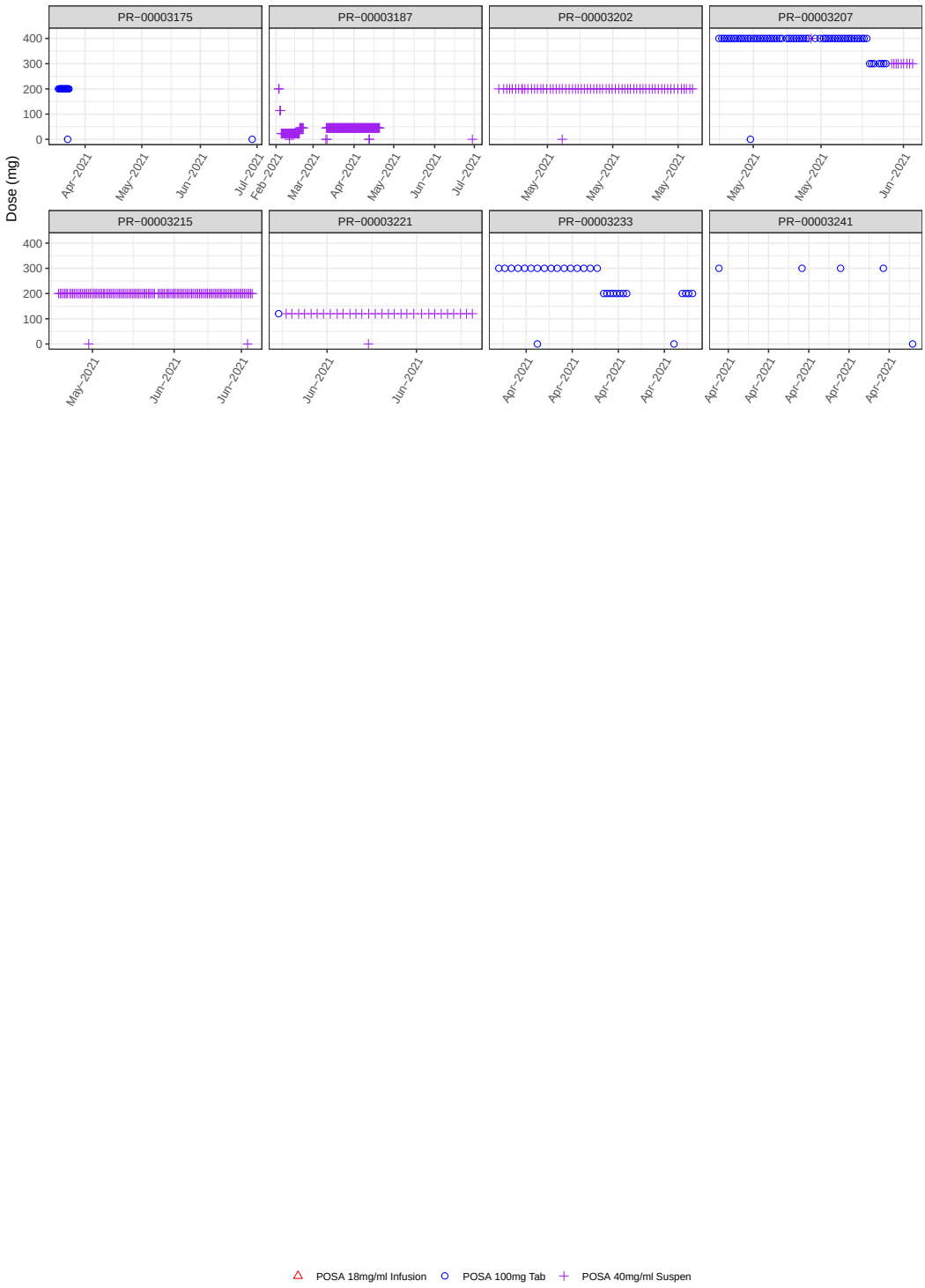

Figure C.6: Posaconazole in-patient dose history plots page 5/5. Red triangle; IV. Blue circle; tablet. Purple cross; suspension. Symbols on the y=0 line show when a TDM blood sample was taken.

Table C.1: Posaconazole Levels which are preceded by less than or equal to 5 days prior in-patient dosing

ID	TIME	DV	Occasion	Days
138	40.50	0.29	1	1.7
1488	449.90	3.47	2	3.9
1609	118.00	0.28	1	4.9
1701	15.55	0.26	1	0.6
1701	7752.80	0.10	2	4.5
1704	107.50	0.10	1	4.5
1726	2590.35	0.24	2	0.8
1731	6446.78	0.77	3	0.6
1732	1693.17	0.42	2	4.5
1784	21.98	0.49	1	0.9
1785	23.83	0.59	1	1.0
1785	26.82	3.10	1	1.1
1864	84.63	1.04	1	3.5
1933	8.25	0.34	1	0.3
1933	1220.00	1.08	2	3.2
1947	1876.42	0.87	2	4.1
1947	3445.42	1.77	3	3.6
1967	30.63	7.24	1	1.3
1967	10600.77	4.50	2	0.7
1970	11.75	2.57	1	0.5
1970	2358.25	0.68	2	4.9
1991	115.28	0.10	1	4.8
1991	3668.53	2.01	3	2.4
1991	6991.78	0.49	4	1.0
2081	3374.40	0.58	2	1.1
2128	39.75	0.75	1	1.7
2128	42.50	2.00	1	1.8
2207	25.98	0.49	1	1.1
2285	11102.60	0.57	3	4.6
2301	4001.23	4.17	3	0.5
2310	1930.40	1.78	3	0.3
2310	7043.15	1.04	5	3.0
2310	7067.70	0.74	5	4.0
2310	9772.35	1.29	6	2.5
2343	23.10	1.32	1	1.0
2343	25.75	2.75	1	1.1
2343	912.80	9.29	2	1.0
2343	977.33	4.74	2	3.7
2343	980.18	5.43	2	3.8
2370	1777.17	0.33	2	3.7
2394	36.12	2.23	1	1.5
2456	6702.25	0.97	4	0.3
2592	11.00	2.28	1	0.5
2592	514.30	0.87	2	0.5
2592	1503.92	1.03	3	3.7
2795	115.15	0.33	1	4.8
2844	36.65	1.25	1	1.5
2844	40.53	1.99	1	1.7
2844	84.90	0.78	1	3.5
2844	87.93	3.43	1	3.7
2888	6025.90	1.50	2	0.5
2961	32.77	1.19	1	1.4
3004	588.47	0.24	2	1.3

Table C.1: Posaconazole Levels which are preceded by less than or equal to 5 days prior in-patient dosing *(continued)*

ID	TIME	DV	Occasion	Days
3061	105.27	1.15	1	4.4
3149	10.80	0.12	1	0.4
3175	116.20	3.51	1	4.8
3187	877.92	1.56	2	0.5
3241	115.55	4.83	1	4.8

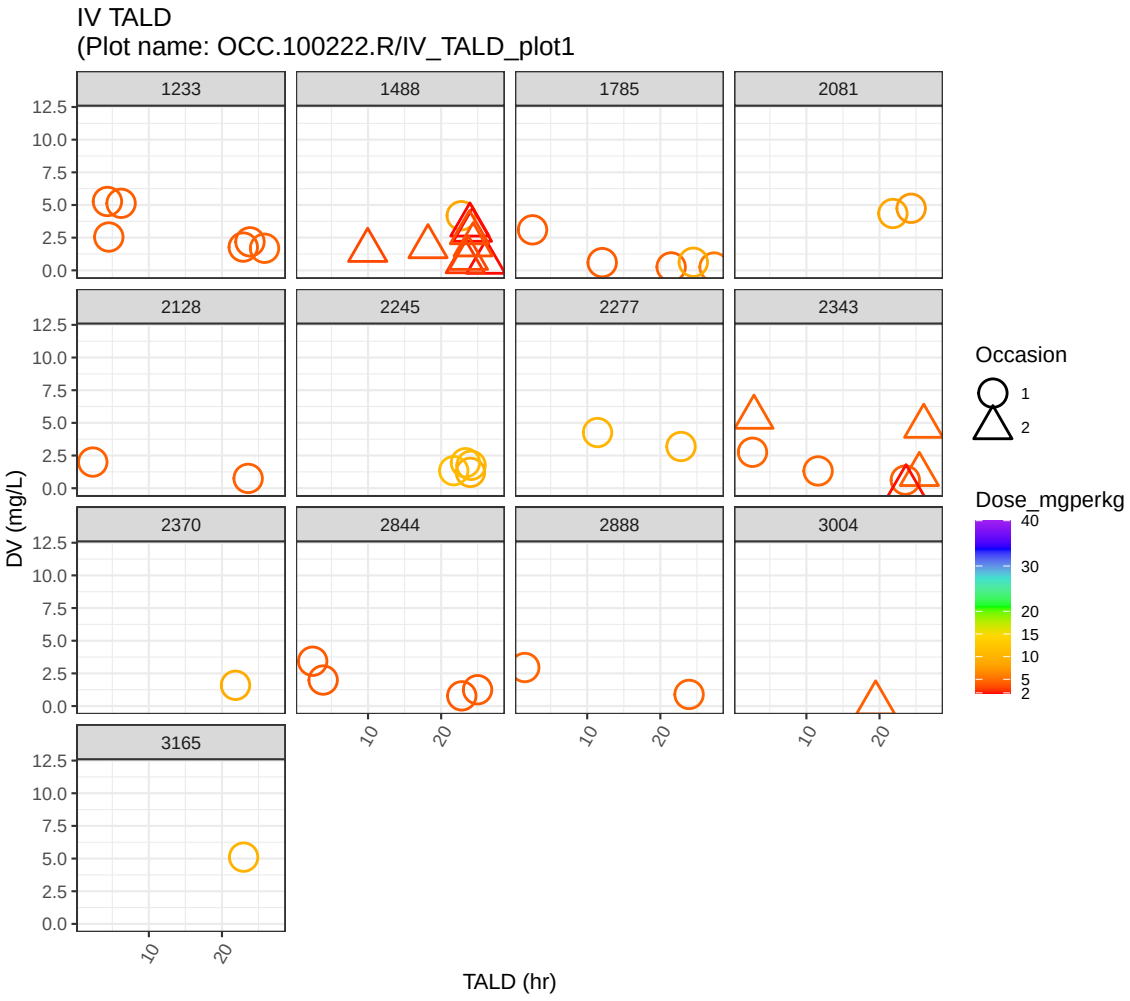

Figure C.7: Observed posaconazole plasma concentration versus time after last dose (TALD) for each subject following intravenous dosing. Colour represents the dose (mg/kg) administered prior to the level and shape the dosing occasion. A new dosing occasion is specified if a gap of >7days in dosing is observed.

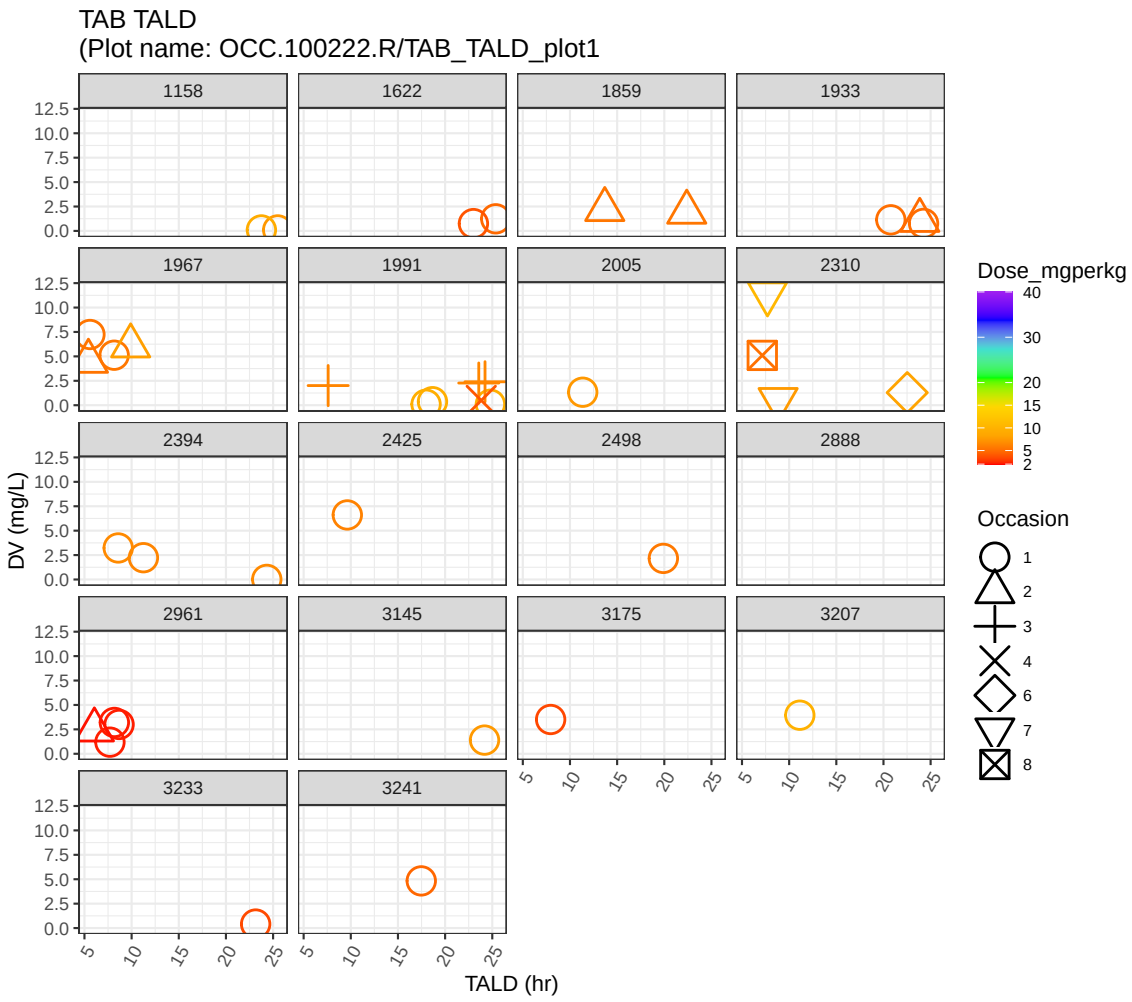

Figure C.8: Observed posaconazole plasma concentration versus time after last dose (TALD) for each subject following tablet dosing. Colour represents the dose (mg/kg) administered prior to the level and shape the dosing occasion. A new dosing occasion is specified if a gap of >7days in dosing is observed.

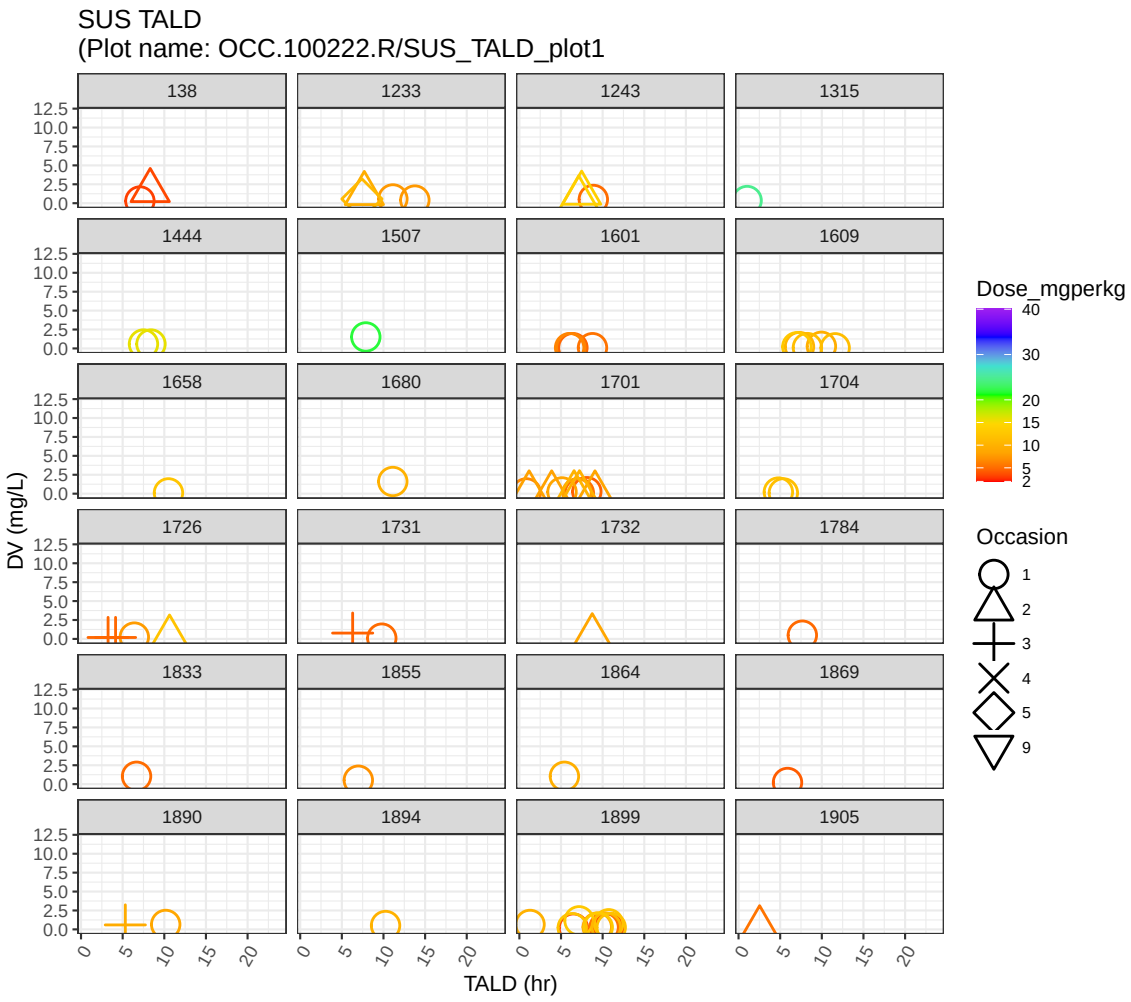

Figure C.9: Observed posaconazole plasma concentration versus time after last dose (TALD) for each subject following suspension dosing (1/4). Colour represents the dose (mg/kg) administered prior to the level and shape the dosing occasion. A new dosing occasion is specified if a gap of >7days in dosing is observed.

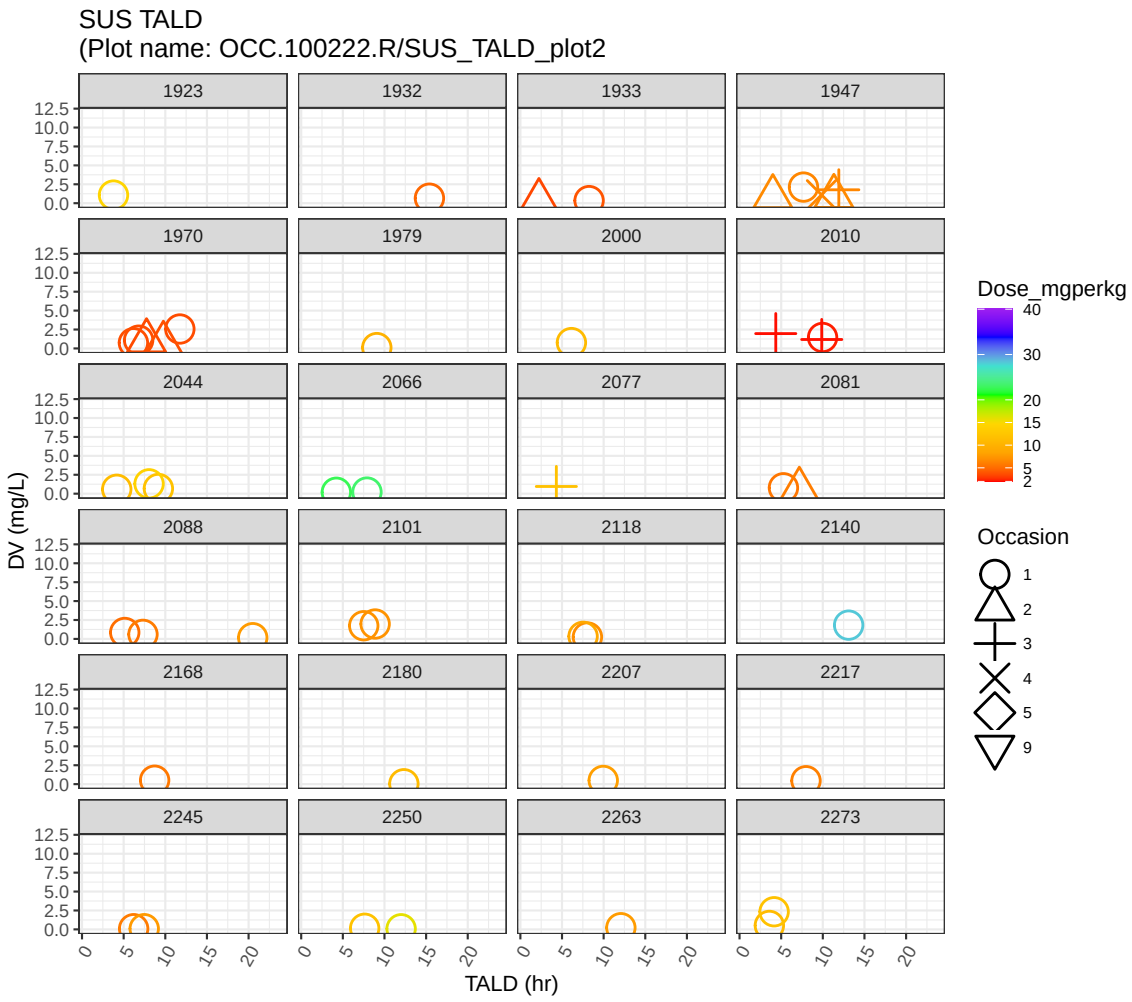

Figure C.10: Observed posaconazole plasma concentration versus time after last dose (TALD) for each subject following suspension dosing (2/4). Colour represents the dose (mg/kg) administered prior to the level and shape the dosing occasion. A new dosing occasion is specified if a gap of >7days in dosing is observed.

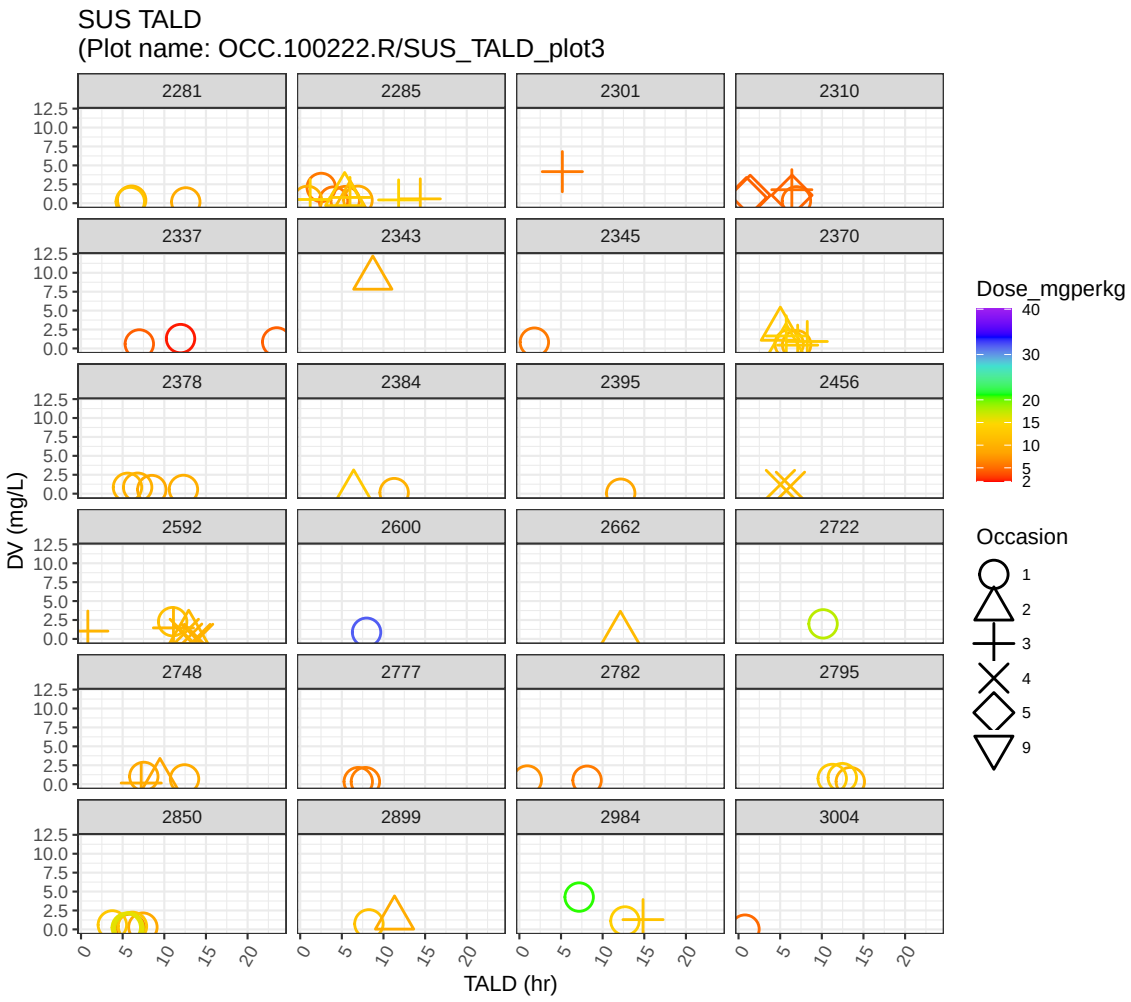

Figure C.11: Observed posaconazole plasma concentration versus time after last dose (TALD) for each subject following suspension dosing (3/4). Colour represents the dose (mg/kg) administered prior to the level and shape the dosing occasion. A new dosing occasion is specified if a gap of >7days in dosing is observed.

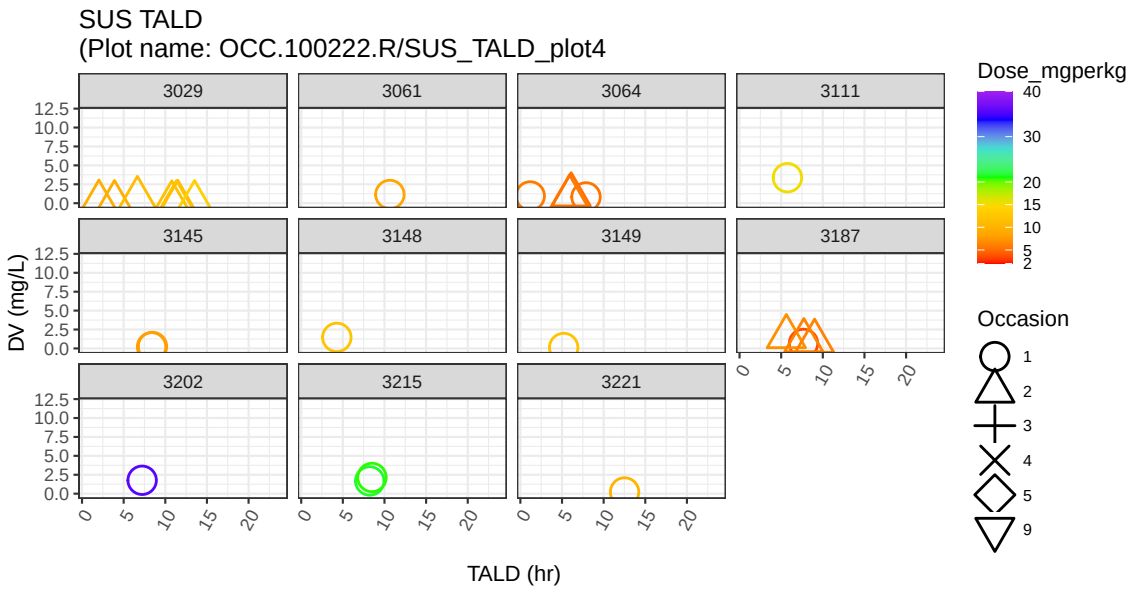

Figure C.12: Observed posaconazole plasma concentration versus time after last dose (TALD) for each subject following suspension dosing (4/4). Colour represents the dose (mg/kg) administered prior to the level and shape the dosing occasion. A new dosing occasion is specified if a gap of >7days in dosing is observed.

Parameter	Estimate (%RSE)	IIV %CV (%RSE)
CL (L/h/70kg)	4.9 (12.7)	28% (70.5)
V (L/70kg)	169.51 (15.2)	–
Add Error (mg/L)	1.17 (37.3)	–
Prop Error (%)	0 (fixed)	–
OFV	72.45	–
Run	Run 3	–

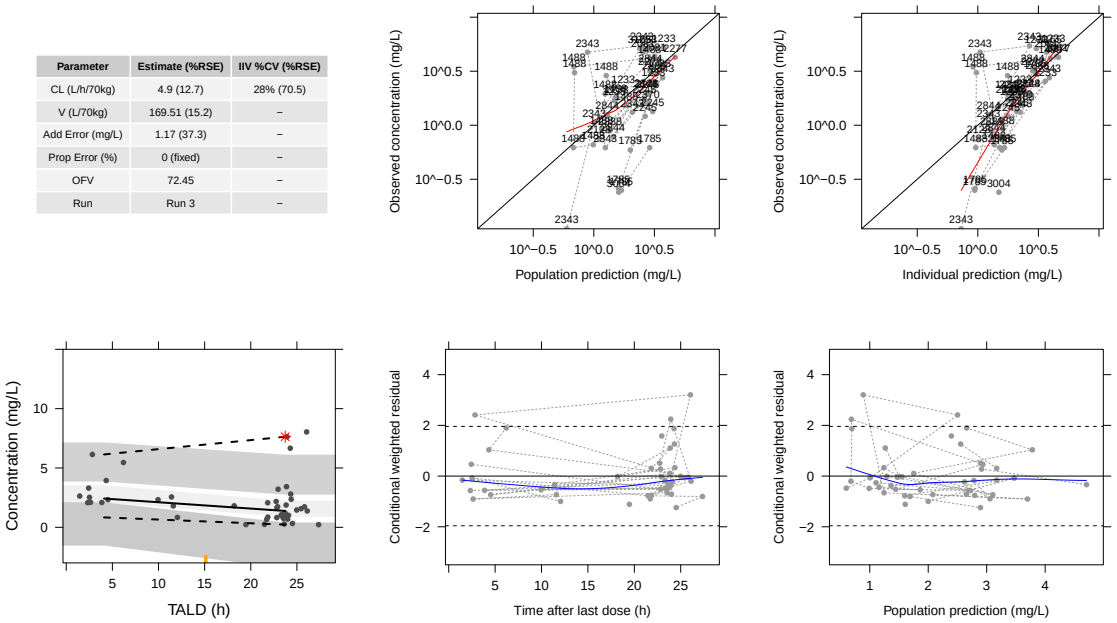

Figure C.13: Parameter Estimates and GOF Plots for a 1-compartment linear CL model with IIV on CL and additive residual error (Run 3 - paediatric IV only modelling)

Parameter	Estimate (%RSE)	IIV %CV (%RSE)
CLsat (L/h/70kg)	10.96(139)	57% (163.4)
Km (mg/L)	2(fixed)	–
V (L/70kg)	413.82(76.1)	48% (315.9)
Prop Error (%)	62.21(156.2)	–
OFV	97.28	–
Run	Run NL−9	–

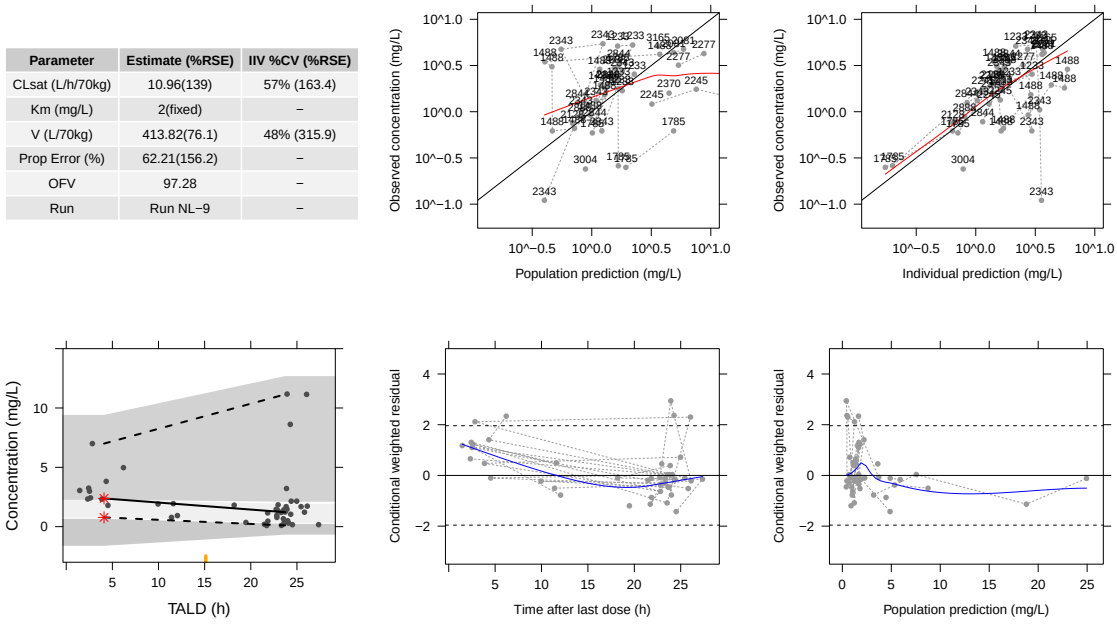

Figure C.14: Parameter Estimates and GOF Plots for a 1-compartment non-linear CL model with IIV on CLmax and V using OMEGA block and proportional residual error (Run NL-9 - paediatric IV only modelling)

A

Parameter	Estimate (%RSE)	IIV %CV (%RSE)
CL (L/h/70 kg)	7.59 (23.6)	55 (40.2)
V (L/70 kg)	124.11 (17.7)	–
KaTAB (/hr)	0.59 (fixed)	–
KaSUS (/hr)	0.2 (fixed)	–
FTAB	1.39 (41.6)	–
FSUS	0.09 (25)	–
Add Error (mg/L)	0.56 (43.8)	–
Prop Error (%)	40 (32.4)	–
OFV	206.37	–
Run	Base Lin: CL and V released	–

B

Parameter	Estimate (%RSE)	IIV %CV (%RSE)
CLsat (L/h/70 kg)	17.54 (25.6)	58 (185.8)
Km (mg/L)	2 (fixed)	–
V (L/70 kg)	342.08 (55)	136 (28.6)
KaTAB (/hr)	0.59 (fixed)	–
KaSUS (/hr)	0.2 (fixed)	–
FTAB	1.06 (52.5)	–
FSUS	0.14 (27.6)	–
Add Error (mg/L)	0.43 (165.1)	–
Prop Error (%)	46 (52.7)	–
OFV	217.83	–
Run	Base Non−Lin: CLmax and V released	–

Figure C.15: Base Model Parameter estimates with clearance and volume terms released. A) Linear clearance. B) Non-linear clearance.

A

Parameter	Estimate (%RSE)	IIV %CV (%RSE)
CLsat (L/h/70 kg)	12 (fixed)	56 (18.7)
Km (mg/L)	2 (fixed)	–
V (L/70 kg)	250 (fixed)	150% (24.2)
KaTAB (/hr)	0.59 (fixed)	–
KaSUS (/hr)	0.2 (fixed)	–
FTAB	0.67 (22.6)	–
D50 SUS (mg/BSA)	40.57 (12.8)	–
theta PPI	−0.43 (−13.4)	–
Add Error (mg/L)	0.01 (105.8)	–
Prop Error (%)	64 (20.3)	–
OFV	145.92	–
Run	Run NL−13	–

Figure C.16: Parameter Estimates for Run NL-13: Non-linear clearance combined covariate model.

C.1 NM Code: Posaconazole Linear CL

```
$PROBLEM posaconazole combined IV/tablet/suspension paediatric TDM

$INPUT ID AMT DV TIME TALD WEIGHT AGEdays AGEyears
       MDV CMT ROUTE RATE FORMULATION PPIFLAG RANITFLAG
       MGPERKG MGPERBSA DIARRHOEA FREQ BLOQ ALBUMIN ALT

$DATA Posa_NM_Sep2022_final.csv IGNORE=@

$SUBROUTINE ADVAN5 TRANS1
$MODEL      COMP(1) ; oral dosing of Tab
            COMP(2) ; oral dosing of Sus
            COMP(3) ; plasma/central compartment
$PK
;--------covariate function
WTCL = (WEIGHT / 70)**0.75  ; WT scaling for CL
WTV  = (WEIGHT / 70)        ; WT scaling for V

;------ Typicl value of parameters
 TVCL  = THETA(1)
 TVV   = THETA(2)
 TVK13 = THETA(3) ; KA for the Tab
 TVK23 = THETA(4) ; KA for the Sus
 TVF1  = THETA(5) ; F for the Tab
 TVD50 = THETA(6) ; dose at which suspension F is 0.5

;------ MU modelling
 MU_1 = DLOG(TVCL)

;------ Individual parameters
;Diarrhoea effect on all formulations as its on CL
IF(DIARRHOEA==0) FDIAR = 1 ; No diarrhoea
IF(DIARRHOEA==1) FDIAR = ( 1 + THETA(7)) ; Fractional effect of DIAR
```

```
;PPI effect
IF(PPIFLAG==0) FPPI = 1 ; Not on PPI
IF(PPIFLAG==1) FPPI = ( 1 + THETA(8)) ; Fractional effect of PPI
IF(FORMULATION==1) FPPI = 1 ; IV, no PPI effect
IF(FORMULATION==2) FPPI = 1 ; Tablet, no PPI effect

 CL   =  DEXP(MU_1+ETA(1)) * WTCL
 V    =  TVV * WTV
 K13  =  TVK13      ; KATab
 K23  =  TVK23      ; Sus KA

IF(FORMULATION==2) F1   = TVF1 ; Tablet

;Dose effect on F2 suspension
DOSF = 0
D50 = 0
IF(AMT>0) DOSE = AMT
DOSEBSA = MGPERBSA
IF(FORMULATION==3) D50 = TVD50
DOSF = (DOSEBSA / (DOSEBSA + D50))
TVF2 = (1 - DOSF)
F2 = TVF2 * FPPI * FDIAR  ; suspension

;------ Rate constants
 K30   = CL/V

$ERROR
CP = A(3)/V
;------ Statistical model
IPRED = CP
Y = IPRED * (1 + EPS(2)) + EPS(1)
;------ Calculate IWRES
 IRES  = DV-IPRED
 ADD   = SQRT(SIGMA(1,1))
 PROP  = SQRT(SIGMA(2,2))*IPRED
 SD    = SQRT(ADD**2 + PROP**2)
```

```
 IF(SD==0) SD=1
 IWRES = IRES/SD

;to remove negative prediction intervals in VPC
TDV=DV
IF(TDV<=0.08) TDV = 0.08

;------ Final parameter estimates
$THETA 5.67 FIX        ; 1. CL
$THETA 143.2 FIX       ; 2. V
$THETA 0.59 FIX        ; 3. K13 KAtab
$THETA 0.2 FIX         ; 4. K23 KAsus
$THETA 1.22        ; 5. Ftab
$THETA 41.36         ; 6. dose at which Fsus is 50%
$THETA -0.93        ; 7. Theta DIAR
$THETA -0.54     ; 8. Theta PPI
;------ Interindividual parameter variability
$OMEGA 0.290      ; IIV on CL, variance for ETA(1)
;------ Residual error
$SIGMA 0.207       ; additive res error
$SIGMA 0.227       ; proportional res error

$ESTIMATION METHOD=1 INTER MAXEVAL=9999 PRINT=1   ; calculation method
$COVARIANCE               ; standard error of estimate is calculated

$TABLE ID TIME TALD MDV IPRED IWRES CWRES NPDE ESAMPLE=300
NOPRINT ONEHEADER FILE=sdtab1
$TABLE ID CL V K13 K23 F1 F2 D50 FPPI FDIAR ETA(1)
NOPRINT NOAPPEND ONEHEADER FILE=patab1
$TABLE ID WEIGHT AGEyears DIARRHOEA FORMULATION ALBUMIN ALT PPIFLAG BLOQ
NOPRINT NOAPPEND ONEHEADER FILE=cotab1
$TABLE ID
NOPRINT NOAPPEND ONEHEADER FILE=catab1
   ; Xpose can read these tables
   ; there must be one empty line after the last command line
```

C.2 NM Code: Posaconazole Non-Linear CL

```
$PROBLEM posaconazole combined IV/tablet/suspension paediatric TDM

$INPUT ID AMT DV TIME TALD WEIGHT AGEdays AGEyears
       MDV CMT ROUTE RATE FORMULATION PPIFLAG RANITFLAG
       MGPERKG MGPERBSA DIARRHOEA FREQ BLOQ ALBUMIN ALT

$DATA Posa_NM_Sep2022_final.csv IGNORE=@

$SUBROUTINE ADVAN6 TOL=6
$MODEL      COMP(1) ; oral dosing of Tab
            COMP(2) ; oral dosing of Sus
            COMP(3) ; plasma/central compartment
$PK
;--------covariate function
WTCL = (WEIGHT / 70)**0.75   ; WT scaling for CLsat
WTV  = (WEIGHT / 70)         ; WT scaling for V3

;------ Typicl value of parameters
 TVCLMAX = THETA(1) ; CL is saturable
 TVKM    = THETA(2) ; Km for non-linear CL
 TVV3    = THETA(3)
 TVK13   = THETA(4) ; KA for the Tab
 TVK23   = THETA(5) ; KA for the Sus
 TVF1    = THETA(6) ; Tab F1
 TVD50S  = THETA(7) ; dose at which suspension F is 0.5

;------ MU modelling
 MU_1 = DLOG(TVCLMAX)
 MU_2 = DLOG(TVV3)

;------ Individual parameters
```

```
;PPI effect
IF(PPIFLAG==0) FPPI = 1 ; Not on PPI
IF(PPIFLAG==1) FPPI = ( 1 + THETA(8)) ; only estimating for Suspension
IF(FORMULATION==1) FPPI = 1           ; IV, no PPI effect
IF(FORMULATION==2) FPPI = 1           ; Tablet, no PPI effect


 CLMAX =  DEXP(MU_1+ETA(1)) * WTCL
 KM    =  TVKM
 V3    =  DEXP(MU_2+ETA(2)) * WTV
 K13   =  TVK13                      ; KATab
 K23   =  TVK23                      ; Sus KA

IF(FORMULATION==2) F1   = TVF1 ; Tablet

;Dose effect on F2 suspension
DOSF = 0
D50 = 0
IF(AMT>0) DOSE = AMT
DOSEBSA = MGPERBSA

IF(FORMULATION==3) D50S = TVD50S
DOSF = (DOSEBSA / (DOSEBSA + D50S))
TVF2 = (1 - DOSF)
F2 = TVF2 * FPPI   ;suspension non-linear F

;------ Rate constants
 K30   = CLMAX/V3
 S3 = V3

$DES
CP= A(3)/S3
DADT(1) = - A(1)*K13
DADT(2) = - A(2)*K23
DADT(3) = - K30*A(3)/(1 + CP/KM) + A(1)*K13 + A(2)*K23
```

```
$ERROR
C1 = A(3)/V3
;------ Statistical model
IPRED = C1
Y = IPRED * (1 + EPS(2)) + EPS(1)
;------ Calculate IWRES
 IRES  = DV-IPRED
 ADD   = SQRT(SIGMA(1,1))
 PROP  = SQRT(SIGMA(2,2))*IPRED
 SD    = SQRT(ADD**2 + PROP**2)
 IF(SD==0) SD=1
 IWRES = IRES/SD

;to remove negative prediction intervals
TDV=DV
IF(TDV<=0.08) TDV = 0.08

;----------Final Parameter Estimates
$THETA 13.47        ; 1. TVCLsat, like Vmax
$THETA 2 FIX         ; 2. TVC50, like Km
$THETA 186.01       ; 3. TVV
$THETA 0.59 FIX      ; 4. TVK13 Tab KA
$THETA 0.2 FIX       ; 5. TVK23 Sus KA
$THETA 0.66      ; 6. F1 Tab
$THETA 43.25       ; 7. Dose at which Fsus is 50%
$THETA -0.41       ; 8. Theta PPI on Fsus

;------ Interindividual parameter variability
$OMEGA BLOCK
0.328      ; IIV on CL, variance for ETA(1), initial estimate
0.149 1.44       ; IIV on V3, variance for ETA(2)
;------ Residual error
$SIGMA 0 FIX       ; variance add res error, initial estimate
$SIGMA 0.402      ; variance prop res error, initial estimate

$ESTIMATION METHOD=1 INTER MAXEVAL=9999 PRINT=1 ; calculation method
```

```
$COVARIANCE                ; standard error of estimate is calculated

$TABLE ID TIME TALD MDV IPRED IWRES CWRES NPDE ESAMPLE=300
NOPRINT ONEHEADER FILE=sdtab1
$TABLE ID CLMAX V3 K13 K23 F1 F2 D50 F1 FPPI ETA(1) ETA(2)
NOPRINT NOAPPEND ONEHEADER FILE=patab1
$TABLE ID WEIGHT AGEyears DIARRHOEA FORMULATION ALBUMIN ALT BLOQ
NOPRINT NOAPPEND ONEHEADER FILE=cotab1
$TABLE ID
NOPRINT NOAPPEND ONEHEADER FILE=catab1
   ; Xpose can read these tables
   ; there must be one empty line after the last command line
```

C.3 Goodness of fit plots: IV, tablet and suspension data combined

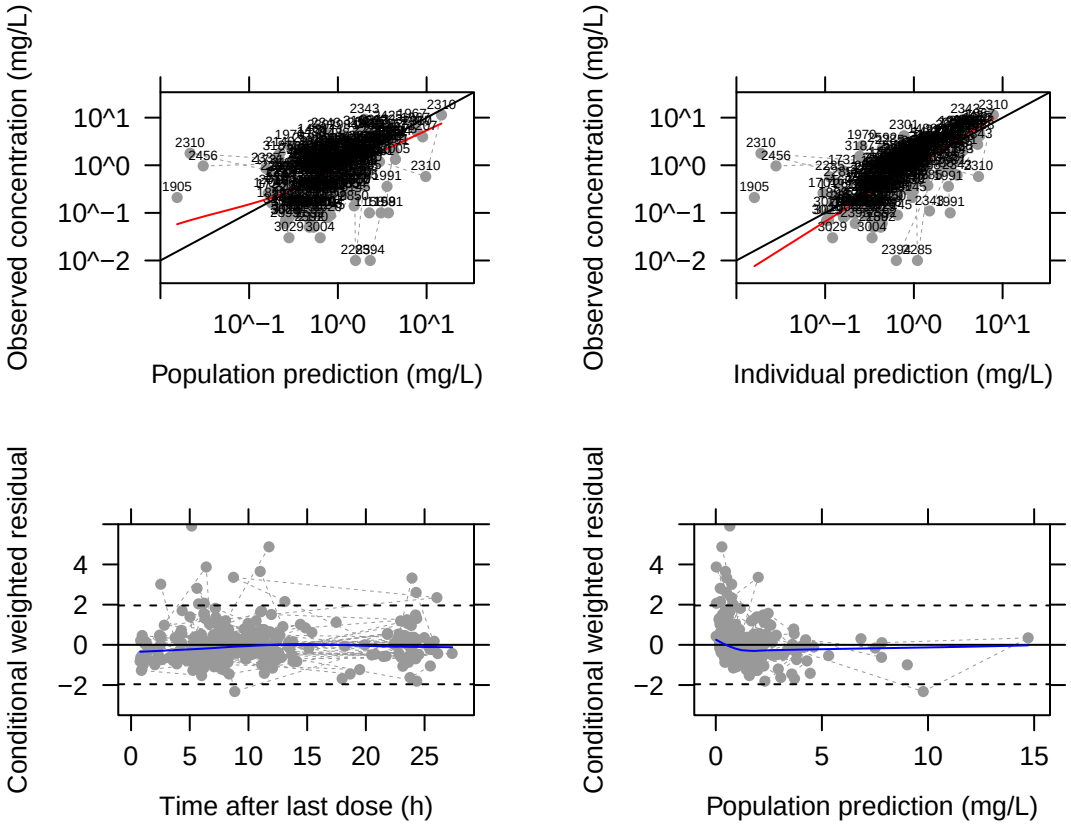

Figure C.17: Final posaconazole linear clearance model. Goodness of fit plots for the combined dataset; IV, tablet and suspension data combined.

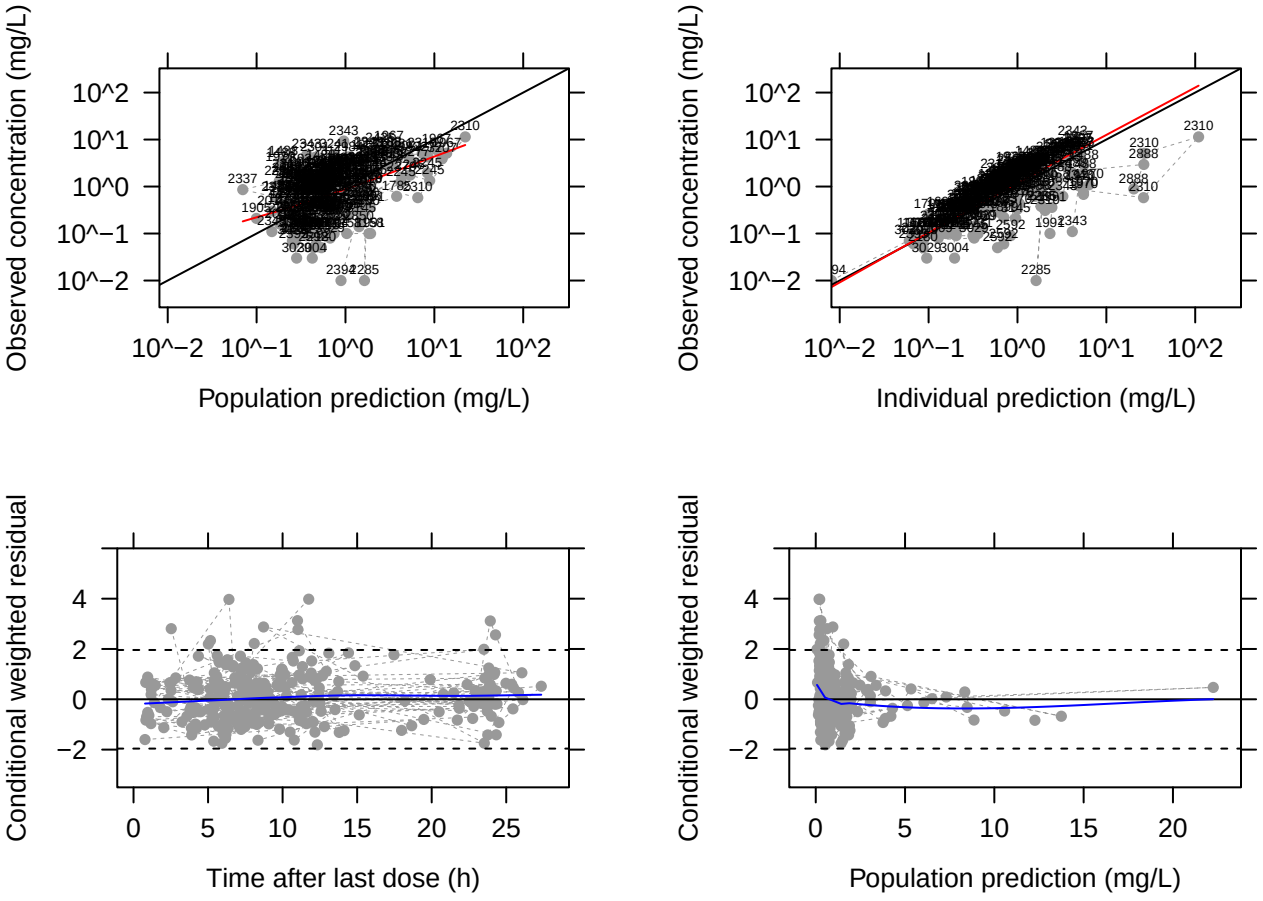

Figure C.18: Final posaconazole non-linear clearance model. Goodness of fit plots for the combined dataset; IV, tablet and suspension data combined.

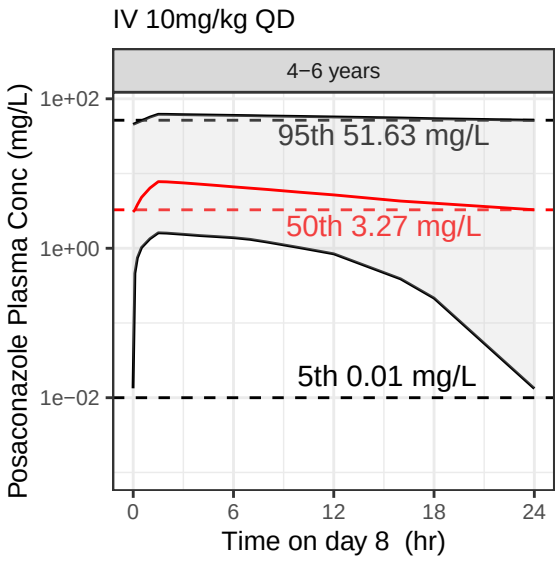

Figure C.19: Concentration-time population simulation for children aged 4-6 years after eight days of 10 mg/kg IV QD dosing.

References

(1) European Medicines Agency (EMEA). Regulation (EC) No 1901/2006 of the EU Parliament and of the Council of 12 December 2006 on Medicinal Products for Paediatric use. **2006**.

(2) Germovsek, E.; Barker, C. I. S.; Sharland, M.; Standing, J. F. Pharmacokinetic–Pharmacodynamic Modeling in Pediatric Drug Development, and the Importance of Standardized Scaling of Clearance. *Clinical Pharmacokinetics* **2019**, *58* (1), 39–52. https://doi.org/10.1007/s40262-018-0659-0.

(3) Hoon, D.; Taylor, M. T.; Kapadia, P.; Gerhard, T.; Strom, B. L.; Horton, D. B. Trends in off-label drug use in ambulatory settings: 2006–2015. *Pediatrics* **2019**, *144* (4). https://doi.org/10.1542/peds.2019-0896.

(4) Pandolfini, C.; Bonati, M. A literature review on off-label drug use in children. *European Journal of Pediatrics* **2005**, *164* (9), 552–558. https://doi.org/10.1007/s00431-005-1698-8.

(5) Rumore, M. M. Medication repurposing in pediatric patients: Teaching old drugs new tricks. *Journal of Pediatric Pharmacology and Therapeutics* **2016**, *21* (1), 36–53. https://doi.org/10.5863/1551-6776-21.1.36.

(6) Tomasi, P. A.; Egger, G. F.; Pallidis, C.; Saint-Raymond, A. Enabling Development of Paediatric Medicines in Europe: 10 Years of the EU Paediatric Regulation. *Pediatric Drugs* **2017**, *19* (6), 505–513. https://doi.org/10.1007/s40272-017-0261-1.

(7) Hwang, T. J.; Tomasi, P. A.; Saint-Raymond, A.; Bourgeois, F. T. Availability of paediatric information in European Medicines Agency approvals. *The Lancet Child and Adolescent Health* **2018**, *2* (5), e9. https://doi.org/10.1016/S2352-4642(18)30101-9.

(8) Neel, D. V.; Shulman, D. S.; DuBois, S. G. Timing of first-in-child trials of FDA-approved oncology drugs. *European Journal of Cancer* **2019**, *112*, 49–56. https://doi.org/10.1016/j.ejca.2019.02.011.

(9) Hirota, S.; Yamaguchi, T. Timing of Pediatric Drug Approval and Clinical Evidence Submitted to Regulatory Authorities: International Comparison Among Japan, the United States, and the European Union. *Clinical Pharmacology and Therapeutics* **2020**, *108* (5), 985–994. https://doi.org/10.1002/cpt.1757.

(10) Hampson, L. V.; Herold, R.; Posch, M.; Saperia, J.; Whitehead, A. Bridging the gap: a review of dose investigations in paediatric investigation plans. *British journal of clinical pharmacology* **2014**, *78* (4), 898–907. https://doi.org/10.1111/bcp.12402.

(11) European Medicines Agency,. Guideline on the Role of Pharmacokinetics in the development of medicinal products in the paediatric population (EMEA/CHMP/EWP/147013/2004). **2007**.

(12) International Council for Harmonisation. Addendum to ICH E11 (R1): Clinical investigation of medicinal products in the paediatric population. **2017**.

(13) European Medicines Agency,. Reflection Paper on Extrapolation of efficacy and safety in paediatric medicine development (EMA/189724/2018). **2018**.

(14) The US Food and Drug Administration. Pediatric Study Plans: Content of and Process for Submitting Initial Pediatric Study Plans and Amended Initial Pediatric Study Plans. **2020**.

(15) International Council for Harmonisation. ICH E11A draft Guideline on Pediatric Extrapolation. **2022**.

(16) Pansa, P.; Hsia, Y.; Bielicki, J.; Lutsar, I.; Walker, A. S.; Sharland, M.; Folgori, L. Evaluating Safety Reporting in Paediatric Antibiotic Trials, 2000–2016: A Systematic Review and Meta-Analysis. *Drugs* **2018**, *78* (2), 231–244. https://doi.org/10.1007/s40265-017-0850-x.

(17) Pansieri, C.; Bonati, M.; Choonara, I.; Jacqz-Aigrain, E. Neonatal drug trials: Impact of EU and US paediatric regulations. *Archives of Disease in Childhood: Fetal and Neonatal Edition* **2014**, *99* (5), F438–E438. https://doi.org/10.1136/archdischild-2013-305900.

(18) Allegaert, K.; Anker, J. V. D. Neonatal Drug Therapy: The First Frontier of Therapeutics for Children. *Clinical Pharmacology and Therapeutics* **2015**, *98* (3), 288–297. https://doi.org/10.1002/cpt.166.

(19) Zanden, T. M. van der; Smeets, N. J. L.; Hoop-Sommen, M. de; Schwerzel, M. F. T.; Huang, H. J.; Barten, L. J. C.; Heijden, J. E. M. van der; Freriksen, J. J. M.; Horstink, A. A. L.; Holsappel, I. H. G.; Mooij, M. G.; Hoog, M. de; Wildt, S. N. de. Off-Label, but on-Evidence? A Review of the Level of Evidence for Pediatric Pharmacotherapy. *Clinical Pharmacology and Therapeutics* **2022**, *112* (6), 1243–1253. https://doi.org/10.1002/cpt.2736.

(20) Balan, S.; Hassali, M. A. A.; Mak, V. S. L. Two decades of off-label prescribing in children: a literature review. *World Journal of Pediatrics* **2018**, *14* (6), 528–540. https://doi.org/10.1007/s12519-018-0186-y.

(21) Khaled, L. A.; Ahmad, F.; Brogan, T.; Fearnley, J.; Graham, J.; MacLeod, S.; McCormick, J. Prescription medicine use by one million Canadian children. *Paediatrics & Child Health* **2001**, *8* (suppl_A), 6A–56A. https://doi.org/10.1093/pch/8.suppl_a.6a.

(22) Servais, J.; Ramage-Morin, P. L.; Gal, J.; Hales, C. M. Prescription medication use among Canadian children and youth, 2012 to 2017. *Health Reports* **2021**, *32* (3), 3–16. https://doi.org/10.25318/82-003-x202100300001-eng.

(23) Reeves, D.; Lovering, A.; Thomson, A. Therapeutic drug monitoring in the past 40 years of the Journal of Antimicrobial Chemotherapy. *Journal of Antimicrobial Chemotherapy* **2016**, *71* (12), 3330–3332. https://doi.org/10.1093/jac/dkw408.

(24) Thomson, A. H.; Elliott, H. L. Designing simple PK-PD studies in children. *Paediatric Anaesthesia* **2011**, *21* (3), 190–196. https://doi.org/10.1111/j.1460-9592.2010.03436.x.

(25) European Medicines Agency (EMEA). Reflection paper on the use of extrapolation in the development of medicines for paediatrics. **2018**.

(26) Ollivier, C.; Thomson, A.; Manolis, E.; Blake, K.; Karlsson, K. E.; Knibbe, C. A. J.; Pons, G.; Hemmings, R. Commentary on the EMA Reflection Paper on the use of extrapolation in the development of medicines for paediatrics. *British Journal of Clinical Pharmacology* **2019**, *85* (4), 659–668. https://doi.org/10.1111/bcp.13883.

(27) UN Inter-agency Group for Child Mortality Estimation. Levels & Trends in Child Mortality Report 2021. **2021**.

(28) Rashed, A. N.; Wong, I. C. K.; Wilton, L.; Tomlin, S.; Neubert, A. Drug Utilisation Patterns in Children Admitted to a Paediatric General Medical Ward in Five Countries. *Drugs - Real World Outcomes* **2015**, *2* (4), 397–410. https://doi.org/10.1007/s40801-015-0049-y.

(29) Lozano, R. et. al. Global and regional mortality from 235 causes of death for 20 age groups in 1990 and 2010: A systematic analysis for the Global Burden of Disease Study 2010. *The Lancet* **2012**, *380* (9859), 2095–2128. https://doi.org/10.1016/S0140-6736(12)61728-0.

(30) Seale, A. C.; Berkley, J. A.; Cous Vergnano, S. Estimates of possible severe bacterial infection in neonates in sub-Saharan Africa, south Asia, and Latin America for 2012: A systematic review and meta-analysis. *The Lancet Infectious Diseases* **2014**, *14* (8), 731–741. https://doi.org/10.1016/S1473-3099(14)70804-7.

(31) Laxminarayan, R.; Matsoso, P.; Pant, S.; Brower, C.; Røttingen, J. A.; Klugman, K.; Davies, S. Access to effective antimicrobials: A worldwide challenge. *The Lancet* **2016**, *387* (10014), 168–175. https://doi.org/10.1016/S0140-6736(15)00474-2.

(32) Kollmann, T. R.; Marchant, A.; Way, S. S. Vaccination strategies to enhance immunity in neonates. *Science* **2020**, *368* (6491), 612–615. https://doi.org/10.1126/science.aaz9447.

(33) Pérez-Molina, J. A.; Molina, I. Chagas disease. *The Lancet* **2018**, *391* (10115), 82–94. https://doi.org/10.1016/S0140-6736(17)31612-4.

(34) World Health Organization. Chagas disease (American trypanosomiasis). **2023**.

(35) Schmunis, G. A.; Yadon, Z. E. Chagas disease: A Latin American health problem becoming a world health problem. *Acta Tropica* **2010**, *115* (1-2), 14–21. https://doi.org/10.1016/j.actatropica.2009.11.003.

(36) Requena-Méndez, A.; Aldasoro, E.; Lazzari, E. de; Sicuri, E.; Brown, M.; Moore, D. A. J.; Gascon, J.; Muñoz, J. Prevalence of Chagas Disease in Latin-American Migrants Living in Europe: A Systematic Review and Meta-analysis. *PLoS Neglected Tropical Diseases* **2015**, *9* (2), e0003540. https://doi.org/10.1371/journal.pntd.0003540.

(37) Bern, C.; Montgomery, S. P. An estimate of the burden of chagas disease in the United States. *Clinical Infectious Diseases* **2009**, *49* (5), e52–e54. https://doi.org/10.1086/605091.

(38) Viotti, R.; Vigliano, C.; Lococo, B.; Alvarez, M. G.; Petti, M.; Bertocchi, G.; Armenti, A. Side effects of benznidazole as treatment in chronic Chagas disease: Fears and realities. *Expert Review of Anti-Infective Therapy* **2009**, *7* (2), 157–163. https://doi.org/10.1586/14787210.7.2.157.

(39) Altcheh, J.; Moscatelli, G.; Moroni, S.; Garcia-Bournissen, F.; Freilij, H. Adverse events after the use of benznidazole in infants and children with Chagas disease. *Pediatrics* **2011**, *127* (1), e212–e218. https://doi.org/10.1542/peds.2010-1172.

(40) Passweg, J. R.; Mohty, M. Use of haploidentical stem cell transplantation continues to increase: The 2015 European Society for Blood and Marrow Transplant activity survey report. *Bone Marrow Transplantation* **2017**, *52* (6), 811–817. https://doi.org/10.1038/bmt.2017.34.

(41) Bosch, M.; Khan, F. M.; Storek, J. Immune reconstitution after hematopoietic cell transplantation. *Current Opinion in Hematology* **2012**, *19* (4), 324–355. https://doi.org/10.1097/MOH.0b013e328353bc7d.

(42) Maertens, J. A.; Cordonnier, C. European guidelines for primary antifungal prophylaxis in adult haematology patients: Summary of the updated recommendations from the European Conference on Infections in Leukaemia. *Journal of Antimicrobial Chemotherapy* **2018**, *73* (12), 3221–3230. https://doi.org/10.1093/jac/dky286.

(43) Groll, A. H.; Townsend, R.; Desai, A.; Azie, N.; Jones, M.; Engelhardt, M.; Schmitt-Hoffman, A. H.; Brüggemann, R. J. M. Drug-drug interactions between triazole antifungal agents used to treat invasive aspergillosis and immunosuppressants metabolized by cytochrome P450 3A4. *Transplant Infectious Disease* **2017**, *19* (5), e12751–n/a. https://doi.org/10.1111/tid.12751.

(44) Groll, A. H.; Castagnola, E.; Cesaro, S.; Dalle, J. H.; Engelhard, D.; Hope, W.; Roilides, E.; Styczynski, J.; Warris, A.; Lehrnbecher, T. Fourth European Conference on Infections in Leukaemia (ECIL-4): Guidelines for diagnosis, prevention, and treatment of invasive fungal diseases in paediatric patients with cancer or allogeneic haemopoietic stem-cell transplantation. *The Lancet Oncology* **2014**, *15* (8), e327–e340. https://doi.org/10.1016/S1470-2045(14)70017-8.

(45) Otto, W. R.; Green, A. M. Fungal infections in children with haematologic malignancies and stem cell transplant recipients. *British Journal of Haematology* **2020**, *189* (4), 607–624. https://doi.org/10.1111/bjh.16452.

(46) Kearns, G. L.; Abdel-Rahman, S. M.; Alander, S. W.; Blowey, D. L.; Leeder, J. S.; Kauffman, R. E. Developmental Pharmacology — Drug Disposition, Action, and Therapy in Infants and Children. *New England Journal of Medicine* **2003**, *349* (12), 1157–1167. https://doi.org/10.1056/nejmra035092.

(47) Mulla, H. Understanding developmental pharmacodynamics: Importance for drug development and clinical practice. *Pediatric Drugs* **2010**, *12* (4), 223–233. https://doi.org/10.2165/11319220-000000000-00000.

(48) Anker, J. van den; Reed, M. D.; Allegaert, K.; Kearns, G. L. Developmental Changes in Pharmacokinetics and Pharmacodynamics. *Journal of Clinical Pharmacology* **2018**, *58* (10), S10–S25. https://doi.org/10.1002/jcph.1284.

(49) Waterbeemd, H. van de; Gifford, E. ADMET in silico modelling: Towards prediction paradise? *Nature Reviews Drug Discovery* **2003**, *2* (3), 192–204. https://doi.org/10.1038/nrd1032.

(50) Amidon, G. L.; Lennernäs, H.; Shah, V. P.; Crison, J. R. A Theoretical Basis for a Biopharmaceutic Drug Classification: The Correlation of in Vitro Drug Product Dissolution and in Vivo Bioavailability. *Pharmaceutical Research: An Official Journal of the American Association of Pharmaceutical Scientists* **1995**, *12* (3), 413–420. https://doi.org/10.1023/A:1016212804288.

(51) European Medicines Agency. ICH M9 on biopharmaceutics classification system based biowaivers (EMA/CHMP/ICH/493213/2018). **2020**.

(52) Zhang, W.; Li, Y.; Zou, P.; Wu, M.; Zhang, Z.; Zhang, T. The Effects of Pharmaceutical Excipients on Gastrointestinal Tract Metabolic Enzymes and Transporters—an Update. *AAPS Journal* **2016**, *18* (4), 830–843. https://doi.org/10.1208/s12248-016-9928-8.

(53) Buggins, T. R.; Dickinson, P. A.; Taylor, G. The effects of pharmaceutical excipients on drug disposition. *Advanced Drug Delivery Reviews* **2007**, *59* (15), 1482–1503. https://doi.org/10.1016/j.addr.2007.08.017.

(54) Watson, C. J.; Hoare, C. J.; Garrod, D. R.; Carlson, G. L.; Warhurst, G. Interferon-γ selectively increases epithelial permeability to large molecules by activating different populations of paracellular pores. *Journal of Cell Science* **2005**, *118* (22), 5221–5230. https://doi.org/10.1242/jcs.02630.

(55) Lee, B.; Moon, K. M.; Kim, C. Y. Tight junction in the intestinal epithelium: Its association with diseases and regulation by phytochemicals. *Journal of Immunology Research* **2018**, *2018*, 2645465–2645411. https://doi.org/10.1155/2018/2645465.

(56) Nicolas, J. M.; Bouzom, F.; Hugues, C.; Ungell, A. L. Oral drug absorption in pediatrics: the intestinal wall, its developmental changes and current tools for predictions. *Biopharmaceutics and Drug Disposition* **2017**, *38* (3), 209–230. https://doi.org/10.1002/bdd.2052.

(57) Bai, J. P. F.; Burckart, G. J.; Mulberg, A. E. Literature Review of Gastrointestinal Physiology in the Elderly, in Pediatric Patients, and in Patients with Gastrointestinal Diseases. *Journal of Pharmaceutical Sciences* **2016**, *105* (2), 476–483. https://doi.org/10.1002/jps.24696.

(58) Effinger, A.; O'Driscoll, C. M.; McAllister, M.; Fotaki, N. Impact of gastrointestinal disease states on oral drug absorption – implications for formulation design – a PEARRL review. *Journal of Pharmacy and Pharmacology* **2019**, *71* (4), 674–698. https://doi.org/10.1111/jphp.12928.

(59) Vaitkute, G.; Panic, G.; Alber, D. G.; Faizura-Yeop, I.; Cloutman-Green, E.; Swann, J.; Veys, P.; Standing, J. F.; Klein, N.; Bajaj-Elliott, M. Linking gastrointestinal microbiota and metabolome dynamics to clinical outcomes in paediatric haematopoietic stem cell transplantation. *Microbiome.* **2022**, *10* (1), 89. https://doi.org/10.1186/s40168-022-01270-7.

(60) Vinarov, Z.; Augustijns, P. Current challenges and future perspectives in oral absorption research: An opinion of the UNGAP network. *Advanced Drug Delivery Reviews* **2021**, *171*, 289–331. https://doi.org/10.1016/j.addr.2021.02.001.

(61) Stillhart, C.; Vučićević, K.; Augustijns, P.; Basit, A. W.; Batchelor, H.; Flanagan, T. R.; Gesquiere, I.; Greupink, R.; Keszthelyi, D.; Koskinen, M.; Madla, C. M.; Matthys, C.; Miljuš, G.; Mooij, M. G.; Parrott, N.; Ungell, A. L.; Wildt, S. N. de; Orlu, M.; Klein, S.; Müllertz, A. Impact of gastrointestinal physiology on drug absorption in special populations—-An UNGAP review. *European Journal of Pharmaceutical Sciences* **2020**, *147*. https://doi.org/10.1016/j.ejps.2020.105280.

(62) Catassi, C.; Bonucci, A.; Coppa, G. V.; Carlucci, A.; Giorgi, P. L. Intestinal permeability changes during the first month: Effect of natural versus artificial feeding. *Journal of Pediatric Gastroenterology and Nutrition* **1995**, *21* (4), 383–386. https://doi.org/10.1097/00005176-199511000-00003.

(63) Saleem, B.; Okogbule-Wonodi, A. C.; Fasano, A.; Magder, L. S.; Ravel, J.; Kapoor, S.; Viscardi, R. M. Intestinal Barrier Maturation in Very Low Birthweight Infants: Relationship to Feeding and Antibiotic Exposure. *Journal of Pediatrics* **2017**, *183*, 31–36.e1. https://doi.org/10.1016/j.jpeds.2017.01.013.

(64) Stenling, R.; Fredrikzon, B.; Nyhlin, H.; Helander, H. F.; Falkmer, S. Surface infrastructure of the small intestine mucosa in healthy children and adults: A scanning electron microscopic study with some methodological aspects. *Ultrastructural Pathology* **1984**, *6* (2-3), 131–140. https://doi.org/10.3109/01913128409018567.

(65) Anderson, B. J.; Woollard, G. A.; Holford, N. H. G. A model for size and age changes in the pharmacokinetics of paracetamol in neonates, infants and children. *British Journal of Clinical Pharmacology* **2000**, *50* (2), 125–134. https://doi.org/10.1046/j.1365-2125.2000.00231.x.

(66) Anderson, B. J.; Van Lingen, R. A.; Hansen, T. G.; Lin, Y. C.; Holford, N. H. G. Acetaminophen developmental pharmacokinetics in premature neonates and infants: A pooled population analysis. *Anesthesiology* **2002**, *96* (6), 1336–1345. https://doi.org/10.1097/00000542-200206000-00012.

(67) Bonner, J. J.; Vajjah, P.; Abduljalil, K.; Jamei, M.; Rostami-Hodjegan, A.; Tucker, G. T.; Johnson, T. N. Does age affect gastric emptying time? A model-based meta-analysis of data from premature neonates through to adults. *Biopharmaceutics and Drug Disposition* **2015**, *36* (4), 245–257. https://doi.org/10.1002/bdd.1937.

(68) Maharaj, A. R.; Edginton, A. N.; Fotaki, N. Assessment of Age-Related Changes in Pediatric Gastrointestinal Solubility. *Pharmaceutical Research* **2016**, *33* (1), 52–71. https://doi.org/10.1007/s11095-015-1762-7.

(69) Shawahna, R. Pediatric biopharmaceutical classification system: Using age-appropriate initial gastric volume. *AAPS Journal* **2016**, *18* (3), 728–736. https://doi.org/10.1208/s12248-016-9885-2.

(70) Johnson, T. N.; Bonner, J. J.; Tucker, G. T.; Turner, D. B.; Jamei, M. Development and applications of a physiologically-based model of paediatric oral drug absorption. *European Journal of Pharmaceutical Sciences* **2018**, *115*, 57–67. https://doi.org/10.1016/j.ejps.2018.01.009.

(71) Somani, A. A.; Thelen, K.; Zheng, S.; Trame, M. N.; Coboeken, K.; Meyer, M.; Schnizler, K.; Ince, I.; Willmann, S.; Schmidt, S. Evaluation of changes in oral drug absorption in preterm and term neonates for Biopharmaceutics Classification System (BCS) class i and II compounds. *British Journal of Clinical Pharmacology* **2016**, *81* (1), 137–147. https://doi.org/10.1111/bcp.12752.

(72) Chan, L. M. S.; Lowes, S.; Hirst, B. H. The ABCs of drug transport in intestine and liver: Efflux proteins limiting drug absorption and bioavailability. *European Journal of Pharmaceutical Sciences* **2004**, *21* (1), 25–51. https://doi.org/10.1016/j.ejps.2003.07.003.

(73) Reznicek, J.; Ceckova, M.; Ptackova, Z.; Martinec, O.; Tupova, L.; Cerveny, L.; Staud, F. MDR1 and BCRP transporter-mediated drug-drug interaction between rilpivirine and abacavir and effect on intestinal absorption. *Antimicrobial Agents and Chemotherapy* **2017**, *61* (9). https://doi.org/10.1128/AAC.00837-17.

(74) Han, T.; Everett, R. S.; Proctor, W. R.; Ng, C. M.; Costales, C. L.; Brouwer, K. L. R.; Thakker, D. R. Organic cation transporter 1 (OCT1/mOct1) is localized in the apical membrane of Caco-2 cell monolayers and enterocytes. *Molecular Pharmacology* **2013**, *84* (2), 182–189. https://doi.org/10.1124/mol.112.084517.

(75) Müller, J.; Keiser, M.; Drozdzik, M.; Oswald, S. Expression, regulation and function of intestinal drug transporters: An update. *Biological Chemistry* **2017**, *398* (2), 175–192. https://doi.org/10.1515/hsz-2016-0259.

(76) Kramer, W. Transporters, Trojan horses and therapeutics: Suitability of bile acid and peptide transporters for drug delivery. *Biological Chemistry* **2011**, *392* (1-2), 77–94. https://doi.org/10.1515/BC.2011.017.

(77) Cheung, K. W. K.; Groen, B. D. van; Burckart, G. J.; Zhang, L.; Wildt, S. N. de; Huang, S. M. Incorporating Ontogeny in Physiologically Based Pharmacokinetic Modeling to Improve Pediatric Drug Development: What We Know About Developmental Changes in Membrane Transporters. *Journal of Clinical Pharmacology* **2019**, *59* (S1), S56–S69. https://doi.org/10.1002/jcph.1489.

(78) Mooij, M. G.; De Koning, B. E. A.; Lindenbergh-Kortleve, D. J.; Simons-Oosterhuis, Y.; Van Groen, B. D.; Tibboel, D.; Samsom, J. N.; De Wildt, S. N. Human intestinal PEPT1 transporter expression and localization in preterm and term infants. *Drug Metabolism and Disposition* **2016**, *44* (7), 1014–1019. https://doi.org/10.1124/dmd.115.068809.

(79) Konieczna, A.; Erdösová, B.; Lichnovská, R.; Jandl, M.; Čížková, K.; Ehrmann, J. Differential expression of ABC transporters (MDR1, MRP1, BCRP) in developing human embryos. *Journal of Molecular Histology* **2011**, *42* (6), 567–574. https://doi.org/10.1007/s10735-011-9363-1.

(80) Mizuno, T.; Fukuda, T.; Masuda, S.; Uemoto, S.; Matsubara, K.; Inui, K. I.; Vinks, A. A. Developmental trajectory of intestinal MDR1/ABCB1 mRNA expression in children. *British Journal of Clinical Pharmacology* **2014**, *77* (5), 910–912. https://doi.org/10.1111/bcp.12211.

(81) Mooij, M. G.; Schwarz, U. I.; De Koning, B. A. E.; Leeder, J. S.; Gaedigk, R.; Samsom, J. N.; Spaans, E.; Van Goudoever, J. B.; Tibboel, D.; Kim, R. B.; De Wildt, S. N. Ontogeny of human hepatic and intestinal transporter gene expression during childhood: Age matters. *Drug Metabolism and Disposition* **2014**, *42* (8), 1268–1274. https://doi.org/10.1124/dmd.114.056929.

(82) Johnson, T. N.; Thomson, M. Intestinal metabolism and transport of drugs in children: The effects of age and disease. *Journal of Pediatric Gastroenterology and Nutrition* **2008**, *47* (1), 3–10. https://doi.org/10.1097/MPG.0b013e31816a8cca.

(83) Fisher, M. B.; Paine, M. F.; Strelevitz, T. J.; Wrighton, S. A. The role of hepatic and extrahepatic UDP-glucuronosyltransferases in human drug metabolism. *Drug Metabolism Reviews* **2001**, *33* (3-4), 273–297. https://doi.org/10.1081/DMR-120000653.

(84) Paine, M. F.; Khalighi, M.; Fisher, J. M.; Shen, D. D.; Kunze, K. L.; Marsh, C. L.; Perkins, J. D.; Thummel, K. E. Characterization of interintestinal and intraintestinal variations in human CYP3A-dependent metabolism. *Journal of Pharmacology and Experimental Therapeutics* **1997**, *283* (3), 1552–1562.

(85) Paine, M. F.; Hart, H. L.; Ludington, S. S.; Haining, R. L.; Rettie, A. E.; Zeldin, D. C. The human intestinal cytochrome P450 "pie". *Drug Metabolism and Disposition* **2006**, *34* (5), 880–886. https://doi.org/10.1124/dmd.105.008672.

(86) Johnson, T. N.; Tanner, M. S.; Taylor, C. J.; Tucker, G. T. Enterocytic CYP3A4 in a paediatric population: Developmental changes and the effect of coeliac disease and cystic fibrosis. *British Journal of Clinical Pharmacology* **2001**, *51* (5), 451–460. https://doi.org/10.1046/j.1365-2125.2001.01370.x.

(87) Brussee, J. M.; Yu, H.; Krekels, E. H. J.; Roos, B. de; Brill, M. J. E.; Anker, J. N. van den; Rostami-Hodjegan, A.; Wildt, S. N. de; Knibbe, C. A. J. First-Pass CYP3A-Mediated Metabolism of Midazolam in the Gut Wall and Liver in Preterm Neonates. *CPT: Pharmacometrics and Systems Pharmacology* **2018**, *7* (6), 374–383. https://doi.org/10.1002/psp4.12295.

(88) Guillemette, C.; Lévesque, É.; Rouleau, M. Pharmacogenomics of human uridine diphospho-glucuronosyltransferases and clinical implications. *Clinical Pharmacology and Therapeutics* **2014**, *96* (3), 324–339. https://doi.org/10.1038/clpt.2014.126.

(89) Patel, P.; Xue, Z.; King, K. S.; Parham, L.; Ford, S.; Lou, Y.; Bakshi, K. K.; Sutton, K.; Margolis, D.; Hughes, A. R.; Spreen, W. R. Evaluation of the effect of UGT1A1 polymorphisms on the pharmacokinetics of oral and long-acting injectable cabotegravir. *The Journal of antimicrobial chemotherapy* **2020**, *75* (8), 2240–2248. https://doi.org/10.1093/jac/dkaa147.

(90) Strassburg, C. P.; Kneip, S.; Topp, J.; Obermayer-Straub, P.; Barut, A.; Tukey, R. H.; Manns, M. P. Polymorphic gene regulation and interindividual variation of UDP-glucuronosyltransferase activity in human small intestine. *Journal of Biological Chemistry* **2000**, *275* (46), 36164–36171. https://doi.org/10.1074/jbc.M002180200.

(91) Sanchez-Dominguez, C. N.; Gallardo-Blanco, H. L.; Salinas-Santander, M. A.; Ortiz-Lopez, R. Uridine 5'-diphospho-glucronosyltrasferase: Its role in pharmacogenomics and human disease (review). *Experimental and Therapeutic Medicine* **2018**, *16* (1), 3–11. https://doi.org/10.3892/etm.2018.6184.

(92) Wright, C. M.; Williams, A. F.; Elliman, D.; Bedford, H.; Birks, E.; Butler, G.; Sachs, M.; Moy, R. J.; Cole, T. J. Using the new UK-WHO growth charts. *BMJ (Online)* **2010**, *340* (7747), 647–650. https://doi.org/10.1136/bmj.c1140.

(93) Haddad, S.; Restieri, C.; Krishnan, K. Characterization of age-related changes in body weight and organ weights from birth to adolescence in humans. *Journal of Toxicology and Environmental Health - Part A* **2001**, *64* (6), 453–464. https://doi.org/10.1080/152873901753215911.

(94) FRIIS-HANSEN, B. Body water compartments in children: changes during growth and related changes in body composition. *Pediatrics* **1961**, *28* (2), 169–181. https://doi.org/10.1542/peds.28.2.169.

(95) Fomon, S. J.; Haschke, F.; Ziegler, E. E.; Nelson, S. E. Body composition of reference children from birth to age 10 years. *American Journal of Clinical Nutrition* **1982**, *35* (5 Suppl.), 1169–1175. https://doi.org/10.1093/ajcn/35.5.1169.

(96) McNamara, P. J.; Alcorn, J. Protein binding predictions in infants. *AAPS PharmSci* **2002**, *4* (1), E4–26. https://doi.org/10.1208/ps040104.

(97) Ehrnebo, M.; Agurell, S.; Jalling, B.; Boréus, L. O. Age differences in drug binding by plasma proteins: Studies on human foetuses, neonates and adults. *European Journal of Clinical Pharmacology* **1971**, *3* (4), 189–193. https://doi.org/10.1007/BF00565004.

(98) Abduljalil, K.; Pan, X.; Pansari, A.; Jamei, M.; Johnson, T. N. A Preterm Physiologically Based Pharmacokinetic Model. Part I: Physiological Parameters and Model Building. *Clinical Pharmacokinetics* **2020**, *59* (4), 485–500. https://doi.org/10.1007/s40262-019-00825-6.

(99) Abduljalil, K.; Jamei, M.; Johnson, T. N. Fetal Physiologically Based Pharmacokinetic Models: Systems Information on Fetal Blood Components and Binding Proteins. *Clinical Pharmacokinetics* **2020**, *59* (5), 629–642. https://doi.org/10.1007/s40262-019-00836-3.

(100) Abduljalil, K.; Jamei, M.; Johnson, T. N. Fetal Physiologically Based Pharmacokinetic Models: Systems Information on the Growth and Composition of Fetal Organs. *Clinical Pharmacokinetics* **2019**, *58* (2), 235–262. https://doi.org/10.1007/s40262-018-0685-y.

(101) Nau, R.; Sörgel, F.; Eiffert, H. Penetration of drugs through the blood-cerebrospinal fluid/blood-brain barrier for treatment of central nervous system infections. *Clinical Microbiology Reviews* **2010**, *23* (4), 858–883. https://doi.org/10.1128/CMR.00007-10.

(102) Sethi, P. K.; White, C. A.; Cummings, B. S.; Hines, R. N.; Muralidhara, S.; Bruckner, J. V. Ontogeny of plasma proteins, albumin and binding of diazepam, cyclosporine, and deltamethrin. *Pediatric Research* **2016**, *79* (3), 409–415. https://doi.org/10.1038/pr.2015.237.

(103) Ince, I.; Knibbe, C. A. J.; Danhof, M.; De Wildt, S. N. Developmental changes in the expression and function of cytochrome p450 3a isoforms: Evidence from in vitro and in vivo investigations. *Clinical Pharmacokinetics* **2013**, *52* (5), 333–345. https://doi.org/10.1007/s40262-013-0041-1.

(104) De Wildt, S. N.; Tibboel, D.; Leeder, J. S. Drug metabolism for the paediatrician. *Archives of Disease in Childhood: Education and Practice Edition* **2014**, *99* (12), 1137–1142. https://doi.org/10.1136/archdischild-2013-305212.

(105) De Wildt, S. N.; Kearns, G. L.; Leeder, J. S.; Van Den Anker, J. N. Cytochrome P450 3A. Ontogeny and drug disposition. *Clinical Pharmacokinetics* **1999**, *37* (6), 485–505. https://doi.org/10.2165/00003088-199937060-00004.

(106) Zhao, W.; Leroux, S.; Biran, V.; Jacqz-Aigrain, E. Developmental pharmacogenetics of CYP2C19 in neonates and young infants: omeprazole as a probe drug. *British Journal of Clinical Pharmacology* **2018**, *84* (5), 997–1005. https://doi.org/10.1111/bcp.13526.

(107) Fanni, D.; Ambu, R.; Gerosa, C.; Nemolato, S.; Castagnola, M.; Van Eyken, P.; Faa, G.; Fanos, V. Cytochrome P450 genetic polymorphism in neonatal drug metabolism: Role and practical consequences towards a new drug culture in neonatology. *International Journal of Immunopathology and Pharmacology* **2014**, *27* (1), 5–13. https://doi.org/10.1177/039463201402700102.

(108) H.J. Krekels, E.; Danhof, M.; Tibboel, D.; A.J. Knibbe, C. Ontogeny of Hepatic Glucuronidation; Methods and Results. *Current Drug Metabolism* **2012**, *13* (6), 728–743. https://doi.org/10.2174/138920012800840455.

(109) Court, M. H.; Zhang, X.; Ding, X.; Yee, K. K.; Hesse, L. M.; Finel, M. Quantitative distribution of mRNAs encoding the 19 human UDP-glucuronosyltransferase enzymes in 26 adult and 3 fetal tissues. *Xenobiotica* **2012**, *42* (3), 266–277. https://doi.org/10.3109/00498254.2011.618954.

(110) Miyagi, S. J.; Collier, A. C. The development of UDP-glucuronosyltransferases 1A1 and 1A6 in the pediatric liver. *Drug Metabolism and Disposition* **2011**, *39* (5), 912–919. https://doi.org/10.1124/dmd.110.037192.

(111) Ladumor, M. K.; Bhatt, D. K.; Gaedigk, A.; Sharma, S.; Thakur, A.; Pearce, R. E.; Leeder, J. S.; Bolger, M. B.; Singh, S.; Prasad, B. Ontogeny of hepatic sulfotransferases and prediction of age-dependent fractional contribution of sulfation in acetaminophen metabolism. *Drug Metabolism and Disposition* **2019**, *47* (8), 818–831. https://doi.org/10.1124/dmd.119.086462.

(112) Mahmood, I.; Balian, J. D. The pharmacokinetic principles behind scaling from preclinical results to phase I protocols. *Clinical Pharmacokinetics* **1999**, *36* (1), 1–11. https://doi.org/10.2165/00003088-199936010-00001.

(113) Boase, S.; Miners, J. O. In vitro-in vivo correlations for drugs eliminated by glucuronidation: Investigations with the model substrate zidovudine. *British Journal of Clinical Pharmacology* **2002**, *54* (5), 493–503. https://doi.org/10.1046/j.1365-2125.2002.01669.x.

(114) Johnson, T. N.; Rostami-Hodjegan, A.; Tucker, G. T. Prediction of the clearance of eleven drugs and associated variability in neonates, infants and children. *Clinical Pharmacokinetics* **2006**, *45* (9), 931–956. https://doi.org/10.2165/00003088-200645090-00005.

(115) Rowland, Malcolm.; Tozer, T. N. *Clinical Pharmacoki-netics and Pharmacodynamics : Concepts and Clinical Applications / Malcolm Rowland and Tom Tozer.*, 4th ed.; Lippincott William & Wilkins: Philadel-phia, 2009.

(116) Fagerholm, U. Prediction of human pharmacokinetics - renal metabolic and excretion clearance. *Journal of pharmacy and pharmacology* **2007**, *59* (11), 1463–1471. https://doi.org/10.1211/jpp.59.11.0002.

(117) Di, L.; Artursson, P.; Avdeef, A.; Benet, L. Z.; Houston, J. B.; Kansy, M.; Kerns, E. H.; Lennernäs, H.; Smith, D. A.; Sugano, K. The Critical Role of Passive Permeability in Designing Successful Drugs. *ChemMedChem* **2020**, *15* (20), 1862–1874. https://doi.org/10.1002/cmdc.202000419.

(118) Boss, K.; Stolpe, S.; Müller, A.; Wagner, B.; Wichert, M.; Assert, R.; Volbracht, L.; Stang, A.; Kowall, B.; Kribben, A. Effect of serum creatinine difference between the Jaffe and the enzymatic method on kidney disease detection and staging. *Clinical Kidney Journal* **2023**, *16* (11), 2147–2155. https://doi.org/10.1093/ckj/sfad178.

(119) Ceriotti, F.; Boyd, J. C.; Klein, G.; Henny, J.; Queraltó, J.; Kairisto, V.; Panteghini, M. Reference intervals for serum creatinine concentrations: Assessment of available data for global application. *Clinical Chemistry* **2008**, *54* (3), 559–566. https://doi.org/10.1373/clinchem.2007.099648.

(120) Rhodin, M. M.; Anderson, B. J.; Peters, A. M.; Coulthard, M. G.; Wilkins, B.; Cole, M.; Chatelut, E.; Grubb, A.; Veal, G. J.; Keir, M. J.; Holford, N. H. G. Human renal function maturation: A quantitative description using weight and postmenstrual age. *Pediatric Nephrology* **2009**, *24* (1), 67–76. https://doi.org/10.1007/s00467-008-0997-5.

(121) Sulemanji, M.; Vakili, K. Neonatal renal physiology. *Seminars in Pediatric Surgery* **2013**, *22* (4), 195–198. https://doi.org/10.1053/j.sempedsurg.2013.10.008.

(122) Anderson, B. J.; McKee, A. D.; Holford, N. H. G. Size, myths and the clinical pharmacokinetics of analgesia in paediatric patients. *Clinical Pharmacokinetics* **1997**, *33* (5), 313–327. https://doi.org/10.2165/00003088-199733050-00001.

(123) Holford, N. H. G. A size standard for pharmacokinetics. *Clinical Pharmacokinetics* **1996**, *30* (5), 329–332. https://doi.org/10.2165/00003088-199630050-00001.

(124) West, G. B.; Brown, J. H.; Enquist, B. J. A general model for the origin of allometric scaling laws in biology. *Science* **1997**, *276* (5309), 122–126. https://doi.org/10.1126/science.276.5309.122.

(125) Mahmood, I. Prediction of drug clearance in children from adults: A comparison of several allometric methods. *British Journal of Clinical Pharmacology* **2006**, *61* (5), 545–557. https://doi.org/10.1111/j.1365-2125.2006.02622.x.

(126) Mahmood, I. Prediction of drug clearance in premature and mature neonates, infants, and children less than 2 years of age: A comparison of the predictive performance of 4 allometric models. *Journal of Clinical Pharmacology* **2016**, *56* (6), 733–739. https://doi.org/10.1002/jcph.652.

(127) Germovsek, E.; Barker, C. I. S.; Sharland, M.; Standing, J. F. Scaling clearance in paediatric pharmacokinetics: All models are wrong, which are useful? *British Journal of Clinical Pharmacology* **2017**, *83* (4), 777–790. https://doi.org/10.1111/bcp.13160.

(128) Mahmood, I.; Tegenge, M. A. A Comparative Study Between Allometric Scaling and Physiologically Based Pharmacokinetic Modeling for the Prediction of Drug Clearance From Neonates to Adolescents. *Journal of Clinical Pharmacology* **2019**, *59* (2), 189–197. https://doi.org/10.1002/jcph.1310.

(129) Mahmood, I. Mechanistic versus allometric models for the prediction of drug clearance in neonates (<3 months of age). *Journal of Clinical Pharmacology* **2015**, *55* (6), 718–720. https://doi.org/10.1002/jcph.487.

(130) Bennett, J. E.; Dolin, R.; Blaser, M. J. *Mandell, Douglas, and Bennett's Principles and Practice of Infectious Diseases e-Book: 2-Volume Set*; Elsevier Health Sciences, 2019.

(131) Brodin, P.; Jojic, V.; Gao, T.; Bhattacharya, S.; Angel, C. J. L.; Furman, D.; Shen-Orr, S.; Dekker, C. L.; Swan, G. E.; Butte, A. J.; Maecker, H. T.; Davis, M. M. Variation in the human immune system is largely driven by non-heritable influences. *Cell* **2015**, *160* (1-2), 37–47. https://doi.org/10.1016/j.cell.2014.12.020.

(132) Heuvel, D. van den; Zelm, M. C. van. Effects of nongenetic factors on immune cell dynamics in early childhood: The Generation R Study. *Journal of Allergy and Clinical Immunology* **2017**, *139* (6), 1923–1934.e17. https://doi.org/10.1016/j.jaci.2016.10.023.

(133) Hill, D. L.; Linterman, M. A. Immune system development varies according to age, location, and anemia in African children. *Science Translational Medicine* **2020**, *12* (529). https://doi.org/10.1126/scitranslmed.aaw9522.

(134) Zhu, H.; Huang, S. M.; Madabushi, R.; Strauss, D. G.; Wang, Y.; Zineh, I. Model-Informed Drug Development: A Regulatory Perspective on Progress. *Clinical Pharmacology and Therapeutics* **2019**, *106* (1), 91–93. https://doi.org/10.1002/cpt.1475.

(135) Bi, Y.; Liu, J.; Li, L.; Yu, J.; Bhattaram, A.; Bewernitz, M.; Li, R. jing; Liu, C.; Earp, J.; Ma, L.; Zhuang, L.; Yang, Y.; Zhang, X.; Zhu, H.; Wang, Y. Role of Model-Informed Drug Development in Pediatric Drug Development, Regulatory Evaluation, and Labeling. *Journal of Clinical Pharmacology* **2019**, *59* (S1), S104–S111. https://doi.org/10.1002/jcph.1478.

(136) Rayner, C. R.; Smith, P. F.; Andes, D.; Andrews, K.; Derendorf, H.; Friberg, L. E.; Hanna, D.; Lepak, A.; Mills, E.; Polasek, T. M.; Roberts, J. A.; Schuck, V.; Shelton, M. J.; Wesche, D.; Rowland-Yeo, K. Model-Informed Drug Development for Anti-Infectives: State of the Art and Future. *Clinical Pharmacology and Therapeutics* **2021**, *109* (4), 867–891. https://doi.org/10.1002/cpt.2198.

(137) Rose, K.; Van Den Anker, J. N. *Guide to Paediatric drug development and clinical research*; S. Karger,: Basel, 2010. https://doi.org/10.1111/j.1442-200x.2010.03300.x.

(138) Noe, D. A. Parameter Estimation and Reporting in Noncompartmental Analysis of Clinical Pharmacokinetic Data. *Clinical Pharmacology in Drug Development* **2020**, *9* (S1), S5–S35. https://doi.org/10.1002/cpdd.810.

(139) Yáñez, J. A.; Remsberg, C. M.; Sayre, C. L.; Forrest, M. L.; Davies, N. M. Flip-flop pharmacokinetics - Delivering a reversal of disposition: Challenges and opportunities during drug development. *Therapeutic Delivery* **2011**, *2* (5), 643–672. https://doi.org/10.4155/tde.11.19.

(140) Mould, D. R.; Upton, R. N. Basic concepts in population modeling, simulation, and model-based drug development - Part 2: Introduction to pharmacokinetic modeling methods. *CPT: Pharmacometrics and Systems Pharmacology* **2013**, *2* (4), 1–14. https://doi.org/10.1038/psp.2013.14.

(141) Reisfeld, Brad.; Mayeno, A. N. *Computational Toxicology : Volume I*, 1st ed. 20.; Reisfeld, Brad., Mayeno, A. N., Eds.; Methods in molecular biology, 929; Humana Press: Totowa, NJ, 2013; pp 377–390. https://doi.org/10.1007/978-1-62703-050-2.

(142) Gabrielsson, J.; Weiner, D. *Pharmacokinetic and Pharmacodynamic Data Analysis: Concepts and Applications, Second Edition*; Swedish Pharmaceutical Society, 1997.

(143) Godfrey, K. *Compartmental Models and Their Application*; Academic Press, 1983.

(144) Bonate, P. L. *Pharmacokinetic-Pharmacodynamic Modeling and Simulation*, 2nd ed. 20.; Springer US: New York, NY, 2011. https://doi.org/10.1007/978-1-4419-9485-1.

(145) Ette, E. I.; Williams, P. J. Population pharmacokinetics II: Estimation methods. *Annals of Pharmacotherapy* **2004**, *38* (11), 1907–1915. https://doi.org/10.1345/aph.1E259.

(146) Sheiner, L. B.; Rosenberg, B.; Marathe, V. V. Estimation of population characteristics of pharmacokinetic parameters from routine clinical data. *Journal of Pharmacokinetics and Biopharmaceutics* **1977**, *5* (5), 445–479. https://doi.org/10.1007/BF01061728.

(147) Mould, D. R.; Upton, R. N. Basic concepts in population modeling, simulation, and model-based drug development. *CPT: Pharmacometrics and Systems Pharmacology* **2012**, *1* (1), 1–14. https://doi.org/10.1038/psp.2012.4.

(148) Ette, E. I.; Williams, P. J. Population pharmacokinetics I: Background, concepts, and models. *Annals of Pharmacotherapy* **2004**, *38* (10), 1702–1706. https://doi.org/10.1345/aph.1D374.

(149) Karlsson, M. O.; Beal, S. L.; Sheiner, L. B. Three new residual error models for population PK/PD analyses. *Journal of Pharmacokinetics and Biopharmaceutics* **1995**, *23* (6), 651–672. https://doi.org/10.1007/BF02353466.

(150) Hooker, A. C.; Staatz, C. E.; Karlsson, M. O. Conditional weighted residuals (CWRES): A model diagnostic for the FOCE method. *Pharmaceutical Research* **2007**, *24* (12), 2187–2197. https://doi.org/10.1007/s11095-007-9361-x.

(151) Bergstrand, M.; Hooker, A. C.; Wallin, J. E.; Karlsson, M. O. Prediction-corrected visual predictive checks for diagnosing nonlinear mixed-effects models. *AAPS Journal* **2011**, *13* (2), 143–151. https://doi.org/10.1208/s12248-011-9255-z.

(152) Kuepfer, L.; Niederalt, C.; Wendl, T.; Schlender, J. F.; Willmann, S.; Lippert, J.; Block, M.; Eissing, T.; Teutonico, D. Applied Concepts in PBPK Modeling: How to Build a PBPK/PD Model. *CPT: Pharmacometrics and Systems Pharmacology* **2016**, *5* (10), 516–531. https://doi.org/10.1002/psp4.12134.

(153) Nestorov, I. Whole-body physiologically based pharmacokinetic models. *Expert Opinion on Drug Metabolism and Toxicology* **2007**, *3* (2), 235–249. https://doi.org/10.1517/17425255.3.2.235.

(154) Wang, L.; Chen, J.; Chen, W.; Ruan, Z.; Lou, H.; Yang, D.; Jiang, B. In silico prediction of bioequivalence of atorvastatin tablets based on GastroPlus™ software. *BMC Pharmacology and Toxicology* **2023**, *24* (1), 69–69. https://doi.org/10.1186/s40360-023-00689-4.

(155) Wedagedera, J. R.; Afuape, A.; Chirumamilla, S. K.; Momiji, H.; Leary, R.; Dunlavey, M.; Matthews, R.; Abduljalil, K.; Jamei, M.; Bois, F. Y. Population PBPK modeling using parametric and nonparametric methods of the Simcyp Simulator, and Bayesian samplers. *CPT: Pharmacometrics and Systems Pharmacology* **2022**, *11* (6), 755–765. https://doi.org/10.1002/psp4.12787.

(156) Krauss, M.; Tappe, K.; Schuppert, A.; Kuepfer, L.; Goerlitz, L. Bayesian population physiologically-based pharmacokinetic (PBPK) approach for a physiologically realistic characterization of interindividual variability in clinically relevant populations. *PLoS ONE* **2015**, *10* (10), e0139423–e0139423. https://doi.org/10.1371/journal.pone.0139423.

(157) Margolskee, A.; Abrahamsson, B. IMI – Oral biopharmaceutics tools project – Evaluation of bottom-up PBPK prediction success part 2: An introduction to the simulation exercise and overview of results. *European Journal of Pharmaceutical Sciences* **2017**, *96*, 610–625. https://doi.org/10.1016/j.ejps.2016.10.036.

(158) Tsamandouras, N.; Rostami-Hodjegan, A.; Aarons, L. Combining the 'bottom up' and 'top down' approaches in pharmacokinetic modelling: Fitting PBPK models to observed clinical data. *British Journal of Clinical Pharmacology* **2015**, *79* (1), 48–55. https://doi.org/10.1111/bcp.12234.

(159) Shebley, M.; Rowland, M. Physiologically Based Pharmacokinetic Model Qualification and Reporting Procedures for Regulatory Submissions: A Consortium Perspective. *Clinical Pharmacology and Therapeutics* **2018**, *104* (1), 88–110. https://doi.org/10.1002/cpt.1013.

(160) The US Food and Drug Administration. Physiologically Based Pharmacokinetic Analyses: Format and Content Guidance for Industry. **2018**.

(161) European Medicines Agency (EMEA). Guideline on the reporting of physiologically based pharmacokinetic (PBPK) modelling and simulation. **2019**.

(162) Yu, L. X.; Lipka, E.; Crison, J. R.; Amidon, G. L. Transport approaches to the biopharmaceutical design of oral drug delivery systems: Prediction of intestinal absorption. *Advanced Drug Delivery Reviews* **1996**, *19* (3), 359–376. https://doi.org/10.1016/0169-409X(96)00009-9.

(163) Yu, L. X.; Amidon, G. L. A compartmental absorption and transit model for estimating oral drug absorption. *International Journal of Pharmaceutics* **1999**, *186* (2), 119–125. https://doi.org/10.1016/S0378-5173(99)00147-7.

(164) Agoram, B.; Woltosz, W. S.; Bolger, M. B. Predicting the impact of physiological and biochemical processes on oral drug bioavailability. *Advanced Drug Delivery Reviews* **2001**, *50* (SUPPL. 1), S41–S67. https://doi.org/10.1016/S0169-409X(01)00179-X.

(165) Lennernäs, H.; Ahrenstedt, Ö.; Hällgren, R.; Knutson, L.; Ryde, M.; Paalzow, L. K. Regional Jejunal Perfusion, a New in Vivo Approach to Study Oral Drug Absorption in Man. *Pharmaceutical Research: An Official Journal of the American Association of Pharmaceutical Scientists* **1992**, *9* (10), 1243–1251. https://doi.org/10.1023/A:1015888813741.

(166) Lennernäs, H.; Lee, I. D.; Fagerholm, U.; Amidon, G. L. A residence-time distribution analysis of the hydrodynamics within the intestine in man during a regional single-pass perfusion with Loc-I-Gut: In-vivo permeability estimation. *Journal of Pharmacy and Pharmacology* **1997**, *49* (7), 682–686. https://doi.org/10.1111/j.2042-7158.1997.tb06092.x.

(167) Lennernäs, H. Human intestinal permeability. *Journal of Pharmaceutical Sciences* **1998**, *87* (4), 403–410. https://doi.org/10.1021/js970332a.

(168) Poulin, P.; Theil, F. P. A priori prediction of tissue: Plasma partition coefficients of drugs to facilitate the use of physiologically-based pharmacokinetic models in drug discovery. *Journal of Pharmaceutical Sciences* **2000**, *89* (1), 16–35. https://doi.org/10.1002/(SICI)1520-6017(200001)89:1%3C16::AID-JPS3%3E3.0.CO;2-E.

(169) Berezhkovskiy, L. M. Volume of distribution at steady state for a linear pharmacokinetic system with peripheral elimination. *Journal of Pharmaceutical Sciences* **2004**, *93* (6), 1628–1640. https://doi.org/10.1002/jps.20073.

(170) Rodgers, T.; Leahy, D.; Rowland, M. Physiologically based pharmacokinetic modeling 1: Predicting the tissue distribution of moderate-to-strong bases. *Journal of Pharmaceutical Sciences* **2005**, *94* (6), 1259–1276. https://doi.org/10.1002/jps.20322.

(171) Rodgers, T.; Rowland, M. Physiologically based pharmacokinetic modelling 2: Predicting the tissue distribution of acids, very weak bases, neutrals and zwitterions. *Journal of Pharmaceutical Sciences* **2006**, *95* (6), 1238–1257. https://doi.org/10.1002/jps.20502.

(172) Parrott, N.; Lavé, T. Prediction of intestinal absorption: Comparative assessment of GASTROPLUS™ and IDEA™. *European Journal of Pharmaceutical Sciences* **2002**, *17* (1-2), 51–61. https://doi.org/10.1016/S0928-0987(02)00132-X.

(173) Lippert, J.; Teutonico, D. Open Systems Pharmacology Community—An Open Access, Open Source, Open Science Approach to Modeling and Simulation in Pharmaceutical Sciences. *CPT: Pharmacometrics and Systems Pharmacology* **2019**, *8* (12), 878–882. https://doi.org/10.1002/psp4.12473.

(174) Rostami-Hodjegan, A.; Tucker, G. 'In silico' simulations to assess the 'in vivo' consequences of 'in vitro' metabolic drug-drug interactions. *Drug Discovery Today: Technologies* **2004**, *1* (4), 441–448. https://doi.org/10.1016/j.ddtec.2004.10.002.
(175) Certara. Simcyp™ Biopharmaceutics, 2023. https://www.certara.com/software/simcyp-biopharmaceutics/.
(176) Simulations Plus. Drug-Drug Interactions, 2023. https://www.simulations-plus.com/software/gastroplus/drug-interaction/.
(177) Ahmad, A.; Rostami-Hodjegan, A. IMI – Oral biopharmaceutics tools project – Evaluation of bottom-up PBPK prediction success part 4: Prediction accuracy and software comparisons with improved data and modelling strategies. *European Journal of Pharmaceutics and Biopharmaceutics* **2020**, *156*, 50–63. https://doi.org/10.1016/j.ejpb.2020.08.006.
(178) Upreti, V. V.; Wahlstrom, J. L. Meta-analysis of hepatic cytochrome P450 ontogeny to underwrite the prediction of pediatric pharmacokinetics using physiologically based pharmacokinetic modeling. *Journal of Clinical Pharmacology* **2016**, *56* (3), 266–283. https://doi.org/10.1002/jcph.585.
(179) Emoto, C.; Johnson, T. N.; Neuhoff, S.; Hahn, D.; Vinks, A. A.; Fukuda, T. PBPK Model of Morphine Incorporating Developmental Changes in Hepatic OCT1 and UGT2B7 Proteins to Explain the Variability in Clearances in Neonates and Small Infants. *CPT: Pharmacometrics and Systems Pharmacology* **2018**, *7* (7), 464–473. https://doi.org/10.1002/psp4.12306.
(180) Abduljalil, K.; Pan, X.; Pansari, A.; Jamei, M.; Johnson, T. N. Preterm Physiologically Based Pharmacokinetic Model. Part II: Applications of the Model to Predict Drug Pharmacokinetics in the Preterm Population. *Clinical Pharmacokinetics* **2020**, *59* (4), 501–518. https://doi.org/10.1007/s40262-019-00827-4.
(181) Templeton, I. E.; Jones, N. S.; Musib, L. Pediatric Dose Selection and Utility of PBPK in Determining Dose. *AAPS Journal* **2018**, *20* (2), 31. https://doi.org/10.1208/s12248-018-0187-8.
(182) Heijden, J. E. M. van der; Freriksen, J. J. M.; Hoop-Sommen, M. A. de; Greupink, R.; de Wildt, S. N. PBPK modeling for drug dosing in pediatric patients: a tutorial for a pragmatic approach in clinical care. *Clinical pharmacology and therapeutics* **2023**. https://doi.org/10.1002/cpt.3023.
(183) Peters, S. A.; Dolgos, H. Requirements to Establishing Confidence in Physiologically Based Pharmacokinetic (PBPK) Models and Overcoming Some of the Challenges to Meeting Them. *Clinical Pharmacokinetics* **2019**, *58* (11), 1355–1371. https://doi.org/10.1007/s40262-019-00790-0.

(184) Obiero, C. W.; Williams, P.; Murunga, S.; Thitiri, J.; Omollo, R.; Walker, A. S.; Egondi, T.; Nyaoke, B.; Correia, E.; Kane, Z.; Gastine, S.; Kipper, K.; Standing, J. F.; Ellis, S.; Sharland, M.; Berkley, J. A. Randomised controlled trial of fosfomycin in neonatal sepsis: pharmacokinetics and safety in relation to sodium overload. *Archives of Disease in Childhood* **2022**, *107* (9), 802–810. https://doi.org/10.1136/archdischild-2021-322483.

(185) Altcheh, J.; García-Bournissen, F. Population Pharmacokinetic Study of Benznidazole in Pediatric Chagas Disease Suggests Efficacy despite Lower Plasma Concentrations than in Adults. *PLoS Neglected Tropical Diseases* **2014**, *8* (5), e2907–e2907. https://doi.org/10.1371/journal.pntd.0002907.

(186) Wellcome Trust. How drug-resistant infections are undermining modern medicine – and why more research is needed now. **2020**.

(187) Laxminarayan, R.; Matsoso, P.; Pant, S.; Brower, C.; Røttingen, J. A.; Klugman, K.; Davies, S. Access to effective antimicrobials: A worldwide challenge. *The Lancet* **2016**, *387* (10014), 168–175. https://doi.org/10.1016/S0140-6736(15)00474-2.

(188) Chaurasia, S.; Sivanandan, S.; Agarwal, R.; Ellis, S.; Sharland, M.; Sankar, M. J. Neonatal sepsis in South Asia: Huge burden and spiralling antimicrobial resistance. *BMJ (Online)* **2019**, *364*, k5314. https://doi.org/10.1136/bmj.k5314.

(189) Tam, P. Y. I.; Musicha, P.; Kawaza, K.; Cornick, J.; Denis, B.; Freyne, B.; Everett, D.; Dube, Q.; French, N.; Feasey, N.; Heyderman, R. Emerging resistance to empiric antimicrobial regimens for pediatric bloodstream infections in Malawi (1998-2017). *Clinical Infectious Diseases* **2019**, *69* (1), 61–68. https://doi.org/10.1093/cid/ciy834.

(190) Thomson, K. M. et. al. (BARNARDS Group). Effects of antibiotic resistance, drug target attainment, bacterial pathogenicity and virulence, and antibiotic access and affordability on outcomes in neonatal sepsis: an international microbiology and drug evaluation prospective substudy (BARNARDS). *The Lancet Infectious Diseases* **2021**, *21* (12), 1677–1688. https://doi.org/10.1016/S1473-3099(21)00050-5.

(191) Hendlin, D.; Stapley, E. O.; Jackson, M.; Wallick, H.; Miller, A. K.; Wolf, F. J.; Miller, T. W.; Chaiet, L.; Kahan, F. M.; Foltz, E. L.; Woodruff, H. B.; Mata, J. M.; Hernandez, S.; Mochales, S. Phosphonomycin, a new antibiotic produced by strains of streptomyces. *Science* **1969**, *166* (3901), 122–123. https://doi.org/10.1126/science.166.3901.122.

(192) Li, G.; Standing, J. F.; Bielicki, J.; Hope, W.; Anker, J. van den; Heath, P. T.; Sharland, M. The Potential Role of Fosfomycin in Neonatal Sepsis Caused by Multidrug-Resistant Bacteria. *Drugs* **2017**, *77* (9), 941–950. https://doi.org/10.1007/s40265-017-0745-x.

(193) Williams, P. C. M.; Waichungo, J.; Gordon, N. C.; Sharland, M.; Murunga, S.; Kamau, A.; Berkley, J. A. The potential of fosfomycin for multi-drug resistant sepsis: An analysis of in vitro activity against invasive paediatric gram-negative bacteria. *Journal of Medical Microbiology* **2019**, *68* (5), 711–719. https://doi.org/10.1099/jmm.0.000973.

(194) Molina, M. A.; Olay, T.; Quero, J. Pharmacodynamic data on fosfomycin in underweight infants during the neonatal period. *Chemotherapy* **1977**, *23*, 217–222. https://doi.org/10.1159/000222051.

(195) Guggenbichler, J. P.; Kienel, G.; Frisch, H. Fosfomycin, Ein Neues Antibiotikum. Pharmakokinetische Untersuchungen Bei Kindern, Fruh- Und Neugeborenen. *Padiatrie und Padologie* **1978**, *13* (4), 429–436.

(196) Guibert, M.; Magny, J. F.; Poudenx, F.; Lebrun, L.; Dehan, M. [Comparative pharmacokinetics of fosfomycin in the neonate: 2 modes of administration]. *Pathologie-biologie* **1987**, *35* (5 Pt 2), 750–752.

(197) Suzuki, S.; Murayama, Y.; Sugiyama, E.; Sekiyama, M.; Sato, H. Dose estimation for renal-excretion drugs in neonates and infants based on physiological development of renal function. *Yakugaku Zasshi* **2009**, *129* (7), 829–842. https://doi.org/10.1248/yakushi.129.829.

(198) Shimizu, K. Fosfomycin: Absorption and excretion. *Chemotherapy* **1977**, *23* (Suppl 1), 153–158. https://doi.org/10.1159/000222042.

(199) Bundgaard, H. Acid-catalyzed hydrolysis of fosfomycin and its implication in oral absorption of the drug. *International Journal of Pharmaceutics* **1980**, *6* (1), 1–9. https://doi.org/10.1016/0378-5173(80)90024-1.

(200) Gobernado, M.; Garcia, J.; Santos, M.; Panadero, J.; Diosdado, N. Renal insufficiency and fosfomycin. *Chemotherapy* **1977**, *23* (SUP I), 200–203. https://doi.org/10.1159/000222048.

(201) Wenzler, E.; Ellis-Grosse, E. J.; Rodvolda, K. A. Pharmacokinetics, Safety, and Tolerability of Single-Dose Intravenous (ZTI-01) and Oral Fosfomycin in Healthy Volunteers. *Antimicrobial Agents and Chemotherapy* **2017**, *61* (9). https://doi.org/10.1128/AAC.00775-17.

(202) Bergan, T.; Thorsteinsson, S. B.; Albini, E. Pharmacokinetic profile of fosfomycin trometamol. *Chemotherapy* **1993**, *39* (5), 297–301. https://doi.org/10.1159/000239140.

(203) Kühnen, E.; Pfeifer, G.; Frenkel, C. Penetration of fosfomycin into cerebrospinal fluid across non-inflamed and inflamed meninges. *Infection* **1987**, *15* (6), 422–424. https://doi.org/10.1007/BF01647220.

(204) Pfausler, B.; Spiss, H.; Dittrich, P.; Zeitlinger, M.; Schmutzhard, E.; Joukhadar, C. Concentrations of fosfomycin in the cerebrospinal fluid of neurointensive care patients with ventriculostomy-associated ventriculitis. *Journal of Antimicrobial Chemotherapy* **2004**, *53* (5), 848–852. https://doi.org/10.1093/jac/dkh158.

(205) Russell, N. J.; Sharland, M. Patterns of antibiotic use, pathogens, and prediction of mortality in hospitalized neonates and young infants with sepsis: A global neonatal sepsis observational cohort study (NeoOBS). *PLoS Medicine* **2023**, *20* (6). https://doi.org/10.1371/journal.pmed.1004179.

(206) Drugs for Neglected Diseases. Intravenous and Oral Fosfomycin in Hospitalised Neonates with Clinical Sepsis (NeoFosfo), 2023. https://www.clinicaltrials.gov/study/NCT03453177.

(207) Drugs for Neglected Diseases. NeoAMR Observational Study in Neonatal Sepsis, 2023. https://www.clinicaltrials.gov/study/NCT03721302.

(208) Stockmann, C.; Barrett, J. S.; Roberts, J. K.; Sherwin, C. M. T. Use of modeling and simulation in the design and conduct of pediatric clinical trials and the optimization of individualized dosing regimens. *CPT: Pharmacometrics and Systems Pharmacology* **2015**, *4* (11), 630–640. https://doi.org/10.1002/psp4.12038.

(209) Ogungbenro, K.; Aarons, L. How many subjects are necessary for population pharmacokinetic experiments? Confidence interval approach. *European Journal of Clinical Pharmacology* **2008**, *64* (7), 705–713. https://doi.org/10.1007/s00228-008-0493-7.

(210) European Medicines Agency, EMEA. Guideline on bioanalytical method validation (EMEA/CHMP/EWP/192217/2009 adopted 2011). **2011**.

(211) Kane, Z.; Gastine, S.; Obiero, C.; Williams, P.; Murunga, S.; Thitiri, J.; Ellis, S.; Correia, E.; Nyaoke, B.; Kipper, K.; Van Den Anker, J.; Sharland, M.; Berkley, J. A.; Standing, J. F. IV and oral fosfomycin pharmacokinetics in neonates with suspected clinical sepsis. *Journal of Antimicrobial Chemotherapy* **2021**, *76* (7), 1855–1864. https://doi.org/10.1093/jac/dkab083.

(212) ICON. ICON's Nonlinear Mixed Effects Modelling Tool, the Industry Standard for Population PK/PD Analysis, 2023. https://www.iconplc.com/solutions/technologies/nonmem.

(213) Germovsek, E.; Kent, A.; Metsvaht, T.; Lutsar, I.; Klein, N.; Turner, M. A.; Sharland, M.; Nielsen, E. I.; Heath, P. T.; Standing, J. F. Development and evaluation of a gentamicin pharmacokinetic model that facilitates opportunistic gentamicin therapeutic drug monitoring in neonates and infants. *Antimicrobial Agents and Chemotherapy* **2016**, *60* (8), 4869–4877. https://doi.org/10.1128/AAC.00577-16.

(214) Germovsek, E.; Sinha, A. Plasma and CSF pharmacokinetics of meropenem in neonates and young infants: Results from the NeoMero studies. *Journal of Antimicrobial Chemotherapy* **2018**, *73* (7), 1908–1916. https://doi.org/10.1093/jac/dky128.

(215) Anderson, B. J.; Holford, N. H. G. Negligible impact of birth on renal function and drug metabolism. *Paediatric Anaesthesia* **2018**, *28* (11), 1015–1021. https://doi.org/10.1111/pan.13497.

(216) Johanson, C. E.; Duncan, J. A.; Klinge, P. M.; Brinker, T.; Stopa, E. G.; Silverberg, G. D. Multiplicity of cerebrospinal fluid functions: New challenges in health and disease. *Cerebrospinal Fluid Research* **2008**, *5* (1), 10–10. https://doi.org/10.1186/1743-8454-5-10.

(217) R Core Team. R: A Language and Environment for Statistical Computing. **2023**.

(218) Lindbom, L.; Pihlgren, P.; Jonsson, N. PsN-Toolkit - A collection of computer intensive statistical methods for non-linear mixed effect modeling using NONMEM. *Computer Methods and Programs in Biomedicine* **2005**, *79* (3), 241–257. https://doi.org/10.1016/j.cmpb.2005.04.005.

(219) Jonsson, E. N.; Karlsson, M. O. Xpose—an S-PLUS based population pharmacokinetic/pharmacodynamic model building aid for NONMEM. *Computer Methods and Programs in Biomedicine* **1998**, *58* (1), 51–64. https://doi.org/10.1016/S0169-2607(98)00067-4.

(220) Upton, R. N. The two-compartment recirculatory pharmacokinetic model - An introduction to recirculatory pharmacokinetic concepts. *British Journal of Anaesthesia* **2004**, *92* (4), 475–484. https://doi.org/10.1093/bja/aeh089.

(221) Benjamin Rich. linpk: Generate Concentration-Time Profiles from Linear PK Systems. **2011**.

(222) Merino-Bohórquez, V.; Docobo-Pérez, F.; Sojo, J.; Morales, I.; Lupión, C.; Martín, D.; Cameán, M.; Hope, W.; Pascual; Rodríguez-Baño, J. Population pharmacokinetics and pharmacodynamics of fosfomycin in non–critically ill patients with bacteremic urinary infection caused by multidrug-resistant Escherichia coli. *Clinical Microbiology and Infection* **2018**, *24* (11), 1177–1183. https://doi.org/10.1016/j.cmi.2018.02.005.

(223) Traunmller, F.; Popovic, M.; Konz, K. H.; Vavken, P.; Leithner, A.; Joukhadar, C. A reappraisal of current dosing strategies for intravenous fosfomycin in children and neonates. *Clinical Pharmacokinetics* **2011**, *50* (8), 493–503. https://doi.org/10.2165/11592670-000000000-00000.

(224) Lepak, A. J.; Zhao, M.; Vanscoy, B.; Taylor, D. S.; Ellis-Grosse, E.; Ambrose, P. G.; Andes, D. R. In Vivo pharmacokinetics and pharmacodynamics of ZTI-01 (fosfomycin for injection) in the neutropenic murine thigh infection model against Escherichia coli, klebsiella pneumoniae, and pseudomonas aeruginosa. *Antimicrobial Agents and Chemotherapy* **2017**, *61* (6). https://doi.org/10.1128/AAC.00476-17.

(225) Docobo-Pérez, F.; Drusano, G. L.; Johnson, A.; Goodwin, J.; Whalley, S.; Ramos-Martín, V.; Ballestero-Tellez, M.; Rodriguez-Martinez, J. M.; Conejo, M. C.; Van Guilder, M.; Rodríguez-Baño, J.; Pascual, A.; Hope, W. W. Pharmacodynamics of fosfomycin: Insights into clinical use for antimicrobial resistance. *Antimicrobial Agents and Chemotherapy* **2015**, *59* (9), 5602–5610. https://doi.org/10.1128/AAC.00752-15.

(226) Standing, J. F.; Ongas, M. O.; Ogwang, C.; Kagwanja, N.; Murunga, S.; Mwaringa, S.; Ali, R.; Mturi, N.; Timbwa, M.; Manyasi, C.; Mwalekwa, L.; Bandika, V. L.; Ogutu, B.; Waichungo, J.; Kipper, K.; Berkley, J. A. Dosing of Ceftriaxone and Metronidazole for Children With Severe Acute Malnutrition. *Clinical Pharmacology and Therapeutics* **2018**, *104* (6), 1165–1174. https://doi.org/10.1002/cpt.1078.

(227) Zeitlinger, M. A.; Sauermann, R.; Traunmüller, F.; Georgopoulos, A.; Müller, M.; Joukhadar, C. Impact of plasma protein binding on antimicrobial activity using time-killing curves. *Journal of Antimicrobial Chemotherapy* **2004**, *54* (5), 876–880. https://doi.org/10.1093/jac/dkh443.

(228) Kirby, W. M. M. Pharmacokinetics of fosfomycin. *Chemotherapy* **1977**, *23* (SUP I), 141–151. https://doi.org/10.1159/000222040.

(229) Botwinski, C. A.; Falco, G. A. Transition to postnatal renal function. *Journal of Perinatal and Neonatal Nursing* **2014**, *28* (2), 150–154. https://doi.org/10.1097/JPN.0000000000000024.

(230) Benet, L. Z.; Broccatelli, F.; Oprea, T. I. BDDCS applied to over 900 drugs. *AAPS Journal* **2011**, *13* (4), 519–547. https://doi.org/10.1208/s12248-011-9290-9.

(231) Umezawa, K.; Hayashi, M.; Awazu, S. Paracellular and Transcellular Permeabilities of Fosfomycin across Small Intestinal Membrane of Rat and Rabbit by Voltage-Clamp Method. *Journal of Pharmacobio-Dynamics* **1991**, *14* (10), 583–589. https://doi.org/10.1248/bpb1978.14.583.

(232) Ishizawa, T.; Sadahiro, S.; Hosoi, K.; Tamai, I.; Terasaki, T.; Tsuji, A. Mechanisms of intestinal absorption of the antibiotic, fosfomycin, in brush-border membrane vesicles in rabbits and humans. *J Pharmacobiodyn* **1992**, *15* (9), 481–489. https://doi.org/10.1248/bpb1978.15.481.

(233) Borsa, F.; Leroy, A.; Fillastre, J. P.; Godin, M.; Moulin, B. Comparative pharmacokinetics of tromethamine fosfomycin and calcium fosfomycin in young and elderly adults. *Antimicrobial Agents and Chemotherapy* **1988**, *32* (6), 938–941. https://doi.org/10.1128/AAC.32.6.938.

(234) Cadorniga, R.; Fierros, M. D.; Olay, T. Pharmacokinetic study of fosfomycin and its bioavailability. *Chemotherapy* **1977**, *23* (SUP I), 159–174. https://doi.org/10.1159/000222043.

(235) Caldas, I. S.; Santos, E. G.; Novaes, R. D. An evaluation of benznidazole as a Chagas disease therapeutic. *Expert Opinion on Pharmacotherapy* **2019**, *20* (15), 1797–1807. https://doi.org/10.1080/14656566.2019.1650915.

(236) World Health Organisation. WHO Global Distribution of Cases of Chagas Disease. **2018**.

(237) Alpern, J. D.; Lopez-Velez, R.; Stauffer, W. M. Access to benznidazole for Chagas disease in the United States—Cautious optimism? *PLoS Neglected Tropical Diseases* **2017**, *11* (9), e0005794–e0005794. https://doi.org/10.1371/journal.pntd.0005794.

(238) Chemo Research S. L. Prescribing Infomation (NDA 209570), 2017. https://www.accessdata.fda.gov/drugsatfda_docs/nda/2017/209570Orig1s000Lbl.pdf.

(239) Wiens, M. O.; Kanters, S.; Mills, E.; Lucano, A. A. P.; Gold, S.; Ayers, D.; Ferrero, L.; Krolewiecki, A. Systematic review and meta-analysis of the pharmacokinetics of benznidazole in the treatment of Chagas disease. *Antimicrobial Agents and Chemotherapy* **2016**, *60* (12), 7035–7042. https://doi.org/10.1128/AAC.01567-16.

(240) Raaflaub, J.; Ziegler, W. H. Single-dose pharmacokinetics of the trypanosomicide benznidazole in man. *Arzneimittel-Forschung/Drug Research* **1979**, *29* (10), 1611–1614.

(241) Raaflaub, J. Multiple-dose kinetics of the trypanosomicide benznidazole in man. *Arzneimittel-Forschung/Drug Research* **1980**, *30* (12), 2192–2194.

(242) Roberts, J. T.; Bleehen, N. M.; Lee, F. Y. F.; Workman, P.; Walton, M. I. A phase I study of the combination of benznidazole and CCNU in man. *International Journal of Radiation Oncology, Biology, Physics* **1984**, *10* (9), 1745–1748. https://doi.org/10.1016/0360-3016(84)90541-8.

(243) Soy, D.; Aldasoro, E.; Guerrero, L.; Posada, E.; Serret, N.; Mejía, T.; Urbina, J. A.; Gascón, J. Population pharmacokinetics of benznidazole in adult patients with Chagas disease. *Antimicrobial Agents and Chemotherapy* **2015**, *59* (6), 3342–3349. https://doi.org/10.1128/AAC.05018-14.

(244) Chemo Research S. L. Clin Pharm and Biopharm Review (NDA 209570) Pg 68-73., 2017. https://www.accessdata.fda.gov/drugsatfda_docs/nda/2017/209570Orig1s000ClinPharmR.pdf.

(245) Molina, I.; Salvador, F.; Sánchez-Montalvá, A.; Artaza, M. A.; Moreno, R.; Perin, L.; Esquisabel, A.; Pinto, L.; Pedrazc, J. L. Pharmacokinetics of benznidazole in healthy volunteers and implications in future clinical trials. *Antimicrobial Agents and Chemotherapy* **2017**, *61* (4). https://doi.org/10.1128/AAC.01912-16.

(246) Nepali, K.; Lee, H. Y.; Liou, J. P. Nitro-Group-Containing Drugs. *Journal of Medicinal Chemistry* **2019**, *62* (6), 2851–2893. https://doi.org/10.1021/acs.jmedchem.8b00147.

(247) Rauth, A. M. Pharmacology and toxicology of sensitizers: Mechanism studies. *International Journal of Radiation Oncology, Biology, Physics* **1984**, *10* (8), 1293–1300. https://doi.org/10.1016/0360-3016(84)90335-3.

(248) Torrico, F.; Asada, M. New regimens of benznidazole monotherapy and in combination with fosravuconazole for treatment of Chagas disease (BENDITA): a phase 2, double-blind, randomised trial. *The Lancet Infectious Diseases* **2021**, *21* (8), 1129–1140. https://doi.org/10.1016/S1473-3099(20)30844-6.

(249) Alteri, E. Benznidazole in Chagas disease study: do the data justify progression to phase 3? *The Lancet. Infectious diseases* **2021**, *21* (8), 1066–1067. https://doi.org/10.1016/S1473-3099(21)00320-0.

(250) Exeltis France. 14C-Benznidazole ADME Study (NCT-03739541), 2018. https://www.clinicaltrials.gov/ct2/show/NCT03739541?term=benznidazole&draw=3&rank=12.

(251) FDA. Fulfilment of Postmarketing Requirement (Study 3247-2), 2019. https://www.accessdata.fda.gov/drugsatfda_docs/appletter/2019/209570Orig1s001ltr.pdf.

(252) Houghton, G.; Thorne, P.; Smith, J.; Templeton, R.; Collier, J. Comparison of the pharmacokinetics of metronidazole in healthy female volunteers following either a single oral or intravenous dose. *British Journal of Clinical Pharmacology* **1979**, *8* (4), 337–341. https://doi.org/10.1111/j.1365-2125.1979.tb04715.x.

(253) Dallmann, A.; Solodenko, J.; Ince, I.; Eissing, T. Applied Concepts in PBPK Modeling: How to Extend an Open Systems Pharmacology Model to the Special Population of Pregnant Women. *CPT: Pharmacometrics and Systems Pharmacology* **2018**, *7* (7), 419–431. https://doi.org/10.1002/psp4.12300.

(254) Houghton, G.; Dennis, M.; Gabriel, R. Pharmacokinetics of metronidazole in patients with varying degrees of renal failure. *British Journal of Clinical Pharmacology* **1985**, *19* (2), 203–209. https://doi.org/10.1111/j.1365-2125.1985.tb02632.x.

(255) Ribeiro, I.; Blum, B.; Fernandes, J.; Santina, G.; Asada, M.; Everson, M.; Schuck, E.; Feleder, E.; Evene, E.; Gualano, V. Drug-drug interaction study of benznidazole and E1224 in healthy male volunteers. *Antimicrobial Agents and Chemotherapy* **2021**, *65* (4). https://doi.org/10.1128/AAC.02150-19.

(256) Frauke Assmus, J. W., Richard M. Hoglund; BENDITA study group, the. Abstract 9778. Population Pharmacokinetics of Benznidazole as Monotherapy and in Combination with Fosravuconazole in Adult Patients with Chronic Chagas Disease (BENDITA Study), 2021. https://www.page-meeting.org/default.asp?abstract=9778.

(257) Lee, F. Y. F.; Workman, P. Nitroimidazoles as modifiers of nitrosourea pharmacokinetics. *International Journal of Radiation Oncology, Biology, Physics* **1984**, *10* (9), 1627–1630. https://doi.org/10.1016/0360-3016(84)90516-9.

(258) Workman, P.; White, R. A.; Walton, M. I.; Owen, L. N.; Twentyman, P. R. Preclinical pharmacokinetics of benznidazole. *British Journal of Cancer* **1984**, *50* (3), 291–303. https://doi.org/10.1038/bjc.1984.176.

(259) Davanço, M. G.; Campos, M. L.; Rosa, T. A.; Padilha, E. C.; Alzate, A. H.; Rolim, L. A.; Rolim-Neto, P. J.; Peccinini, R. G. Benznidazole Extended-Release tablets for improved treatment of chagas disease: Preclinical pharmacokinetic study. *Antimicrobial Agents and Chemotherapy* **2016**, *60* (4), 2492–2498. https://doi.org/10.1128/AAC.02506-15.

(260) Plus, S. Simulations Plus ADMET Predictor Platform, 2022. https://www.simulations-plus.com/software/admetpredictor/.

(261) Gonzalez Hernandez, F.; Lilaonitkul, W.; Kloprogge, F.; Standing, J. F.; Carter, S. J.; Iso-Sipilä, J.; Goldsmith, P.; Almousa, A. A.; Gastine, S. An automated approach to identify scientific publications reporting pharmacokinetic parameters. *Wellcome Open Research* **2021**, *6*, 88. https://doi.org/10.12688/wellcomeopenres.16718.1.

(262) Ankit Rohatgi. WebPlotDigitizer Version 4.5. https://github.com/ankitrohatgi/WebPlotDigitizer.

(263) Simulations Plus. GastroPlus® PBBM / PBPK, 2023. https://www.simulations-plus.com/software/gastroplus/.

(264) Varma, M. V.; Steyn, S. J.; Allerton, C.; El-Kattan, A. F. Predicting Clearance Mechanism in Drug Discovery: Extended Clearance Classification System (ECCS). *Pharmaceutical Research* **2015**, *32* (12), 3785–3802. https://doi.org/10.1007/s11095-015-1749-4.

(265) Williamson, B.; Harlfinger, S.; McGinnity, D. F. Evaluation of the disconnect between hepatocyte and microsome intrinsic clearance and in vitro in vivo extrapolation performances. *Drug Metabolism and Disposition* **2020**, *48* (11), 1137–1146. https://doi.org/10.1124/DMD.120.000131.

(266) Mahmood, I. Prediction of human drug clearance from animal data: Application of the rule of exponents and 'fu Corrected Intercept Method' (FCIM). *Journal of Pharmaceutical Sciences* **2006**, *95* (8), 1810–1821. https://doi.org/10.1002/jps.20650.

(267) Mahmood, I.; Balian, J. D. The pharmacokinetic principles behind scaling from preclinical results to phase I protocols. *Clinical Pharmacokinetics* **1999**, *36* (1), 1–11. https://doi.org/10.2165/00003088-199936010-00001.

(268) Morilla, M. J.; Montanari, J. A.; Prieto, M. J.; Lopez, M. O.; Petray, P. B.; Romero, E. L. Intravenous liposomal benznidazole as trypanocidal agent: Increasing drug delivery to liver is not enough. *International Journal of Pharmaceutics* **2004**, *278* (2), 311–318. https://doi.org/10.1016/j.ijpharm.2004.03.025.

(269) Tang, H.; Mayersohn, M. A novel model for prediction of human drug clearance by allometric scaling. *Drug Metabolism and Disposition* **2005**, *33* (9), 1297–1303. https://doi.org/10.1124/dmd.105.004143.

(270) Margolskee, A.; Abrahamsson, B. IMI – Oral biopharmaceutics tools project – Evaluation of bottom-up PBPK prediction success part 2: An introduction to the simulation exercise and overview of results. *European Journal of Pharmaceutical Sciences* **2017**, *96*, 610–625. https://doi.org/10.1016/j.ejps.2016.10.036.

(271) Bedor, D. C. G.; Bedor, N. C. T. C.; Da Silva, J. W. V.; Sousa, G. D.; De Santana, D. P.; Garcia-Bournissen, F.; Altcheh, J.; Blum, B.; Alves, F.; Ribeiro, I. Dried blood spot technique-based liquid chromatography-tandem mass spectrometry method as a simple alternative for benznidazole pharmacokinetic assessment. *Antimicrobial Agents and Chemotherapy* **2018**, *62* (12). https://doi.org/10.1128/AAC.00845-18.

(272) Marson, M. E.; Bournissen, F. G.; Altcheh, J.; Moscatelli, G.; Moroni, S.; Mastrantonio, G. E. Presence of benznidazole conjugated metabolites in urine identified by β-glucuronidase treatment. *Brazilian Journal of Pharmaceutical Sciences* **2020**, *56*. https://doi.org/10.1590/s2175-97902019000218034.

(273) Lombardo, F.; Berellini, G.; Obach, R. S. Trend analysis of a database of intravenous pharmacokinetic parameters in humans for 1352 drug compounds. *Drug Metabolism and Disposition* **2018**, *46* (11), 1466–1477. https://doi.org/10.1124/dmd.118.082966.

(274) Scotcher, D.; Jones, C.; Rostami-Hodjegan, A.; Galetin, A. Novel minimal physiologically-based model for the prediction of passive tubular reabsorption and renal excretion clearance. *European Journal of Pharmaceutical Sciences* **2016**, *94*, 59–71. https://doi.org/10.1016/j.ejps.2016.03.018.

(275) Zhong, K.; Li, X.; Xie, C.; Zhang, Y.; Zhong, D.; Chen, X. Effects of renal impairment on the pharmacokinetics of morinidazole: Uptake transporter-mediated renal clearance of the conjugated metabolites. *Antimicrobial Agents and Chemotherapy* **2014**, *58* (7), 4153–4161. https://doi.org/10.1128/AAC.02414-14.

(276) Ivanyuk, A.; Livio, F.; Biollaz, J.; Buclin, T. Renal Drug Transporters and Drug Interactions. *Clinical Pharmacokinetics* **2017**, *56* (8), 825–892. https://doi.org/10.1007/s40262-017-0506-8.

(277) Perdomo, V. G.; Rigalli, J. P.; Villanueva, S. S. M.; Ruiz, M. L.; Luquita, M. G.; Echenique, C. G.; Catania, V. A. Modulation of biotransformation systems and ABC transporters by benznidazole in rats. *Antimicrobial Agents and Chemotherapy* **2013**, *57* (10), 4894–4902. https://doi.org/10.1128/AAC.02531-12.

(278) Rigalli, J. P.; Perdomo, V. G.; Luquita, M. G.; Villanueva, S. S. M.; Arias, A.; Theile, D.; Weiss, J.; Mottino, A. D.; Ruiz, M. L.; Catania, V. A. Regulation of Biotransformation Systems and ABC Transporters by Benznidazole in HepG2 Cells: Involvement of Pregnane X-Receptor. *PLoS Neglected Tropical Diseases* **2012**, *6* (12), e1951. https://doi.org/10.1371/journal.pntd.0001951.

(279) Lennernäs, H. Intestinal permeability and its relevance for absorption and elimination. *Xenobiotica* **2007**, *37* (10-11), 1015–1051. https://doi.org/10.1080/00498250701704819.

(280) European Medicines Agency. ICH M9 on Biopharmaceutics Classification System Based Biowaivers - Scientific Guideline, 2020. https://www.ema.europa.eu/en/ich-m9-biopharmaceutics-classification-system-based-biowaivers-scientific-guideline.

(281) Food & Drug Administration. M9 Biopharmaceutics Classification System Based Biowaivers - Guidance for Industry, 2021. https://www.fda.gov/media/148472/download.

(282) Kansy, M.; Senner, F.; Gubernator, K. Physicochemical high throughput screening: Parallel artificial membrane permeation assay in the description of passive absorption processes. *Journal of Medicinal Chemistry* **1998**, *41* (7), 1007–1010. https://doi.org/10.1021/jm970530e.

(283) Sun, D.; Lennernas, H.; Welage, L. S.; Barnett, J. L.; Landowski, C. P.; Foster, D.; Fleisher, D.; Lee, K. D.; Amidon, G. L. Comparison of human duodenum and Caco-2 gene expression profiles for 12,000 gene sequences tags and correlation with permeability of 26 drugs. *Pharmaceutical Research* **2002**, *19* (10), 1400–1416. https://doi.org/10.1023/A:1020483911355.

(284) Maximiano, F. P.; Costa, G. H. Y.; De Souza, J.; Da Cunha-Filho, M. S. S. Physicochemical characterization of antichagasic benznidazole. *Quimica Nova* **2010**, *33* (8), 1714–1719. https://doi.org/10.1590/s0100-40422010000800018.

(285) Honorato, S. B.; Mendonça, J. S.; Boechat, N.; Oliveira, A. C.; Mendes Filho, J.; Ellena, J.; Ayala, A. P. Novel polymorphs of the anti-Trypanosoma cruzi drug benznidazole. *Spectrochimica Acta - Part A: Molecular and Biomolecular Spectroscopy* **2014**, *118*, 389–394. https://doi.org/10.1016/j.saa.2013.08.096.

(286) Workman, P.; Brown, J. M. Structure-pharmacokinetic relationships for misonidazole analogues in mice. *Cancer Chemotherapy and Pharmacology* **1981**, *6* (1), 39–49. https://doi.org/10.1007/BF00253009.

(287) Johnson, K. C. Dissolution and absorption modeling: Model expansion to simulate the effects of precipitation, water absorption, longitudinally changing intestinal permeability, and controlled release on drug absorption. *Drug Development and Industrial Pharmacy* **2003**, *29* (8), 833–842. https://doi.org/10.1081/DDC-120024179.

(288) Hintz, R. J.; Johnson, K. C. The effect of particle size distribution on dissolution rate and oral absorption. *International Journal of Pharmaceutics* **1989**, *51* (1), 9–17. https://doi.org/10.1016/0378-5173(89)90069-0.

(289) Pearce, R. E.; Cohen-Wolkowiez, M.; Sampson, M. R.; Kearns, G. L. The role of human cytochrome P450 enzymes in the formation of 2-hydroxymetronidazole: CYP2A6 is the high affinity (low Km) catalyst. *Drug Metabolism and Disposition* **2013**, *41* (9), 1686–1694. https://doi.org/10.1124/dmd.113.052548.

(290) Lindell, M.; Karlsson, M. O.; Lennernäs, H.; Påhlman, L.; Lang, M. A. Variable expression of CYP and Pgp genes in the human small intestine. *European Journal of Clinical Investigation* **2003**, *33* (6), 493–499. https://doi.org/10.1046/j.1365-2362.2003.01154.x.

(291) Zhang, Q. Y.; Dunbar, D.; Ostrowska, A.; Zeisloft, S.; Yang, J.; Kaminsky, L. S. Characterization of human small intestinal cytochromes P-450. *Drug Metabolism and Disposition* **1999**, *27* (7), 804–809.

(292) Song, G.; Sun, X.; Hines, R. N.; McCarver, D. G.; Lake, B. G.; Osimitz, T. G.; Creek, M. R.; Clewell, H. J.; Yoon, M. Determination of human hepatic CYP2C8 and CYP1A2 age-dependent expression to support human health risk assessment for early ages. *Drug Metabolism and Disposition* **2017**, *45* (5), 468–475. https://doi.org/10.1124/dmd.116.074583.

(293) Kiss, M.; Mbasu, R.; Nicolaï, J.; Barnouin, K.; Kotian, A.; Mooij, M. G.; Kist, N.; Wijnen, R. M. H.; Ungell, A. L.; Cutler, P.; Russel, F. G. M.; Wildt, S. N. de. Ontogeny of small intestinal drug transporters and metabolizing enzymes based on targeted quantitative proteomicsS. *Drug Metabolism and Disposition* **2021**, *49* (12), 1038–1046. https://doi.org/10.1124/dmd.121.000559.

(294) Brouwer, K. L. R.; Aleksunes, L. M.; Brandys, B.; Giacoia, G. P.; Knipp, G.; Lukacova, V.; Meibohm, B.; Nigam, S.; M Rieder, M.; Wildt, S. D. Human Ontogeny of Drug Transporters: Review and Recommendations of the Pediatric Transporter Working Group. *Clinical Pharmacology and Therapeutics* **2015**, *98* (3), 266–287. https://doi.org/10.1002/cpt.176.

(295) Merck Sharp & Dohme Corp. NDA Approval (214770) Noxafil PowderMix for Delayed-Release Oral Suspension, 2021. https://www.accessdata.fda.gov/drugsatfda_docs/nda/2021/214770Orig1s000Approv.pdf.

(296) Hens, B.; Pathak, S. M.; Mitra, A.; Patel, N.; Liu, B.; Patel, S.; Jamei, M.; Brouwers, J.; Augustijns, P.; Turner, D. B. In Silico Modeling Approach for the Evaluation of Gastrointestinal Dissolution, Supersaturation, and Precipitation of Posaconazole. *Molecular Pharmaceutics* **2017**, *14* (12), 4321–4333. https://doi.org/10.1021/acs.molpharmaceut.7b00396.

(297) Kersemaekers, W. M.; Van Iersel, T.; Nassander, U.; O'Mara, E.; Waskin, H.; Caceres, M.; Van Iersela, M. L. P. S. Pharmacokinetics and safety study of posaconazole intravenous solution administered peripherally to healthy subjects. *Antimicrobial Agents and Chemotherapy* **2015**, *59* (2), 1246–1251. https://doi.org/10.1128/AAC.04223-14.

(298) Merck Sharp Dohme. Noxafil IV Clin Pharm Review (NDA 205596), 2014. https://www.accessdata.fda.gov/drugsatfda_docs/nda/2014/205596Orig1s000ClinPharmR.pdf.

(299) Merck Sharp & Dohme Corp. FDA Noxafil Prescribing Information, 2022. https://www.merck.com/product/usa/pi_circulars/n/noxafil/noxafil_pi.pdf.

(300) Krieter, P.; Flannery, B.; Musick, T.; Gohdes, M.; Martinho, M.; Courtney, R. Disposition of posaconazole following single-dose oral administration in healthy subjects. *Antimicrobial Agents and Chemotherapy* **2004**, *48* (9), 3543–3551. https://doi.org/10.1128/AAC.48.9.3543-3551.2004.

(301) Krishna, G.; Moton, A.; Lei, M.; Medlock, M. M.; McLeod, J. Pharmacokinetics and absorption of posaconazole oral suspension under various gastric conditions in healthy volunteers. *Antimicrobial Agents and Chemotherapy* **2009**, *53* (3), 958–966. https://doi.org/10.1128/AAC.01034-08.

(302) Krishna, G.; Martinho, M.; Chandrasekar, P.; Ullmann, A. J.; Patino, H. Pharmacokinetics of oral posaconazole in allogeneic hematopoietic stem cell transplant recipients with graft-versus-host disease. *Pharmacotherapy* **2007**, *27* (12 I), 1627–1636. https://doi.org/10.1592/phco.27.12.1627.

(303) Krishna, G.; Ma, L.; Vickery, D.; Yu, X.; Wu, I.; Power, E.; Beresford, E.; Komjathy, S. Effect of varying amounts of a liquid nutritional supplement on the pharmacokinetics of posaconazole in healthy volunteers. *Antimicrobial Agents and Chemotherapy* **2009**, *53* (11), 4749–4752. https://doi.org/10.1128/AAC.00889-09.

(304) Courtney, R.; Pai, S.; Laughlin, M.; Lim, J.; Batra, V. Pharmacokinetics, safety, and tolerability of oral posaconazole administered in single and multiple doses in healthy adults. *Antimicrobial Agents and Chemotherapy* **2003**, *47* (9), 2788–2795. https://doi.org/10.1128/AAC.47.9.2788-2795.2003.

(305) Abutarif, M. A.; Krishna, G.; Statkevich, P. Population pharmacokinetics of posaconazole in neutropenic patients receiving chemotherapy for acute myelogenous leukemia or myelodysplastic syndrome. *Current Medical Research and Opinion* **2010**, *26* (2), 397–405. https://doi.org/10.1185/03007990903485056.

(306) Courtney, R.; Wexler, D.; Radwanski, E.; Lim, J.; Laughlin, M. Effect of food on the relative bioavailability of two oral formulations of posaconazole in healthy adults. *British Journal of Clinical Pharmacology* **2004**, *57* (2), 218–222. https://doi.org/10.1046/j.1365-2125.2003.01977.x.

(307) Boonsathorn, S.; Cheng, I.; Kloprogge, F.; Alonso, C.; Lee, C.; Doncheva, B.; Booth, J.; Chiesa, R.; Irwin, A.; Standing, J. F. Correction to: Clinical Pharmacokinetics and Dose Recommendations for Posaconazole in Infants and Children (Clinical Pharmacokinetics, (2019), 58, 1, (53-61), 10.1007/s40262-018-0658-1). *Clinical Pharmacokinetics* **2019**, *58* (1), 141. https://doi.org/10.1007/s40262-018-0722-x.

(308) Wiederhold, N. P. Pharmacokinetics and safety of posaconazole delayed-release tablets for invasive fungal infections. *Clinical Pharmacology: Advances and Applications* **2015**, *8*, 1–8. https://doi.org/10.2147/CPAA.S60933.

(309) Krishna, G.; Ma, L.; Martinho, M.; O'Mara, E. Single-dose phase I study to evaluate the pharmacokinetics of posaconazole in new tablet and capsule formulations relative to oral suspension. *Antimicrobial Agents and Chemotherapy* **2012**, *56* (8), 4196–4201. https://doi.org/10.1128/AAC.00222-12.

(310) Merck Sharp & Dohme Corp. EMEA Assessment Report (EMA/159150/2014), 2014. https://www.ema.europa.eu/en/documents/variation-report/noxafil-h-c-610-x-0028-epar-scientific-discussion-extension_en.pdf.

(311) Li, H.; Wei, Y.; Zhang, S.; Xu, L.; Jiang, J.; Qiu, Y.; Mangin, E.; Zhao, X. M.; Xie, S. Pharmacokinetics and Safety of Posaconazole Administered by Intravenous Solution and Oral Tablet in Healthy Chinese Subjects and Effect of Food on Tablet Bioavailability. *Clinical Drug Investigation* **2019**, *39* (11), 1109–1116. https://doi.org/10.1007/s40261-019-00833-1.

(312) Krishna, G.; Ma, L.; Martinho, M.; Preston, R. A.; O'mara, E. A new solid oral tablet formulation of posaconazole: A randomized clinical trial to investigate rising single- and multiple-dose pharmacokinetics and safety in healthy volunteers. *Journal of Antimicrobial Chemotherapy* **2012**, *67* (11), 2725–2730. https://doi.org/10.1093/jac/dks268.

(313) Merck Sharp Dohme. Noxafil Tablet Clin Pharm Review (NDA 205053), 2013. https://www.accessdata.fda.gov/drugsatfda_docs/nda/2013/205053Orig1s000ClinPharmR.pdf.

(314) Dolton, M. J.; Brüggemann, R. J. M.; Burger, D. M.; McLachlan, A. J. Understanding variability in posaconazole exposure using an integrated population pharmacokinetic analysis. *Antimicrobial Agents and Chemotherapy* **2014**, *58* (11), 6879–6885. https://doi.org/10.1128/AAC.03777-14.

(315) Kohl, V.; Müller, C.; Cornely, O. A.; Abduljalil, K.; Fuhr, U.; Vehreschild, J. J.; Scheid, C.; Hallek, M.; Rüping, M. J. G. T. Factors influencing pharmacokinetics of prophylactic posaconazole in patients undergoing allogeneic stem cell transplantation. *Antimicrobial Agents and Chemotherapy* **2010**, *54* (1), 207–212. https://doi.org/10.1128/AAC.01027-09.

(316) Vehreschild, J. J.; Müller, C.; Farowski, F.; Vehreschild, M. J. G. T.; Cornely, O. A.; Fuhr, U.; Kreuzer, K. A.; Hallek, M.; Kohl, V. Factors influencing the pharmacokinetics of prophylactic posaconazole oral suspension in patients with acute myeloid leukemia or myelodysplastic syndrome. *European Journal of Clinical Pharmacology* **2012**, *68* (6), 987–995. https://doi.org/10.1007/s00228-012-1212-y.

(317) Peña-Lorenzo, D.; Rebollo, N.; Sánchez-Hernández, J. G.; Zarzuelo-Castañeda, A.; Vázquez-López, L.; Otero, M. J.; Pérez-Blanco, J. S. Population pharmacokinetics of a posaconazole tablet formulation in transplant adult allogeneic stem cell recipients. *European Journal of Pharmaceutical Sciences* **2022**, *168*, 106049–106049. https://doi.org/10.1016/j.ejps.2021.106049.

(318) Petitcollin, A.; Boglione-Kerrien, C.; Tron, C.; Nimubona, S.; Lalanne, S.; Lemaitre, F.; Bellissant, E.; Verdiera, M. C. Population pharmacokinetics of posaconazole tablets and monte carlo simulations to determine whether all patients should receive the same dose. *Antimicrobial Agents and Chemotherapy* **2017**, *61* (11). https://doi.org/10.1128/AAC.01166-17.

(319) Ezzet, F.; Wexler, D.; Courtney, R.; Krishna, G.; Lim, J.; Laughlin, M. Oral bioavailability of posaconazole in fasted healthy subjects: Comparison between three regimens and basis for clinical dosage recommendations. *Clinical Pharmacokinetics* **2005**, *44* (2), 211–220. https://doi.org/10.2165/00003088-200544020-00006.

(320) Bentley, S.; Davies, J. C.; Gastine, S.; Donovan, J.; Standing, J. F. Clinical pharmacokinetics and dose recommendations for posaconazole gastroresistant tablets in children with cystic fibrosis. *Journal of Antimicrobial Chemotherapy* **2021**. https://doi.org/10.1093/jac/dkab312.

(321) Bhatnagar, S.; Mukherjee, D.; Salem, A. H.; Miles, D.; Menon, R. M.; Gibbs, J. P. Dose adjustment of venetoclax when co-administered with posaconazole: clinical drug–drug interaction predictions using a PBPK approach. *Cancer Chemotherapy and Pharmacology* **2021**, *87* (4), 465–474. https://doi.org/10.1007/s00280-020-04179-w.

(322) Lu Chen. PAGE2022 Abstract 10036: An Integrated Population Pharmacokinetic Analysis for Posaconazole Oral Suspension, Delayed-Release Tablet, and Intravenous Infusion in Healthy Volunteers, 2022. https://www.page-meeting.org/default.asp?abstract=10036.

(323) Groll, A. H.; Abdel-Azim, H.; Lehrnbecher, T.; Steinbach, W. J.; Paschke, A.; Mangin, E.; Winchell, G. A.; Waskin, H.; Bruno, C. J. Pharmacokinetics and safety of posaconazole intravenous solution and powder for oral suspension in children with neutropenia: an open-label, sequential dose-escalation trial. *International Journal of Antimicrobial Agents* **2020**, *56* (3), 106084. https://doi.org/10.1016/j.ijantimicag.2020.106084.

(324) Kraft, W. K.; Chang, P. S.; Van Iersel, M. L. P. S.; Waskin, H.; Krishna, G.; Kersemaekers, W. M. Posaconazole tablet pharmacokinetics: Lack of effect of concomitant medications altering gastric pH and gastric motility in healthy subjects. *Antimicrobial Agents and Chemotherapy* **2014**, *58* (7), 4020–4025. https://doi.org/10.1128/AAC.02448-13.

(325) GOSH. About GOSH DRIVE, 2023. https://www.gosh.nhs.uk/about-us/about-gosh-drive/.

(326) Aridhia. Your Next-Generation Research Environment, 2023. https://www.aridhia.com/.

(327) Michaelis, L.; Menten, M. L.; others. Die Kinetik Der Invertinwirkung. *Biochem. z* **1913**, *49* (333-369), 352.

(328) Johnson, K. A.; Goody, R. S. The original Michaelis constant: Translation of the 1913 Michaelis-Menten Paper. *Biochemistry* **2011**, *50* (39), 8264–8269. https://doi.org/10.1021/bi201284u.

(329) Shafer, S.; Fisher, D. Fisher/Shafer NONMEM Workshop Pharmacokinetic and Pharmacodynamic Analysis with NONMEM Basic Concepts, 2007. https://www.google.com/url?sa=t&rct=j&q=&esrc=s&source=web&cd=&cad=rja&uact=8&ved=2ahUKEwjwxsrq5uGCAxUJWkEAHZcODfcQFnoECA4QAQ&url=https%3A%2F%2Fwiki.ucl.ac.uk%2Fdownload%2Fattachments%2F23206987%2FShafer%2520NONMEM.pdf&usg=AOvVaw0nn63QWGt8-1Q4h0shRS94&opi=89978449.

(330) Patil, I. Visualizations with statistical details: The 'ggstatsplot' approach. *Journal of Open Source Software* **2021**, *6* (61), 3167. https://doi.org/10.21105/joss.03167.

(331) Epic. With the Patient at the Heart, 2023. https://www.epic.com/.

(332) Beal, S. L. Ways to fit a PK model with some data below the quantification limit. *Journal of Pharmacokinetics and Pharmacodynamics* **2001**, *28* (5), 481–504. https://doi.org/10.1023/A:1012299115260.

(333) Bergstrand, M.; Karlsson, M. O. Handling data below the limit of quantification in mixed effect models. *AAPS Journal* **2009**, *11* (2), 371–380. https://doi.org/10.1208/s12248-009-9112-5.

(334) Sharkey, I.; Boddy, A. V.; Wallace, H.; Mycroft, J.; Hollis, R.; Picton, S. Body surface area estimation in children using weight alone: Application in paediatric oncology. *British Journal of Cancer* **2001**, *85* (1), 23–28. https://doi.org/10.1054/bjoc.2001.1859.

(335) Boyd, E. *The Growth of the Surface Area of the Human Body.*; Milford, Univ. Minnesota Press, 1935.

(336) Gastine, S.; Hope, W.; Hempel, G.; Petraitiene, R.; Petraitis, V.; Mickiene, D.; Bacher, J.; Walsh, T. J.; Groll, A. H. Pharmacodynamics of posaconazole in experimental invasive pulmonary aspergillosis: Utility of serum galactomannan as a dynamic endpoint of antifungal efficacy. *Antimicrobial Agents and Chemotherapy* **2021**, *65* (2). https://doi.org/10.1128/AAC.01574-20.

(337) Pohlert, T. kwAllPairsDunnTest, 2023. https://rdrr.io/cran/PMCMRplus/man/kwAllPairsDunnTest.html.

(338) Dunn, O. J. Multiple Comparisons Using Rank Sums. *Technometrics* **1964**, *6* (3), 241–252. https://doi.org/10.1080/00401706.1964.10490181.

(339) Kendall, J.; Papich, M. G. Posaconazole pharmacokinetics after administration of an intravenous solution, oral suspension, and delayed-release tablet to dogs. *American Journal of Veterinary Research* **2015**, *76* (5), 454–459. https://doi.org/10.2460/ajvr.76.5.454.

(340) Jang, S. H.; Colangelo, P. M.; Gobburu, J. V. S. Exposure-response of posaconazole used for prophylaxis against invasive fungal infections: Evaluating the need to adjust doses based on drug concentrations in plasma. *Clinical Pharmacology and Therapeutics* **2010**, *88* (1), 115–119. https://doi.org/10.1038/clpt.2010.64.

(341) Smits, A.; Annaert, P.; Cavallaro, G.; De Cock, P. A. J. G.; Wildt, S. N. de; Kindblom, J. M.; Lagler, F. B.; Moreno, C.; Pokorna, P.; Schreuder, M. F.; Standing, J. F.; Turner, M. A.; Vitiello, B.; Zhao, W.; Weingberg, A. M.; Willmann, R.; Anker, J. van den; Allegaert, K. Current knowledge, challenges and innovations in developmental pharmacology: A combined conect4children Expert Group and European Society for Developmental, Perinatal and Paediatric Pharmacology White Paper. *British Journal of Clinical Pharmacology* **2022**, *88* (12), 4965–4984. https://doi.org/10.1111/bcp.14958.

(342) Liu, X. I.; Anker, J. N. van den; Burckart, G. J.; Dallmann, A. Evaluation of Physiologically Based Pharmacokinetic Models to Predict the Absorption of BCS Class I Drugs in Different Pediatric Age Groups. *Journal of Clinical Pharmacology* **2021**, *61* (S1), S94–S107. https://doi.org/10.1002/jcph.1845.